UNIVERSITÉ FRANÇOIS – RABELAIS DE TOURS

ÉCOLE DOCTORALE « Santé, Sciences Biologiques et Chimie du Vivant »

EA 6295 « Nanomédicaments et Nanosondes »

THÈSE présentée par :

Juliette GAUTIER

soutenue le : **19 juin 2013**

pour obtenir le grade de : **Docteur de l'université François – Rabelais de Tours**

Discipline/ Spécialité : Sciences de la Vie

Nanoparticules d'oxydes de fer PEGylées pour la délivrance de la doxorubicine : développement et évaluation de leur potentiel théragnostique

THÈSE dirigée par :

M. CHOURPA Igor	Professeur, Université François Rabelais de Tours

RAPPORTEURS :

Mme GEZE Annabelle	Maître de Conférences, Université Joseph Fourier de Grenoble
M. OLIVIER Jean-Christophe	Professeur, Université de Poitiers

---

JURY :

Mme ALLARD-VANNIER Emilie	Maître de Conférences, Université François Rabelais de Tours
M. CHOURPA Igor	Professeur, Université François Rabelais de Tours
Mme GEZE Annabelle	Maître de Conférences, Université Joseph Fourier de Grenoble
M. MANFAIT Michel	Professeur, Université de Reims Champagne-Ardenne
M. OLIVIER Jean-Christophe	Professeur, Université de Poitiers
Mme PASSIRANI Catherine	Professeur, Université d'Angers

À mon père.

Remerciements

Je tiens à exprimer mes plus sincères remerciements aux membres du jury, pour avoir accepté et pris de leur temps pour juger ce travail.

Je remercie Mme Annabelle Geze, Maître de Conférences à l'université de Grenoble, membre du Département de Pharmacochimie Moléculaire, UMR5063 UJF/CNRS, et M. Jean-Christophe Olivier, Professeur à l'université de Poitiers, membre de l'équipe « Pharmacology of Antimicrobial Agents », INSERM U1070, de me faire l'honneur d'être rapporteurs de cette thèse.

Je remercie Mme Emilie Allard-Vannier, Maître de Conférences à l'université de Tours, membre de l'équipe EA 6295 « Nanomédicaments et Nanosondes », Mme Catherine Passirani, Professeur à l'université d'Angers et membre de l'équipe « Micro et nanomédecines Biomimétiques », MINT UMR INSERM 1066, et M. Michel Manfait, Professeur à l'université de Reims, responsable de l'équipe « Biophotonique, Médicaments, Dynamique Cellulaire et Tissulaire » de l'URCA CNRS UMR 6237 MEDyC, d'avoir accepté de faire partie du jury en tant qu'examinateurs.

Je tiens à remercier M. Igor Chourpa, Professeur à l'Université de Tours, directeur de l'EA 6295 « Nanomédicaments et nanosondes », pour m'avoir accueillie dans son équipe et m'avoir fait confiance pour mener à bien ces travaux. Je le remercie également pour ses conseils, les opportunités offertes d'élargir mes champs de compétence, et la liberté qu'il m'a laissée.

Je tiens à remercier tous les membres des laboratoires de Pharmacie Galénique et de Chimie Analytique de la Faculté des Sciences Pharmaceutiques de Tours.

Au docteur Emilie Munnier, pour avoir guidé mes premiers pas en tant que doctorante, pour ses conseils toujours avisés, sa franchise et son humour pince-sans-rire.

Au docteur Emilie Allard-Vannier, pour m'avoir fait découvrir les joies de l'expérimentation animale, pour sa vision scientifique aiguisée, sa célérité dans les corrections de manuscrits, et sa bonne humeur indéboulonnable.

Au docteur Katel Hervé-Aubert, pour son soutien sans faille, et son aide précieuse pour les enseignements. Merci également pour les éclats de rire et les pâtisseries ! Quel dommage de ne pas avoir plus travaillé ensemble !

Au docteur Laurence Douziech-Eyrolles, pour les collaborations scientifiques et sa gentillesse.

Au docteur Simone Cohen-Jonathan, et au Professeur Pierre Dubois, pour leur bienveillance à mon égard.

Au docteur Hervé Marchais, pour m'avoir fait confiance pour mes premiers enseignements dans le supérieur.

Au docteur Martin Soucé, pour le temps infini passé à corriger mon anglais déplorable, et pour avoir contribué à l'améliorer, merci également pour les discussions scientifiques, la patience, l'indulgence et le temps déployés pour une petite étudiante noyée sous les TP.

À mes techniciens préférés, Didier, Jean-François et Xavier. Je ne compte plus le nombre de fois où ils m'ont sauvé la mise. Ils m'ont épaulé d'une façon magistrale, j'ai beaucoup appris d'eux. Merci aussi pour les bises façon hérisson, les blagues vaseuses et le café à réveiller les morts!

Cela a été une réelle joie de travailler au sein de cette équipe.

Je remercie également le docteur Marek Procházka et sa doctorante Petra Šimáková de l'Institut de Physique de la Charles University de Prague, pour m'avoir accueillie au sein de son laboratoire, et pour notre collaboration scientifique fructueuse et amicale.

Je remercie le Professeur Jorge Domenech, de l'unité CNRS UMR 7292 de l'UFR de Médecine de Tours, pour le temps consacré à l'analyse des données hématologiques de nos petites souris, et Julien Gaillard, du Plateau Technologique Analyse des Systèmes Biologiques, pour les clichés en MET. Je remercie Sandra Même et Jean-Claude Beloeil, de l'UPR 4301, équipe « IRM, signaux, images et expression des gènes » du CBM d'Orléans, pour l'acquisition et le traitement des données IRM.

Je remercie le personnel de l'animalerie, Thierry et Benjamin, pour leur accompagnement et leur disponibilité.

Je remercie les stagiaires, doctorants, post-doctorants et ATER que j'ai côtoyés pendant ces années : Karine, Roland, Archibald, Manuela, Yaël, Clément, Xavier, Stéphanie, Phuong, Ambre, Christophe… Ça a été un plaisir de travailler avec eux, surtout en partageant un minuscule bureau !!!

Pour finir, une pensée pour ma famille : ma petite maman, qui attendait ça impatiemment, depuis le temps que je suis étudiante !!! Et mes sœurs, Charlotte et Alice (et les beaux-frères !), qui ont su m'écouter et m'encourager.

Mon dernier remerciement sera pour toi, Fabien. Merci d'être là.

Résumé

Des nanoparticules d'oxydes de fer superparamagnétiques (SPIONs) PEGylées ont servi de plateforme pour la formulation de nanovecteurs théragnostiques d'un agent anticancéreux, la doxorubicine (DOX).

La DOX a été chargée sur ces nanovecteurs sous forme d'un complexe du médicament avec l'ion fer (II). Ce complexe DOX-Fe^{2+} se dissocie en milieu acide, typique de l'environnement tumoral et des compartiments intracellulaires tels que les endosomes et les lysosomes : la libération de la DOX est ainsi accélérée. Le chargement de la DOX sur les nanovecteurs a été optimisé, et la spectroscopie Raman exaltée de surface (SERS) a confirmé que les nanovecteurs libèrent la DOX sous forme non complexée.

La cytotoxicité *in vitro* induite par la libération de la DOX à partir des nanovecteurs a été évaluée sur différentes lignées cellulaires de cancer du sein, et comparée à celle de la DOX en solution. Les voies d'internalisation des nanovecteurs ont été explorées en microscopie électronique en transmission (MET) : les nano-objets entrent dans les cellules par la voie des clathrines et la voie des cavéoles. Le devenir intracellulaire de la DOX a été suivi en imagerie confocale multispectrale de fluorescence (ICMS) : après internalisation initiale des nanovecteurs dans les compartiments cytoplasmiques, la DOX est progressivement libérée vers le noyau.

Enfin, un protocole thérapeutique *in vivo* chez la souris tumorisée a permis d'évaluer la capacité de la nanoformulation à limiter la croissance tumorale, avec ou sans application d'un champ magnétique externe, et la réduction des effets secondaires hématologiques induits par la DOX.

Mots-clés

Nanoparticules d'oxydes de fer superparamagnétiques (SPIONs), doxorubicine (DOX), complexe DOX-Fe^{2+}, nanovecteur théragnostique, délivrance, protocole thérapeutique, furtivité, imagerie

Abstract

PEGylated superparamagnetic iron oxide nanoparticles (SPIONs) were used as a platform to build theranostic nanovectors for an anticancer drug, doxorubicin (DOX).

The DOX molecule was loaded on nanocarriers via a complex between drug and iron (II). The DOX-Fe^{2+} complex dissociates at low pH, typical of tumoral environment and intracellular compartments like endosomes or lysosomes: the DOX release is accelerated in cells. The DOX loading on nanovectors via the DOX-Fe^{2+} complex was optimized, and surface enhanced Raman scattering (SERS) confirmed that the nanovectors released DOX under free form.

In vitro cytotoxicity due to DOX loaded on nanocarriers was performed on different breast cancer cells, and compared to that of DOX in solution. Internalization pathways of nanovectors were explored with transmission electron microscopy (TEM): nanocarriers enter cells via clathrin- and caveolae-mediated endocytosis. The intracellular fate of DOX was monitored by confocal spectral imaging (CSI): after internalization of the nanocarriers into intracellular compartments, DOX is progressively released and found in the nucleus.

Finally, a therapeutical protocol was performed on tumorized mice, in order to evaluate the efficacy of the nanoformulation on tumor reduction, with and without the application of an external magnetic field, and the decrease of hematologic side effects induced by DOX.

Keywords

Superparamagnetic iron oxide nanoparticles (SPIONs), doxorubicin (DOX), DOX-Fe^{2+} complex, theranostic nanovector, delivery, therapeutical protocol, stealthiness, imaging

Table des matières

Liste des figures

Liste des annexes

Introduction

Dans le cadre de la lutte contre le cancer, la chimiothérapie est, avec la radiothérapie et la chirurgie, une arme de choix. Les classes de molécules anticancéreuses classiques (comme les agents alkylants, les antimétabolites, les alcaloïdes végétaux, les inhibiteurs des topoisomérases et les antibiotiques antitumoraux) présentent cependant des points faibles, de par leur administration systémique :

- une biodistribution des molécules dans l'ensemble de l'organisme ;
- le manque d'affinité spécifique de la molécule pour le site pathologique ;
- la nécessité d'une dose totale importante de façon à assurer une concentration locale suffisante ;
- une toxicité non spécifique et autres effets indésirables dus à la dose importante employée [1].

Ces dernières années, l'arsenal thérapeutique s'est enrichi de thérapies plus ciblées comme les modificateurs de la transduction du signal (Gleevec®), les inhibiteurs enzymatiques (Iressa® et Tarceva®), les anticorps humanisés (Avastin® et Cetuximab®), la thérapie cellulaire ou la thérapie génique. Même si les molécules en question sont prometteuses, et présentent plus de spécificité pour le site tumoral, elles présentent toujours une toxicité systémique, et la plasticité et l'instabilité génétique des tumeurs se sont révélées être un facteur limitant à ce type de thérapie ciblée [2]. De plus, de nombreuses tumeurs développent une multirésistance aux médicaments, phénomène appelé MDR (ou multidrug resistance) [3–5].

Face à ces constatations, la recherche s'est orientée vers une autre stratégie : la vectorisation des agents anticancéreux usuels, déjà bien connus, mais non spécifiques. Associer une molécule à un vecteur permet de modifier sa pharmacocinétique et sa biodistribution [6]. Le but recherché est de favoriser la concentration du principe actif au niveau du tissu pathologique, de façon à potentialiser son action locale, tout en diminuant la toxicité systémique [1].

1. La vectorisation

La stratégie de vectorisation passe par l'association d'une molécule à un objet de dimensions nanométriques (macromolécule ou nano-objet). La formulation des nanovecteurs est donc un élément clé pour contrôler le devenir de la molécule dans l'organisme.

1.1. Les différentes architectures de nanovecteurs

La formulation de nanovecteurs fait appel à des matériaux divers, naturels comme des phospholipides [7,8], des polysaccharides tels que le chitosan [9,10], des protéines comme l'albumine [11–13], ou de synthèse comme de nombreux polymères ou copolymères [14–19]. Le critère principal de choix de ces matériaux est leur biocompatibilité, ainsi que l'affinité de la molécule active à vectoriser pour des matériaux hydrophiles ou lipophiles. Les architectures possibles (quelque unes sont présentées à la figure 1) et les méthodes de chargement des anticancéreux sur des nanovecteurs sont ainsi très variées.

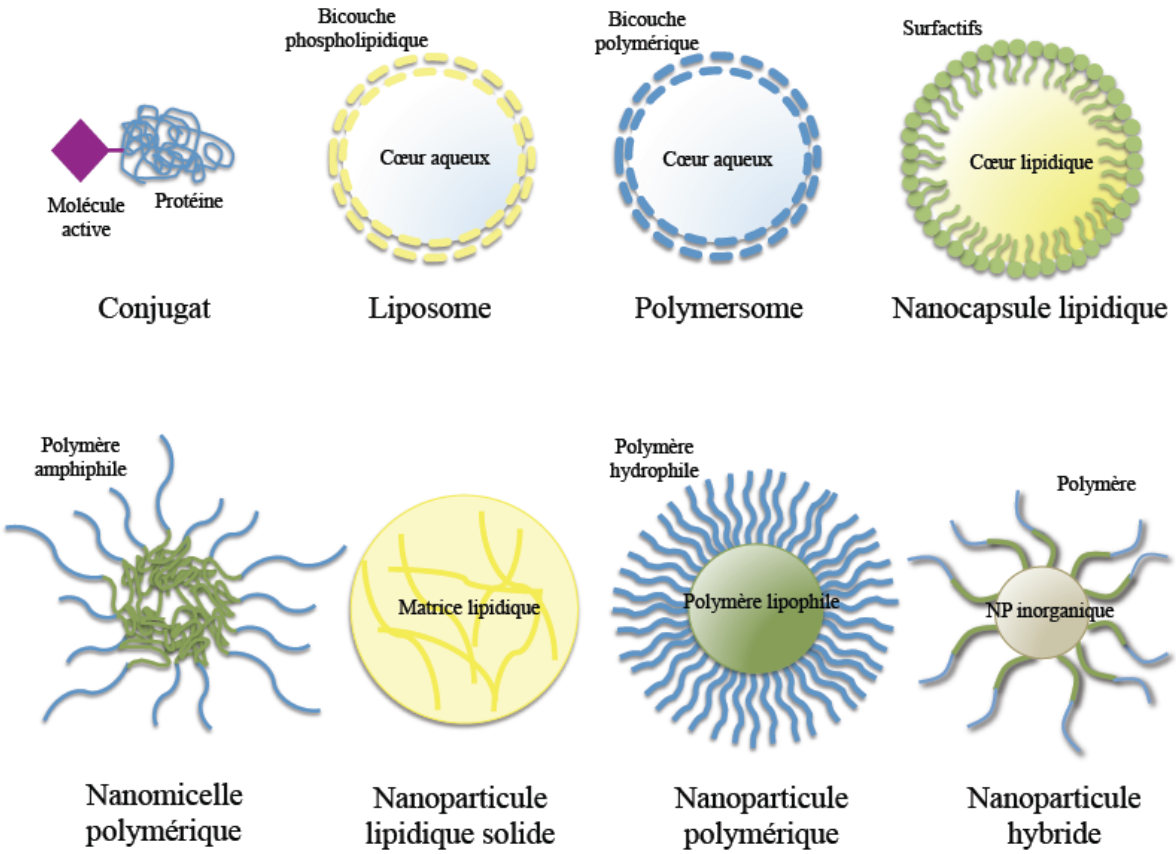

Figure 1 : Différentes formulations de nanovecteurs.

Les conjugats (figure 1) consistent à associer chimiquement une molécule active à une autre, de haut poids moléculaire, généralement une protéine, comme l'albumine. L'ensemble présente donc un poids moléculaire très supérieur à celui de la molécule seule, ce qui modifie sa biodistribution dans l'organisme, ainsi que ses interactions avec les cellules. Cette solution a été mise en œuvre avec succès pour le paclitaxel, lié à de l'albumine dans l'Abraxane® [20]. La liaison chimique utilisée pour l'association ne doit pas mettre en œuvre le site actif de la

molécule, sous peine de perdre l'efficacité antitumorale de cette dernière, ou doit pouvoir être clivée pour libérer l'anticancéreux sur son site d'action.

Les liposomes (figure 1) sont constitués d'une bicouche phospholipidique, généralement stabilisée par des surfactifs et rigidifiée par du cholestérol, renfermant un cœur aqueux. Le principe actif peut donc être inclus dans le cœur s'il est hydrophile, plus rarement dans la bicouche s'il est lipophile. La molécule est libérée lorsque le liposome fusionne avec la membrane cellulaire. Des liposomes à base de doxorubicine sont déjà disponibles sur le marché (Myocet® et Doxil®) [21,22]. La bicouche peut être également constituée de polymères amphiphiles autoassemblés. Des copolymères à base de polypeptides (notamment acide glutamique) constituent ainsi des polymersomes (figure 1) [23–25]. Ces polymères peuvent aussi être assemblés en nanomicelles (figure 1) [26–29]. Dans ce cas, le chargement et libération de l'anticancéreux sont conditionnés par la plus ou moins grande affinité de l'anticancéreux pour ces matériaux, et la fonctionnalisation de surface des polymersomes et des nanomicelles est généralement plus aisée que pour des systèmes à base de lipides.

Pour des molécules lipophiles, des matériaux lipidiques peuvent être assemblés sous forme de nanocapsules ou LNC (lipid nanocapsules) (figure 1) : le cœur lipidique composé de triglycérides est stabilisé par des phospholipides et des surfactifs. Lorsque les matériaux lipidiques se présentent sous forme cristalline, le nanovecteur est appelé nanoparticule lipidique solide ou SLN (solid lipid nanoparticle, figure 1) [10,30,31]. Ces deux types de vecteurs présentent cependant l'inconvénient d'un chargement en principe actif souvent faible, accompagné d'une libération trop rapide, et incomplète [30].

Pour finir, de nombreux types de polymères et copolymères sont mis en œuvre pour la fabrication de nanoparticules polymériques (figure 1) : acide poly(lactique-co-glycolique) ou PLGA [16], poly-ε-caprolactone ou PCL [17], dérivés d'acide malique [19], le plus couramment utilisé restant le polyéthylène glycol ou PEG [18,32–36]. Ce dernier a en effet été approuvé par la FDA pour les applications biomédicales. Les nanoparticules polymériques sont des systèmes très versatiles : le chargement du principe actif se fait dans le cœur ou dans l'enveloppe, et leur fonctionnalisation de surface est aisée, d'où leur étude intensive dans la littérature [37–43]. Ces mêmes polymères sont retrouvés dans la formulation de nanoparticules hybrides (figure 1). Dans ce cas, le cœur des nanovecteurs est inorganique, à base par exemple de silice mésoporeuse [44–47], de cristaux semi-conducteurs comme les quantum dots (souvent à base de CdSe) [48,49], ou de métaux comme des oxydes de

manganèse [50], des oxydes de fer [51–54], ou même à base d'or [55–59]. Les polymères servent donc à fonctionnaliser leur surface. Les principes actifs sont chargés à la surface des nanoparticules, ou emprisonnés dans le revêtement polymérique. Ce type de nanovecteurs sera largement étudié dans la première partie de cette thèse.

1.2. Propriétés des nanovecteurs dans l'organisme : intérêts de la vectorisation

Pour une molécule vectorisée, sa biodistribution n'est plus régie par des phénomènes de diffusion, hors du flux sanguin jusqu'aux organes et aux cellules ; le nanovecteur doit franchir de nombreuses barrières biologiques (capture par les phagocytes, dégradation enzymatique, endothélium vasculaire, membranes cellulaires, organites subcellulaires comme les endosomes). Arrivé sur son site d'action, le nanovecteur entre dans les cellules par un phénomène actif d'endocytose [60–62], ou dans le cas des liposomes, par fusion avec la membrane plasmique [62,63]. La taille des nanovecteurs joue un rôle prépondérant concernant l'élimination de l'organisme. Les nano-objets sont préférentiellement éliminés par voie rénale (taille inférieure à 10 nm) ou hépatique (taille supérieure à 10 nm) [2]. Les nano-objets de taille inférieure à 200 nm font l'objet d'une capture diminuée par les cellules phagocytaires, ce qui retarde leur élimination du flux sanguin [2]. La vectorisation peut donc permettre d'augmenter le temps de circulation d'un anticancéreux, en le protégeant d'une élimination rapide.

La vectorisation peut aussi permettre d'augmenter l'exposition des cellules tumorales à un anticancéreux. C'est le cas de l'Abraxane®, où le paclitaxel est lié à des macromolécules d'albumine, formant des complexes solubles de 10 nm. Le paclitaxel étant lipophile, cette formulation permet de le solubiliser, tout en évitant l'utilisation d'huile de ricin polyoxyéthylénée et d'alcool éthylique, excipients à effets notoires présents dans la forme conventionnelle pour augmenter la solubilité de la molécule. De plus, l'albumine, connue pour faciliter la transcytose endothéliale, favorise le transport du paclitaxel à travers les cellules endothéliales, permettant d'augmenter son accumulation dans la zone tumorale. Le volume de distribution de la molécule n'est pas modifié, mais la liaison aux protéines plasmatiques du paclitaxel est réduite lorsqu'il est complexé avec l'albumine, ce qui augmente l'exposition totale de l'organisme à la molécule.

La vectorisation peut aussi permettre de diminuer les effets secondaires. Dans le cas du Doxil®, la vectorisation de la doxorubicine sous forme liposomale a permis de modifier le volume de distribution de la molécule, le réduisant drastiquement (4 L au lieu de 254 L) [21]. Si l'efficacité de la forme vectorisée est identique à celle de la forme conventionnelle dans ses indications officielles, la faible diffusion dans les tissus sains a permis de diminuer significativement l'incidence des pathologies cardiaques classiquement associées à l'administration de la doxorubicine [64].

1.3. Délivrance des anticancéreux : les stratégies de ciblage et de délivrance

Ciblage passif et actif

L'objectif principal de la vectorisation est de favoriser l'accumulation de l'agent anticancéreux au niveau de la tumeur. Ce ciblage de l'environnement tumoral peut tout d'abord être passif : une injection ou une implantation directement dans le site tumoral permet une délivrance localisée, évitant ainsi le franchissement de nombreuses barrières biologiques, mais il s'agit d'une technique invasive. Une administration systémique mène aussi à une accumulation passive des nanovecteurs dans l'environnement tumoral, par un phénomène appelé « effet EPR », pour « enhanced retention and permeation » [65–67]. En effet, la néoangiogénèse au niveau des tumeurs est imparfaite, les nouveaux vaisseaux présentant des fenestrations plus grandes que les vaisseaux sains, 200 nm en moyenne et jusqu'à 700 nm, au lieu de 70 nm. L'extravasation et l'accumulation des nanovecteurs (de 20 à 200 nm) dans l'espace interstitiel sont donc facilitées. De plus, les vaisseaux lymphatiques sont absents ou non fonctionnels au sein des tumeurs, ce qui contribue à un drainage lymphatique inefficace, les nanovecteurs ne sont donc pas chassés de l'environnement tumoral. C'est cet effet EPR qui a été exploité avec succès pour la première génération de nanovecteurs, comme le Doxil® [21].

Cependant le ciblage passif reste insuffisant, une partie non négligeable des molécules anticancéreuses se distribuant dans l'organisme. C'est pourquoi la plupart des nanovecteurs développés récemment ajoutent une stratégie de ciblage actif biochimique et/ou physique à la formulation. Pour le ciblage biochimique, il s'agit d'habiller les vecteurs avec une molécule permettant une meilleure reconnaissance des cibles tumorales, notamment des ligands spécifiques de certains récepteurs surexprimés au niveau des cellules tumorales [65,68–70].

Ces ligands peuvent aider au ciblage des cellules tumorales, mais aussi faciliter l'entrée des nanovecteurs au sein de ces cellules. L'exemple le plus connu est l'utilisation de l'acide folique, son récepteur étant très largement surexprimé dans bon nombre de types de cancers [71]. À côté de ce ciblage actif de nature biologique, s'est développé dans les années 70 le concept de ciblage physique, au moyen d'un champ magnétique appliqué au niveau des tumeurs [52,72]. La vectorisation magnétique repose sur l'utilisation de nanoparticules magnétiques, classiquement à base d'oxydes de fer [52,53,73–75]. Après injection systémique, l'application d'un champ magnétique externe focalisé sur la tumeur permet de retenir les nanovecteurs au niveau de l'environnement tumoral. Le principe de ce ciblage actif macroscopique est schématisé par la figure 2. Il est particulièrement adapté aux tumeurs solides superficielles. Certaines stratégies de ciblage actif seront étudiées dans la première partie de cette thèse.

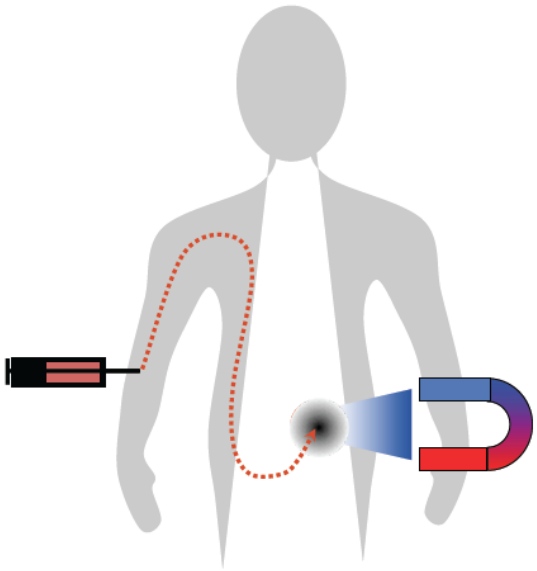

Figure 2 : principe de la vectorisation magnétique d'agents anticancéreux, utilisant des vecteurs magnétiques injectables et un champ magnétique externe appliqué au niveau de la tumeur cible.

Délivrance en réponse à un stimulus

En plus du ciblage des tumeurs, les études récentes rapportent la mise au point de nanovecteurs « activables » [37,76,77]. Ces nanosystèmes assurent le transport de l'agent anticancéreux dans l'organisme, et à proximité de la tumeur, un stimulus interne ou externe permet d'activer l'interaction avec les cellules cibles, ou même de déclencher/d'accélérer la libération de la molécule active.

Le cas le plus simple est une réponse à un stimulus interne, comme le changement de pH de l'environnement. L'environnement tumoral possède en effet un pH plus faible que le sang et les tissus sains (entre 6 et 7, au lieu de 7,4) [65]. De plus, après endocytose par les cellules, les nanovecteurs se retrouvent fréquemment dans des endosomes (pH 6) ou des lysosomes (pH 5) [78]. Les stratégies de délivrance mettant en œuvre une libération pH-dépendante de l'agent anticancéreux sont donc nombreuses. Des polymères sensibles au pH ont été employés sous forme de micelles polymériques [27], ou comme revêtement de nanoparticules inorganiques [79]. À faible pH, les micelles sont déstabilisées, le revêtement polymérique se désagrège, libérant la molécule active par destruction du nanovecteur. Une autre approche est la liaison de la molécule active au nanovecteur par une liaison chimique pH-dépendante, comme les liaisons hydrazone [80–82] ou ester [83], se dissociant à pH acide. Le but est identique, favoriser la libération de l'anticancéreux après internalisation des nanovecteurs par les cellules, lorsqu'ils sont stockés dans les compartiments endosomaux et lysosomaux, tout en évitant sa libération dans le reste de l'organisme.

D'autres formulations utilisent un stimulus externe pour activer les nanovecteurs. Les systèmes thermosensibles sont nombreux. Des polymersomes [23,24] ou des liposomes [7] contenant des nanoparticules magnétiques ont été exposés à un champ magnétique, provoquant un échauffement, et une fluidification des polymères ou des lipides, facilitant ainsi la libération de l'agent anticancéreux. Des nanoparticules hybrides à base d'or [84–86] exposées à un laser infrarouge ont permis un échauffement du cœur inorganique des nanosystèmes et une libération accélérée de la molécule active. Au lieu d'une réponse à un échauffement provoqué par l'application d'un champ magnétique ou d'un laser, d'autres formulations utilisent des ultra-sons [77].

Un nombre croissant de publications associe à la fois un ciblage de l'environnement tumoral ou des cellules cancéreuses avec une délivrance stimuli-répondante de l'agent anticancéreux, elles seront développées dans la première partie de cette thèse.

1.4. Vers des nanosystèmes multifonctionnels

En plus de la délivrance des agents anticancéreux, les nanovecteurs nouvellement mis au point offrent des fonctionnalités supplémentaires. On parle de nanovecteurs théragnostiques [87–89], c'est-à-dire permettant à la fois la délivrance d'une molécule active, une stratégie de ciblage, et des fonctions d'imagerie pour le suivi du traitement ou le diagnostic.

L'utilisation en imagerie est surtout envisageable pour les nanoparticules hybrides, dont le cœur inorganique est à base de métaux. Les nanoparticules d'or peuvent en effet servir d'agents de contraste en tomographie à cohérence optique, en tomographie acoustique, en tomographie aux rayons X (scanner) ou en tomographie à émission de positrons (PET scan) [90–92]. Les nanoparticules d'oxydes de fer sont utilisées depuis une quinzaine d'années comme agents de contraste en imagerie à résonance magnétique (IRM) [53,75,93–96]. Quant aux quantum dots, elles possèdent une très large gamme de longueurs d'onde excitatrices, des spectres d'émission allant de l'ultraviolet au proche infrarouge, en fonction des semi-conducteurs utilisés et de la taille des nanoparticules [48,49,97,98]. De plus, elles sont capables d'émettre pendant plusieurs dizaines de minutes, contrairement aux fluorophores organiques classiques, et ont un meilleur rendement quantique. Elles sont donc largement mises en œuvre en imagerie de fluorescence [99–101]. Les nanosystèmes exclusivement à base de polymère ou de lipides doivent en revanche être marqués (liaison à un fluorophore, ajout d'un isotope) pour pouvoir être suivis dans l'organisme.

Enfin, certains nanosystèmes théragnostiques vont encore plus loin. L'utilisation de certains matériaux comme l'or ou les oxydes de fer permet de compléter l'effet anticancéreux de la molécule active par une thérapie complémentaire. Lorsque des nanoparticules oxydes de fer sont soumises à un champ magnétique alternatif, ou que des nanoparticules d'or sont soumises à un rayonnement proche infrarouge, l'échauffement local généré peut provoquer la mort des cellules cancéreuses. Il s'agit de thérapie ou d'ablation thermique [56,91,102]. Ce concept a été récemment mis en œuvre dans des évaluations in vivo [84,86].

La première partie de cette thèse traitera plus particulièrement des nanosystèmes théragnostiques à base d'or et d'oxydes de fer.

2. La doxorubicine

La doxorubicine (DOX) est une anthracycline (famille d'antibiotiques). Elle permet de traiter une large variété de cancers, dont des leucémies, des cancers ovariens, et particulièrement des cancers du sein avancés [103]. Cette thèse est focalisée sur cet agent anticancéreux.

2.1. Structure de la molécule et propriétés physico-chimiques

La molécule de doxorubicine est composée d'un noyau aglycone et d'un sucre. Le noyau aglycone est une structure tétracyclique, avec des groupements quinone–hydroquinone sur les cycles B et C, un substituant méthoxy en C_4 sur le cycle D, et une chaîne courte en C_9 avec un carbonyle en C_{13}. Le sucre aminé ou daunosamine (3-amino-2,3,6-trideoxy-L-fucosyl) est attaché au cycle A (C_7) par une liaison glycosidique (voir la figure 3) [104]. La partie sucre est hydrophile, le noyau anthraquinone est plutôt lipophile, en fonction de l'état de protonation des groupements phénoliques. En effet, la molécule possède des fonctions ionisables (deux groupements phénoliques sur le cycle B en position C11 et C6, pKa 9,5 and 10,2 respectivement, et un groupement amine sur le sucre, pKa 8,3) [103]. La protonation du groupement amine sur le sucre permet d'améliorer son hydrosolubilité par rapport à la forme moléculaire : le chlorhydrate de doxorubicine est souvent utilisé pour cette raison. La conséquence du port de charges et de la structure de la molécule est sa facilité à se lier avec les protéines et les membranes cellulaires. Une autre conséquence est qu'elle peut être utilisée à la fois dans des matériaux hydrophiles et lipophiles, et que son affinité pour de tels matériaux dépend étroitement des conditions de pH [105].

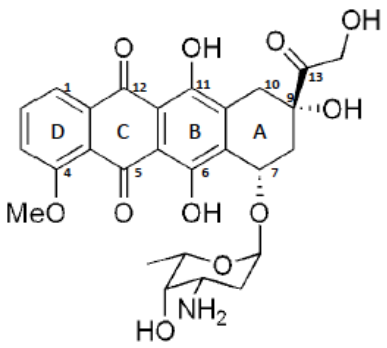

Figure 3 : structure de la doxorubicine.

La doxorubicine est un objet de recherche populaire: son noyau anthracycline est responsable des ses propriétés optiques, et de la fluorescence intrinsèque de la molécule. Cette molécule

peut donc être facilement dosée en spectrophotométrie UV-visible. La distribution de la DOX peut aussi être visualisée dans les tissus ou les cellules, grâce à l'imagerie de fluorescence [103]. Néanmoins, les interprétations doivent être faites avec précaution, car l'intensité et les spectres de fluorescence de la DOX dépendent fortement de sa concentration et de la nature de son microenvironnement. De plus, l'attachement de la DOX sur les nanovecteurs via la partie anthracycline éteint sa fluorescence et peut diminuer ses propriétés thérapeutiques. C'est donc souvent la partie sucre qui est utilisée pour les liaisons avec des nanovecteurs.

2.2. Mécanismes responsables de la toxicité et des effets secondaires

L'activité cytostatique et cytotoxique de la doxorubicine peut être expliquée par plusieurs mécanismes. Le principal est l'intercalation de la partie anthracycline, qui est plane, entre les paires de bases de l'ADN, inhibant ainsi l'activité de l'enzyme topoisomérase II, qui réalise la coupure double-brin de l'ADN, indispensable à la transcription [103]. Cela provoque la mort cellulaire en interférant avec l'étape de réplication, en arrêtant le cycle cellulaire, ou en induisant l'apoptose. Un autre mécanisme est la production de radicaux libres oxygénés (ROS ou reactive oxygen species), notamment des radicaux hydroxyles, générés par la réduction enzymatique de la DOX complexée par des ions cuivre ou fer (notamment Fe(III)). Ces radicaux libres endommagent l'ADN et provoquent l'apoptose [104].

Le principal effet secondaire de la DOX est sa toxicité cardiaque. Comme les cardiomyocytes ne se multiplient pas, la toxicité n'est pas due à l'intercalation de la molécule au sein de l'ADN, mais aux radicaux libres oxygénés : les systèmes enzymatiques antioxydants ont une activité très réduite dans ce type de cellule. De plus, cette cardiotoxicité est dose-dépendante: la dose totale cumulée lors du traitement ne doit pas excéder 450-550 mg/m^2 [64]. L'hématotoxicité de la DOX est un autre facteur limitant son utilisation [106].

Cette toxicité est aussi due à l'importance des doses utilisées. Comme c'est une petite molécule, son temps de demi-vie dans le sang est très court ($t_{1/2} \approx 2$ min) [107]. Ainsi, peu de molécules de DOX peuvent atteindre l'environnement tumoral, en raison des nombreuses barrières biologiques à franchir évoquées précédemment. De plus, les cellules cancéreuses développent des mécanismes de résistance à de multiples traitements, phénomène appelé multidrug resistance ou MDR. Ces mécanismes de résistance limitent l'accès au noyau, pour des molécules arrivées jusqu'aux compartiments cytoplasmiques. Il peut s'agir de la surexpression de pompes effluant les molécules actives hors de la cellule, par exemple la glycoprotéine P ou P-gp, ou la superfamille des transporteurs ABC (pour ATP-binding

cassettes), ou de l'activation de défenses cellulaires antiapoptotiques (par exemple la surexpression du gène Bcl-2) [5,108]. Dans ces conditions, seules de très petites quantités de DOX peuvent atteindre le noyau des cellules tumorales, environ 1 sur 10 000 à 1 sur 100 000, ce qui nécessite d'augmenter les doses pour obtenir une efficacité thérapeutique [109].

2.3. La doxorubicine, un candidat idéal pour la vectorisation

Même si d'importants efforts de recherche ont été faits dans cette direction, peu de vecteurs ont conduit à des essais cliniques, et une poignée seulement a été approuvée pour un usage clinique chez l'homme. La doxorubicine fait partie des quelques molécules vectorisées disponibles sur le marché, avec le Myocet®, une formulation à base de liposomes (Enzon Pharmaceuticals, Piscataway, New Jersey), et Doxil®/Caelyx®, qui sont des liposomes PEGylés (Centocor Ortho Biotech, Horsham, Pennsylvanie, et Shering-Plough, North Ryde, New South Wales, Australie, respectivement) [110]. Ces systèmes permettent de cibler passivement les tumeurs par effet EPR (Enhanced Permeation and Retention) [67]. La doxorubicine liposomale est efficace [6], mais elle n'est généralement utilisée qu'en traitement de seconde intention, en cas de rechute [111]. Les effets secondaires sont certes réduits, mais pas totalement supprimés, notamment à cause de la persistance d'une accumulation non spécifique [22]. En plus de la cardiotoxicité, il existe notamment des problèmes persistants d'érythrodysesthésie palmo-plantaire (syndrome main-pied).

Face à ce constat, des stratégies consistent à associer ces formulations liposomales de DOX à d'autres chimiothérapies, de façon à réduire les quantités de médicament administrées, comme dans plusieurs essais cliniques récents de phase II (association avec la gemcitabine [112], le carboplatine [113] ou l'ifosfamide [114]). D'autres pistes de recherche explorent la modification de ces liposomes avec des ligands spécifiques, de façon à augmenter la spécificité de la capture par les cellules tumorales : ligands pour le récepteur à intégrine [115], le récepteur au folate [7], des récepteurs spécifiques de certaines lignées cellulaires [8,116,117], et parmi eux des anticorps et des peptides, comme l'anticorps anti αv intégrine [118] et le peptide HVGGSSV [117]. Une autre stratégie est la transfection de petits ARN interférents (siRNA) pour outrepasser les phénomènes de résistance et faire taire l'expression des pompes à efflux [115].

Dans ce contexte, la mise au point de vecteurs autres que des liposomes pour la délivrance de la DOX est une nécessité. Les nanoparticules hybrides offrent une plateforme idéale pour construire de tels nano-objets.

3. Les nanovecteurs magnétiques pour la délivrance de la DOX

Formulation des nanovecteurs

Notre équipe de recherche développe des nanovecteurs magnétiques pour la délivrance de la doxorubicine. Le cœur inorganique de ces nanovecteurs est constitué de nanoparticules d'oxydes de fer superparamagnétiques, appelées aussi SPIONs (superparamagnetic iron oxide nanoparticles) [2]. Ces nanoparticules inorganiques offrent de nombreux avantages comme plateformes pour bâtir des nanovecteurs :

- D'abord, les oxydes de fer offrent une toxicité inférieure à celle des autres métaux et oxydes métalliques [119], et le métabolisme du fer dans l'organisme est capable de gérer un apport externe relativement important [93].
- Ces nanoparticules sont superparamagnétiques, c'est-à-dire qu'elles offrent une magnétisation importante dans le champ, tout en ne possédant pas de rémanence magnétique après leur exposition à un champ magnétique [51,120]. Elles sont donc indiquées pour réaliser un ciblage magnétique, tout en limitant les risques de thromboses dues à une agrégation magnétique hors champ magnétique.
- Des SPIONs sont déjà disponibles sur le marché depuis une quinzaine d'années, comme agents de contraste pour l'imagerie par résonance magnétique (IRM) des organes du système endothélial, comme le foie et la rate [51,93–95,121,122]. Leur moment magnétique important distord les caractéristiques magnétiques locales des tissus, générant ainsi un contraste négatif. Ces systèmes offrent donc un certain recul quant à leur utilisation parentérale. De plus, des nanovecteurs à base de SPIONs permettant à la fois la délivrance d'une molécule active et des applications en imagerie pour le diagnostic et/ou le suivi de la délivrance, sont impatiemment attendus comme la nouvelle génération de nanovecteurs, appelés « théragnostiques ». C'est un avantage que ne possèdent pas les nanoparticules exclusivement polymériques.

Ces SPIONs sont fonctionnalisés à l'aide de polyéthylène glycol (PEG), un polymère hydrophile biocompatible [123]. Ce revêtement de surface permet d'assurer leur stabilité colloïdale en suspension par encombrement stérique. De plus, l'absence de charges de surface permet de limiter l'opsonisation et la capture par les cellules phagocytaires, rendant ces nanovecteurs « furtifs » dans l'organisme [124]. Leur temps de demi-vie dans l'organisme est également augmenté, et leur biodistribution modifiée en comparaison de vecteurs non PEGylés.

La doxorubicine peut être chargée sur les SPIONs PEGylés sous forme d'un complexe avec un ion Fe^{2+}. La doxorubicine, qui ne se fixe pas spontanément à la surface des SPIONs, est connue pour former facilement des complexes stables avec le fer. L'ion fer sert alors d'intermédiaire pour la fixation de la DOX à la surface des SPIONs, par adsorption. Cette stratégie permet de fixer la DOX sur les nanovecteurs, contrairement à une simple adsorption dans le revêtement polymérique. De plus, comme le complexe se dissocie à pH inférieur à 6, la libération de la DOX se réalise sous forme non complexée, et est facilitée par rapport à une liaison covalente [125]. La pH-dépendance est un atout, car l'environnement tumoral est connu pour être plus acide que les tissus sains [94,126]. Après l'internalisation des nanovecteurs par les cellules, ceux-ci sont dirigés vers certains compartiments intracellulaires, comme les lysosomes, qui présentent un pH très acide (pH 5,0) [78]. La libération de la DOX peut donc être facilitée et accélérée au niveau des cellules tumorales ciblées. Notre choix s'est porté sur des ions Fe^{2+} plutôt que Fe^{3+}, car la formation du complexe DOX-Fe^{3+} *in vivo* est fortement suspectée d'entraîner la formation de radicaux libres, et donc d'induire une part substantielle de la cardiotoxicité de la DOX [127–129].

Les travaux de thèse

Le but de ces travaux de thèse a été d'optimiser le protocole de chargement du complexe DOX-Fe^{2+} sur des SPIONs PEGylés, puis de caractériser les nanovecteurs chargés de DOX, et de les évaluer *in vitro* puis *in vivo.*

- Les premières caractérisations physico-chimiques ont permis de s'assurer que ces nanovecteurs possèdent les propriétés requises pour un usage ultérieur *in vivo.* Leur taille et leur charge de surface est compatible avec une administration systémique, la quantité d'agent anticancéreux chargée est compatible avec une dose thérapeutique, et la cinétique de libération de la DOX est compatible avec un ciblage magnétique des tumeurs.
- Pour s'assurer de l'efficacité d'un futur traitement, la cytotoxicité *in vitro* de ces nanovecteurs de DOX a été comparée à celle de la DOX en solution. Leur furtivité vis à vis du système immunitaire a aussi été vérifiée *in vitro*.
- Du point de vue des mécanismes responsables de la cytotoxicité des nanovecteurs de DOX, leurs voies d'entrée dans les cellules ont été révélées en microscopie électronique en transmission (MET), leur devenir intracellulaire et la libération de la DOX étant suivis par imagerie confocale multispectrale de fluorescence (ICMS). La question de la forme sous laquelle la DOX est libérée à partir des nanovecteurs (forme

libre ou complexée avec le fer) a été explorée, notamment grâce à la technique du SERS (surface enhanced Raman scattering).

- Enfin, les évaluations *in vivo* ont été entamées, avec une étude de biodistribution des nanovecteurs sans DOX sur souris saines, puis la mise en place d'un protocole thérapeutique avec les nanovecteurs chagés de DOX sur un modèle de souris nude tumorisées, comportant l'évaluation du ciblage magnétique et de l'hémotoxicité. Les études en imagerie sur souris saines et tumorisées sont en cours de réalisation, pour évaluer le potentiel de ces nanovecteurs comme outils diagnostiques.

Cette thèse est divisée en trois parties :

- La première partie est une étude bibliographique de l'état de l'art. Le premier chapitre traite de la formulation de nanovecteurs hybrides (à base d'oxydes de fer ou d'or fonctionnalisés) pour la délivrance de molécules anticancéreuses. Le deuxième chapitre s'attache aux différentes stratégies de chargement et de libération de la doxorubicine sur ces mêmes vecteurs hybrides, et à leur évaluation *in vitro* et *in vivo*.
- La deuxième partie est consacrée aux nanovecteurs magnétiques pour la délivrance de la doxorubicine développés dans le cadre de cette thèse.

⇒ Le premier chapitre traite du développement et des caractérisations physico-chimiques des SPIONs PEGylés chargés de DOX, ainsi que de l'évaluation *in vitro* de leur cytotoxicité.

⇒ Le deuxième chapitre de cette deuxième partie est plus particulièrement consacré à l'étude du complexe DOX-Fe^{2+} par spectroscopie de diffusion Raman exaltée de surface (SERS), et de la forme sous laquelle la DOX est libérée à partir de SPIONs citratés ou PEGylés.

⇒ Enfin, le troisième chapitre aborde l'évaluation *in vivo* de ces nanovecteurs sur un modèle animal de souris tumorisées.

- La troisième partie est une discussion générale, abordant les problématiques liées à l'évaluation *in vitro* et *in vivo* de ces nanovecteurs, ainsi que les problématiques liées à la construction d'un nanovecteur théragnostique.

Première partie
Les nanovecteurs hybrides pour la délivrance d'agents anticancéreux

Chapitre 1 : Formulation de nanovecteurs à base de nanoparticules d'oxydes de fer et d'or pour la délivrance d'agents anticancéreux

Publication 1 : Design of hybrid metallic nanocarriers for drug delivery and imaging

Soumise dans Nanotechnology, 2013

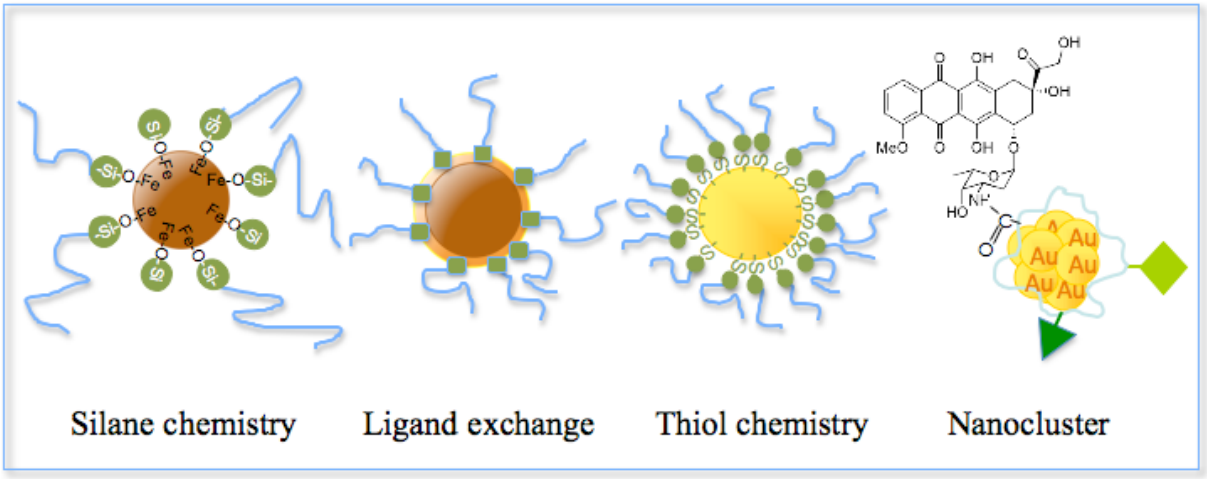

Cette revue traite de la formulation de nanovecteurs hydrides à base de nanoparticules d'oxydes de fer et d'or pour la délivrance de molécules anticancéreuses. Les nanoparticules d'oxydes de fer et d'or constituent des plateformes intéressantes : la possibilité de les utiliser en imagerie constitue un avantage par rapport aux nanoparticules exclusivement organiques. Par contre, leur surface doit être fonctionnalisée pour une utilisation *in vivo*. La méthode la plus courante consiste à modifier la surface de ces nanoparticules après synthèse, le plus souvent avec des matériaux organiques biocompatibles. Ces matériaux apportent au nanovecteur (i) un état de surface compatible avec une administration systémique, mais aussi (ii) des sites de fonctionnalisation potentielle avec des ligands de ciblage, et (iii) un environnement propice au chargement de molécules anticancéreuses et/ou de molécules pour l'imagerie.

La variété des nanosystèmes hybrides existants étant très grande, cette revue s'est focalisée sur les systèmes permettant la délivrance de la doxorubicine. En effet, cette molécule peut être mise en œuvre à la fois dans des matériaux hydrophiles ou hydrophobes, ce qui permet de présenter des nanosystèmes très variés, adaptés pour la délivrance de molécules hydrophiles et/ou lipophiles.

Les nanoparticules à base d'oxydes de fer ou d'or peuvent être mises en œuvre selon deux stratégies. La première consiste à formuler des systèmes cœur-enveloppe, où la nanoparticule est recouverte individuellement d'une couche de matériau. Beaucoup de nanosystèmes mettent en œuvre du PEG, mais d'autres types de revêtements, à base de chitosan, de copolymères ou de protéines sont également proposés. La deuxième stratégie consiste à inclure les nanoparticules d'oxydes de fer ou d'or dans une matrice lipidique ou polymérique.

La littérature fait apparaître plusieurs nouvelles tendances quant à la formulation de nanovecteurs hybrides. Le cœur inorganique peut être remplacé par des nanoclusters, de taille plus restreinte que les nanoparticules. Des revêtements alternatifs sont proposés, comme les polymères zwitterioniques ou les lipoprotéines haute densité, et la chimie « click » se développe.

Cette revue démontre la grande variété des formulations existantes, correspondant toutes à des stratégies différentes pour la délivrance de molécules anticancéreuses.

Nanotechnology XX (2013) XXXXXX (Xpp) doi:10.1039/b000000x

Design of hybrid metallic nanocarriers for drug delivery and imaging

J Gautier[1], E Allard-Vannier[1], K Hervé-Aubert[1], M Soucé[1] and I Chourpa[1]

[1] EA 6295 « Nanomédicaments et Nanosondes », Université François-Rabelais, Tours, F-37200 France.

E-mail : emilie.allard@univ-tours.fr

Received XXX, XXX
Published XXX, XXX
Online at XXX, XXX

Abstract
Metallic nanoparticles (MNPs) like iron oxide and gold nanoparticles are interesting platforms to build nanocarriers not only for drug delivery, but also for nano-based imaging. These cargos are so called “theragnostic nanocarriers” as they combine diagnostic and therapeutic capabilities. Their surface must be functionalized to be suitable for *in vivo* applications. Surface functionalization also provides binding sites for targeting ligands, and also for drug loading. This review focuses on materials and surface chemistry used to build hybrid nanocarriers that are inorganic cores functionalized with organic materials. The surface state of MNPs largely depends on their synthesis routes, and defines the strategies used for functionalization. Two main designs can be found in the literature: core-shell nanosystems, or organic materials embedding nanoparticles. Emerging tendencies like the use of clusters or alternative coating materials are also evoked. To present both hydrophilic and lipophilic nanosystems, we chose the doxorubicin anticancer agent as an example, because the molecule presents affinity for both types of materials.

1. Introduction

Metallic nanoparticles (MNPs) are interesting cargos used as drug delivery systems for numerous reasons [1]. The inorganic core confers to them attractive properties: material and size-dependent physico-chemical properties, easy surface functionalization, stability and biocompatibility. MNPs often present interesting nanosizes below 100 nm allowing their intravenous administration and their uptake by the target cells [2]. Surface charge can be easily modified to obtain neutral nanocarriers considered as “stealth” nanocargos, i.e., almost undetectable by the immune system [3]. Moreover, compared to lipidic/polymeric drug delivery systems, additional functionalities become possible with MNPs. They can be used as “theragnostic agents”, which facilitates simultaneous drug delivery and imaging, representing an important breakthrough in nanomedicine. They can be also used for hyperthermia (also called thermal therapy or thermotherapy), which consists in a type of cancer treatment in which body tissue is exposed to high temperatures. Research has shown that high temperatures can damage and kill cancer cells, usually with minimal injury to normal tissues [4].

Magnetic nanoparticles based on iron oxides such as magnetite (Fe_3O_4) or its oxidized form maghemite (γ-Fe_2O_3), known as superparamagnetic iron oxide nanoparticles (SPIONs) or ultrasmall superparamagnetic iron oxide nanoparticles (USPIOs), are widely described as safe materials for biomedical applications [2]. Magnetic ferrofluids are stable colloidal suspensions of MNPs dispersed in organic or inorganic liquid phases. The core crystal size is generally equal to or below 10 nm. This size confers them « superparamagnetic properties ». Superparamagnetic behaviour means that the NPs are highly magnetized in a magnetic field but loose their magnetization when the field is switched off. This behaviour is important for injectable formulations, because it reduces the risk of thrombosis from magnetically aggregated NPs. Furthermore their magnetic properties allow the realization of magnetic drug targeting (MDT), magnetic resonance imaging (MRI) contrast, and thermal therapy.

The second MNPs treated in this review are gold nanoparticles (Au-NPs). Their optical properties make them useful for molecular cancer imaging [5], and for analytical methods like Surface Enhanced Raman Scattering (SERS) spectroscopy [6–9]. Indeed, Au-NPs present interesting optical properties such as light absorption and light scattering, and exhibit a plasmon resonance [10]. Light induces collective oscillations of conductive metal electrons at the NP surface, inducing a surface electromagnetic field. This light-induced plasmon resonance is tuneable to different wavelengths by varying the Au-NP size, and the plasmonic field is able to enhance Raman scattering and fluorescence emission of adjacent molecules. Au-NPs have been widely exploited for imaging, but are now used as theragnostic systems, and for hyperthermia.

To illustrate our discussion on the design of theragnostic nanosystems based on SPIONs and Au-NPs for the delivery of anticancer molecules, we restricted our search to the doxorubicin (DOX) anticancer drug, because it is the drug model used in numerous published studies on nanocarriers. Furthermore, the protonated form presents an increased aqueous solubility compared to the molecular form. So DOX can be loaded into hydrophilic or lipophilic materials, which is adequate to overview numerous design strategies, DOX exemplifying for both hydrophilic and lipophilic anticancer drugs.

This review focuses on the design of metallic nanoparticles (MNPs) for theragnostic applications. Synthesis methods of SPIONs and Au-NPs, and their surface functionalization are crucial because it governs their physicochemical properties, their colloidal stability, and their biological fate. While the chemical composition of a nanoparticle is important, even more important are the size and shape of the nanoparticle and its surface/colloidal properties. As the hybrid nano-objects built with MNPs are complex in composition and structure, we particularly focused on the materials used and the chemistry involved in functionalization. Organic molecules can be grafted on inorganic cores, for the design of hybrid core-shell nanosystems. The inorganic core can also be embedded in organic materials, for the design of composite nanosystems. The nature and properties of materials used are discussed, as well as the chemistry involved, and the main consequences for *in vivo* applications. We also highlighted the emerging tendencies for the design of such nanosystems.

2. Conception and stabilization of metallic cores

2.1. Colloid synthesis routes

The size and surface properties of SPIONs and Au-NPs play an important role in their colloidal stability in suspension, their magnetic and optical properties, their fate in the organism and pharmacokinetics. Their ability to be modified depends widely on synthesis routes, and plays an important role on the loading and delivery of small molecules like the DOX. Production routes have been reviewed elsewhere in detail [10–17]. The main ones, summarized in figure 1, are briefly discussed here, because they remain the most used to date.

2.1.1. SPIONs synthesis. The most common method of SPION synthesis is chemical: coprecipitation was first reported by Massart *et al.* [18] (figure 1A). This approach presents numerous advantages: low cost precursors and materials, ease of scale up, simple chemistry in aqueous medium (which is necessary for ulterior biological applications). This method leads to spherical magnetite nanocrystallites of relatively uniform sizes, generally below 20 nm. Many synthesis methods inspired from Massart *et al.* [18] add a passivation step by addition of ferric nitrate. The maghemite passivation shell [19] prevents further anarchic oxidation. Surface stabilization and modification are facilitated.

Precipitation within reverse micro emulsions has also been successfully applied [20] (figure 1B). Controlling water droplet size in the oily phase permits to monitor the size of NPs. Surfactants used for micellisation of the aqueous phase can also be used for dispersion of iron oxide NPs, since they present an hydrophobic surface. But the addition of such components can hinder subsequent reactions with the surface and complicate the NP modification. One may also consider that NPs obtained by micro emulsion methods present a larger size than those obtained by aqueous precipitation, but with a narrower size distribution. In spite of this advantage, micro emulsions generally have low yields of production.

Finally, thermal decomposition of organometallic compounds has recently gained considerable attention [21,22] (figure 1C). The choice of solvent and surfactant as well as the addition rate of iron pentacarbonyl, offers good control over the final particle size, shape, and crystal structure compared to other methods: particles are smaller and more monodisperse [23]. However, the reaction occurs in organic solvents containing hydrophobic stabilizers (like benzylamine [24], oleic acid and octyl ether [25], pentanedione and dioctyl ether [26]), which requires additional surface modification in order to obtain nanoparticles that are stable in aqueous medium and non toxic for biomedical applications.

2.1.2. Au-NPs synthesis. The chemical reduction method (figure 2A) is the most common technique used to prepare Au-NPs, because it is simple and yields controllable sizes and shapes of Au-NPs [27]. This method leads to spherical Au-NPs in the 10-20 nm diameter range [16]. The ratio citrate/$HAuCl_4$ permits to control the Au-NP size [7]: a high concentration of citrate rapidly produces small Au-NPs, while a low ratio leads to incomplete stabilization and aggregation, resulting in larger NPs. If growth is isotropic on the surface of gold nuclei, this leads to an increase of the particle size, and eventually a spherical shape. But an anisotropic growth of particles will induce the formation of particular shaped Au-NPs. For example, the introduction of a surfactant delays the crystal growth on certain faces; the use of cetyltrimethylammonium bromide (CTAB) leads to the production of nanorods, while polyvinylpyrrolidone (PVP) can lead to triangular-plate or star Au-NPs (figure 2). The shape of gold nano-objects is one of the parameters affecting the frequency of their surface plasmon resonance, thus modifying their optical properties [7]. To finely control the size of Au-NPs and obtain a narrower size distribution, one can use seed-mediated growth [28]. The new metal atoms generated by reduction reactions are deposited on the surface of the seed particles without further nucleation.

Gold hollow nanospheres can be produced by a sacrificial

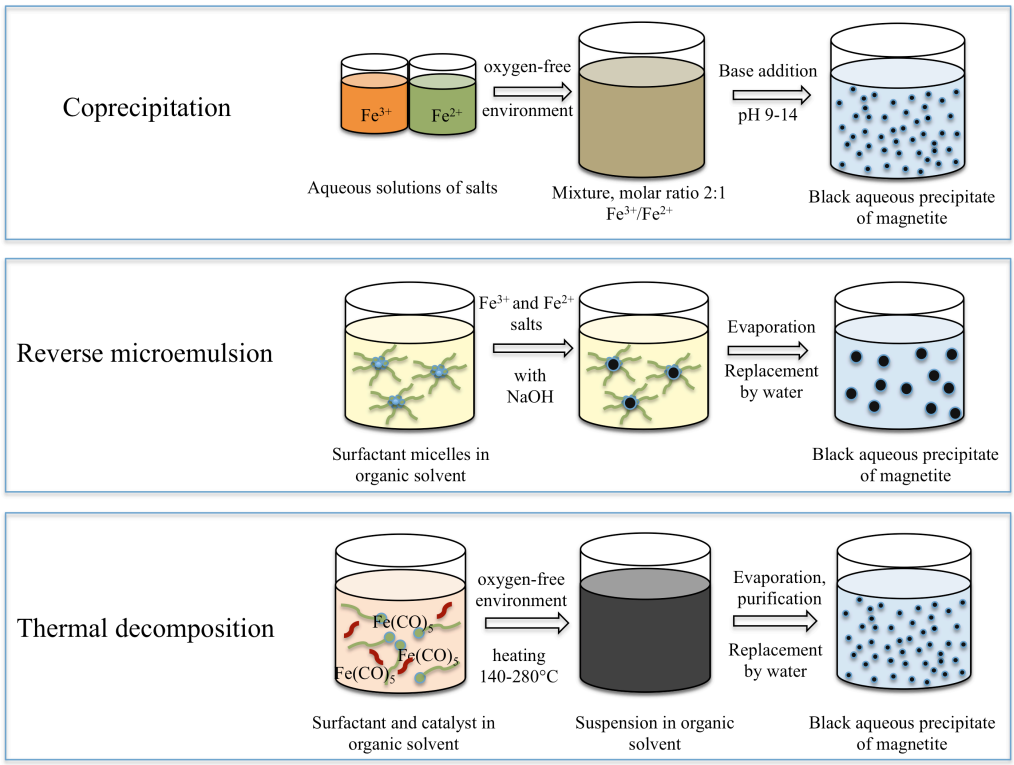

Figure 1. Main synthesis routes for SPIONs.

reduction method [29]. The resulting NPs are a shell, with roughly the same diameter as the initial NPs. This technique is used with silver or cobalt NPs, using the redox potential between metallic silver or cobalt and gold salt in solution [30]. When the Au^{3+} ions come in contact with the silver or cobalt atoms, there is an electroless plating that reduces the Au^{3+} ions to gold atoms and oxidizes the silver or the cobalt to ionic form (figure 2B).

Even if production routes permit to precisely control quality and properties of Au-NPs and to obtain considerable quantities, the cost of production can limit their clinical application.

2.2. Stabilization of MNP colloids

In aqueous medium, iron atoms on the SPION surface can act as Lewis acids, and coordinate with water molecules to accept lone-pair electrons: thus the SPION surface presents hydroxyl groups, due to water dissociation [31]. Consequently, their surface charge changes with pH (isoelectric point approximately 6.8). This surface state has a main consequence as SPIONs experience colloidal instability around this pH: in contrast to the colloids of charged NPs stabilised by electrostatic repulsion, the colloids of neutral NPs tend to precipitate. NPs have a great surface-to-volume ratio, so hydrophobic interactions and Van der Waals forces can lead to aggregation of SPIONs, minimizing total surface and interfacial energy. The progressive growth of clusters, beyond a critical size, can lead to precipitation because of gravitation [11]. As aggregation could be dangerous when injected intravenously, such surface properties are not compatible with a biological use, even though magnetic susceptibility increases with cluster size. The same aggregation phenomena can occur with Au-NPs.

As a consequence, to become suitable for theragnostic applications, the surface of SPIONs and Au-NPs has to be necessarily modified. In order to avoid aggregation, strategies for the stabilization of the NPs surface use mainly organic molecules. Post-synthesis addition of coating materials is the most common way for inorganic NP cores, introducing electrostatic or steric hindrance [32].

2.2.1. Stabilization via electrostatic repulsion. Electrostatic stabilization consists in the adsorption of charged groups (citrates…) to the surface, generating repulsion between NPs of equal electric charge [6,33]. Unfortunately, surface charge mainly depends on pH, and electrostatically stabilized nanoparticles are prone to aggregation in biological media due to neutralization of the surface charge by ionic species present *in situ*. Moreover, charged NPs tend to adsorb proteins in biological media through electrostatic interaction. The adsorption of proteins on the NP surface tends to increase the particle size, which can lead to particle precipitation [21] and to a rapid uptake by phagocytes [34].

An example is the citrate reduction method for the production of Au-NPs. This method produces Au-NPs with negative surface charge, as a consequence of a weakly bound citrate coating. These ionically stabilised NPs can easily loose or gain protons, and then are highly sensitive to pH, as it affects the surface charge (ζ potential). Anionic ligands like citrates are only suitable for stabilisation in basic to mildly acidic conditions, at a pH greater than the pKa values [7]. This implies that they are not suitable for biological applications, because ionic interactions with charged species in biological media can affect the stability of the citrate shell. Mirza *et al.* developed citrate modified Au-

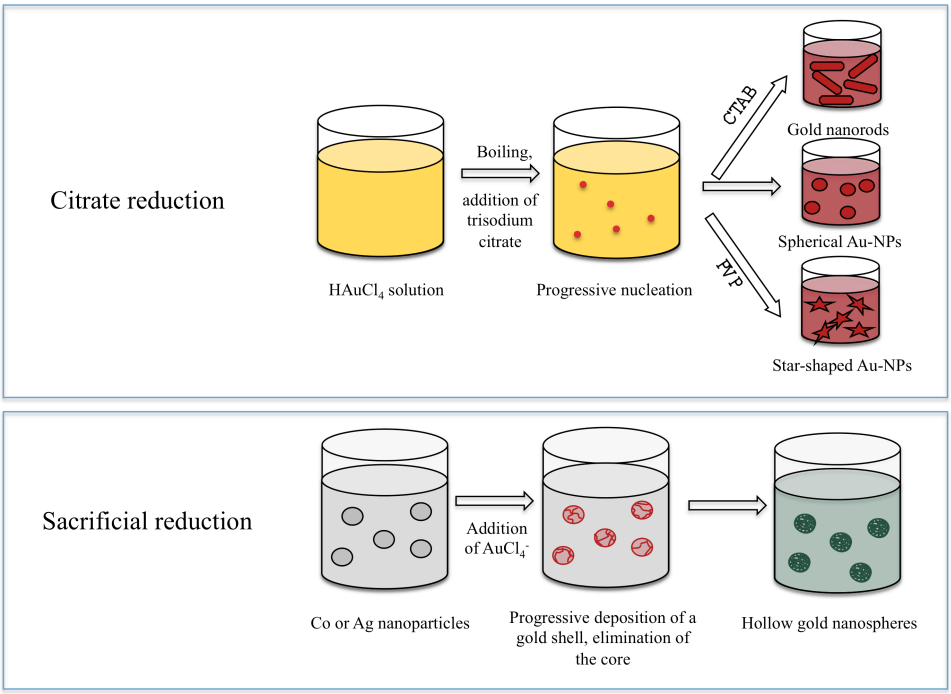

Figure 2. Main synthesis routes for Au-NPs.

NPs and found that these nanostructures formed aggregates in acidic buffers (pH 1 and 2.4) and in PBS (pH 7.4, probably due to an insufficient citrate coverage) [6].

2.2.2. Stabilization via steric hindrance. Steric hindrance of the SPION surface is widely used, because of enhanced stability of the nanotheragnostic systems. Besides stabilizing NPs in biological media, surface modification can also provide functional groups for further derivatization, and avoid or delay uptake by the reticuloendothelial system (RES). This also permits a variety of strategies for attachment of DOX or other anticancer molecules to the NP: organic molecules can play the role of reactive sites or serve as a trap for DOX loading, and help to modulate the drug release.

The FDA-approved biocompatible neutral polymer PEG (polyethylene glycol) is the material most currently used, due to its enhanced hydrophilicity and flexibility [35]. It prevents aggregation of NPs and increases colloidal stability in a pH-independent manner [34,36–40]. In addition, the coating of NPs with biocompatible PEG is also used because it offers stealthiness to nanocarriers. The presence of PEG reduces opsonisation because of its hydrophilicity, non-immunogenicity and absence of electric charge, preventing interactions with plasma proteins [34]. The polymer molecular weight, its density and its conformation on the particle surface modulate the level of stealthiness [41]. As a consequence, it increases the NP blood half-life *in vivo*.

In this context, Allard-Vannier *et al*. studied the stealthiness of PEGylated SPIONs (PEG 5000), in which DOX was loaded through the polymer layer [34]. The *in vitro* stealthiness was evaluated by measuring the ability for NPs to activate the complement system (CH_{50} test) and the uptake of NPs by monocytes and macrophage like cells. The results confirmed that stealthiness was not altered by the presence of the drug that is buried inside the polymer layer.

This is possibly the reason why PEG are used in the formulation of most present DOX-loaded nanocarriers [21,29,42–44]. Nevertheless, other types of polymers or coating materials are developed, with various stealth properties. They are discussed in the following part.

3. Design of hybrid core-shell systems

Hybrid core-shell nanosystems are composed of an inorganic core (in our case SPION or Au-NP), covered by a layer of organic molecules. The shell is of primary interest for drug delivery strategies. Most nanosystems described in this part are schematized in figure 3. The addition of functionalization materials is often made post-synthesis, because the reactive groups at the SPION and Au-NP surface allow a varied chemistry.

In case of SPIONs produced by co-precipitation, the hydroxyl groups on the surface are very reactive to silane functions, and permit to functionalize the surface with various groups, carried by silanes molecules [42]. In case of SPIONs produced by thermal decomposition, the hydrophobic stabilizers on the SPION surface can be replaced in a ligand exchange reaction by another molecule, to stabilize the system [21,45].

Due to the strong interaction between Au and thiol, the surface modification of Au-NPs is mainly done by the addition of thiolated species [46]. Thiols are good soft Lewis bases which make them complementary to the soft acid properties of Au-NPs: they offer a strong conjugation via Au-S covalent bonding [46]. This type of linkage is convenient and sufficient to prepare stable Au-NP conjugates, but it can be an issue when exposed to a reducing environment, such as glutathione that may be present at high concentrations in a living subject [5].

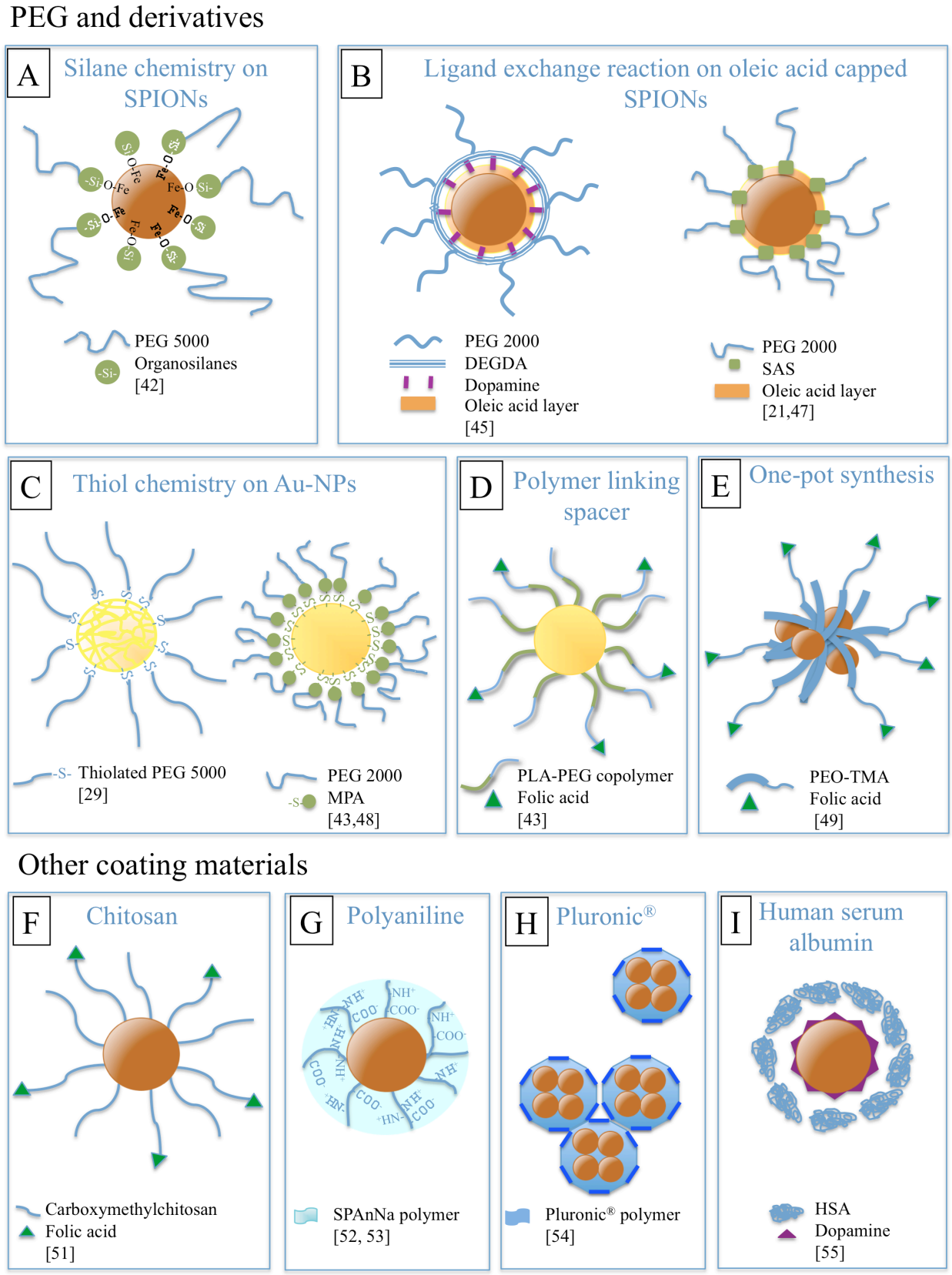

Figure 3. Main synthesis routes for Au-NPs Hybrid core-shell nanosystems based on SPIONs ( ) or Au-NPs ( ). A-E: grafting strategies for PEG and derivatives on MNPs; F-I: other materials used to coat SPIONs.
DEGDA di(ethylene glycol) diacrylate; HSA human serum albumin; MPA 3-mercaptopropionic acid; PEG polyethylene glycol; PEO polyethylene oxide; PLA poly (L-aspartate); SAS triethoxysilylpropylsuccinic anhydride; SPAnNa poly[aniline-co-sodium N-(1-one-butyric acid) aniline]; TMA trimellitic anhydride chloride.

3.1. PEG and derivatives

Even if PEG coating is considered as a classical process, the chemistry used to bind this polymer on NPs is quite varied, and some studies report the use of PEG copolymers, or PEG in association with other coating agents.

3.1.1. Silane chemistry and ligand exchange reactions on SPIONs. Hervé *et al.* added chains of PEG 5000 by a post-synthesis method, using silane chemistry with the hydroxyl groups present at the SPION surface (figure 3A). SPIONs were silanized by contacting iron oxide cores with APTES (3-aminopropyltriethoxysilane). Firstly, ethoxy silane groups react with hydroxyl groups of the surface, and in a second step, amino groups form an amide bond with the activated ester group of PEG [42]. If the polymer density is sufficient, the covalent bond guarantees the stability of the linkage, and the protection of NPs against opsonisation and aggregation.

Fang *et al*. coated SPIONs with a derivative of PEG named PBAE (poly(beta-amino ester)) [45]. This is a copolymer of DEGDA (di(ethylene glycol) diacrylate) and PEG-NH_2 that is linked to dopamine and DOX thanks to a reaction between bifunctional amines and diacrylate monomers (Michael reaction) (figure 3B). This preformed DOX-loaded polymer was bound to oleic acid capped SPIONs via a ligand exchange reaction, i.e., the oleic acid molecules on the surface of SPIONs were replaced by the dopamine units of the PBAE molecules. The copolymer offers the same steric protection as classical PEG, but at the same time DOX and targeting ligands are integrated into the same polymer. The polymer backbone is pH-sensitive: acidic pH promotes the degradation of the ester linkages, so the release of the active molecule.

Kievit *et al.* used the same process, with oleic acid capped SPIONs, but first made a ligand exchange reaction with triethoxysilylpropylsuccinic anhydride (SAS) [21,47]. This offered a binding site for amine functionalized PEG (figure 3B). The PEG coating was highly stable, because of the strong affinity of SAS to oxide surfaces, and the formation of silanol-silanol bridges or siloxane bonds between PEG chains. Both nanocarriers coated by ligand exchange reaction had a d_H below 100 nm (80.5 [45] and 91 nm [47]).

3.1.2. Thiol chemistry on Au-NPs. You *et al*. observed that the average size of gold nanospheres was about 38.5 ± 1.7 nm before coating, and the addition of long chains of PEG-SH (MW 5000) did not increase dramatically their hydrodynamic diameter (d_H 48.6 ± 1.3 nm), thanks to a limited quantity of PEG in the reactive medium [29]. They chose a classical and convenient chemistry: thiolated PEGs (PEG-SH) that interact with Au on the nanocarrier surface, inducing strong Au-S covalent bonds (figure 3C).

Instead of direct PEG bonding on the NP surface via thiol linkage, Gu *et al*. immobilized PEG chains (MW 2000) on their Au-NPs using an intermediary reaction [43,48]. They first added 3-mercaptopropionic acid (MPA) to their Au-NPs (figure 3C). The thiol group interacted with the Au surface, and then the carboxyl group permitted an amidation with the amine groups of NH_2-PEG-NH_2. This two-step reaction avoids the thiolation of the PEG before the addition on Au-NPs, and offers more versatility, since polymers with terminal amine groups are more numerous and cheaper than the thiolated ones.

3.1.3. Polymer linking spacer. Prabaharan *et al*. also bound PEG via a two-step procedure, but not directly on the Au-NPs [44]. Their Au-NP core, first reacted with aminoethanethiol to furnish amine groups, was functionalized with a hydrophobic poly (L-aspartate) (PLA) inner shell (figure 3D). PEG was then attached to this hydrophobic polymer (amidation between PEG-COOH and terminal amine groups), forming an outer shell. The Au-NP core was thus covered with a shell of an amphiphilic copolymer monolayer. This model presents the advantage of offering both hydrophobic and hydrophilic environments for drug loading. Even though this copolymer is quite bulky (MW 5910), the resulting nanoparticles were small (average hydrodynamic diameter 34 nm) and monodisperse (polydispersity index 0.029). This regularity in size induces homogeneous optical properties and uniform behaviour in the organism, which is the goal for any nanoformulation.

3.1.4. One-pot synthesis. Maeng *et al*. manufactured aggregates of SPIONs and PEO-TMA-FA polymer (poly(ethylene oxide)-(trimellitic anhydride chloride)-folate) [49]. This original nanocarrier presented an average hydrodynamic diameter of 84.7 nm, and a narrow and unimodal distribution. This process was original as it was a one-pot synthesis process. They directly added polymer with DOX and iron oxide in DMSO: the self-assembly of the polymer entrapped DOX and SPIONs (figure 3E). The *in situ* formation of nanoaggregates permitted to control their size and shape by changing the polymer-to-iron ratios. Although the PEO is well known to be biocompatible, hydrophilic and non-ionic [50], the association with TMA raises the matter of toxicity/tolerance of such composite polymers.

3.2. Other coating materials

3.2.1. Chitosan derivatives. Sahu *et al.* coated SPIONs with a derivative of chitosan (figure 3F) [51]. Carboxymethylchitosan (CMC) is an amphoteric polyelectrolyte that demonstrated ion sensitivity in aqueous solutions at different pH due to abundant carboxyl (–COOH) and amine (–NH_2) groups. Here, the carboxylate (–COO^-) anions present on CMC attach to the surface of NPs. The primary amine groups on the NP surface are further reacted with acrylic acid (vinyl monomers) in order to increase the number of carboxylic groups. This strategy of adsorption involves the construction of a polyelectrolyte multi-layer at the NP surface. The use of a natural biodegradable and biocompatible polymer derivative is interesting since it does not increase the intrinsic toxicity of the nanosystems, and confers bioadhesion properties (namely a prolonged interaction with biological tissue, and direct interaction with the cell membrane) [31]. But this polysaccharide is produced from chitin, naturally extracted from shellfish or fungi: this leads to seasonal production, and of variable quality, which can hamper process reproducibility.

In addition, Sahu *et al*. modulated the thickness of the CMC layer, and verified that the saturation magnetization, which is necessary for magnetic targeting and which often decreases by coating processes, was not compromised [51]. After coating, the

hydrodynamic diameter d_H did not exceed 100 nm, which is the optimal size in terms of long *in vivo* circulation times [31]. But amine groups persist on the surface of nanocarriers, and pH variations can provoke size and zeta potential changes, and thus can lead to colloidal instability.

3.2.2. Polyaniline derivatives. Hua *et al.* modified a polymer of polyaniline (Pan) with succinic anhydride in order to coat SPIONs [52,53]. Whereas polyaniline is biocompatible but not very hydrophilic, the formed self-doped polymer named SPAnNa (poly[aniline-co-sodium N-(1-one-butyric acid) aniline]) is water-soluble, thus increasing its usefulness for biomedical applications. Furthermore, this polymer, in the presence of acid, can form a shell around SPIONs without any cross-linking agent, representing thus a simplified coating process. The carboxylic functions of grafted chain COO^- react with the secondary amines NH^+ in the SpanH backbone, inducing a self-assembly (figure 3G).

3.2.3. Copolymers. Copolymers are also widely represented in the literature. Park *et al.* chose Pluronic®, a tri-block co-polymer based on PEO and PPO (poly-ethylene oxide-co-propylene oxide-co-ethylene oxide), to coat magnetite nanoparticles (3H) [54]. Terminal hydroxyl groups of Pluronic® were transformed in thiol groups, to react directly with ferric oxide groups on the surface of SPIONs. They studied the critical densities of polymeric coating on nanoparticle surfaces. The thickness of the layer influenced the size and shape of nanoparticles, as well as their ability to load and release DOX. Pluronic®, which is a thermo-responsive polymer, ensures the stability of the system, but it undergoes structural transition between relaxed and collapsed states as temperature changes across its lower critical solution temperature (LCST). Changes in process temperature (37°C instead of 4°C) dramatically increased the diameter of aggregates (about 300 nm to 1000 nm), reducing their interest as biomimetic nanovectors. On the other hand, increased DOX loading on the NPs was obtained. This could be due to the PPO blocks that become more hydrophobic at 37°C, thus favouring aggregation and modifying hydrophobic interactions with DOX. If in this paper, Pluronic® did not permit to build nanocarriers suitable for *in vivo* applications, because of the possible aggregation, thermo-responsive polymers like Pluronic® are an interesting way to modulate the loading and release of drugs on nanovectors *in vivo*.

3.2.4. Proteins. Quan *et al.* bonded Human Serum Albumin (HSA) to SPIONs covered by oleate [55]. HSA has long been used for biomedical applications (for example in hypovolemia, haemorrhage treatment, or as implantable biomaterials). It has proven to extend the drug circulation half-life and to improve the tumour homing rate, namely in the case of FDA-approved Abraxane® (HSA-bound paclitaxel) [56–58].

To disperse oleate SPIONs in water, the surface was modified via a two-step procedure. First, the contact of SPIONs with an excess of dopamine allowed the formation of chelates with the iron atoms present at the SPION surface (figure 3I). Then, HSA easily adsorbed on the amine-rich surface of the SPIONs, generating NPs with a 50 nm d_H. They remarked that their nanocarriers were smaller than DOX-HSA complex particles found in the literature (150 to 500 nm, [59]). A similar process was used by Xie *et al.*, to design multifunctional imaging tools [56]. They also noticed a small d_H for their labelled SPIONs (29.4 nm). The compact coating layer and the limited size should be advantageous to obtain extravasation and high retention rates in the tumour sites. This effect could be enhanced because of the HSA affinity for the cell surface, and a limited activation of the immune system by the HSA-coated SPIONs.

4. Composite nanocarriers with embedded metallic cores

A second option consists in the "encapsulation" of SPIONs or Au-NPs in a bigger structure, generally composed of lipids and/or polymers. Examples in the literature mainly concern SPIONs, because of their magnetic properties (magnetic targeting of anticancer drugs [60], for MRI imaging and cancer treatment by hyperthermia [61]). Most nanosystems described in this part are schematized in figure 4.

4.1. MNPs embedded in lipids

4.1.1. Magnetoliposomes. Bothun *et al*. reported the original design of folate-targeted magnetoliposomes loaded with DOX [61]. They made an interesting suite of strategic choices for the design of the nanocarrier. They co-encapsulated maghemite SPIONs and DOX in a bilayer composed of cholesterol, DOPC (a derivative of phosphocholine) and DTAP (dipalmitoyl-trimethylammonium-propane), in order to provide drug delivery in a temperature-dependent manner (figure 4A). To achieve drug release from liposomes at low NP concentrations and low magnetic fields, contrary to a related work [62,63], the heating should be localized near the bilayer surface. An electrostatic attraction between a limited quantity of anionic NPs and cationic inner lipids must have permitted to cover the inner surface of liposomes with SPIONs.

Liposomes generally are bigger than other nanosystems, in this case 174 ± 53 nm [61], and restructuration and/or fusion after extrusion led to structures of up to 300 nm. This poses problems with extravasation, cellular uptake, pharmacokinetics and elimination routes of these systems, all the more so as the size distribution is generally large. Liposomes of ~100 nm have been shown to be optimal for the delivery of chemotherapeutics in tumours [64]. Next, Bothun *el al.* chose their compounds to generate a fluid phase bilayer [61]. Kawano *et al.* have shown that greater bilayer fluidity enhanced the antitumour activity of liposomes, but this involves spontaneous restructuration and growth, as they could observe cupping and budding in their magnetoliposomes [65,66]. And finally, Bothun *et al.* observed heterogeneous encapsulation of SPIONs (none, single or aggregates), which could be a clue to the instability of nanoliposomes, due for example to surface defunctionalisation during the manufacturing process.

Deng *et al.* resolved the problem of poor SPION encapsulation using covalent binding (figure 4A) [67]. They used dextran-coated SPIONs, and oxidized them to generate aldehyde groups. These functions were then able to link to the amino groups of aminophospholipids DOPE (dioleoylphosphatidylethanolamine) during liposome preparation at high pH. SPIONs were thus

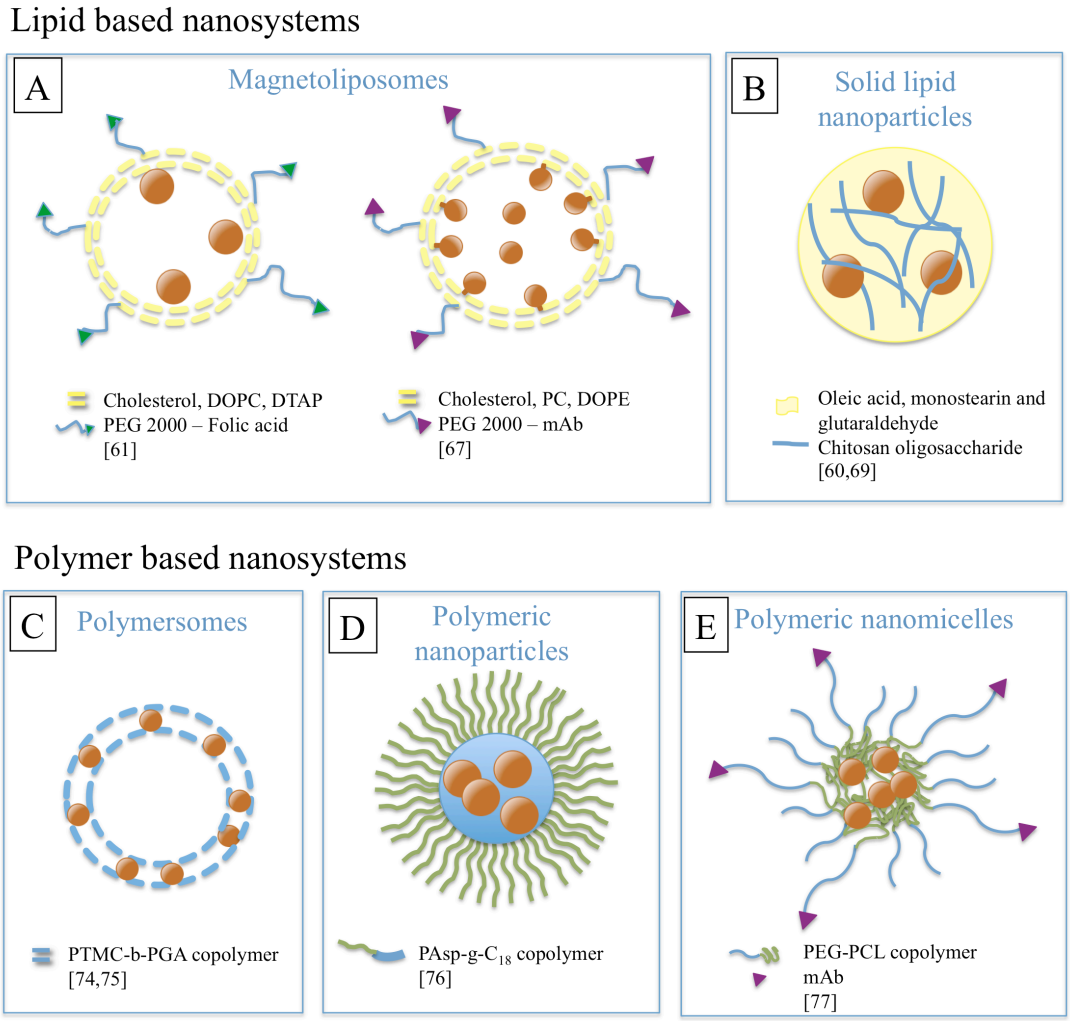

Figure 4. Hybrid nanosystems embedding SPIONs ( ). A-B: nanosystems based on lipids; C-E: nanosystems based on polymers. DOPC 2-dioleoyl-sn-glycero-3-phosphocholine; DOPE dioleoyl-phosphatidyl-ethanolamine; DTAP dipalmitoyl-trimethylammonium-propane; mAb monoclonal antibody; PAsp-g-C_{18} poly(aspartic acid) grafting an octadecyl chain; PC phophatidylcholine; PEG polyethylene glycol; PCL poly(ε-caprolactone); PTMC-b-PGA poly(trimethylene carbonate)-poly(L-glutamic acid).

successfully bound to the interior surface of the lipid bilayer. At the same time, SPIONs were also passively encapsulated in the internal aqueous phase. This permitted to increase the quantity of SPIONs in liposomes. But as Bothun *et al.* observed, the nanocarriers thus designed are rather big (d_H ~175-185 nm), mainly due to the PEGylation step.

4.1.2. Solid lipid nanoparticles. Recently, Ying *et al.* used another type of lipids to design magnetic solid lipid nanoparticles (SLN) [60]. SLNs are an interesting alternative to emulsions, liposomes and polymeric NPs, developed at the beginning of the 1990's [68]. They are generally made of well-tolerated and biodegradable triglycerides. Ying *et al*. chose to stabilize SPIONs (prepared by an ultrasound technique in aqueous medium) with oleic acid (figure 4B). This fatty acid is adsorbed on the surface of SPIONs, generates stable colloidal suspensions in apolar media, and then favours the inclusion of NP in solid lipid nanoparticles by its affinity with monostearin. It is thus possible to introduce SPIONs in SLNs without any functionalization of the SPION surface. Nevertheless, to reinforce their drug delivery performance, these nanovectors still need a surface functionalization of their lipid outer surface.

Ying *et al.* functionalized glutaraldehyde SLNs with chitosan oligosaccharide, thus modulating the SLN size and zeta potential, the DOX content, and its *in vitro* release, as well as the SLN uptake by tumour cells [69]. Contrary to magnetoliposomes, where simple amphiphilic molecules can be included in the bilayer by autoassembly, SLN often need the use of block copolymers or cross-linking techniques [70–73]. This functionalization process involved supplementary steps of chemical synthesis, complicating the process.

Similar to liposomes, the size of SLNs is generally greater than that of core-shell systems, in this case between 83.7 and 308.3 nm [69], which leads to the same critical considerations about cellular uptake and elimination routes. Secondly, the use of anionic lipids induces a negative surface charge. This prevents nanosystems from aggregating and offers a longer circulation time in the organism compared to positively charged ones, but it

also favours capture by lymph nodes [30].

To conclude, Veiseh *et al*. remarked that "when applying these coatings (liposomes and lipids), there is a danger of coating agglomerates rather than discrete SPION cores in micellar or phospholipid structures, leading to poor physicochemical and magnetic properties" [14].

4.2. MNPs embedded in polymers

The use of poly(amino acid)s received considerable attention for the design of nanocarriers, because of their biodegradability and solubility in water. In addition, these polymers can be easily modified by chemical reactions to obtain new properties, like hydrophobic domains, or stimuli-responsive behaviour.

4.2.1. Polymersomes. Recently, Sanson *et al.* designed USPIO and DOX-loaded polymersomes by nanoprecipitation [74,75]. The addition of water to a DMSO solution of poly(trimethylene carbonate)-poly(L-glutamic acid) block copolymer (PTMC-b-PGA) promoted the formation of bilayer vesicles (figure 4C). During their formation, DOX and USPIOs present in the DMSO solution, were loaded into the inner hydrophobic part (PTMC) of the bilayer. The choice to load both USPIOs and anticancer drug into the bilayer can be discussed. First, the thickness of the bilayer could limit the quantity of DOX and USPIOs loaded. This is even more important since high loading rates can compromise the integrity of the bilayer, and alter its self-assembly. Still, the volume available in a 10 nm thick bilayer of a 50 nm diameter hollow sphere is equivalent to the volume of a 40 nm diameter full sphere. Furthermore, the PTMC part of the polymer is thermo-sensitive. Organized in a bilayer, the polymer would be easier to stimulate than in a compact spherical form.

4.2.2. Polymeric nanoparticles and nanomicelles. Yang *et al*. reported the design of poly(aspartic acid)-based nanoparticles, loaded with SPIONs and DOX [76]. They modified the poly(aspartic acid) polymer (PAsp) by grafting an octadecyl chain. The resulting copolymer, named Pasp-g-C_{18}, allowed the self-assembly in compact nanoparticles, with a hydrophobic core of C_{18} chains, and an outer layer of hydrophilic PAsp (figure 4D). By mixing the copolymer with oleic acid-coated SPIONs (obtained by thermal decomposition), the oxide nanoparticles were entrapped in a 100 nm polymeric nanocarrier. This also allowed the entrapment of hydrophobic molecular DOX at basic pH conditions.

Liao *et al.* designed comparable systems using others types of copolymers, monomethoxy PEG-block-poly(ε-caprolactone) ($MPEG_{2000}$-PCL), mixed with maleimide-$MPEG_{3000}$-PCL [77]. The copolymers self-assembled to a hydrophobic PCL core, entrapping SPIONs and DOX, and a hydrophilic shell of PEG (figure 4E). Their strategy to add a targeting ligand on the nanomicelles was original. Here, the maleimide functions protrude from the corona and can be used for conjugation. The targeting ligand (here cetuximab) can thus be added post-synthesis after thiolation, on the maleimide part. This choice permits to vary the surface functionalization of polymeric nanomicelles without modifying the structural polymers.

The choice of polymeric materials instead of lipids presents several advantages. The hydrophilic outer shell makes the nanocarriers directly water-soluble, without any supplementary functionalization. The polymer can be directly grafted with targeting ligands. Unfortunately, the use of poly(aspartic acid) in polymeric nanoparticles and poly(glutamic acid) in polymersomes creates negative charges at the nanocarrier surface (ζ potential around -40 mV), which as in the case of lipids facilitates the capture by lymph nodes.

5. Emerging tendencies for anticancer drugs delivery with inorganic cores

5.1. Nanoclusters instead of nanoparticles

For the delivery of DOX, Chen *et al*. chose the use of nanoclusters that are aggregates of a few tens of Au atoms (figure 5A) [78]. These ultrasmall nanostructures (5.6 nm in hydrodynamic diameter, polydispersity 0.118) keep the same optical properties as gold nanoparticles, have a prolonged blood circulation time compared to PEGylated materials, and enter tumours effectively by EPR effect [79]. They are mainly eliminated via the kidneys, due to their size under 10 nm.

Metal nanoclusters are more and more frequently used, particularly as a novel class of luminescent nanomaterials, and multifunctional nanoclusters appear in recent studies with biological applications [80–82]. Interactions of these ultrasmall structures with the biological environment still need to be explored in more detail, specifically in respect to their intracellular behaviour and degradation [83]. Chen *et al.* protected nanoclusters with bovine serum albumin (BSA), and directly conjugated targeting ligand and DOX. This type of nanoclusters combined with plasma proteins to form larger aggregates in blood, demonstrating the necessity of improving their stability [84].

Because of the ultra small size of these carriers, covalent linkage is the only solution to keep a certain stability of these systems, and design a "prodrug" with DOX [78]. BSA (bovine serum albumin) carboxyl groups protecting the nanoclusters were activated by contact with EDC/NHS to permit the covalent linkage with the sugar moiety of DOX, as well as with methionine as targeting ligand. In another recent publication, the same group improved the nanoclusters by adding a folate group conjugated to the surface in the same way [85].

5.2. Alternative coating materials for inorganic cores

5.2.1. Zwitterionic polymers to limit the size of nanocarriers. PEG, dextran and chitosan have been extensively used for NP coating. However, the increase of the hydrodynamic diameter of these nanosystems can limit the access to cellular compartments and modify their biodistribution and their clearance.

Surface coating with zwitterionic functional groups can be an alternative. A few examples are mentioned in recent reviews [10,86]. Biocompatible Au-NPs with zwitterionic head-groups were designed to encapsulate hydrophobic drugs (tamoxifen and β-lapachone) in their hydrophobic pockets [87]. This coating minimized non-specific binding with biomacromolecules, but unfortunately also prevented cellular uptake. The release was realized by membrane-mediated diffusion. The same type of zwitterionic coating was also reported on quantum dots [88–90]:

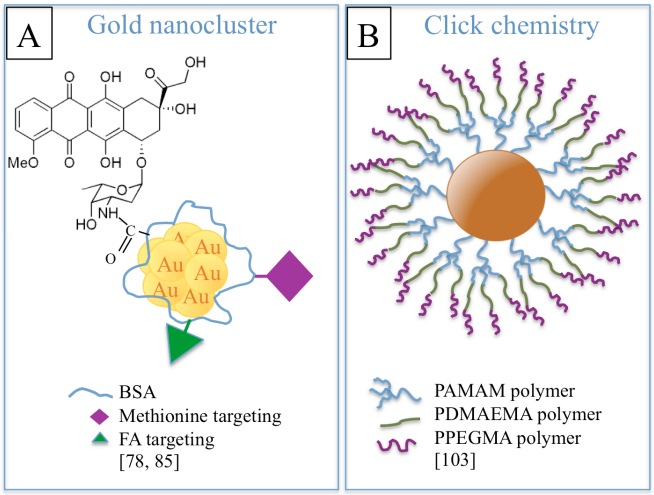

Figure 5. Emerging tendencies for the design of hybrid nanosystems. A: Clusters; B: Click chemistry. BSA bovine serum albumin; FA folic acid; PAMAM polyamidoamine; PDMAEMA poly(2-(dimethylamino)ethyl methacrylate; PPEGMA poly(poly(ethylene glycol) methyl ether methacrylate.

dihydrolipoic acid (DHLA) derivatives conferred high stability to nanosystems, regardless of the pH or ionic strength, and formed a layer less then 2 nm thick [88]. Park et al. even designed mixed coatings (50% zwitterionic coating, 50% other functional groups). This allows maintaining colloidal stability and low non-specific adsorption due to the zwitterionic material, offering at the same time binding groups such as carboxyls or amines for further functionalization [88]. This kind of coatings should multiply in the future, especially for SPIONs and Au-NPs.

5.2.2. High-density lipoproteins to mimic biological structures. NP coating with lipids evolved towards biomimetic high-density lipoproteins (HDL), mimicking biological structures. Indeed, the role of HDL in cancer pathogenesis is increasingly appreciated: the rapid uncontrolled cell growth requires a significant cellular uptake of cholesterol [91].

The use of HDL as coating for Au-NPs, SPIONs and quantum dots has been reported for imaging applications [92]. A classical synthesis involves thiolated lipids like apolipoprotein A1 (an HDL protein) adsorbed onto the Au-NP surface, covered with a second lipid layer adsorbed by hydrophobic interactions. The use of HDL as coating agent for anticancer drug delivery is emerging now, since the biological properties of HDL-coated SPIONs have been verified *in vitro* and *in vivo* [93]: with these systems (non loaded with any active ingredient) there seems to be no significant decrease in cell viability. Unfortunately, they accumulate in atherosclerotic plaques and liver tissue in mice, suggesting that a targeting strategy would be necessary for a use as a drug delivery system, in order to reduce this non-specific accumulation.

5.2.3. Dendrimers as coating agents for inorganic cores. Dendrimers or dendritic architectures are more and more developed for biomedical applications. Their highly tuneable surface chemistry, as well as their precise composition and structure make them attractive for NP coating, especially for magnetic nanoparticles [94–96], but also for Au-NPs [97].

For instance, publications report design and characterization of such systems [95,97], and imaging studies in MRI [96], demonstrating good contrast properties. On the other hand, there are very few studies on drug delivery from dendrimers. Taratula *et al.* designed complexes with SPIONs, poly(propyleneimine) generation 5 dendrimers (PPI 5) and siRNA [94], with a co-delivery of cisplatin and a luteinizing hormone-releasing hormone (LHRH) decapeptide as targeting agent. The *in vitro* and *in vivo* studies showed an excellent cell-targeted selectivity, with a significant limitation of the tumour growth.

Studies on dendrimer coated SPIONs or Au-NPs for drug delivery can be expected multiply, especially with DOX as a model drug.

5.3. Click-chemistry applied to DOX-loaded inorganic cores

Click-chemistry is a modular synthetic approach for the assembly of new molecular entities, offering stereospecificity and high reaction efficiencies [98]. The concept is already 10 years old. Its application to NPs led to nano-objects with original coatings. For instance, SPIONs and Au-NPs engineered with click-chemistry led to sensor applications [99,100], or imaging applications [101]. But few recent publications are interested in the delivery of molecules into the cell [102].

A system of NPs coated by click-chemistry, and loaded with DOX as a model drug was reported by He *et al.* (SPIONs with a dendritic-linear-brush-like tri-block copolymer, figure 5B) [103]. They prepared SPIONs coated with the triblock copolymer polyamidoamine-*b*-poly(2-(dimethylamino)ethyl methacrylate)-*b*-poly(poly(ethylene glycol) methyl ether methacrylate) (PAMAM-*b*-PDMAEMA-*b*-PPEGMA) via a two-step copper-mediated atom transfer radical polymerization (ATRP) method. The copper(I)-catalyzed 1,2,3-triazole-forming reaction between azides and terminal alkynes has become the most used 'click chemistry' method, because of its reliability, specificity, and biocompatibility [98].

The macroinitiators were immobilized on the surface of Fe_3O_4 nanoparticles via ligand exchange of oleic acid with PAMAM-type dendron, following a click reaction with 2′-azidoethyl-2-bromoisobutylate (AEBIB). PDMAEMA and PPEGMA were grown gradually from the nanoparticle surfaces using the "grafting from" approach, which rendered the SPIONs soluble in water and which reversed aggregation [103].

In the classical "grafting onto" approach, the polymers must be entirely synthesized before the coating step, the steric hindering renders the grafting density difficult to control, and polymer chains can bind more than a particle, creating nanoparticle clusters. On the contrary, the "grafting from" approach to coat nanoparticles is interesting since the coating polymers are grown directly on the surface, and bypass these difficulties. So click-chemistry is a simple solution with prospects for the design of nanocarriers.

6. Conclusion

The shell/matrix of the nanosystems described in this review presents hydrophilic and/or lipophilic environment to load small anticancer molecules by diffusion. It also offers binding sites for

covalent linkages with these small molecules as well as targeting ligands. The organic materials used were first chosen for stability and biocompatibility of the nanocarriers. Nevertheless, most of the nanosystems described in this review are more than simple nanocargos for the transport of active molecules. The NP designs are chosen in function of the release strategies of the molecules loaded. The stimuli-sensitive strategies like the use of temperature-responsive materials (polymers or lipids) or pH-sensitive bindings modulate the release of the active molecules by the modification of the shell conformation, or by its degradation in the organism. The final size of nanocarriers is taken into account, to modulate the clearance pathways, as shown by the emerging formulations of nanoclusters. Production routes of nanocarriers tend to be simplified (one-pot synthesis) for easier transposition. The perfect master of nanocarrier structure (for exemple with click-chemistry) is essential for further investigations *in vivo*, and for marketing authorizations. Nanocarrier design is a multidisciplinary research field destined to expand in the years to come.

Notes and references

[1] Huang H-C, Barua S, Sharma G, Dey S K and Rege K 2011 Inorganic nanoparticles for cancer imaging and therapy *J Control Release* 155 344–57

[2] Klostergaard J and Seeney C E 2012 Magnetic nanovectors for drug delivery *Maturitas* 73 33–44

[3] Owens III D E and Peppas N A 2006 Opsonization, biodistribution, and pharmacokinetics of polymeric nanoparticles *International Journal of Pharmaceutics* 307 93–102

[4] Van der Zee J 2002 Heating the patient: a promising approach? *Ann. Oncol.* 13 1173–84

[5] Xie J, Lee S and Chen X 2010 Nanoparticle-based theranostic agents *Adv. Drug Deliv. Rev.* 62 1064–79

[6] Mirza A Z and Shamshad H 2011 Preparation and characterization of doxorubicin functionalized gold nanoparticles *Eur J Med Chem* 46 1857–60

[7] Nguyen D T, Kim D-J and Kim K-S 2011 Controlled synthesis and biomolecular probe application of gold nanoparticles *Micron* 42 207–27

[8] Zong S, Wang Z, Yang J, Wang C, Xu S and Cui Y 2012 A SERS and fluorescence dual mode cancer cell targeting probe based on silica coated Au@Ag core–shell nanorods *Talanta* 97 368–75

[9] Wang Z, Zong S, Yang J, Song C, Li J and Cui Y 2010 One-step functionalized gold nanorods as intracellular probe with improved SERS performance and reduced cytotoxicity *Biosens Bioelectron* 26 241–7

[10] Rana S, Bajaj A, Mout R and Rotello V M 2012 Monolayer coated gold nanoparticles for delivery applications *Adv. Drug Deliv. Rev.* 64 200–16

[11] Mahmoudi M, Sant S, Wang B, Laurent S and Sen T 2011 Superparamagnetic iron oxide nanoparticles (SPIONs): Development, surface modification and applications in chemotherapy *Adv. Drug Deliv. Rev.* 63 24–46

[12] Gupta A K and Gupta M 2005 Synthesis and surface engineering of iron oxide nanoparticles for biomedical applications *Biomaterials* 26 3995–4021

[13] Petcharoen K and Sirivat A 2012 Synthesis and characterization of magnetite nanoparticles via the chemical co-precipitation method *Mat Sci Eng B-Solid* 177 421–7

[14] Veiseh O, Gunn J W and Zhang M 2010 Design and fabrication of magnetic nanoparticles for targeted drug delivery and imaging *Adv. Drug Deliv. Rev.* 62 284–304

[15] Duncan B, Kim C and Rotello V M 2010 Gold nanoparticle platforms as drug and biomacromolecule delivery systems *J Control Release* 148 122–7

[16] Frens G 1973 Controlled nucleation for regulation of particle size in monodisperse gold suspensions *Nature Phys. Sci.* 241 20–2

[17] Vigderman L and Zubarev E R 2012 Therapeutic platforms based on gold nanoparticles and their covalent conjugates with drug molecules *Adv. Drug Deliv. Rev.*

[18] Massart R 1981 Preparation of aqueous magnetic liquids in alkaline and acidic media *IEEE T Magn* 17 1247–8

[19] Chourpa I, Douziech-Eyrolles L, Ngaboni-Okassa L, Fouquenet J-F, Cohen-Jonathan S, Soucé M, Marchais H and Dubois P 2005 Molecular composition of iron oxide nanoparticles, precursors for magnetic drug targeting, as characterized by confocal Raman microspectroscopy *Analyst* 130 1395–403

[20] Zhang D, Tong Z, Li S, Zhang X and Ying A 2008 Fabrication and characterization of hollow Fe3O4 nanospheres in a microemulsion *Mater Lett* 62 4053–5

[21] Fang C, Bhattarai N, Sun C and Zhang M 2009 Functionalized nanoparticles with long-term stability in biological media *Small* 5 1637–41

[22] Yang X, Hong H, Grailer J J, Rowland I J, Javadi A, Hurley S A, Xiao Y, Yang Y, Zhang Y, Nickles R J, Cai W, Steeber D A and Gong S 2011 cRGD-functionalized, DOX-conjugated, and 64Cu-labeled superparamagnetic iron oxide nanoparticles for targeted anticancer drug delivery and PET/MR imaging *Biomaterials* 32 4151–60

[23] Huber D 2005 Synthesis, Properties, and Applications of Iron Nanoparticles *Small* 1 482–501

[24] Pinna N, Garnweitner G, Antonietti M and Niederberger M 2005 A General Nonaqueous Route to Binary Metal Oxide Nanocrystals Involving a C−C Bond Cleavage *J Am Chem Soc* 127 5608–12

[25] Lee S-Y and Harris M T 2006 Surface modification of magnetic nanoparticles capped by oleic acids: Characterization and colloidal stability in polar solvents *J Colloid Interf Sci* 293 401–8

[26] Huber D L, Venturini E L, Martin J E, Provencio P P and Patel R J 2004 Synthesis of highly magnetic iron nanoparticles suitable for field structuring using a β-diketone surfactant *J Magn Magn Mater* 278 311–6

[27] Huang X and El-Sayed M A 2010 Gold nanoparticles: Optical properties and implementations in cancer diagnosis and photothermal therapy *J Adv Res* 1 13–28

[28] De Dios A S and Díaz-García M E 2010 Multifunctional nanoparticles: Analytical prospects *Anal Chim Acta* 666 1–22

[29] You J, Zhang G and Li C 2012 Exceptionally High Payload of Doxorubicin in Hollow Gold Nanospheres for Near-Infrared Light-Triggered Drug Release *ACS Nano* 4 1033–41

[30] Thanh N T K and Green L A W 2010 Functionalisation of nanoparticles for biomedical applications *Nano Today* 5 213–30

[31] Dias A M G C, Hussain A, Marcos A S and Roque A C A 2011 A biotechnological perspective on the application of iron oxide magnetic colloids modified with polysaccharides *Biotechnol. Adv.* 29 142–55

[32] Neuberger T, Schöpf B, Hofmann H, Hofmann M and von Rechenberg B 2005 Superparamagnetic nanoparticles for biomedical applications: Possibilities and limitations of a new drug delivery system *J Magn Magn Mater* 293 483–96

[33] Munnier E, Cohen-Jonathan S, Linassier C, Douziech-Eyrolles L, Marchais H, Soucé M, Hervé K, Dubois P and Chourpa I 2008 Novel method of doxorubicin–SPION reversible association for magnetic drug targeting *Int J Pharm* 363 170–6

[34] Allard-Vannier E, Cohen-Jonathan S, Gautier J, Hervé-Aubert K, Munnier E, Soucé M, Legras P, Passirani C and Chourpa I 2012 Pegylated magnetic nanocarriers for doxorubicin delivery: A quantitative determination of stealthiness in vitro and in vivo *Eur J Pharm Biopharm* 81 498–505

[35] Wang M and Thanou M 2010 Targeting nanoparticles to cancer *Pharmacol Res* 62 90–9

[36] Cao N, Cheng D, Zou S, Ai H, Gao J and Shuai X 2011 The synergistic effect of hierarchical assemblies of siRNA and chemotherapeutic drugs co-delivered into hepatic cancer cells *Biomaterials* 32 2222–32

[37] Gautier J, Munnier E, Paillard A, Hervé K, Douziech-Eyrolles L, Soucé M, Dubois P and Chourpa I 2012 A pharmaceutical study of

doxorubicin-loaded PEGylated nanoparticles for magnetic drug targeting *Int J Pharm* 423 16–25

[38] Kaaki K, Hervé-Aubert K, Chiper M, Shkilnyy A, Soucé M, Benoit R, Paillard A, Dubois P, Saboungi M-L and Chourpa I 2012 Magnetic nanocarriers of doxorubicin coated with poly(ethylene glycol) and folic acid: relation between coating structure, surface properties, colloidal stability, and cancer cell targeting *Langmuir* 28 1496–505

[39] Lee H, Yu M K, Park S, Moon S, Min J J, Jeong Y Y, Kang H-W and Jon S 2012 Thermally Cross-Linked Superparamagnetic Iron Oxide Nanoparticles: Synthesis and Application as a Dual Imaging Probe for Cancer in Vivo *J. Am. Chem. Soc.* 129 12739–45

[40] Barenholz Y (Chezy) 2012 Doxil® — The first FDA-approved nano-drug: Lessons learned *J Control Release* 160 117–34

[41] Gref R, Lück M, Quellec P, Marchand M, Dellacherie E, Harnisch S, Blunk T and Müller R . 2000 "Stealth" corona-core nanoparticles surface modified by polyethylene glycol (PEG): influences of the corona (PEG chain length and surface density) and of the core composition on phagocytic uptake and plasma protein adsorption *Colloid Surface B* 18 301–13

[42] Hervé K, Douziech-Eyrolles L, Munnier E, Cohen-Jonathan S, Soucé M, Marchais H, Limelette P, Warmont F, Saboungi M L, Dubois P and Chourpa I 2008 The development of stable aqueous suspensions of PEGylated SPIONs for biomedical applications *Nanotechnology* 19 465608

[43] Gu Y-J, Cheng J, Man C W-Y, Wong W-T and Cheng S H 2012 Gold-doxorubicin nanoconjugates for overcoming multidrug resistance *Nanomedicine* 8 204–11

[44] Prabaharan M, Grailer J J, Pilla S, Steeber D A and Gong S 2009 Gold nanoparticles with a monolayer of doxorubicin-conjugated amphiphilic block copolymer for tumor-targeted drug delivery *Biomaterials* 30 6065–75

[45] Fang C, Kievit F M, Veiseh O, Stephen Z R, Wang T, Lee D, Ellenbogen R G and Zhang M 2012 Fabrication of magnetic nanoparticles with controllable drug loading and release through a simple assembly approach *J Control Release* 162 233–41

[46] Schwartzberg A M, Olson T Y, Talley C E and Zhang J Z 2006 Synthesis, characterization, and tunable optical properties of hollow gold nanospheres *J Phys Chem B* 110 19935–44

[47] Kievit F M, Wang F Y, Fang C, Mok H, Wang K, Silber J R, Ellenbogen R G and Zhang M 2011 Doxorubicin loaded iron oxide nanoparticles overcome multidrug resistance in cancer in vitro *J Control Release* 152 76–83

[48] Gu Y-J, Cheng J, Lin C-C, Lam Y W, Cheng S H and Wong W-T 2009 Nuclear penetration of surface functionalized gold nanoparticles *Toxicol. Appl. Pharmacol.* 237 196–204

[49] Maeng J H, Lee D-H, Jung K H, Bae Y-H, Park I-S, Jeong S, Jeon Y-S, Shim C-K, Kim W, Kim J, Lee J, Lee Y-M, Kim J-H, Kim W-H and Hong S-S 2010 Multifunctional doxorubicin loaded superparamagnetic iron oxide nanoparticles for chemotherapy and magnetic resonance imaging in liver cancer *Biomaterials* 31 4995–5006

[50] Agrawal S K, Sanabria-DeLong N, Coburn J M, Tew G N and Bhatia S R 2006 Novel drug release profiles from micellar solutions of PLA–PEO–PLA triblock copolymers *J Control Release* 112 64–71

[51] Sahu S K, Maiti S, Pramanik A, Ghosh S K and Pramanik P 2012 Controlling the thickness of polymeric shell on magnetic nanoparticles loaded with doxorubicin for targeted delivery and MRI contrast agent *Carbohyd Polym* 87 2593–604

[52] Hua M-Y, Yang H-W, Liu H-L, Tsai R-Y, Pang S-T, Chuang K-L, Chang Y-S, Hwang T-L, Chang Y-H, Chuang H-C and Chuang C-K 2011 Superhigh-magnetization nanocarrier as a doxorubicin delivery platform for magnetic targeting therapy *Biomaterials* 32 8999–9010

[53] Hua M-Y, Yang H-W, Chuang C-K, Tsai R-Y, Chen W-J, Chuang K-L, Chang Y-H, Chuang H-C and Pang S-T 2010 Magnetic-nanoparticle-modified paclitaxel for targeted therapy for prostate cancer *Biomaterials* 31 7355–63

[54] Park S, Kim H S, Kim W J and Yoo H S 2012 Pluronic@Fe3O4 nanoparticles with robust incorporation of doxorubicin by thermo-responsiveness *Int J Pharm* 424 107–14

[55] Quan Q, Xie J, Gao H, Yang M, Zhang F, Liu G, Lin X, Wang A, Eden H S, Lee S, Zhang G and Chen X 2011 HSA coated iron oxide nanoparticles as drug delivery vehicles for cancer therapy *Mol. Pharm.* 8 1669–76

[56] Xie J, Chen K, Huang J, Lee S, Wang J, Gao J, Li X and Chen X 2010 PET/NIRF/MRI triple functional iron oxide nanoparticles *Biomaterials* 31 3016–22

[57] Dufort S, Sancey L and Coll J-L 2012 Physico-chemical parameters that govern nanoparticles fate also dictate rules for their molecular evolution *Adv. Drug Deliv. Rev.* 64 179–89

[58] Fanali G, di Masi A, Trezza V, Marino M, Fasano M and Ascenzi P 2012 Human serum albumin: From bench to bedside *Mol Aspects Med* 33 209–90

[59] Dreis S, Rothweiler F, Michaelis M, Cinatl J Jr, Kreuter J and Langer K 2007 Preparation, characterisation and maintenance of drug efficacy of doxorubicin-loaded human serum albumin (HSA) nanoparticles *Int J Pharm* 341 207–14

[60] Ying X-Y, Du Y-Z, Hong L-H, Yuan H and Hu F-Q 2011 Magnetic lipid nanoparticles loading doxorubicin for intracellular delivery: Preparation and characteristics *J Magn Magn Mater* 323 1088–93

[61] Bothun G D, Lelis A, Chen Y, Scully K, Anderson L E and Stoner M A 2011 Multicomponent folate-targeted magnetoliposomes: design, characterization, and cellular uptake *Nanomedicine: NBM* 7 797–805

[62] Pradhan P, Banerjee R, Bahadur D, Koch C, Mykhaylyk O and Plank C 2010 Targeted magnetic liposomes loaded with doxorubicin *Methods Mol. Biol.* 605 279–93

[63] Pradhan P, Giri J, Rieken F, Koch C, Mykhaylyk O, Döblinger M, Banerjee R, Bahadur D and Plank C 2010 Targeted temperature sensitive magnetic liposomes for thermo-chemotherapy *J Control Release* 142 108–21

[64] Cukierman E and Khan D R 2010 The benefits and challenges associated with the use of drug delivery systems in cancer therapy *Biochem Pharmacol* 80 762–70

[65] Kawano K, Onose E, Hattori Y and Maitani Y 2009 Higher liposomal membrane fluidity enhances the in vitro antitumor activity of folate-targeted liposomal mitoxantrone *Mol. Pharm.* 6 98–104

[66] Kawano K and Maitani Y 2011 Effects of polyethylene glycol spacer length and ligand density on folate receptor targeting of liposomal Doxorubicin in vitro *J Drug Deliv* 2011 160967

[67] Deng L, Ke X, He Z, Yang D, Gong H, Zhang Y, Jing X, Yao J and Chen J 2012 A MSLN-targeted multifunctional nanoimmunoliposome for MRI and targeting therapy in pancreatic cancer *Int J Nanomedicine* 7 5053–65

[68] Parveen S, Misra R and Sahoo S K 2012 Nanoparticles: a boon to drug delivery, therapeutics, diagnostics and imaging *Nanomedicine* 8 147–66

[69] Ying X-Y, Cui D, Yu L and Du Y-Z 2011 Solid lipid nanoparticles modified with chitosan oligosaccharides for the controlled release of doxorubicin *Carbohyd Polym* 84 1357–64

[70] Prasad P, Cai P, Shuhendler A, Rauth A M and Wu X Y 2012 Doxorubicin and mitomycin C co-loaded polymer-lipid hybrid nanoparticles inhibit growth of sensitive and multidrug resistant human mammary tumor xenografts *Cancer Lett.*

[71] Kuo Y-C and Liang C-T 2011 Catanionic solid lipid nanoparticles carrying doxorubicin for inhibiting the growth of U87MG cells *Colloid Surface B* 85 131–7

[72] Kang K W, Chun M-K, Kim O, Subedi R K, Ahn S-G, Yoon J-H and Choi H-K 2010 Doxorubicin-loaded solid lipid nanoparticles to overcome multidrug resistance in cancer therapy *Nanomedicine: NBM* 6 210–3

[73] Subedi R K, Kang K W and Choi H-K 2009 Preparation and characterization of solid lipid nanoparticles loaded with doxorubicin *Eur J Pharm Sci* 37 508–13

[74] Sanson C, Schatz C, Le Meins J-F, Soum A, Thévenot J, Garanger E and Lecommandoux S 2010 A simple method to achieve high doxorubicin loading in biodegradable polymersomes *J Control Release* 147 428–35

[75] Sanson C, Diou O, Thévenot J, Ibarboure E, Soum A, Brûlet A, Miraux S, Thiaudière E, Tan S, Brisson A, Dupuis V, Sandre O and Lecommandoux S 2011 Doxorubicin Loaded Magnetic

Polymersomes: Theranostic Nanocarriers for MR Imaging and Magneto-Chemotherapy *ACS Nano* 5 1122–40

[76] Yang H-M, Oh B C, Kim J H, Ahn T, Nam H-S, Park C W and Kim J-D 2011 Multifunctional poly(aspartic acid) nanoparticles containing iron oxide nanocrystals and doxorubicin for simultaneous cancer diagnosis and therapy *Colloid Surface A* 391 208–15

[77] Liao C, Sun Q, Liang B, Shen J and Shuai X 2011 Targeting EGFR-overexpressing tumor cells using Cetuximab-immunomicelles loaded with doxorubicin and superparamagnetic iron oxide *Eur J Radiol* 80 699–705

[78] Chen H, Li B, Ren X, Li S, Ma Y, Cui S and Gu Y 2012 Multifunctional near-infrared-emitting nano-conjugates based on gold clusters for tumor imaging and therapy *Biomaterials*

[79] Wu X, He X, Wang K, Xie C, Zhou B and Qing Z 2010 Ultrasmall near-infrared gold nanoclusters for tumor fluorescence imaging in vivo *Nanoscale* 2 2244–9

[80] Safari D, Marradi M, Chiodo F, Th Dekker H A, Shan Y, Adamo R, Oscarson S, Rijkers G T, Lahmann M, Kamerling J P, Penadés S and Snippe H 2012 Gold nanoparticles as carriers for a synthetic Streptococcus pneumoniae type 14 conjugate vaccine *Nanomedicine (Lond)* 7 651–62

[81] Sapozhnikova V, Willsey B, Asmis R, Wang T, Jenkins J T, Mancuso J, Ma L L, Kuranov R, Milner T E, Johnston K and Feldman M D 2012 Use of near-infrared luminescent gold nanoclusters for detection of macrophages *J Biomed Opt* 17 026006

[82] Wang Y, Chen J and Irudayaraj J 2011 Nuclear targeting dynamics of gold nanoclusters for enhanced therapy of HER2+ breast cancer *ACS Nano* 5 9718–25

[83] Shang L, Dong S and Nienhaus G U 2011 Ultra-small fluorescent metal nanoclusters: Synthesis and biological applications *Nano Today* 6 401–18

[84] Zhang X-D, Wu D, Shen X, Liu P-X, Fan F-Y and Fan S-J 2012 In vivo renal clearance, biodistribution, toxicity of gold nanoclusters *Biomaterials* 33 4628–38

[85] Chen H, Li S, Li B, Ren X, Li S, Mahounga D M, Cui S, Gu Y and Achilefu S 2012 Folate-modified gold nanoclusters as near-infrared fluorescent probes for tumor imaging and therapy *Nanoscale* 4 6050–64

[86] Nam J, Won N, Bang J, Jin H, Park J, Jung S, Jung S, Park Y and Kim S Surface engineering of inorganic nanoparticles for imaging and therapy *Advanced Drug Delivery Reviews*

[87] Kim C K, Ghosh P, Pagliuca C, Zhu Z-J, Menichetti S and Rotello V M 2009 Entrapment of hydrophobic drugs in nanoparticle monolayers with efficient release into cancer cells *J. Am. Chem. Soc.* 131 1360–1

[88] Park J, Nam J, Won N, Jin H, Jung S, Jung S, Cho S-H and Kim S 2011 Compact and Stable Quantum Dots with Positive, Negative, or Zwitterionic Surface: Specific Cell Interactions and Non-Specific Adsorptions by the Surface Charges *Adv Funct Mater* 21 1558–66

[89] Muro E, Pons T, Lequeux N, Fragola A, Sanson N, Lenkei Z and Dubertret B 2010 Small and stable sulfobetaine zwitterionic quantum dots for functional live-cell imaging *J. Am. Chem. Soc.* 132 4556–7

[90] Susumu K, Oh E, Delehanty J B, Blanco-Canosa J B, Johnson B J, Jain V, Hervey W J 4th, Algar W R, Boeneman K, Dawson P E and Medintz I L 2011 Multifunctional compact zwitterionic ligands for preparing robust biocompatible semiconductor quantum dots and gold nanoparticles *J. Am. Chem. Soc.* 133 9480–96

[91] Damiano M G, Mutharasan R K, Tripathy S, McMahon K M and Thaxton C S 2012 Templated high density lipoprotein nanoparticles as potential therapies and for molecular delivery *Adv. Drug Deliv. Rev.*

[92] Cormode D P, Skajaa T, van Schooneveld M M, Koole R, Jarzyna P, Lobatto M E, Calcagno C, Barazza A, Gordon R E, Zanzonico P, Fisher E A, Fayad Z A and Mulder W J M 2008 Nanocrystal Core High-Density Lipoproteins: A Multimodality Contrast Agent Platform *Nano Letters* 8 3715–23

[93] Skajaa T, Cormode D P, Jarzyna P A, Delshad A, Blachford C, Barazza A, Fisher E A, Gordon R E, Fayad Z A and Mulder W J M 2011 The biological properties of iron oxide core high-density lipoprotein in experimental atherosclerosis *Biomaterials* 32 206–13

[94] Taratula O, Garbuzenko O, Savla R, Wang Y A, He H and Minko T 2011 Multifunctional nanomedicine platform for cancer specific delivery of siRNA by superparamagnetic iron oxide nanoparticles-dendrimer complexes *Curr Drug Deliv* 8 59–69

[95] Dietrich S, Chandra S, Georgi C, Thomas S, Makarov D, Schulze S, Hietschold M, Albrecht M, Bahadur D and Lang H 2012 Design, characterization and magnetic properties of Fe3O4-nanoparticle arrays coated with PEGylated-dendrimers *Mater Chem Phys* 132 292–9

[96] Lamanna G, Kueny-Stotz M, Mamlouk-Chaouachi H, Ghobril C, Basly B, Bertin A, Miladi I, Billotey C, Pourroy G, Begin-Colin S and Felder-Flesch D 2011 Dendronized iron oxide nanoparticles for multimodal imaging *Biomaterials* 32 8562–73

[97] Dietrich S, Schulze S, Hietschold M and Lang H 2011 Au nanoparticles stabilised by PEGylated low generation PAMAM dendrimers: Design, characterisation and properties *J Colloid Interf Sci* 359 454–60

[98] Agalave S G, Maujan S R and Pore V S 2011 Click chemistry: 1,2,3-triazoles as pharmacophores *Chem Asian J* 6 2696–718

[99] Yao Y, Sun Z, Zou Z and Li H 2011 Quinolino-triazole linked gold nanoparticles as sensitive "turn-on" fluorescent Cd(2+) probes *Nanotechnology* 22 435502

[100] Hua C, Zhang W H, De Almeida S R M, Ciampi S, Gloria D, Liu G, Harper J B and Gooding J J 2012 A novel route to copper(II) detection using "click" chemistry-induced aggregation of gold nanoparticles *Analyst* 137 82–6

[101] Locatelli E, Ori G, Fournelle M, Lemor R, Montorsi M and Comes Franchini M 2011 Click chemistry for the assembly of gold nanorods and silver nanoparticles *Chemistry* 17 9052–6

[102] Voliani V, Ricci F, Signore G, Nifosì R, Luin S and Beltram F 2011 Multiphoton molecular photorelease in click-chemistry-functionalized gold nanoparticles *Small* 7 3271–5

[103] He X, Wu X, Cai X, Lin S, Xie M, Zhu X and Yan D 2012 Functionalization of magnetic nanoparticles with dendritic-linear-brush-like triblock copolymers and their drug release properties *Langmuir* 28 11929–38

Chapitre 2 : Nanovecteurs théragnostiques pour la délivrance de la DOX

Publication 2 : Recent advances in theragnostic nanocarriers of doxorubicin based on iron oxide and gold nanoparticles

Publiée dans Journal of Controlled Release, 2013

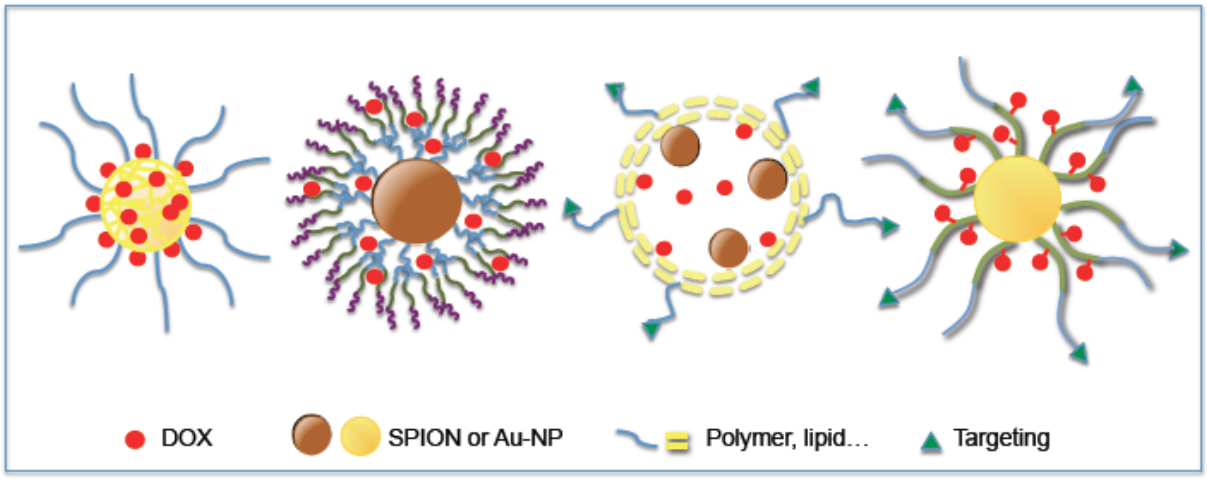

Cette revue fait le point sur les recherches actuelles concernant les stratégies de délivrance de la DOX et d'imagerie proposées avec des nanovecteurs hybrides à base de nanoparticules d'oxydes de fer et d'or. L'exemple de la doxorubicine a servi de fil conducteur pour cette étude, car comme cela a été dit précédemment, elle est fréquemment utilisée comme molécule modèle dans de nombreuses études.

Les stratégies mises en œuvre pour charger la doxorubicine sur les nanovecteurs sont de première importance, car elles conditionnent les modalités et les cinétiques de libération de cette molécule.

- Le fait d'adsorber électrostatiquement la doxorubicine à la surface de nanovecteurs conduit souvent à une libération massive et non contrôlée. C'est pourquoi la doxorubicine est chargée sous forme de complexes dans certaines études, la dissociation du complexe étant soumise à des stimuli extérieurs (acidification du milieu, activité enzymatique), permettant de réguler plus finement la libération de la doxorubicine.
- Une stratégie proche consiste à mettre en œuvre des liaisons clivables par des stimuli intracellulaires, comme un changement de pH ou un environnement réducteur présents dans les compartiments intracellulaires. Dans ce cas, la libération de la doxorubicine est favorisée après l'internalisation des nanovecteurs dans les cellules.
- L'affinité de la doxorubicine moléculaire pour les matériaux lipophiles et de ses formes ionisées pour les matériaux plus hydrophiles permet de la faire diffuser dans les matériaux de revêtement, ou de la piéger lors de la formulation. Dans ce cas, la libération est conditionnée par la plus ou moins grande affinité de la DOX pour ces matériaux.

Les évaluations *in vitro* et *in vivo* des nanovecteurs ainsi formulés s'appuient sur de nombreuses techniques pour élucider leur comportement au sein de la cellules ou de l'organisme.

- La fluorescence de la DOX a permis de suivre son devenir intracellulaire après internalisation de nanovecteurs magnétiques dans des cellules. Les nanovecteurs peuvent être suivis indépendamment de la DOX, par exemple par dosage de l'or par spectrométrie de masse ou par dosage du fer par spectrométrie d'absorption atomique.
- D'autres études se sont attachées à l'intérêt de tels nanovecteurs dans le cas de multirésistance aux médicaments. La vectorisation de la DOX lui permet en effet de

ne pas être effluée hors des cellules, démontrant une cytotoxicité accrue par rapport à la molécule seule.

- Ces nanovecteurs hybrides sont aussi des outils diagnostiques potentiels, aussi bien *in vitro* qu'*in vivo*. Leur fort contraste en microscopie électronique en transmission (MET) permet de les visualiser aisément dans les cellules ou les tissus. Les oxydes de fer, du fait de leur moment magnétique important, déforment les caractéristiques magnétiques locales et augmentent le contraste en imagerie à résonance magnétique (IRM). Les nanoparticules d'or, quant à elles, possèdent une résonance plasmonique exploitable en spectroscopie SERS, et le numéro atomique important de l'or permet une bonne atténuation des rayons X, en faisant un bon candidat comme agent de contraste en tomographie à émission de positrons (ou PET scan).
- La formulation des nanovecteurs hybrides s'appuie souvent sur une stratégie de ciblage de la tumeur. Des études sont régulièrement publiées sur la mise en œuvre d'un ciblage magnétique pour les nanovecteurs à base de SPIONs. Parallèlement, les études présentant des ciblages biologiques (récepteur au folate, cRGD ou anticorps monoclonaux) se multiplient.
- Par contre, les études de réduction tumorale concernant des nanovecteurs hybrides chargés de DOX sont très peu nombreuses à ce jour. Deux sont présentées dans cet article, dont une associant effet antitumoral de la DOX et thérapie thermique. Ce type d'association entre molécule antitumorale et thérapie alternative devient de plus en plus courant.

L'article de synthèse présenté ici démontre que la doxorubicine, bien que connue depuis les années soixante-dix, reste un élément de choix dans l'arsenal thérapeutique, et un modèle d'étude intéressant, puisqu'il permet de mettre en évidence les tendances actuelles de formulation et les résultats récents obtenus.

Journal of Controlled Release 169 (2013) 48–61

Contents lists available at SciVerse ScienceDirect

Journal of Controlled Release

journal homepage: www.elsevier.com/locate/jconrel

Review

Recent advances in theranostic nanocarriers of doxorubicin based on iron oxide and gold nanoparticles

J. Gautier, E. Allard-Vannier *, E. Munnier, M. Soucé, I. Chourpa

EA 6295 "Nanomédicaments et Nanosondes", Université François-Rabelais, Tours F-37200, France

ARTICLE INFO

Article history:
Received 11 December 2012
Accepted 9 March 2013
Available online 6 April 2013

Keywords:
Drug delivery
Doxorubicin
Iron oxide nanocarriers
Gold nanocarriers

ABSTRACT

Hybrid (organic/inorganic) nanoparticles emerged as a simple solution to build "theranostic" systems. Due to their physical properties, superparamagnetic iron oxide nanoparticles (SPIONs) and plasmonic gold nanoparticles (Au-NPs) are extensively studied as a part of diagnostic and therapeutic strategies in cancer treatments. They can be used as agents for in vitro or in vivo imaging, for magnetic drug targeting and/or thermal therapy. Their functionalization with organic shells enhances their potential performance in tumor targeting and drug delivery. The advances in such hybrid nanocarriers are well illustrated with the example of the anticancer drug doxorubicin (DOX).

The aim of this review is to give a multidisciplinary overview of such smart nanosystems loaded with DOX, based on examples taken from recent publications. From a physico-chemical point of view, we discuss the choices for the strategies for loading DOX and the consequences on drug release. From a biological point of view, we analyze the in vitro and in vivo assays concerning tumor imaging, targeted drug delivery and anticancer efficiency. Future opportunities and challenges are also addressed.

Contents

* Corresponding author at: Laboratoire de Pharmacie Galénique, UFR de Pharmacie, 31 Avenue Monge, 37200 Tours, France. Tel.: +33 247367200; fax: +33 247367198.
E-mail address: emilie.allard@univ-tours.fr (E. Allard-Vannier).

0168-3659/$ – see front matter © 2013 Elsevier B.V. All rights reserved.
http://dx.doi.org/10.1016/j.jconrel.2013.03.018

1. Introduction

Applications of "nanomedicine" are becoming common, particularly in the field of oncology, with contrast agents for imaging and diagnosis (Feridex®/Endorem®, Resovist®/Clavist®), or for anticancer drug delivery (Doxil®, Abraxane®). This first generation of nano-objects reached the tumor environment by the so-called "enhanced permeation and retention" (EPR) effect [1]. The EPR effect consists in extravasation from leaky fenestrations of tumor neovascularization, and accumulation of nanocarriers in tumor and inflamed tissues, because of inefficient lymphatic drainage. The second generation of nanocarriers complemented the EPR effect with a specific targeting in order to reach the tumor environment and vectorize drugs.

In our days, the third generation of nano-objects, with additional functionalities, called "theranostics", is impatiently expected [2]. The delivery of an anticancer drug by such a nano-object would be coupled to a specific targeting of the tumor micro-environment, with triggered or controlled release, and it would allow diagnosis with imaging functions. The number of publications concerning theranostic platforms exploded in recent years [2–10].

As a platform for such smart nano-objects, hybrid nanosystems based on metallic nanoparticles (MNPs) gained significant attention because of their unique characteristics [7]. The inorganic core confers to them attractive properties: material and size-dependent physicochemical properties, easy surface functionalization, stability, and inertness. MNPs often present interesting sizes comprised between 10 and 100 nm. A size above 10 nm prevents rapid elimination through the kidneys. A size under 100 nm prevents the recognition by phagocytic cells [11]. By surface modification, it can be easily obtained selected surface charges, avoid opsonization phenomena, that is the adsorption of serum proteins to the surface of the particles, thereby making them more visible to phagocytic cells [12]. The charged ones can interact with proteins, but negative charges on nanoparticles (NPs) are known to facilitate deep penetration into tumors in vivo. Thus, compared to classical liposomes or polymeric nanocarriers, additional functionalities become possible with hybrid nanosystems: they can be used as a) contrast agents, b) "theranostic agents" and for c) complementary anticancer effects, like thermal therapy, which consists in local heating by varied stimuli, leading to tissue destruction [13,14]. Compared to structures based only on polymers, nanohybrids also permit the use of a large panel of analytical methods, which facilitates their characterization, and their monitoring in vitro and in vivo.

This review focuses on nanohybrids made of two types of MNPs. MNPs in iron oxides such as magnetite (Fe_3O_4) or its oxidized form maghemite (γ-Fe_2O_3), known as superparamagnetic iron oxide nanoparticles (SPIONs) or ultrasmall superparamagnetic iron oxide nanoparticles (USPIOs), are by far the most commonly employed materials for biomedical applications [11]. The term USPIO is generally used when the hydrodynamic diameter (d_H) of the NPs, that is its diameter with the solvatation layer, is around 20 nm [15]. Magnetic ferrofluids are stable colloidal suspensions of magnetic NPs dispersed in organic or inorganic liquids, normally in water for biomedical applications. They generally present a core crystal size equal to or below 10 nm. The size of the crystals confers them "superparamagnetic properties". The magnetic moment of NPs arises from the coupling of many atomic spins. Compared to paramagnetic materials, their magnetization is much higher, similar to ferromagnetic materials, but it disappears as soon as the magnetic field is switched off. Their magnetic properties are useful for magnetic targeting, magnetic resonance imaging (MRI) contrast, and thermal therapy, in addition to a chemotherapeutic treatment. We focus this review on SPION-based nanohybrids, because they have been studied for a long time, and have been used in a variety of innovative strategies [16].

The second type of MNPs treated in this review is gold nanoparticles (Au-NPs). The Au-NPs present interesting optical properties such as light absorption and light scattering. These particles possess a plasmon resonance [17]: this is a resonant phenomenon whereby light induces collective oscillations of conductive metal electrons at the NP surface. The electron oscillation induces a surface electromagnetic field. The light-induced plasmon resonance of the Au-NPs is tunable to different wavelengths by varying the NP size. Their plasmonic field is able to enhance Raman scattering and fluorescence emission of adjacent molecules. It makes them very useful for molecular cancer imaging [10], and for analytical methods like Surface Enhanced Raman Scattering (SERS) spectroscopy [18–21]. We focus this review on Au-NPs-based nanohybrids, because they have been widely exploited for imaging, and just begin to be used as drug delivery systems.

To explore drug delivery with SPIONs and Au-NPs, we focused our discussion on hybrid nanocarriers for doxorubicin (DOX) anticancer drug delivery. DOX appears as a good candidate, because it is one of the most commonly used therapeutic agents [22]. This is the drug model used in numerous published studies on nanocarriers, due to the central anthracycline group, responsible for the intrinsic fluorescence of the DOX molecule (Fig. 1). DOX distribution can be visualized in tissues or cells by fluorescence-based microscopy and imaging [22]. It is also one of the few drugs to be on the market in vectorized form (Doxil®/Caelyx®, PEGylated liposomal formulations). Modifying its biodistribution and clearance by vectorization should reduce its cardiotoxicity [23] and hemotoxicity [24] which limited the use in its molecular form.

The aim of this paper is to give an overview of recent publications and advances in the delivery of DOX with hybrid nanocarriers based on SPIONs and Au-NPs. We develop examples of the methods used for loading DOX on SPION- and Au-NP-based nanocarriers and their consequences on drug release, as well as in vitro and in vivo evaluations of such systems. We also discuss the expected efficacy of such nanosystems and the real needs for DOX delivery.

2. DOX loading and release strategies with hybrid nanocarriers

DOX loading on SPIONs and Au-NPs largely depends on the chemical and physical properties of NP surfaces and coating. Several methods can be used to load DOX: a) by adsorption on the nanocarrier inorganic core; b) by diffusion or entrapment in the coating materials; and c) by chemical bonds with the coating of the nanocarrier.

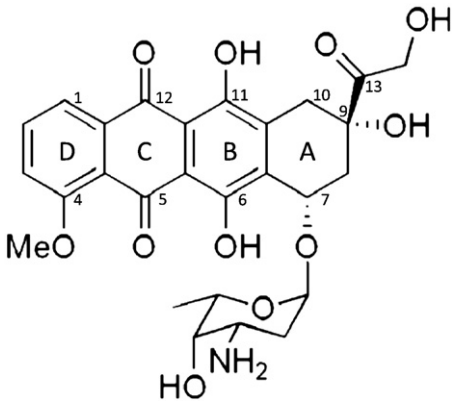

Fig. 1. Doxorubicin structure.

Because DOX is both amphiphilic (hydrophilic sugar part, lipophilic anthraquinone part) and amphoteric (ionizable functions) (Fig. 1), the molecule can be loaded into hydrophilic or lipophilic materials, and its affinity for materials is closely related to pH conditions [25]. DOX affinity for coating materials can consist in the interaction of DOX base with hydrophobic polymers, ion exchange of its protonated form with anionic polymers, or hydrogen bonds. When covalent bonds are used, they have to be cleavable to release the drug. Moreover, the attachment of the DOX molecule on nanocarriers via the anthracycline moiety quenches its fluorescence, so the amine group of the sugar is most often used for linkage (Fig. 1).

Most nanosystems described in this part are schematized in Fig. 2. Depending on the coating material used, very different release profiles can be obtained. Besides, many systems use stimuli-responsive strategies, like reduction-dependent, temperature-dependent or NIR light-dependent release. The most popular strategy is a pH-dependent release, since nanocarriers are usually internalized into cells by endocytosis, and end up in endosomes/lysosomes where the decreasing pH values (6.5 to 4.5) can accelerate the release. In addition, the tumor environment is known to be more acidic (6.8–6.9) than healthy tissues (7.4), making pH-dependent release especially attractive for achieving tumor targeting [26].

We are conscious that the observed release kinetics are only in vitro models and cannot be directly extrapolated to intracellular or in vivo kinetics; but they supply clues about the future behavior of nanocarriers in vivo, and raise important questions. The development of DOX nanocarriers, or more generally nanosystems for in vivo applications, must keep in mind the feasibility of the final formulation, industrial scale-up and parameters related to the patient.

2.1. Adsorption of DOX on nanocarrier surface

2.1.1. Free DOX

You et al. chose an adsorption method, by mixing hollow gold nanospheres (PEGylated or not, via Au – S strong covalent bonding) with DOX for 24 h at room temperature, and washing repeatedly to remove unbound DOX [27]. They suggest that DOX, positively charged at pH 7.4, was adsorbed onto the gold surface, stabilized by negatively charged citrates, via electrostatic interaction (Fig. 2A). They also suggest that their high DOX payload (63% DOX by weight, ~1.7 μg DOX/μg Au) is due to the geometry of their carriers. Indeed, the shell of their hollow carriers seems to be porous, and with their inner and outer surface areas combined, they possess a 3.2-fold greater surface area than solid nanoparticles for the same quantity of gold.

A burst effect (significant initial release) was observed with PEGylated or non-PEGylated hollow gold nanospheres releasing 15–20% of total DOX load over a 2-day period [27]. No further release was observed in different media (water, PBS pH 7.0 or cell culture medium). The group suggests that the electrostatic adsorption of DOX is quite stable.

But several other elements must be taken into account: a) release studies were performed at room temperature; a temperature elevation could enhance molecular agitation and DOX release; and b) the release volume chosen might not be well adapted to the nanosystem concentration; a greater volume should displace the equilibrium and favor DOX release.

The influence of pH on DOX release was tested because at low pH the citrate groups on the surface become protonated, which reduces the electrostatic interaction with DOX, and at the same time the fully protonated amine of the DOX increases the water solubility of the molecule. As expected, the release of DOX after 24 h is increased at low pH: around 50% at pH 3.0, around 25% at pH 5.0 against 10% at pH 7.4 [27]. Like several other DOX-loaded nano-objects, a total DOX release is not obtained [28,29].

Finally, You et al. also studied DOX release aided by a 5 min NIR laser irradiation (4.0 W/cm^2 output power). The cumulative release increased significantly from 4.1 to 31.9% for PEGylated hollow gold nanospheres during the 5 min of laser application, but stopped when it was switched off. A second laser irradiation after one hour induced a lesser DOX release, and a third one did not increase the yield any further. The effect of irradiation is due to plasmon absorption of these hollow nanostructures in the near infrared, translating into an increase in temperature (by 30 °C for PEGylated hollow nanospheres).

This model could be an interesting approach, with NIR induced DOX release for chemotherapy, and photothermal ablation of a tumor. The behavior of the system must be studied in vivo to confirm the robustness of the concept, namely a) the poor loss of DOX on the first two days, b) the behavior at 37 °C, c) the total quantity of DOX released, and d) the feasibility of NIR irradiation.

2.1.2. DOX complexes

2.1.2.1. DOX–Fe^{2+} complex. Munnier et al. developed an original approach for loading DOX on SPIONs, using a pre-formed complex of the drug with ferrous ion (Fe^{2+}) (Fig. 2B) [30]. The iron promoted the deprotonation of the phenolic groups at positions C6 and C11 and linked the complex to the iron oxide particle surface. Munnier et al. were able to load 14% w/w DOX on citrated SPIONs [30]. This method can also be used with PEG-coated SPIONs, since the diffusion of the complex through the polymer is similar to that of free DOX. Gautier et al. noticed a saturation of DOX loading at 3% w/w on PEGylated SPIONs [31]. This result was expected, since the access of the DOX–Fe^{2+} complex to the SPION surface was limited: coating materials occupied the hydroxyl groups on the surface, and PEG chains generated steric hindrance.

This leads to a progressive release of 60% of total DOX in 2 h at physiological pH, and 100% in 1 h in acidic conditions [30,31]. We suppose that only a part of the DOX–Fe^{2+} complex interacts with the surface of SPIONs (Fig. 3), but an appreciable part may be entrapped in the polymer. At acidic pH, the DOX–Fe^{2+} complex dissociates and its release by diffusion will be facilitated (Fig. 3).

2.1.2.2. Intercalation of DOX with aptamers. Min et al. loaded DOX on SPIONs by intercalation with targeting aptamers [32]. Aptamers are oligonucleic acid or peptide molecules that bind to a specific target molecule. In this study, the RNA aptamer A10 targets a membrane glycoprotein over-expressed in prostate cancer cells, and the peptide aptamer DUP-1 targets prostate cancer cells without this marker: so the nanosystems were designed to exhibit good selectivity for both types of cancer cell lines. As DOX can bind to double-strand nucleotides like A10 (Fig. 2C), associating drug and ligand has certain analytical advantages: DOX fluorescence is quenched by intercalation, which permits to monitor the DOX binding on aptamers and its binding efficacy by measuring the decrease of the fluorescence signal. Furthermore, as loaded nanocarriers do not fluoresce, DOX release can be followed in real time in the cell.

Unfortunately, fluorescence measurements in cells are only semi-quantitative, as the intensity can vary as a function of the environment of the DOX molecule. This loading by intercalation also raises the question of the quantity of DOX loaded: one DOX molecule for two aptamer ligands, with an unknown quantity of ligands loaded on SPIONs. Another problem is the evaluation of DOX release. Aptamers specifically bind to membrane glycoproteins, and can favor the entry of nanosystems into targeted tumorous cells. But in order to reach the nucleus, DOX has to be released from aptamers. In these conditions, a classical in vitro release study would not be relevant.

2.2. Affinity of DOX for coating materials

2.2.1. DOX diffusion in coating materials

2.2.1.1. Lipid based systems. Ying et al. chose to dissolve DOX in its molecular form by diffusion in a layer of oleic acid and monostearin,

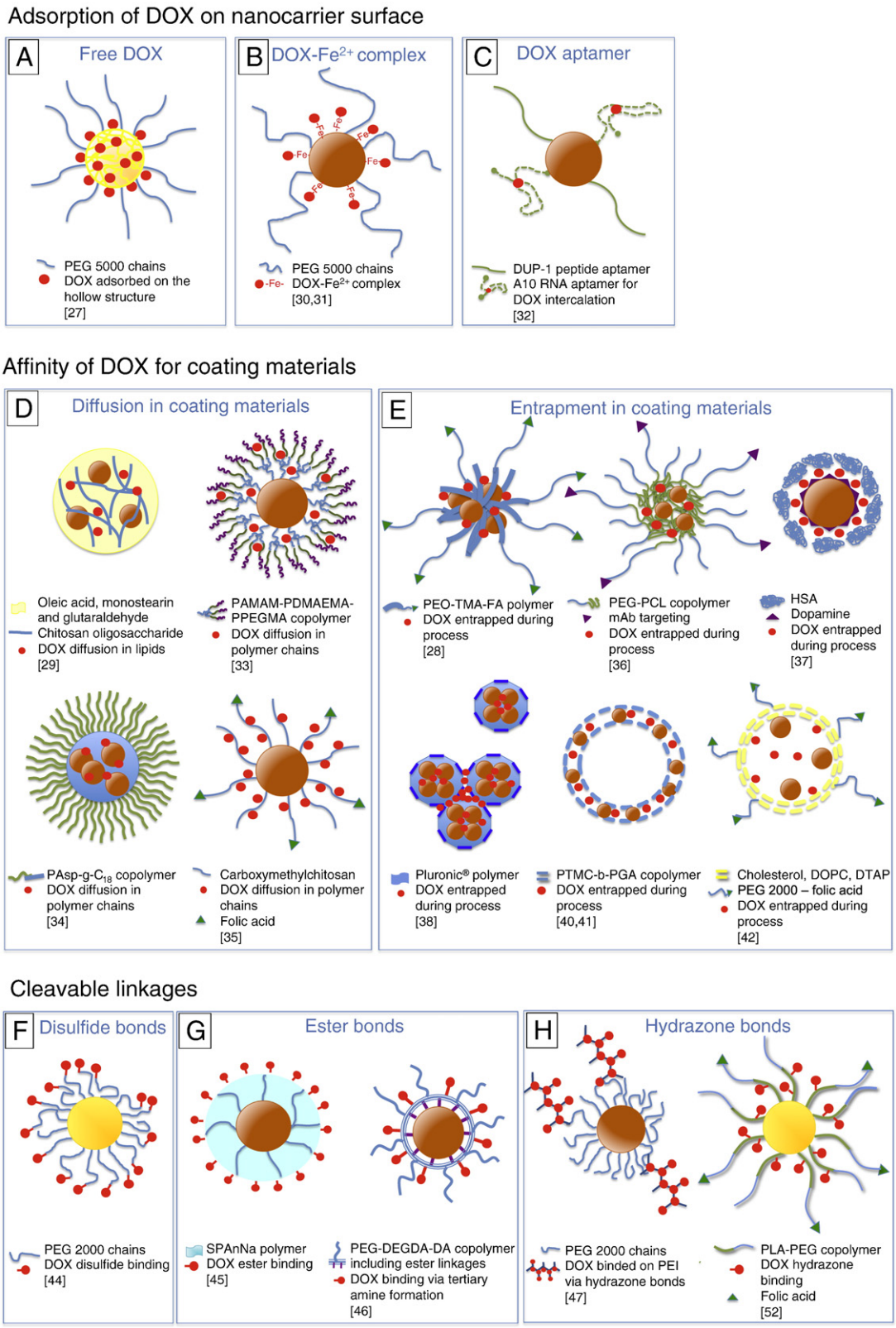

Fig. 2. DOX loading and release strategies on hybrid nanosystems based on SPIONs (●) and Au-NPs (●). A–C: DOX adsorbed on the surface of MNPs; D: DOX diffused in coating materials; E: DOX entrapped in coating materials during process; F–H: cleavable linkages used for DOX loading/release on coating materials. DA dopamine; DEGDA di(ethylene glycol) diacrylate; DOPC 1,2-dioleoyl-glycero-3-phosphocholine; DTAP dipalmitoyl-trimethylammonium-propane; FA folic acid; HAS human serum albumin; PAMAM polyamidoamine; Pasp-g-C18 poly(aspartic acid) grafted with octadecyl; PCL poly(ε-caprolactone); PDMAEMA poly(2-(dimethylamino)ethyl methacrylate); PEG polyethylene glycol; PEI polyethylene imine; PEO polyethylene oxide; PLA poly(L-aspartate); PPEGMA poly(poly(ethylene glycol) methyl ether methacrylate); PTMC-b-PGA poly(trimethylene carbonate)-poly(L-glutamic acid); SPAnNa polyaniline-co-sodium N-(1-one-butyric acid) aniline; TMA trimellitic anhydride chloride.

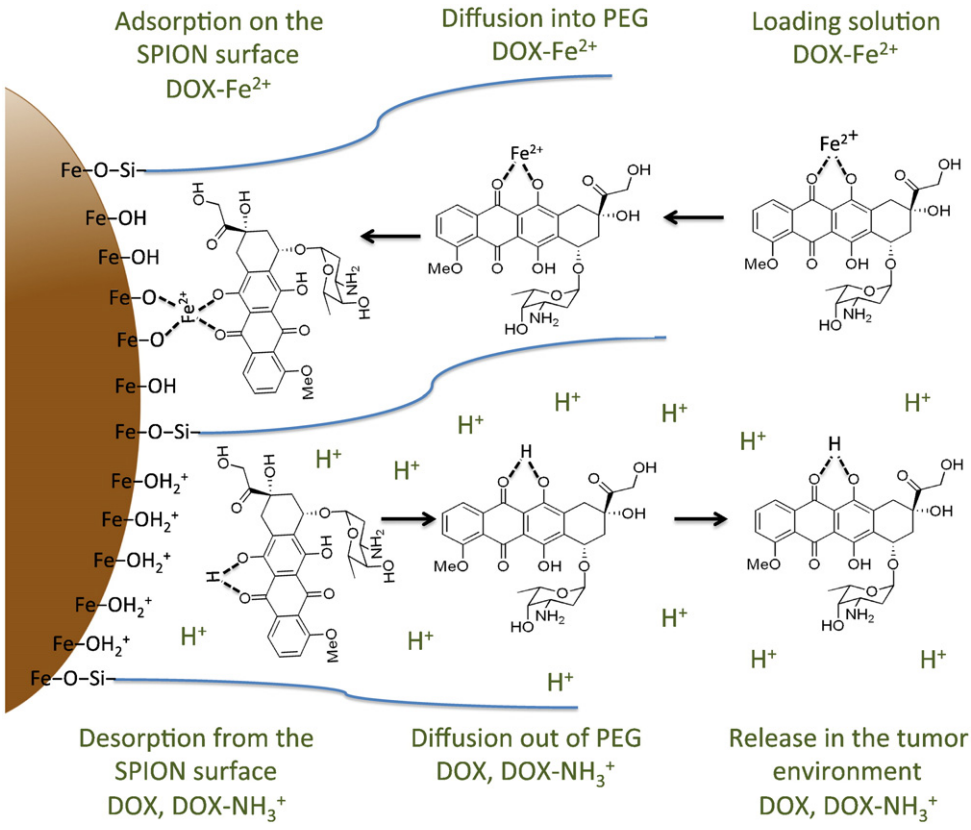

Fig. 3. Schematic diagram of DOX–Fe^{2+} complex binding to the PEGylated SPION surface (pH 7.4) and subsequent drug release (acidic pH 6.5 to 4.5). Adapted from [31].

composing solid lipid nanoparticles (SLN) entrapping SPIONs (Fig. 2D) [29]. The nanovectors were functionalized with chitosan oligosaccharide cross-linked with glutaraldehyde, thus modulating the SLN size and zeta potential, DOX content and its in vitro release, as well as the SLN uptake by tumor cells. The diffusion of DOX in lipid layers requires the use of organic solvents (here DMSO and ethanol, quite difficult to eliminate from the suspensions), and such systems often lead to very low loaded quantities of DOX (here, between 1.1% and 12.3% as a function of the ratios of oleic acid, monostearin and DOX). Indeed, the DOX loading must be sufficient to obtain a therapeutic dose on the site of action, while minimizing the quantity and concentration of nanocarriers administered.

The authors observed a marked burst effect with the release in 2 h of about 40% of DOX loaded on one of magnetic SLN formulations. The choice of loading DOX by diffusion implies a concentration gradient in the lipidic material, the surface being in equilibrium with a relatively concentrated DOX solution. As DOX loaded carriers are diluted in PBS, a burst effect can be observed.

With diffusion methods in such systems, DOX is under its free form, and its optical properties like UV–vis absorbance and fluorescence are conserved, which is an advantage for the nanocarrier characterization, and its monitoring in vitro. The rapid release implies that the nanosystems have to reach their target in vivo in less than 2 h, in order to avoid distribution in the whole organism and in organs subject to side effects.

2.2.1.2. Amphiphilic polymer based systems. He et al. also chose diffusion to load DOX on dendritic–linear–brush-like triblock copolymer-grafted SPIONs, prepared by click-chemistry (Fig. 2D) [33]. Here DOX is loaded for 24 h via hydrophobic interactions with PDMAEMA (poly(2-(dimethylamino)ethyl methacrylate)) chains, the hydrophobic central part of the copolymer. The loaded quantities are estimated about 6% w/w. This relatively low loading is probably due to the thickness of the polymer shell.

Yang et al. loaded DOX into their copolymer-coated SPION nanocarriers at basic pH by diffusion (Fig. 2D) [34]. They modified the poly(aspartic acid) polymer (PAsp) by grafting an octadecyl chain. The resulting copolymer, named Pasp-g-C_{18}, allowed the self-assembly in compact nanoparticles, with a hydrophobic core of C_{18} chains, and an outer shell of hydrophilic Pasp. The hydrophobic core contained only 2.9 ± 0.2 wt.% of DOX. This could be due to the reduced time of contact (30 min) between DOX and nanocarriers, or to the difficulty for DOX to cross the hydrophilic outer layer.

Contrary to lipid-based systems, the use of both hydrophilic and hydrophobic copolymers permits to load DOX in the hydrophobic part, but modulate the release with the hydrophilic part. Thus He et al. observed a rapid initial release, followed by a slow and sustained release, at pH 7.4 and 4.7. The maximum quantity released is observed at acidic pH, 83% within 48 h [33]. At low pH, both DOX and the polymer are protonated, decreasing their affinity. Furthermore, PDMAEMA chains tend to swell at acidic pH due to the protonated tertiary amino groups, which could accelerate DOX release. Yang et al. observed the same behavior, with markedly higher retention, since polymeric nanocarriers release only about 30% of DOX loaded [34]. This difference can be explained by the different affinity of DOX for the polymers used.

2.2.1.3. Hydrophilic polymer based systems. Sahu et al. loaded water-soluble DOX hydrochloride into the SPION chitosan layer by diffusion (Fig. 2D, see also Section 3.3.2 for targeting with folic acid) [35]. As they noticed, the thickness of the layer determined the quantity of DOX loaded. This type of loading has the advantage of giving useful loaded quantities (37% w/w), but often needs a long time of contact (12 h), because of slow diffusion in a concentration gradient.

After a first burst effect, the polysaccharide layer of Sahu et al. modulated release: after 96 h, only about 50% of DOX was released at pH 7.4 [35]. They also observed pH-dependent release: at lower pH the protonation of the free amino groups of chitosan led to a looser structure of the polymer, facilitating the diffusion of cationic DOX: approximately 21% of DOX loaded was released within 24 h at pH 7.4, against 52% at pH 5.1.

2.2.2. DOX entrapment in coating materials

2.2.2.1. Entrapment in a layer. Maeng et al. incorporated DOX base during preparation of polymer/SPION aggregates (Fig. 2E), and loaded 0.84 mg DOX/mg iron [28]. This remarkable quantity of drug loaded was obtained thanks to the protocol, where DOX base was mixed with Fe_3O_4 and the polymer (PEO–TMA–FA, poly(ethylene oxide)–(trimellitic anhydride chloride)–folate). In the aggregates, DOX was entrapped in the hydrophobic environment of the polymer. Liao et al. used a similar process for entrapment of DOX in copolymeric micelles (Fig. 2E). They used others types of copolymers, monomethoxy PEG–block–poly(ε-caprolactone) ($MPEG_{2000}$–PCL), mixed with maleimide–$MPEG_{3000}$–PCL [36]. The copolymers self-assembled to a hydrophobic PCL core, entrapping SPIONs and DOX, and a hydrophilic shell of PEG (Fig. 2E) [36]. This "one-pot" process gave better loading rates compared to simple diffusion in a polymer.

Quan et al. also obtained a high DOX loading, upon mixing DOX during the preparation of HSA (Human Serum Albumin)-coated SPIONs [37]. SPIONs were first modified with dopamine, offering an amine-rich surface for the adsorption of HSA. DOX was entrapped simultaneously in the protein layer, presumably via hydrogen bonding (Fig. 2E). The loaded DOX/Fe/HSA ratio was 1:2:20 (w/w/w). The entire quantity of DOX loaded was released in about 75 h in a sustained manner. Unfortunately, release profiles were measured only at pH 7.4. The authors suppose that a lower pH could weaken the interaction between DOX and HSA, and the release could be accelerated.

Park et al. chose a tri-block co-polymer Pluronic® (PEO–PPO–PEO, F127), to coat magnetite nanoparticles [38]. As this polymer is thermoresponsive, a self-assembly was observed when increasing the temperature of the mixture to 37 °C. At this temperature, the copolymer contracts and hydrophobic PPO blocks can be anchored to each other, to form aggregates of coated SPIONs. During the self-association of the copolymer, the hydrophobic form of doxorubicin, in the presence of tri-ethylamine, is simultaneously co-encapsulated in nanoparticle aggregates (Fig. 2E). A high ratio of Pluronic® to SPIONs permitted to cluster a high quantity of nanoparticles, and the higher NP surface areas subsequently maximized strong hydrophobic interactions between DOX and nanoparticles, increasing the quantity of DOX loaded.

As the Fe_30_4–thiol linkage used to attach Pluronic® on NPs can be cleaved by chemical reduction, the release rate of DOX was significantly enhanced by addition of DTT (dithiothreitol, a reducing agent): around 40% in 24 h, instead of 10% in PBS only. Thus, DOX is more completely released due to the liberation of Pluronic® moieties from the nanoparticles. This release under reducing conditions is an original approach for the delivery of DOX in cancer cells, because small cytosolic organelles such as endosomes and lysosomes are known to possess reducing power [39]. The authors speculate that "DOX can only be dissociated from the MNPs (magnetic nanoparticles) within cells, but not during the systemic circulation when those particles are intravenously administered". Of course, such drug delivery to tumors without any premature drug release in the blood flow would be ideal.

2.2.2.2. Entrapment in a bilayer. Another original approach was the entrapment of DOX and USPIOs in the bilayer of a polymeric vesicle (Fig. 2E) [40,41]. Sanson et al. added water to a DMSO solution of poly(trimethylene carbonate)–poly(L-glutamic acid) block copolymer (PTMC–b–PGA), promoting the formation of bilayer vesicles. During their formation, DOX and USPIOs present in the DMSO solution, were loaded into the inner hydrophobic part (PTMC) of the bilayer. The available volume of the bilayer limited the quantity of DOX and SPIONs loaded. More importantly, PTMC is temperature-sensitive due to its semi-crystalline structure. The release kinetics observed for different temperatures possessed the same profile: after an early burst effect, a plateau appeared after 8 h. However, the total amount of DOX released depended strongly on temperature: 5% at 5 °C, 30% at 20 °C, 60% at 37 °C, and 85% at 45 °C. The heat is believed to increase the fluidity of this polymer, increasing dramatically the diffusion of the entrapped DOX out of the membrane. With the application of an oscillating magnetic field of frequency 500 kHz, USPIOs sequestrated in the bilayer are known to dissipate heat originating from "friction losses" of their magnetic dipoles. After 7 h of magnetic field, the amount of DOX released was 2-fold higher than without the field. No macroscopic elevation of temperature was observed. These polymeric vesicles may be an interesting design to modulate the DOX release directly at the targeted site.

2.2.2.3. Entrapment in a core. Bothun et al. entrapped DOX in magnetoliposomes (Fig. 2E), by hydration of dry lipid films with a DOX solution and SPIONs, in order to provide drug delivery by hyperthermia [42]. The lipid bilayer was composed of cholesterol, DOPC (a phospholipid) and DPTAP (dipalmitoyl–trimethylammonium–propane). The electrostatic attraction between anionic SPIONs and the cationic inner lipids must have permitted to cover the inner surface of liposomes with SPIONs.

As expected, the entrapment efficacy of DOX was high (89%). But what about the release of DOX through a hydrophobic bilayer? Bothun et al. tested the DOX release with and without the application of an alternative electromagnetic field at radio frequencies (RF-heating). The 2 h release kinetics were monitored by the ratio of fluorescence intensities I_{RF}/I_0 obtained with (I_{RF}) or without (I_0) the RF-heating. After 80 min of dialysis, the DOX fluorescence intensities were 4-fold higher in the presence of RF-heating than without heating. Hayashi et al. also showed in vitro that their system (SPIONs functionalized with β-cyclodextrin as drug carrier and folic acid as a ligand) could generate heat, which accelerated the release of different fluorescent molecules [43].

Contrary to the study of polymeric vesicles made by Sanson et al. and described in the previous section [40], Bothun et al. observed with their magnetoliposomes a significant increase of temperature in vitro (about 9 °C) that may favor a faster release of DOX [42]. The authors suggested that the accelerated release of DOX could not be due to the heating of the lipids that were chosen to be in a fluid state, and therefore should not undergo any phase transition. They rather believe that the drug release could be mechanically stimulated by the oscillation of SPIONs bound to the lipid bilayer or situated near it.

2.3. Cleavable linkages

2.3.1. Disulfide bonds

Gu et al. coated their Au-NPs with PEG–NH_2, thus incorporating functional groups for DOX conjugation [44]. By the incorporation of a terminal thiol on the polymer (PEG–SH), the thiol-modified DOX could be bound to the end of the polymer chains via a disulfide bond (Fig. 2F). They postulated that upon endocytic entry, the disulfide bond could be cleaved by thiol-reducing enzymes, aided by the acidic pH in lysosomes. DOX was located outside the polymer chains, and then possessed a limited number of linking sites. Nevertheless, they estimated a concentration of 70 μM of DOX/240 μM of Au in their Au–PEG–SS–DOX NPs, which represents 0.3 μM of DOX/μM Au.

2.3.2. Ester bonds

Hua et al. activated the carboxyl groups at the surface of SPAnNa-coated SPIONs (poly [aniline-co-sodium N-(1-one-butyric acid) aniline]), in order to couple primary amine groups of DOX with resultant

active esters (Fig. 2G) [45]. The quantity of loaded DOX was 271 μg/mg of nanosystems, which corresponded to a 27.1% w/w payload. Unfortunately, the release kinetics at different pH were not reported.

Fang et al. also used ester bonds in the structure of the polymer layer to modulate the release of DOX as a function of pH [46]. In order to increase the number of potential binding sites for DOX, Fang et al. directly incorporated DOX into the backbone of their PBAE polymer (poly(beta-amino ester), a PEG-based copolymer with DEGDA (di(ethylene glycol) diacrylate) and dopamine), via its primary amine group (Fig. 2G) [46]. Thus the PBAE backbone contained tertiary amine groups close to ester bonds. The polymer was then conjugated on the surface of SPIONs. The high DOX content (9.5% of the total PBAE weight) permitted to produce nanoparticles with 679 μg of DOX/mg of iron. Fang et al. underlined that a "high drug loading is preferable since it would reduce the dose of pharmaceutically inactive ingredients, minimizing unintended toxicity and improving the safety profile of nanoparticle-based therapeutics". Furthermore, the stability of the bonds between DOX and the polymer would allow sufficient delay for the nanosystem to reach the tumor site and to be internalized by tumor cells, without releasing DOX prematurely. Besides, the polymer backbone is pH-sensitive: acidic pH promotes the degradation of the polymer (ester linkages), followed by the release of DOX. At 72 h, over 30% of loaded DOX was released at pH 7.4, against 40% at pH 6.4 and 55% at pH 5.5.

2.3.3. Hydrazone bonds

Instead of loading DOX in a polymer layer, Kievit et al. used PEI (polyethylene imine) as a docking molecule for the attachment of DOX to PEGylated SPIONs (Fig. 2H) [47]. A high quantity of DOX, i.e. 1089 ± 21 molecules per NP was covalently attached to PEI by a pH-sensitive hydrazone bond. This work, however, raises the problem of cytotoxicity of PEI, which penetrates easily into the nucleus. There, it interacts with DNA and prevents its normal transcription [48,49]. Its buffering capacity also prevents normal acidification of endosomal vesicles and degradation of endosomal content. Kievit et al. used a low molecular weight PEI, known to be less toxic. PEI conjugation to biocompatible polymers (here PEG) greatly reduces cytotoxic effects while maintaining a significant buffering capacity [50]. When monitoring the release, Kievit et al. observed a burst effect in 1 h followed by a plateau, at any pH between 4.5 and 7.5 [47]. The pH-sensitive hydrazone linkage did not modify release kinetics, but permitted to enhance the quantity released under acidic conditions. Unfortunately, the percentage of DOX released did not exceed 30% of its initial quantity. This could be due to hydrophobic interactions between DOX and the polymer after cleavage of the hydrazone bound [51].

On the NPs developed by Prabaharan's group, which are Au-NPs coated by an amphiphilic block copolymer, DOX was conjugated onto the hydrophobic inner shell by an acid-cleavable hydrazone linkage (Fig. 2H) [52]. To be loaded onto NPs, DOX had to cross the outer PEG shell (MW 3000) to reach hydrazide sites in the hydrophobic poly (L-aspartate) (PLA) inner shell. Diffusion kinetics imposed 24 h of contact between DOX and NPs, and 48 h of dialysis to remove unreacted DOX. Although this technique takes some time, DOX loading was high and equivalent to 17% w/w, which corresponded to 47 DOX molecules per Au-NP.

The release was strongly pH-dependent, and certainly modulated by the polymer. Only 10% of DOX was released at pH 7.4 after 3 days, whereas the 45 h release at lower pH was almost total: 94 and 83% at pH 5.3 and 6.6 respectively. This should be particularly adapted for in vivo applications, avoiding premature DOX loss in the organism during nanocarrier circulation in blood and limiting side effects, releasing DOX preferentially in the more acidic tumor environment.

To conclude this part, we can make two general remarks. Firstly, most of the polymer or lipid-coated drug delivery nanosystems described in the literature release DOX only partially. Maeng et al. recovered only 56% of total DOX entrapped in PEO–TMA–FA coated magnetic nanoparticles in 24 h at pH 5.1 [28]; Yang's PEGylated multifunctional SPIONs only released 35% of DOX after 24 h at pH 5.3, and 40% after more than 75 h [53]; Fang et al. found 55% of the loaded DOX released in 72 h at pH 5.5, with copolymer coated SPIONs [46].

Secondly, the methods used for evaluating release, involving either dialysis or centrifugation after incubation, are open to criticism: DOX release can be underestimated because of adsorption of DOX on the dialysis membrane or precipitation of DOX in centrifugation tubes. The data must be interpreted with caution. Furthermore, the release profiles must be discussed with regard to in vitro and in vivo studies.

3. In vitro and in vivo evaluations

Hybrid nanocarriers based on MNPs loaded with DOX are particularly useful to explore the in vitro and in vivo behavior of such nanosystems. Using fluorescence imaging and elementary analysis of the metal it is possible to monitor the subcellular fate of DOX and nanocarriers in vitro and observe the effect of multidrug resistant cells in cytotoxicity assays. Moreover, the metallic core renders the DOX-loaded hybrid nanocarriers efficient as imaging diagnostic tools. Next to routine techniques like TEM (Transmission Electronic Microscopy) or MRI (Magnetic Resonance Imaging), emerging tools appear in the literature, like SERS (Surface-Enhanced Raman Scattering) and CT (Computed Tomography). The evaluation of the efficacy of targeting with biological ligands is increasingly reported in the literature, and targeting thanks to the magnetic properties of SPIONs is still relevant today. Last but not least, more and more studies explore the tumor reduction efficacy of DOX loaded on hybrid nanocarriers, with the development of complementary techniques like thermal therapy.

3.1. Hybrid nanocarriers as intracellular vehicle for DOX

3.1.1. To monitor the subcellular fate of vectorized DOX

As DOX can be visualized by its fluorescence, several assays use DOX as fluorescent marker [28,46,47,54]. The use of other fluorescent markers (like octadecylamine–fluorescein isothiocyanate (FITC–ODA) [29] or rhodamine isothiocyanate (RITC) [35]) permitted to monitor nanosystems by fluorescence microscopy, independently of DOX behavior. The optical properties of inorganic cores allow other techniques [44,55]. The intracellular DOX is usually detected by microscopic methods which most often do not allow to distinguish the drug released from that still attached to a carrier. This is why data obtained from cells treated with the drug-loaded nanocarriers are systematically compared with those treated with DOX solution.

3.1.1.1. DOX release in cells. Our group recently shed a light on the intracellular behavior of vectorized DOX on PEGylated SPIONs (Fig. 2B), thanks to confocal spectral imaging (CSI) [31,56]. Unlike conventional confocal fluorescence microscopy, CSI allows collecting not only the intensity of DOX fluorescence at a given wavelength, but its total emission spectrum, for each point scanned in living cells. This permits a) to distinguish very subtle modifications of DOX intrinsic fluorescence as a function of its molecular environment or its interactions (Fig. 4A), b) to build maps with a localization of the different spectra (Fig. 4B), and c) to make a semi-quantitative evaluation of the subcellular distribution of DOX (Fig. 4C). Thanks to spectral changes (wavelength shifts and increase/decrease of peak widths) induced by variations of the polarity and by DNA intercalation [57], one can distinguish the DOX molecules still inside the PEG coating of SPIONs (cytoplasmic spectrum in a more apolar environment, Cyt 1), from the DOX released into the cytoplasm (cytoplasmic spectrum Cyt 2, corresponding to a more polar environment than that of PEG) and the DOX having reached the nucleus (nuclear spectrum Nuc, with wavelength shifts due to DNA intercalation) [56].

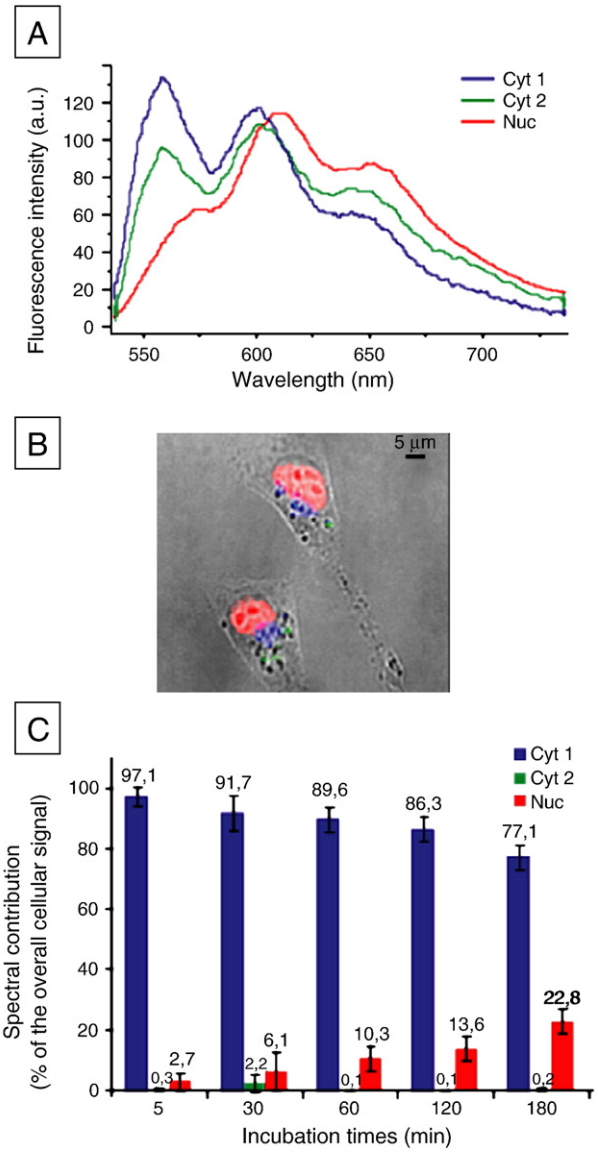

Fig. 4. Confocal spectral imaging results on the subcellular DOX distribution in live MCF-7 cancer cells. A: reference spectra used to fit the intracellular fluorescence (nuclear spectrum Nuc, and two cytoplasmic spectra Cyt 1 and Cyt 2, corresponding respectively to a more and less apolar molecular environment). B: Superposition of the maps of intracellular distribution of the spectra, using an extended intensity scale for colorization and encoded with pseudo colors. C: Contribution to the cellular fluorescence of the three spectra of DOX, as a function of time.
Adapted from [31].

The percentage of each contribution to fluorescence permitted to visualize the kinetics of DOX entering the nucleus. For example, it was found that the PEGylated nanocarriers were preferentially accumulated in lysosomes, and that the polymeric coating delayed the arrival of DOX in the nucleus, since after 180 min only 22.8% of the cellular signal was located in the nucleus (Fig. 4C) [31]. The progressive release of DOX from the lysosomes into the cytoplasm was ensured thanks to the acidic conditions in lysosomes.

Book Newell et al. monitored the uptake of DOX-loaded gold nanorods, DOX release and localization in living cells by multiphoton microscopy using fluorescence intensity and lifetime imaging [58]. As the DOX is directly bound on the surface of gold nanorods by electrostatic forces, its fluorescence is quenched until it is released from the carrier by pH changes. By the observation of the intrinsic photoluminescence of gold nanorods and variations of DOX fluorescence intensity, the fate of both DOX and nanocarriers can be observed as a function of time. After 2 h of incubation, nanorods are located in the cytoplasm, and spots of DOX fluorescence show its release in acidic medium, as in lysosomes. After 4 h, a greater quantity of DOX was released, but its proximity with the nanorods in the cytoplasm quenched its fluorescence, whereas after 16 h, DOX was detached from nanorods and its fluorescence was no longer quenched.

Quan et al. observed different kinetics for the entry of DOX into cells, with HSA-coated SPIONs (Fig. 2E) [37]. They monitored the DOX using fluorescence microscopy. After 5 min incubation of DOX-loaded HSA coated SPIONs, DOX was found in the nucleus, whereas treatment with DOX solution needed more time to reach the nucleus. The vectorization permitted to accelerate the entry process of DOX. But this could also be a clue concerning the behavior of nanocarriers. The fact that DOX reaches the cell nucleus in less than 5 min cannot be attributed to a rapid internalization of nanocarriers, followed by the release of DOX in intracellular compartments. The fast internalization of nanocarriers could explain the sustained effect of DOX in time, but not the early kinetics. The high affinity of HSA with cell membranes must be considered, facilitating the entry of DOX under free form. The authors noted that even if the mechanism is unknown at this stage, they hope it could be due to the design of their nanocarriers.

3.1.1.2. Intracellular behavior of nanocarriers. Gu et al. confirmed the entry of PEGylated Au-NPs (Fig. 2F) into the cells, with the gold concentration determined by inductively coupled plasma mass spectroscopy (ICP–MS) as a function of time [55]. Cellular uptake increased significantly for the first 6 h, and then reached a plateau. As the cellular uptake is dramatically reduced at 4 °C compared to 37 °C, this suggests an active phenomenon, like endocytosis. TEM images confirmed the internalization of PEGylated Au-NPs into cells and labelling the NPs with FITC resulted in fluorescence detected in nuclei. Purified nuclear fractions examined by confocal spectroscopy and ICP–MS confirmed the nuclear localization of NPs (ratio 1/3.6 between nucleus and cytoplasm), maybe due to a reduced size of the nanocarrier (28.2 ± 0.2 nm, against around 40 nm for nucleus pores). This could enhance treatment efficacy, since gold nanoparticles were recently reported to interact with DNA to induce oxidative stress and to have adverse effects on cytoskeletal structure and cell viability [59,60]. A supplementary study revealed that DOX was accumulated in cells, but preferentially in the lysosomes [44]. They hypothesized that after endocytic entry, thiol-reducing enzymes and acidic pH in lysosomes cleaved the disulfide bond between DOX and Au-NP. This implies that even if the entire nanocarrier can penetrate into the nucleus, delivery of DOX is more likely due to the drug released from lysosomes into the cytoplasm, rather than to nanoparticles reaching the nucleus.

3.1.2. To bypass the multi drug resistance (MDR) effect

This phenomenon, which limits the effectiveness of chemotherapy, is particularly important for DOX. It is generally due to the overexpression of ATP-binding cassette (ABC) or P-gp transporters that increase the efflux of a broad class of small molecules from cancer cells [61]. The activation of anti-apoptotic cellular defenses (e.g. overexpression of BCL2) is another mechanism of MDR [62,63]. Nanocarriers are particularly indicated to overcome MDR, and DOX bound to NPs bypasses the efflux pumps.

Kievit et al. evaluated in vitro PEG and PEI-coated SPIONs, designed in order to circumvent MDR (Fig. 2H) [47]. In this study, Kievit et al. developed a DOX resistant cell line (rat glioma C6-ADR cells). The cellular uptake showed an increase of intracellular DOX when incubated with the nanovectors, compared to free DOX, which seems to be pumped out of the cells. These results were completed with fluorescence imaging, showing an accumulation of DOX in the cell nucleus. On sensitive cells, the DOX-loaded nanocarriers were less efficient (IC_{50} about 520 ng/mL DOX) than DOX in solution after 72 h of

incubation (100 ng/mL). However, on resistant cells, the ratio was reversed (1700 ng/mL for nanocarriers and 5600 ng/mL for free DOX): the IC_{50} of DOX-loaded nanocarriers was 3 to 5-fold lower than of free DOX.

Fang et al. also used C6-ADR cells to evaluate PBAE-coated SPIONs (Fig. 2G) [46]. If between DOX-loaded nanoparticles and free DOX the IC_{50} was comparable for an incubation of 24 h, this was not the case for longer incubation times. Nanocarriers showed a 3-fold lower value (0.39 μg/mL, which is around 0.7 μM) than free DOX (1.10 μg/mL, which is around 2 μM) after an incubation of 72 h. These IC_{50} values are in accordance with the results published by Kievit et al. [47]. Similar results were obtained with Au-NPs: Gu et al. compared the cytotoxicity of DOX-loaded PEGylated Au-NPs (Fig. 2F) with that of free DOX on two cell lines (human hepatoma cells HepG2, and HepG2-R, a MDR subline) [44]. Over 24 h, and for a wide range of concentrations (from 1 to 20 μM of DOX), nanosystems were more cytotoxic for MDR cells compared to free DOX, but less effective on the sensitive cell line.

The cellular uptake of free DOX is greater than with DOX-loaded nanosystems, which explains why DOX is more effective than carriers for DOX sensitive cell lines. Furthermore, the NP uptake and drug release kinetics disadvantage the anticancer effect of nanocarried drug, in vitro, compared to free DOX. In contrast, MDR cells actively pump out free DOX, whereas nanocarriers bypass this system, enhancing their efficacy on these cell lines. The use of drug resistant cells seems to be an appropriate alternative compared to classical cell lines, since the main advantage for the nanocarriers is the pump efflux bypassing. One should also consider that the incubation times chosen are often quite long, because of the nature of the nanosystems: the sustained release of DOX explains that the short-term cytotoxicity is often reduced, compared to free DOX. Whereas free DOX is rapidly internalized and reaches the cell nucleus, the nanocarried drug needs time for diffusion out of the coating [29,35], or for bond cleavage under particular conditions (acidic [31], reducing environment [38]).

3.2. Hybrid nanocarriers as diagnostic tools

3.2.1. In vitro imaging

3.2.1.1. Transmission Electronic Microscopy (TEM). The high atomic number of gold provides good contrast for visualizing Au-NPs by transmission electron microscopy (TEM). SPIONs are less contrasting but can also be quite easily visualized by TEM. This high-resolution bio-imaging tool permits to examine the biodistribution of Au-NPs and SPIONs and the respective hybrids of gold and iron oxide nanoparticle cores at different times in cells and tissue samples, hinting at the presence of hybrid nanocarriers.

The TEM images found in the literature concern thin sections of organs or cell cultures, and are mainly employed to observe the intracellular distribution of nanocarriers. The goals of these studies may be quite varied.

For example, in a toxicity study, Mahmoudi et al. observed the presence of gas vesicles in the vicinity of uncoated SPIONs in L929 cells, after 72 h of incubation [64]. Kneipp et al. used TEM imaging to observe the aggregation of gold NPs in intracellular compartments as a function of time and correlated them with SERS signal enhancement (see paragraph below) for intracellular biosensoring [65]. Nativo et al. followed the interactions between HeLa cells and gold NPs with different ligand shells (stabilized with citrates, coated with PEG derivatives or with pentapeptides) [66]. They observed caveolae and clathrin-mediated endocytosis, internalization in endosomes, and a nuclear entry of NPs.

3.2.1.2. Surface-Enhanced Raman Scattering (SERS). Au-NPs offer numerous advantages compared to other materials, particularly for Raman spectroscopy. These surface properties of Au-NPs mainly depend on their size and shape. Spherical gold particles display a single resonance at approximately 530 nm, whereas nanorods have a resonance shifted and broken into two absorption bands, one for the shorter axis, or transverse mode, and another for the longer axis, or longitudinal mode. The longitudinal mode has lower energy corresponding to an absorption at higher wavelengths than the transverse mode. In aggregated systems, there are multiple resonances within each given cluster of particles [19], and the Raman scattering efficiencies of adsorbed molecules are amplified, as much as 10^6 or even 10^{10}-fold [67]. This allows the use of Au-NPs for an analytical method like Surface-Enhanced Raman Scattering or SERS. SERS spectroscopy yields very structure-specific vibrational spectra, characteristic of a molecule [68]. Fine analysis of molecules like DOX by SERS on the surface of Ag and Au-NPs [18], in solution, or directly in cell cultures, was the subject of numerous published studies [20,21].

3.2.2. In vivo imaging

The diagnostic methods most often applied to cancer detection are magnetic resonance imaging (MRI), computed tomography (CT) and positron emission tomography (PET). A review of numerous imaging techniques available with Au-NPs is given elsewhere [69]. Unfortunately, to our knowledge, such imaging with Au-NPs based hybrid nanocarriers of DOX has not been reported yet. On the contrary, studies using SPIONs as contrast agents loaded with DOX can be found in the literature.

3.2.2.1. Magnetic resonance imaging (MRI). SPIONs can be used as contrast agents in MRI. Due to their significant magnetic moment, SPIONs can distort the local magnetic characteristics of the tissues, and thus enhance the imaging contrast. Certain types of SPIONs with core sizes of 3–6 nm and dextran coating (with hydrodynamic sizes of 20–150 nm) such as Feridex®/Endorem®, and Resovist®/Cliavist® have been approved for liver MRI in patients. Some of them were recently withdrawn from the market.

This MRI can be combined with the DOX delivery, in order to monitor the treatment. Such nanotheranostic carriers are widely studied in recent work [28,35].

Maeng et al. compared their SPION-based hybrid nanosystems (also called YCC, in reference to a sponsor of the work, Fig. 2E) to Resovist® [28]. In order to evaluate the usefulness of their nanohybrids as MRI contrast agents, they measured the signal intensity in vitro (on dilutions in plates) and in vivo (after intravenous injection in animals) using a MRI scanner. The MRI signal enhancement by the nanoparticles with or without DOX was higher compared to Resovist®, at the same iron concentration, both in vitro and in vivo. Hua et al. made the same observation with a similar DOX-loaded SPION-based system (Fig. 2G) [45]. Maeng et al. concluded that YCC–DOX and YCC are good candidates as MRI contrast agents. In the same way, Yang et al. used SPIONs coated with cyclic RGD (a peptide which targets neoangiogenesis in general, see Section 3.3.2). They verified the magnetic relaxivity of cRGD-coated and PEGylated SPIONs against Feridex I.V.® as a control, for MRI applications [53]. They especially designed DOX loaded ^{64}Cu-labeled SPIONs, in order to realize PET scans in mice tumorized by subcutaneous injection of U87MG cells. After intravenous injections, the uptake of nanocarriers in mouse liver was prominent at early time points and gradually declined over time. As expected, an appreciable amount of nanoparticles reached the tumor. The quantity of nanocarriers in the tumor was lower than in the liver but higher than in all other organs examined, indicating a certain tumor-targeting capability, thanks to cRGD.

MRI would be a perfect method with high spatial resolution and good contrast, if its sensibility was not too low [67]. This is why complementary techniques with better sensitivities are needed.

3.2.2.2. Computed Tomography (CT) and Positron Emission Tomography (PET) imaging. CT provides anatomical information thanks to the measurement of X-ray absorption of tissues. Discrimination between

the different tissues can be made, since the attenuation of X-rays depends on the electron density of the tissue. Even if CT offers a high spatial resolution, it suffers from a poor contrast in soft tissues. On the contrary, Positron Emission Tomography (PET) is very sensitive, but has a limited spatial resolution.

Gold possesses a high atomic number and electron density, so it should have a higher X-ray attenuation than iodine-based contrast agents, and therefore an increased sensitivity for CT imaging [70]. Thus gold-based contrast agents would be safer than iodine-based ones (causing severe allergies), would enhance the tissue contrast, and limit the X-ray exposition dose. In these conditions, CT could compete with MRI as a routine technique. Very recent papers present gold nanoparticles for CT, with various coatings (Au-NPs entrapped in dendrimers [71], coated with PEG [70], with transferrin [72] or with horse serum proteins [73]).

3.3. Hybrid nanocarriers as targeted drug delivery systems

3.3.1. Magnetic drug targeting (MDT)

In the late 1970's, Freeman et al. proposed the concept of using an external magnetic field coupled with magnetic carriers [74]. Because they are superparamagnetic, SPIONs can be used for macroscopic targeting of tumors, by focusing on them an external magnetic field. Properties of SPIONs are often studied for MRI contrast, but less frequently for magnetic targeting. Some reasons for this situation are exposed in the following.

3.3.1.1. Feasibility studies. Ganguly et al. studied the behavior of a ferrofluid droplet in a forced flow, mimicking basically blood or biological fluid flow [75]. They showed that the magnetic field, or rather its gradient, was there too weak to overcome the hydrodynamic force, and the ferrofluid droplet was transported downstream with the flow. The linear blood flow rates in tissues (>10 cm/s in arteries, >0.05 cm/s in capillaries) can limit the magnetic retention phenomena in the targeted tissues and, consequently, tumoral cell uptake.

Nevertheless, in vitro/in vivo studies establishing the feasibility of tumor targeting in mice with an extracorporeal magnet are published every once in a while [76,77]. Fortin-Ripoche et al. glued magnets (neodymium, iron, boron, magnetic field 0.29 T) on the outside of subcutaneous induced tumors in mice, and left them in place for 1–24 h, to test the concept of magnetic targeting with 200 nm magnetoliposomes [77]. The magnet-exposed tumors showed significantly higher enhancement in MRI signal than the contralateral control tumors. The signal was proportional to the doses of the nanosystem administered. The magnetoliposomes were preferentially situated in the vicinity of the magnet surface and in the vascular region, and remained in the tumor, as shown by the persistence of the signal after 16 h. The vascular uptake into the tumor was significantly higher with the use of an external magnet (15.9 ± 6.3% of injected NPs), than without magnet application (5 ± 1.3%) [77]. Another study demonstrated the accumulation of magnetic nanocarriers in tumor capillaries, followed by mild retention in the tumor interstitium, by using an external magnet with a magnetic field of 0.3 T and a field gradient of 11 T/m [76]. However, Fortin-Ripoche et al. reported that the use of a small extracorporeal magnet limited the technique to superficial tumors, without preventing significant liver uptake [76].

The feasibility of the concept was also demonstrated on humans. In 1999, Lübbe et al. reported the first phase I trial with a ferrofluid (SPIONs coated with a starch derivative) loaded with epirubicin, a doxorubicin analogue, on 14 patients with advanced solid tumors [78]. An external magnetic field (0.5 T to 0.8 T) was applied during infusion of ferrofluids, for 60 to 120 min, with a distance between tumor and magnet less than 0.5 cm. They demonstrated the feasibility of the concept by guiding ferrofluids into tumors in about half of the patients, as well as the safety of the ferrofluids used. It was nevertheless concluded that improvements were necessary, namely in ferrofluid design and properties, to increase the targeting efficacy, and make it less dependent on patient- or disease-related parameters. It also has to be considered that the efficacy of magnetic targeting by the application of an external field is dependent not only on SPION properties, but also on the choice of shell and type of drug linkage, as well as physiological parameters. If patient parameters like body weight and blood volume are naturally considered, the cardiac output and peripheral resistance of the circulation system must be taken into account [16,78].

3.3.1.2. DOX delivery with MDT. If feasibility studies are published, articles about the effect of magnetic targeting on DOX release and efficacy are very few. A recent study reports the magnetic targeting of DOX in cells and tumorized mice via polyaniline coated SPIONs (Fig. 2G) [45]. Drug resistant bladder-cancer cells (MGH-U1) were used to appreciate the effect of the application of a magnetic field. An in vitro cytotoxicity assay was performed with a 300 or 900 Gauss magnetic field applied beneath the culture plate. They showed that the cytotoxicity was enhanced by the combination of nanoparticles and magnetic field; the lowest IC_{50} values are obtained with higher magnetic field, and with nanocarriers possessing higher magnetization. In all cases, even without a magnetic field, IC_{50} values are lower than those observed for free DOX. In vivo studies led to the same conclusions as Fortin-Ripoche et al. [77]. They demonstrated an efficient accumulation of carriers not only in the tumor, but also in the liver. Unfortunately, no studies of the efficacy in tumor reduction were reported for the DOX-loaded hybrid nanocarriers.

Such a study was published by Dandamudi et al. for magnetic liposomes loaded with vinblastine [76], and not with DOX. They concluded that the application of a magnet of 1.2 T on the tumor for 1 h after injection of nanocarriers improved the tumor vascular uptake, prevented metastasis (no metastasis in the pleural cavity of mice treated with the magnet, contrary to all others groups) and limited the tumor growth. Indeed, the percentage of changes in tumor volume was significantly lower for the group of mice treated with the formulation in the presence of a magnet ($+24$%) when compared to the no-magnet group ($+94$%), mice treated with free vinblastine ($+270$%), and untreated animals ($+378$%).

In all the studies, it was noticed that magnetic targeting with an external magnet is only possible with superficial tumors. In fact, the field of commercial magnets is sufficient to retain nanoparticles up to a depth of a few millimeters into the tissue. Lübbe et al. were already aware of technical difficulties related to the generation of magnetic fields [78]. They noted that "the currently available inhomogeneous fields (were) only strong enough for the manipulation of particles against the diffusion and blood stream velocities found in living systems over a distance of a few centimeters from the sharp edge of a magnet pole." More recently, Ruenraroengsak et al. suggested that the wait for the arrival of more powerful and focused magnets has been the delaying factor for the development of such systems [79].

3.3.2. Biological targeting

Park et al. used A 549 cells (human lung cancer) incubated with DOX concentrations of 0 to 160 μM for 48 h to evaluate non-targeted Pluronic® coated SPIONs (Fig. 2E) [38]. They observed a 10-fold higher IC_{50} for their DOX-loaded nanocarriers compared to free DOX [38]. They attributed this result to a lack of release, due to the strong hydrophobic interactions between DOX and nanoparticles, but a possible lack of specificity of the nanocarriers may be also considered.

He et al. observed an IC_{50} of 2.72 and 0.72 μg/mL (about 5 and 1.3 μM), respectively, for non-targeted DOX-loaded SPIONs (Fig. 2D) and free DOX, after 24 h incubation on Hela cells (human cervix carcinoma cell line) [38]. This represents a 4-fold decreased cytotoxicity compared to free DOX.

In brief, non-targeted systems often present a reduced cytotoxic efficacy compared to free DOX. Targeting strategies seem to be

essential to gain a sufficient efficacy of tumorous cell uptake, and to make up slow release kinetics of DOX.

3.3.2.1. Folate. The folate (FA) receptor is a well-known target for drug delivery systems [80]. This receptor is highly expressed in several human cancers including breast, lung, ovarian and brain cancers. Folate-targeted NPs can enter the receptor-expressing cells via folate receptor-mediated endocytosis. This targeting method has been used for a long time and demonstrated its efficiency as simple tumor marker, as well as in nanocarrier targeting to tumors [81,82].

Prabaharan et al. compared DOX-loaded Au-NPs (Fig. 2H) to DOX in solution on two cell lines: mouse metastatic breast cancer 4T1 cells, with over-expression of FA receptor, and healthy mouse embryonic fibroblast NIH-3T3 cells, with normal expression of FA receptor [80]. The cytotoxicity of FA-targeted or non-targeted nanosystems was equivalent on normal cells. On the over-expressing cell line, only targeted systems promoted a decrease of cell viability (whereas non-targeted nanosystems had little effect). The addition of free folic acid to the culture medium hampered the targeted nanosystem uptake and increased its cytotoxicity. Unfortunately, the cytotoxicity of FA-targeted Au-NPs remained lower than that of free DOX in both cases, even if the efficacy of the targeting was demonstrated. The authors attribute the difference of cytotoxicity between nanocarriers and free DOX to the fast diffusion of the DOX molecule into the cell nuclei. One can also consider the slow and progressive release kinetics of DOX from nanocarriers.

Encouraging results were obtained by Maeng et al., who compared the in vitro toxicity of DOX-loaded PEO–TMA–FA coated SPIONs (Fig. 2E) with results obtained with free DOX and Doxil® (Hep3B human liver cancer cells, 24 and 48 h incubation, DOX concentrations 0.01 to 10 μM) [28]. A cell viability of 50% was obtained with free DOX concentrations around 10 μM for a 24 h incubation, and from 1 to 10 μM after 48 h. With FA-targeted nanosystems, the cell viability was equivalent to free DOX and significantly lower than Doxil®.

3.3.2.2. cRGD. Another well-known target for cancer cell drug delivery is the integrin $\alpha_v\beta_3$, highly expressed on the luminal surface of the endothelia cells during angiogenesis. One integrin $\alpha_v\beta_3$ antagonist is the cRGD peptide (cyclic arginine–glycine-aspartic acid).

Yang et al. used U87MG cells (human glioblastoma cells) with DOX concentrations from 10 to 40 μg/mL (20 to 80 μM) for 48 h to evaluate DOX-loaded SPIONs, with and without cRGD targeting [53]. The cytotoxicity of nanocarriers with a cRGD targeting peptide developed by Yang et al. was not significantly different from that of free DOX for a DOX concentration of 10 μg/mL. For higher DOX concentrations, the ligand permits to enhance the cytotoxicity compared to non-targeted systems, but not as much as free DOX.

3.3.2.3. Monoclonal antibodies (mAb). Liao et al. chose the epidermal growth factor receptor (EGFR) as target for polymeric micelles containing SPIONs and DOX (Fig. 2E) [36]. The broad expression of this receptor family in several tumor types and the possibility to block their signaling in cells (specifically involved in cancer proliferation) stimulated research in this domain [83]. Liao et al. used cetuximab, a human–murine chimeric anti EGFR IgG monoclonal antibody (mAb). In vitro assays (confocal laser scanning microscopy, flow cytometry and MRI studies) revealed an increased uptake of nanocarriers in EGFR-expressing cell lines. The decrease of cell viability due to DOX was accentuated after exposition to DOX-loaded targeted systems, compared to nontargeted systems. With non-expressing cell lines, the cell viability was equivalent. If this study hints at the interest of this targeted nanosystem, further points must be explored in more detail (the DOX release mechanism, the cell viability with free DOX), and in vivo studies are expected.

Deng et al. coated DOX-loaded PEGylated liposomes with a monoclonal antibody directed against mesothelin [15]. This is a differentiative antigen highly expressed in several human tumors, but not in adjacent healthy tissues. It is closely associated with tumor progression and migration in pancreatic cancer. They compared targeted and non-targeted DOX-loaded nanocarriers on Panc-1 cells (human pancreatic cancer line expressing mesothelin) in vitro and in vivo. MTT assays revealed an increased cytotoxicity of targeted nanocarriers (IC_{50} 1.95 μM instead of 3.5 μM for non-targeted nanocarriers). But both formulations exhibited less cytotoxicity than free DOX (IC_{50} 0.53 μM) for 24 h of incubation. The authors attribute this to the gradual DOX release from liposomes. Unfortunately, no release studies were performed. More interestingly, targeting seemed to increase the entry of nanocarriers into cells (studied by flow cytometry) and played a role in the increased accumulation in tumor tissues (as seen by MRI on tumorized mice). Effects on tumor growth seemed promising (see Section 3.4.1).

3.4. Metallic nanocarriers in tumor reduction

In a recent review about theranostic systems, Mura and Couvreur noted that even if articles with physico-chemical characterization and in vitro evaluations were numerous, the in vivo evaluations were limited [84].

3.4.1. Antitumor effect of DOX

Maeng et al. published one of the few studies of tumor reduction using SPIONs to vectorize the DOX molecule. They used rats and rabbits with induced or implanted liver tumors for the in vivo evaluation of DOX-loaded SPIONs (2.1 mg DOX/2.5 mg iron) coated with PEO–TMA–FA (Fig. 2E) [28]. The efficacy was compared with free DOX and Doxil® treatment (2 mg DOX equivalent/kg three times at 5-day intervals). The results showed that animals treated with nanocarriers developed tumors with volumes comparable to those treated with free DOX, but significantly lower than animals treated with Doxil® (Fig. 5). The efficiency to limit tumor growth was coupled with a decrease of classical side effects usually observed with DOX and Doxil®. The weight loss was insignificant, and other signs like hair loss and oral mucositis (observed with Doxil®), cell mortality or inflammatory cells in the heart (observed with free DOX and Doxil® treatment) were absent.

Quan et al. tested DOX-loaded SPIONs (0.5 mg DOX/mg SPION) coated with HSA (Fig. 2E) on nude mice bearing 4T1 breast tumors [37]. The comparison was made with free DOX and Doxil® treatment (3 mg DOX equivalent/kg, once a day for 4 days). In animals treated with DOX-loaded hybrid nanocarriers and Doxil®, the increase in tumor volume was equivalent and significantly lower than with PBS or with free DOX. A slight weight loss was also observed. If both studies suggest a clear anticancer effect of DOX-loaded nanocarriers, results are different between DOX and Doxil® treatment. In one case, Doxil® proved to be superior to free DOX in tumor reduction, whereas the other study concluded to the opposite. This highlights the difficulty to choose a pertinent protocol (DOX dose, number of injections, type of cells) and to correctly interpret the results.

The comparison with Doxil® is not systematic. For example, Deng et al. evaluated liposomes loaded with USPIO and DOX (0.228 mg DOX/0.470 mg Fe/mL formulation), on nude mice bearing Panc-1 (human pancreatic cancer cells) tumors (2 mg DOX equivalent/kg three times at 7-day intervals) [15]. Their goal was an increased anticancer efficacy in tumor growth for targeted nanocarriers with a monoclonal antibody, compared to the formulation without targeting. The tumors in mice treated with targeted nanosystems were significantly smaller than those in mice treated with DOX in solution, and they also highlighted a difference with nontargeted systems (but with a lower significance level).

As reports of DOX-loaded Au-NPs are not very numerous, in vivo studies are still fewer. Chen et al. used mice tumorized with S180 cells (murine sarcoma) subcutaneously injected in the axillary fossa to evaluate DOX covalently linked to gold nanoclusters (aggregates of a few ten gold atoms, coated with bovine serum albumin) [85].

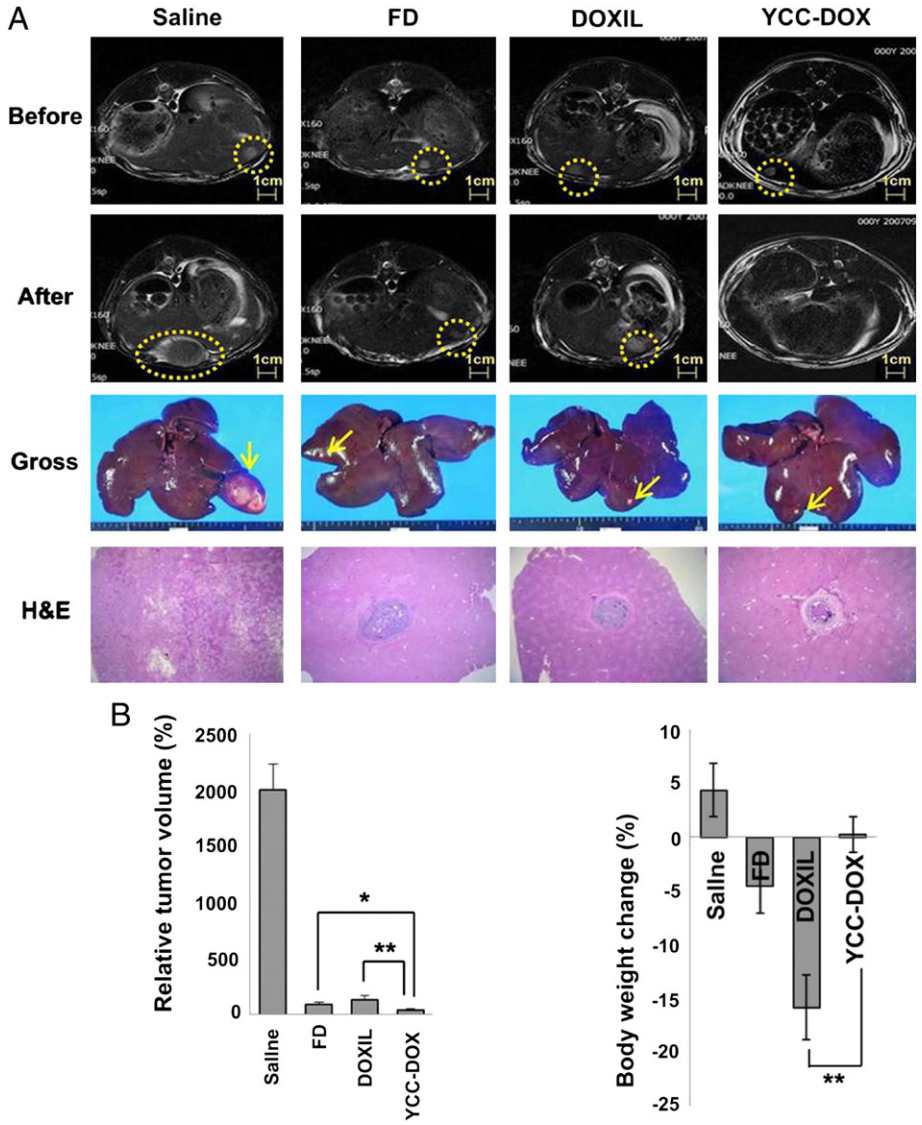

Fig. 5. Anticancer effects of treatment (2 mg/kg DOX or equivalent 3 times at 5-day intervals) with saline, DOX in solution (FD), Doxil® or DOX-loaded nanocarriers (YCC–DOX) in rabbit models. A: Representative MR images before and after the treatments, gross images, and H&E (hematoxylin–eosin) images. B: Relative tumor volumes and weight changes of rabbits treated with saline, DOX in solution, Doxil® and YCC–DOX. Reprinted with permission from [28].

NIR imaging system permitted to follow the dynamic distribution of their nanocarriers. Organs were removed after 8 h and examined with confocal microscopy and fluorescence intensities were recorded. Mice received 5 injections (one per day) of 5.5 mg/kg of DOX in solution or DOX-loaded nanoclusters. This model showed a good tumor targeting capability, and the bright fluorescence signal reached a maximum at 7–10 h not only in the tumor, but also in elimination organs like liver and kidneys. Better survival rates, an increase in body weight, and limited tumor growth for the animals confirmed the therapeutic effect of the nanosystem, especially compared to free DOX.

3.4.2. Antitumor effect of DOX combined with thermal therapy

As described above, Au-NPs possess size-dependent optical and photothermal properties due to plasmons — the collective oscillation of conductive free electrons on their surface [17]. For thermal therapy, the near infrared light (NIR) (650–900 nm) is preferentially used because it penetrates human tissue from half a millimeter up to a few centimeters, due to a minimal absorption by water and blood in this region of the wavelength spectrum. Consequently, exposure to NIR light results in the generation of heat and its dissipation to the surrounding tissue, leading to cellular death and tumor ablation.

SPIONs can also be used as hyperthermia agents by application of an alternating magnetic field: the Brownian and Néel relaxation mechanisms lead to an increase in temperature of the particles [7]. As tumor cells are more vulnerable to heat than normal cells, tumor ablation can be achieved by using only 5–10 mg of SPIONs/cm^3 of tissue [7]. Nevertheless, there is a lack of in vivo studies of DOX delivery associated to magnetically-induced thermal therapy with SPIONs.

You et al. studied photothermal therapy/ablation (PTA) for their DOX-loaded gold hollow nanospheres (Fig. 2A), and added a targeting for a specific receptor of multiple tumors and angiogenic blood vessels (EphB4) [27,86,87]. In both cases, the in vivo release of DOX triggered by NIR laser was confirmed by a dual radiotracer technique. Treatment with their nanosystems followed by near-infrared laser irradiation resulted in significantly decreased tumor growth, when compared to treatments without laser, to gold nanospheres with laser, or to free DOX. Moreover, targeted nanosystems gave better results compared to non-targeted ones. The tumors in six of the eight mice treated with targeted DOX-loaded hollow nanospheres plus laser regressed completely with only residual scar tissue after 22 days following injection. None of the treatment groups experienced a loss in body weight, contrary to groups treated with free DOX. These in vivo assays

gave encouraging results for the association of DOX delivery and thermal ablation.

4. Remarks and conclusions

If DOX seems to be surpassed by more recent treatments, it remains an essential tool for research, precisely because the molecule, its chemistry, its activity mechanisms and its behavior and efficacy in vitro and in vivo are so well known. The use of DOX as a model to evaluate the potential of hybrid nanocarriers based on MNPs highlights the design tendencies. "One-pot" processes, that is the mixing of the active molecule, MNPs and coating materials, are increasingly reported in the literature. Coating materials are more and more varied, and play not only a passive role (for example for stealthiness) but also an active and stimuli-responsive role to control the release of DOX.

The DOX loading strategies and release profiles reported in the literature also open up a number of reflections about the rational aims of research in this domain. The quantity of DOX loaded on nanocarriers does not have to be great, as long as it is sufficient for a therapeutic effect. The aim of targeting is to decrease the loss of drug in non-targeted sites. It is rather the quantity of nanocarriers reaching the cells that must be considered.

The in vitro release kinetics can vary from a few minutes to often quite long, 48 h or more. This must be compatible with an in vivo use, considering the time for the nanocarriers to reach the targeted site and enter cells. In a clinical study, Lübbe et al. applied a magnetic field for 60–120 min in order to accumulate their SPIONs in the tumor [78]. An ideal release profile would have only a moderate release during the time of magnetic focalization, to avoid disseminating a high percentage of DOX in the organism. This delay in DOX release must also be considered for theranostic nanosystems (DOX release and imaging). The residence time of nanocarriers in cells must be explored, to evaluate the interest of a long sustained release.

The necessity to obtain an equivalent or higher cytotoxicity of nanocarriers compared to free DOX may discourage some researchers from further developing new nanosystems. However, a lower cytotoxicity could be acceptable since the targeting permits to deliver DOX preferentially to tumor cells. Targeting strategies for nanocarriers seem to be essential to gain a sufficient efficacy to compensate for slow release kinetics and a lack of cell specificity. This implies that in vitro cytotoxicity evaluation has to be completed with in vivo tumor reduction assays, to appreciate the real impact of the targeting on tumor toxicity. Unfortunately, in vivo studies are very few, and supplementary publications could shed some light on these aspects. The current tendency to multidisciplinary studies is a real need for researchers.

To conclude, the development of such theranostic systems is only very difficult, and requires extensive studies and characterization before it can lead to routine processes and marketing authorizations, but it also opens up new horizons to research. Exciting work remains to be done in the years ahead, as expressed by Barenholz and Gabizon, the fathers of Doxil® [88,89].

References

[1] H. Maeda, J. Wu, T. Sawa, Y. Matsumura, K. Hori, Tumor vascular permeability and the EPR effect in macromolecular therapeutics: a review, J. Control. Release 65 (2000) 271–284.
[2] R.E. Serda, B. Godin, E. Blanco, C. Chiappini, M. Ferrari, Multi-stage delivery nanoparticle systems for therapeutic applications, BBA-Gen. Subj. 1810 (2011) 317–329.
[3] S. Chandra, K.C. Barick, D. Bahadur, Oxide and hybrid nanostructures for therapeutic applications, Adv. Drug Deliv. Rev. 63 (2011) 1267–1281.
[4] A.J. Cole, V.C. Yang, A.E. David, Cancer theranostics: the rise of targeted magnetic nanoparticles, Trends Biotechnol. 29 (2011) 323–332.
[5] E. Cukierman, D.R. Khan, The benefits and challenges associated with the use of drug delivery systems in cancer therapy, Biochem. Pharmacol. 80 (2010) 762–770.
[6] A.S. de Dios, M.E. Díaz-García, Multifunctional nanoparticles: analytical prospects, Anal. Chim. Acta 666 (2010) 1–22.
[7] H.-C. Huang, S. Barua, G. Sharma, S.K. Dey, K. Rege, Inorganic nanoparticles for cancer imaging and therapy, J. Control. Release 155 (2011) 344–357.
[8] S. Parveen, R. Misra, S.K. Sahoo, Nanoparticles: a boon to drug delivery, therapeutics, diagnostics and imaging, Nanomedicine 8 (2012) 147–166.
[9] N.T.K. Thanh, L.A.W. Green, Functionalisation of nanoparticles for biomedical applications, Nano Today 5 (2010) 213–230.
[10] J. Xie, S. Lee, X. Chen, Nanoparticle-based theranostic agents, Adv. Drug Deliv. Rev. 62 (2010) 1064–1079.
[11] J. Klostergaard, C.E. Seeney, Magnetic nanovectors for drug delivery, Maturitas 73 (2012) 33–44.
[12] D.E. Owens III, N.A. Peppas, Opsonization, biodistribution, and pharmacokinetics of polymeric nanoparticles, Int. J. Pharm. 307 (2006) 93–102.
[13] C.S.S.R. Kumar, F. Mohammad, Magnetic nanomaterials for hyperthermia-based therapy and controlled drug delivery, Adv. Drug Deliv. Rev. 63 (2011) 789–808.
[14] P. Rai, S. Mallidi, X. Zheng, R. Rahmanzadeh, Y. Mir, S. Elrington, A. Khurshid, T. Hasan, Development and applications of photo-triggered theranostic agents, Adv. Drug Deliv. Rev. 62 (2010) 1094–1124.
[15] L. Deng, X. Ke, Z. He, D. Yang, H. Gong, Y. Zhang, X. Jing, J. Yao, J. Chen, A MSLN-targeted multifunctional nanoimmunoliposome for MRI and targeting therapy in pancreatic cancer, Int. J. Nanomedicine 7 (2012) 5053–5065.
[16] A.S. Lübbe, C. Bergemann, J. Brock, D.G. McClure, Physiological aspects in magnetic drug-targeting, J. Magn. Magn. Mater. 194 (1999) 149–155.
[17] S. Rana, A. Bajaj, R. Mout, V.M. Rotello, Monolayer coated gold nanoparticles for delivery applications, Adv. Drug Deliv. Rev. 64 (2012) 200–216.
[18] A.Z. Mirza, H. Shamshad, Preparation and characterization of doxorubicin functionalized gold nanoparticles, Eur. J. Med. Chem. 46 (2011) 1857–1860.
[19] D.T. Nguyen, D.-J. Kim, K.-S. Kim, Controlled synthesis and biomolecular probe application of gold nanoparticles, Micron 42 (2011) 207–227.
[20] S. Zong, Z. Wang, J. Yang, C. Wang, S. Xu, Y. Cui, A SERS and fluorescence dual mode cancer cell targeting probe based on silica coated Au@Ag core–shell nanorods, Talanta 97 (2012) 368–375.
[21] Z. Wang, S. Zong, J. Yang, C. Song, J. Li, Y. Cui, One-step functionalized gold nanorods as intracellular probe with improved SERS performance and reduced cytotoxicity, Biosens Bioelectron. 26 (2010) 241–247.
[22] P. Mohan, N. Rapoport, Doxorubicin as a molecular nanotheranostic agent: effect of doxorubicin encapsulation in micelles or nanoemulsions on the ultrasound-mediated intracellular delivery and nuclear trafficking, 7 (2010) 1959–1973.
[23] Y. Octavia, C.G. Tocchetti, K.L. Gabrielson, S. Janssens, H.J. Crijns, A.L. Moens, Doxorubicin-induced cardiomyopathy: from molecular mechanisms to therapeutic strategies, J. Mol. Cell. Cardiol. 52 (2012) 1213–1225.
[24] G. Molyneux, M. Andrews, W. Sones, M. York, A. Barnett, E. Quirk, W. Yeung, J. Turton, Haemotoxicity of busulphan, doxorubicin, cisplatin and cyclophosphamide in the female BALB/c mouse using a brief regimen of drug administration, Cell Biol. Toxicol. 27 (2010) 13–40.
[25] X. Li, D.J. Hirsh, D. Cabral-Lilly, A. Zirkel, S.M. Gruner, A.S. Janoff, W.R. Perkins, Doxorubicin physical state in solution and inside liposomes loaded via a pH gradient, BBA-Biomembr. 1415 (1998) 23–40.
[26] S.F. Medeiros, A.M. Santos, H. Fessi, A. Elaissari, Stimuli-responsive magnetic particles for biomedical applications, Int. J. Pharm. 403 (2011) 139–161.
[27] J. You, G. Zhang, C. Li, Exceptionally high payload of doxorubicin in hollow gold nanospheres for near-infrared light-triggered drug release, ACS Nanosci. 4 (2012) 1033–1041.
[28] J.H. Maeng, D.-H. Lee, K.H. Jung, Y.-H. Bae, I.-S. Park, S. Jeong, Y.-S. Jeon, C.-K. Shim, W. Kim, J. Kim, Multifunctional doxorubicin loaded superparamagnetic iron oxide nanoparticles for chemotherapy and magnetic resonance imaging in liver cancer, Biomaterials 31 (2010) 4995–5006.
[29] X.-Y. Ying, Y.-Z. Du, L.-H. Hong, H. Yuan, F.-Q. Hu, Magnetic lipid nanoparticles loading doxorubicin for intracellular delivery: preparation and characteristics, J. Magn. Magn. Mater. 323 (2011) 1088–1093.
[30] E. Munnier, S. Cohen-Jonathan, C. Linassier, L. Douziech-Eyrolles, H. Marchais, M. Soucé, K. Hervé, P. Dubois, I. Chourpa, Novel method of doxorubicin–SPION reversible association for magnetic drug targeting, Int. J. Pharm. 363 (2008) 170–176.
[31] J. Gautier, E. Munnier, A. Paillard, K. Hervé, L. Douziech-Eyrolles, M. Soucé, K. Hervé, P. Dubois, I. Chourpa, A pharmaceutical study of doxorubicin-loaded PEGylated nanoparticles for magnetic drug targeting, Int. J. Pharm. 423 (2012) 16–25.
[32] K. Min, H. Jo, K. Song, M. Cho, Y.-S. Chun, S. Jon, W.J. Kim, C. Ban, Dual-aptamer-based delivery vehicle of doxorubicin to both PSMA (+) and PSMA (−) prostate cancers, Biomaterials 32 (2011) 2124–2132.
[33] X. He, X. Wu, X. Cai, S. Lin, M. Xie, X. Zhu, D. Yan, Functionalization of magnetic nanoparticles with dendritic–linear–brush-like triblock copolymers and their drug release properties, Langmuir 28 (2012) 11929–11938.
[34] H.-M. Yang, B.C. Oh, J.H. Kim, T. Ahn, H.-S. Nam, C.W. Park, J.-D. Kim, Multifunctional poly(aspartic acid) nanoparticles containing iron oxide nanocrystals and doxorubicin for simultaneous cancer diagnosis and therapy, Colloid Surf. A 391 (2011) 208–215.
[35] S.K. Sahu, S. Maiti, A. Pramanik, S.K. Ghosh, P. Pramanik, Controlling the thickness of polymeric shell on magnetic nanoparticles loaded with doxorubicin for targeted delivery and MRI contrast agent, Carbohydr. Polym. 87 (2012) 2593–2604.
[36] C. Liao, Q. Sun, B. Liang, J. Shen, X. Shuai, Targeting EGFR-overexpressing tumor cells using cetuximab–immunomicelles loaded with doxorubicin and superparamagnetic iron oxide, Eur. J. Radiol. 80 (2011) 699–705.
[37] Q. Quan, J. Xie, H. Gao, M. Yang, F. Zhang, G. Liu, X. Lin, A. Wang, H.S. Eden, S. Lee, G. Zhang, X. Chen, HSA coated iron oxide nanoparticles as drug delivery vehicles for cancer therapy, Mol. Pharm. 8 (2011) 1669–1676.

[38] S. Park, H.S. Kim, W.J. Kim, H.S. Yoo, S. Park, H.S. Kim, W.J. Kim, H.S. Yoo, Pluronic@Fe3O4 nanoparticles with robust incorporation of doxorubicin by thermo-responsiveness, Int. J. Pharm. 424 (2012) 107–114.
[39] W. Wang, N. Ballatori, Endogenous glutathione conjugates: occurrence and biological functions, Pharmacol. Rev. 50 (1998) 335–356.
[40] C. Sanson, C. Schatz, J.-F. Le Meins, A. Soum, J. Thévenot, E. Garanger, S. Lecommandoux, A simple method to achieve high doxorubicin loading in biodegradable polymersomes, J. Control. Release 147 (2010) 428–435.
[41] C. Sanson, O. Diou, J. Thévenot, E. Ibarboure, A. Soum, A. Brûlet, S. Miraux, E. Thiaudière, S. Tan, A. Brisson, V. Dupuis, O. Sandre, S. Lecommandoux, Doxorubicin loaded magnetic polymersomes: theranostic nanocarriers for MR imaging and magneto-chemotherapy, ACS Nanosci. 5 (2011) 1122–1140.
[42] G.D. Bothun, A. Lelis, Y. Chen, K. Scully, L.E. Anderson, M.A. Stoner, Multicomponent folate-targeted magnetoliposomes: design, characterization, and cellular uptake, Nanomedicine: NBM 7 (2011) 797–805.
[43] K. Hayashi, K. Ono, H. Suzuki, M. Sawada, M. Moriya, W. Sakamoto, T. Yobo, High-frequency, magnetic-field-responsive drug release from magnetic nanoparticle/organic hybrid based on hyperthermic effect, ACS Appl. Mater. Interfaces 2 (2010) 1903–1911.
[44] Y.-J. Gu, J. Cheng, C.W.-Y. Man, W.-T. Wong, S.H. Cheng, Gold–doxorubicin nanoconjugates for overcoming multidrug resistance, Nanomedicine 8 (2012) 204–211.
[45] M.-Y. Hua, H.-W. Yang, H.-L. Liu, R.-Y. Tsai, S.-T. Pang, K.-L. Chuang, Y.-S. Chang, T.-S. Hwang, Y.-H. Chang, H.-C. Chuang, C.-K. Chuang, Superhigh-magnetization nanocarrier as a doxorubicin delivery platform for magnetic targeting therapy, Biomaterials 32 (2011) 8999–9010.
[46] C. Fang, F.M. Kievit, O. Veiseh, Z.R. Stephen, T. Wang, D. Lee, R.G. Ellenbogen, M. Zhang, Fabrication of magnetic nanoparticles with controllable drug loading and release through a simple assembly approach, J. Control. Release 162 (2012) 233–241.
[47] F.M. Kievit, F.Y. Wang, C. Fang, H. Mok, K. Wang, J.R. Silber, R.G. Ellenbogen, M. Zhang, Doxorubicin loaded iron oxide nanoparticles overcome multidrug resistance in cancer in vitro, J. Control. Release 152 (2011) 76–83.
[48] A. Brownlie, I. Uchegbu, A. Schätzlein, PEI-based vesicle-polymer hybrid gene delivery system with improved biocompatibility, Int. J. Pharm. 274 (2004) 41–52.
[49] J. Robbens, C. Vanparys, I. Nobels, R. Blust, K. Van Hoecke, C. Janssen, K. De Schamphelaere, K. Roland, G. Blanchard, F. Silvestre, Eco-, geno- and human toxicology of bio-active nanoparticles for biomedical applications, Toxicology 269 (2010) 170–181.
[50] L.-Y. Su, T.-Y. Fang, W.-C. Tseng, The effect of pendant hydrophobicity on the biological efficacy of polyethylenimine conjugate, Biochem. Eng. J. 49 (2010) 21–27.
[51] S.K. Agrawal, N. Sanabria-DeLong, J.M. Coburn, G.N. Tew, S.R. Bhatia, Novel drug release profiles from micellar solutions of PLA–PEO–PLA triblock copolymers, J. Control. Release 112 (2006) 64–71.
[52] M. Prabaharan, J.J. Grailer, S. Pilla, D.A. Steeber, S. Gong, Gold nanoparticles with a monolayer of doxorubicin-conjugated amphiphilic block copolymer for tumor-targeted drug delivery, Biomaterials 30 (2009) 6065–6075.
[53] X. Yang, H. Hong, J.J. Grailer, I.J. Rowland, A. Javadi, S.A. Hurley, Y. Xiao, Y. Yang, Y. Zhang, R.J. Nickles, W. Cai, D.A. Steeber, S. Gong, cRGD-functionalized, DOX-conjugated, and 64Cu-labeled superparamagnetic iron oxide nanoparticles for targeted anticancer drug delivery and PET/MR imaging, Biomaterials 32 (2011) 4151–4160.
[54] X.-Y. Ying, D. Cui, L. Yu, Y.-Z. Du, Solid lipid nanoparticles modified with chitosan oligosaccharides for the controlled release of doxorubicin, Carbohydr. Polym. 84 (2011) 1357–1364.
[55] Y.-J. Gu, J. Cheng, C.-C. Lin, Y.W. Lam, S.H. Cheng, W.-T. Wong, Nuclear penetration of surface functionalized gold nanoparticles, Toxicol. Appl. Pharmacol. 237 (2009) 196–204.
[56] E. Munnier, S. Cohen-Jonathan, K. Hervé, C. Linassier, M. Soucé, P. Dubois, I. Chourpa, Doxorubicin delivered to MCF-7 cancer cells by superparamagnetic iron oxide nanoparticles: effects on subcellular distribution and cytotoxicity, J. Nanopart. Res. 13 (2011) 959–971.
[57] A. Shkilnyy, E. Munnier, K. Hervé, M. Soucé, R. Benoit, S. Cohen-Jonathan, C. Linassier, P. Limelette, M.-L. Saboungi, P. Dubois, I. Chourpa, Synthesis and evaluation of novel biocompatible super-paramagnetic iron oxide nanoparticles as magnetic anticancer drug carrier and fluorescence active label, J. Phys. Chem. C 114 (2010) 5850–5858.
[58] B. Book Newell, Y. Wang, J. Irudayaraj, Multifunctional gold nanorod theragnostics probed by multi-photon imaging, Eur. J. Med. Chem. 48 (2012) 330–337.
[59] A. Chompoosor, K. Saha, P.S. Ghosh, D.J. Macarthy, O.R. Miranda, Z.-J. Zhu, K.F. Arcaro, V.M. Rotello, The role of surface functionality on acute cytotoxicity, ROS generation and DNA damage by cationic gold nanoparticles, Small 6 (2010) 2246–2249.
[60] N. Khlebtsov, L. Dykman, Biodistribution and toxicity of engineered gold nanoparticles: a review of in vitro and in vivo studies, Chem. Soc. Rev. 40 (2011) 1647–1671.
[61] G. Szakács, J.K. Paterson, J.A. Ludwig, C. Booth-Genthe, M.M. Gottesman, Targeting multidrug resistance in cancer, Nat. Rev. Drug Discov. 5 (2006) 219–234.
[62] A. Shapira, Y.D. Livney, H.J. Broxterman, Y.G. Assaraf, Nanomedicine for targeted cancer therapy: towards the overcoming of drug resistance, Drug Resist. Update 14 (2011) 150–163.
[63] M. Sui, W. Liu, Y. Shen, Nuclear drug delivery for cancer chemotherapy, J. Control. Release 155 (2011) 227–236.
[64] M. Mahmoudi, A. Simchi, M. Imani, M.A. Shokrgozar, A.S. Milani, U.O. Häfeli, P. Stroeve, A new approach for the in vitro identification of the cytotoxicity of superparamagnetic iron oxide nanoparticles, Colloid Surf. B 75 (2010) 300–309.
[65] J. Kneipp, H. Kneipp, M. McLaughlin, D. Brown, K. Kneipp, In vivo molecular probing of cellular compartments with gold nanoparticles and nanoaggregates, Nano Lett. 6 (2006) 2225–2231.
[66] P. Nativo, I.A. Prior, M. Brust, Uptake and intracellular fate of surface-modified gold nanoparticles, ACS Nanosci. 2 (2008) 1639–1644.
[67] D. Kim, S. Jon, Gold nanoparticles in image-guided cancer therapy, Inorg. Chim. Acta 393 (2012) 154–164.
[68] A.M. Schwartzberg, T.Y. Olson, C.E. Talley, J.Z. Zhang, Synthesis, characterization, and tunable optical properties of hollow gold nanospheres, J. Phys. Chem. B 110 (2006) 19935–19944.
[69] X. Huang, M.A. El-Sayed, Gold nanoparticles: optical properties and implementations in cancer diagnosis and photothermal therapy, J. Adv. Res. 1 (2010) 13–28.
[70] C. Peng, L. Zheng, Q. Chen, M. Shen, R. Guo, H. Wang, X. Cao, G. Zhang, X. Shi, PEGylated dendrimer-entrapped gold nanoparticles for in vivo blood pool and tumor imaging by computed tomography, Biomaterials 33 (2012) 1107–1119.
[71] H. Wang, L. Zheng, C. Peng, R. Guo, M. Shen, X. Shi, G. Zhang, Computed tomography imaging of cancer cells using acetylated dendrimer-entrapped gold nanoparticles, Biomaterials 32 (2011) 2979–2988.
[72] J.-L. Li, L. Wang, X.-Y. Liu, Z.-P. Zhang, H.-C. Guo, W.-M. Liu, S.-H. Tang, In vitro cancer cell imaging and therapy using transferrin-conjugated gold nanoparticles, Cancer Lett. 274 (2009) 319–326.
[73] A. Astolfo, E. Schültke, R.H. Menk, R.D. Kirch, B.H.J. Juurlink, C. Hall, L.-A. Harsan, M. Stebel, D. Barbetta, G. Tromba, F. Arfelli, In vivo visualization of gold-loaded cells in mice using x-ray computed tomography, Nanomedicine: NBM 9 (2012) 284–292.
[74] M.W. Freeman, A. Arrott, J.H.L. Watson, Magnetism in medicine, J. Appl. Phys. 31 (1960) S404.
[75] R. Ganguly, A.P. Gaind, S. Sen, I.K. Puri, Analyzing ferrofluid transport for magnetic drug targeting, J. Magn. Magn. Mater. 289 (2005) 331–334.
[76] S. Dandamudi, V. Patil, W. Fowle, B.-A. Khaw, R.B. Campbell, External magnet improves antitumor effect of vinblastine and the suppression of metastasis, Cancer Sci. 100 (2009) 1537–1543.
[77] J.-P. Fortin-Ripoche, M.S. Martina, F. Gazeau, C. Ménager, C. Wilhelm, J.-C. Bacri, S. Lesieur, O. Clément, Magnetic targeting of magnetoliposomes to solid tumors with MR imaging monitoring in mice: feasibility, Radiology 239 (2006) 415–424.
[78] A.S. Lübbe, C. Alexiou, C. Bergemann, Clinical applications of magnetic drug targeting, J. Surg. Res. 95 (2001) 200–206.
[79] P. Ruenraroengsak, J.M. Cook, A.T. Florence, Nanosystem drug targeting: facing up to complex realities, J. Control. Release 141 (2010) 265–276.
[80] Y. Lu, P.S. Low, Folate-mediated delivery of macromolecular anticancer therapeutic agents, Adv. Drug Deliv. Rev. 54 (2012) 675–693.
[81] Y.-J. Lu, K.-C. Wei, C.-C.M. Ma, S.-Y. Yang, J.-P. Chen, Dual targeted delivery of doxorubicin to cancer cells using folate-conjugated magnetic multi-walled carbon nanotubes, Colloid Surf. B 89 (2012) 1–9.
[82] A. Garcia-Bennett, M. Nees, B. Fadeel, In search of the Holy Grail: folate-targeted nanoparticles for cancer therapy, Biochem. Pharmacol. 81 (2011) 976–984.
[83] I. Altintas, R.J. Kok, R.M. Schiffelers, Targeting epidermal growth factor receptor in tumors: from conventional monoclonal antibodies via heavy chain-only antibodies to nanobodies, Eur. J. Pharm. Sci. 45 (2012) 399–407.
[84] S. Mura, P. Couvreur, Nanotheranostics for personalized medicine, Adv. Drug Deliv. Rev. 64 (2012) 1394–1416.
[85] H. Chen, B. Li, X. Ren, S. Li, Y. Ma, S. Cui, Y. Gu, Multifunctional near-infrared-emitting nano-conjugates based on gold clusters for tumor imaging and therapy, Biomaterials 33 (2012) 8461–8476.
[86] J. You, C. Xiong, M. Zhong, M. Melancon, S. Gupta, A.M. Nick, A.K. Sood, C. Li, Effective photothermal chemotherapy using doxorubicin-loaded gold nanospheres that target EphB4 receptors in tumors, Cancer Res. 72 (2012) 4777–4786.
[87] J. You, R. Zhang, G. Zhang, M. Zhong, Y. Liu, C.S. Van Pelt, D. Liang, W. Wei, A.K. Sood, C. Li, Photothermal-chemotherapy with doxorubicin-loaded hollow gold nanospheres: a platform for near-infrared light-trigged drug release, J. Control. Release 158 (2012) 319–328.
[88] A. Gabizon, H. Shmeeda, T. Grenader, Pharmacological basis of pegylated liposomal doxorubicin: impact on cancer therapy, Eur. J. Pharm. Sci. 45 (2012) 388–398.
[89] Y. (Chezy) Barenholz, Doxil® — the first FDA-approved nano-drug: lessons learned, J. Control. Release 160 (2012) 117–134.

Deuxième partie
Nanovecteurs magnétiques pour la délivrance de la doxorubicine : design, caractérisations et études in vitro/in vivo

Chapitre 1 : Développement et caractérisations des nanovecteurs magnétiques pour la délivrance de la DOX

Publication 3 : A pharmaceutical study of doxorubicin-loaded PEGylated nanoparticles for magnetic drug targeting

Publiée dans International Journal of Pharmaceutics, 2012

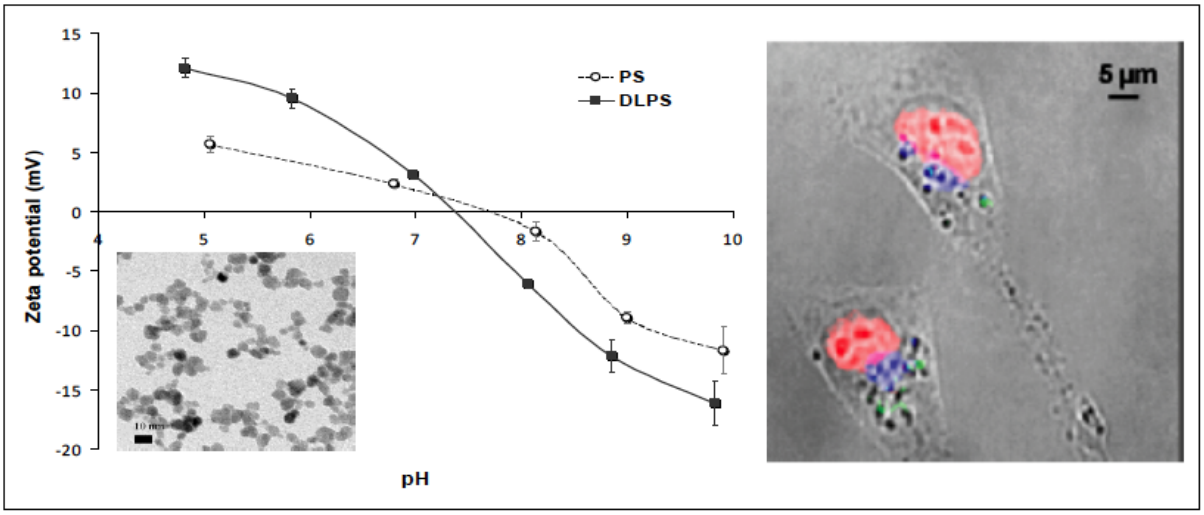

Dans cette étude, le complexe DOX-Fe^{2+} précédemment développé par Munnier et al. [125] a été chargé sur les SPIONs PEGylés développés par Hervé *et al.* [123]. L'optimisation du protocole a permis de mettre au point une technique de chargement rapide (30 min), à température ambiante et facilement transposable à l'échelle industrielle. La quantité de DOX chargée représente environ 3% de la masse des oxydes de fer. Cette quantité est inférieure à celle chargée sur des SPIONs citratés (14% m/m) [125]. L'encombrement stérique des chaînes de PEG limite en effet les interactions entre le complexe DOX-Fe^{2+} et la surface disponible des SPIONs. Néanmoins, les PEG offrent la possibilité de retenir une partie non négligeable du complexe.

L'étude *in vitro* de la libération du complexe DOX-Fe^{2+} à partir des nanovecteurs a révélé une libération continue sur 2h à pH 7,4. Le revêtement de PEG permet donc de moduler cette libération, et la rend compatible avec un ciblage magnétique. En effet, Lübbe et al. [52] ont mené une étude clinique de phase I avec des ferrofluides chez l'homme en appliquant un champ magnétique externe pendant 60 à 120 min au niveau des tumeurs. Dans notre cas, cette cinétique de libération permettrait aux nanovecteurs se s'accumuler au niveau de la tumeur, sans disséminer une grande quantité de DOX dans l'organisme, limitant ainsi les effets indésirables. De plus, en environnement acide, la libération est accélérée, et totale en 1h à pH 4. Cette caractéristique semble prometteuse, dans la mesure où la littérature rapporte qu'après internalisation, de nombreux nanovecteurs sont retrouvés au niveau des lysosomes, où règne un pH de 5 [78,93,130]. La libération de la DOX serait donc favorisée après internalisation des nanovecteurs par les cellules cancéreuses.

Après leur mise en contact avec des cellules MCF-7 (cancer du sein humain), l'imagerie confocale multispectrale a révélé que les nanovecteurs étaient internalisés, et la DOX progressivement libérée depuis les compartiments cytoplasmiques comme les lysosomes, vers les noyaux des cellules. L'intensité de la fluorescence de la DOX augmente progressivement dans le noyau cellulaire (2,7% de l'intensité totale à 5 min, 22,8% à 180 min). L'essai de viabilité cellulaire au MTT (test au tétrazolium) a également montré que nanovecteurs chargés de DOX génèrent une cytotoxicité comparable à celle de la DOX en solution, après 96 h d'incubation.

Cette étude *in vitro* des nanovecteurs magnétiques pour la délivrance de la doxorubicine pose des bases permettant d'étudier le potentiel de ce type de vecteurs *in vivo*.

International Journal of Pharmaceutics 423 (2012) 16–25

Contents lists available at ScienceDirect

International Journal of Pharmaceutics

journal homepage: www.elsevier.com/locate/ijpharm

A pharmaceutical study of doxorubicin-loaded PEGylated nanoparticles for magnetic drug targeting

J. Gautier[a,b], E. Munnier[a,b,*], A. Paillard[a,b], K. Hervé[a,b], L. Douziech-Eyrolles[a,b], M. Soucé[a,b], P. Dubois[a,b], I. Chourpa[a,b]

[a] Université François-Rabelais, EA 4244 «Physico-Chimie des Matériaux et des Biomolécules», équipe «Nanovecteurs Magnétiques pour la Chimiothérapie», Tours F-37200, France
[b] Institut Fédératif de Recherche 135 "Imagerie Fonctionnelle", Tours F-37000, France

ARTICLE INFO

Article history:
Received 17 February 2011
Received in revised form 25 May 2011
Accepted 6 June 2011
Available online 14 June 2011

Keywords:
Doxorubicin (DOX)
Superparamagnetic iron oxide nanoparticles (SPION)
Polyethylene glycol
Release kinetics
Intracellular distribution

ABSTRACT

One of the new strategies to improve cancer chemotherapy is based on new drug delivery systems, like the polyethylene glycol-coated superparamagnetic iron oxide nanoparticles (PEG-SPION, thereafter called PS). In this study, PS are loaded with doxorubicin (DOX) anticancer drug, using a pre-formed DOX–Fe^{2+} complex reversible at lower pH of tumour tissues and cancer cells. The DOX loaded PS (DLPS, 3% w/w DOX/iron oxide) present a hydrodynamic size around 60 nm and a zeta potential near zero at physiological pH, both parameters being favourable for increased colloidal stability in biological media and decreased elimination by the immune system. At physiological pH of 7.4, 60% of the loaded drug is gradually released from the DLPS in ~2 h. The intracellular release and distribution of DOX is followed by means of confocal spectral imaging (CSI) of the drug fluorescence. The in vitro cytotoxicity of the DLPS on MCF-7 breast cancer cells is equivalent to that of a DOX solution. The reversible association of DOX to the SPION surface and the role of polymer coating on the drug loading/release are discussed, both being critical for the design of novel stealth magnetic nanovectors for chemotherapy.

1. Introduction

Doxorubicin (DOX) is an antineoplastic agent of the anthracycline family frequently used in association with other drugs to treat a large number of cancers, like leukaemia, ovarian cancers and particularly last stage breast cancers (Lankelma et al., 1999). The clinical use of DOX is limited by its side effects, the most dangerous being a cumulative dose-dependent cardiotoxicity (Leonard et al., 2009). To minimize the side effects, DOX can be vectorized, that is associated to drug carriers that will favour its accumulation on the site of action and limit its dispersion in healthy tissues. Such a minimization has already been obtained with liposomal forms commercialized for nearly ten years (Leonard et al., 2009; Pütz et al., 2009). These forms increase the drug intratumoural concentration mainly due to their nanometric size: liposomes accumulate in tumours by a passive mechanism known as the enhanced permeation and retention effect (EPR effect). Indeed, the leaky fenestrations of neovasculature in tumours, combined with their inefficient lymphatic drainage, enable extravasation and accumulation of such small objects (Veiseh et al., 2010).

In addition to this passive targeting, nanovectors of a new generation are developed to permit an active targeting of tumours. Several concepts of active targeting are being investigated in the literature, namely at a molecular scale, as the functionalization of vector surfaces with targeting ligands complementary to specific or overexpressed receptors on cancer cells (Fan et al., 2010; Veiseh et al., 2010), or at a macroscopic scale, for example by means of an external magnetic field (Douziech-Eyrolles et al., 2007; Lübbe et al., 1996a,b, 2001; Maeng et al., 2010; Yang et al., 2010). Magnetic drug targeting is thus based on the association of a drug and magnetic nanoparticles. These magnetic drug delivery systems are essentially based on iron oxides (Aqil et al., 2008; Sabaté et al., 2008; Wassel et al., 2007; Ying et al., 2011), known to be non-toxic (Weissleder et al., 1989; Ying and Hwang, 2010).

To benefit from the EPR effect, the size of the final systems has to be below the dimensions of vascular permeativity in tumours, i.e. ~150 nm (Veiseh et al., 2010). The size of initial iron oxide nanoparticles is also determining for their magnetic properties:

* Corresponding author at: Laboratoire de Pharmacie Galénique, UFR de Pharmacie, 31 avenue Monge, 37200 Tours, France. Tel.: +33 247367201; fax: +33 247367198.
E-mail address: emilie.munnier@univ-tours.fr (E. Munnier).

0378-5173/$ – see front matter © 2011 Elsevier B.V. All rights reserved.
doi:10.1016/j.ijpharm.2011.06.010

below 30 nm diameter, the particles are superparamagnetic, i.e. highly magnetisable in the presence of magnetic fields but void of magnetic memory (remanence) (Mahmoudi et al., 2009). This is a critical requirement to avoid thrombotic risk related to magnetic aggregation of injectable delivery systems. The initial particles used for these purposes are commonly called SPION (superparamagnetic iron oxide nanoparticles) or USPIO (ultrasmall superparamagnetic iron oxide), the latter term being reserved for particle sizes below 20 nm (Roch et al., 2005).

The surface properties of the nanovectors are also essential for their biocompatibility. The presence of hydrophobic functions and/or charges favours nanoparticle opsonisation, i.e. nonspecific adsorption of plasma proteins (opsonins), which accelerates their recognition and elimination by the immune system before they reach their target tissue (Veiseh et al., 2010). In order to reduce the opsonisation and to ensure a colloidal stability by sterical repulsion, the surface of the magnetic systems must be coated with a hydrophilic and neutral moiety, such as a biocompatible polymer. For example, polymer molecules like polyethylene glycol (PEG) or dextran are known to reduce the opsonisation phenomenon and to lengthen the duration of circulation of the nanovectors (Harris and Chess, 2003). In addition, the coating can provide various chemical groups to conjugate drugs or targeting ligands (Wang and Thanou, 2010), in order to combine macroscopic and microscopic targeting. Nevertheless, the coating may lead to modified drug loading and release that must be taken into account (Zhu et al., 2010). The activity of the drug loaded on nanovectors must be respected through the formulation steps. The most common protocols of drug loading on the magnetic systems in the literature imply either covalent binding or entrapment of the drug into a polymer layer (Mahmoudi et al., 2010). Covalent linkage can be too strong to be cleaved by cellular enzymes, in particular if access to the drug is hindered by the polymeric coating (Shkilnyy et al., 2010). The entrapment of the drug within a polymer often leads to a burst effect (fast initial release) and/or to a low release in the absence of stimuli (Dilnawaz et al., 2010; Yang et al., 2010). We developed a novel method of reversible association of doxorubicin to SPION (Munnier et al., 2008): DOX is adsorbed on the iron oxide surface after being chelated with a Fe(II) ion (Fig. 1). The chelated iron binds to OH groups on the SPION surface and thus plays the role of an intermediary between the drug and nanoparticles. In this model, the drug release is pH-dependent as the DOX–Fe^{2+} complex dissociates in acidic conditions (Munnier et al., 2008). This release is expected to be tumour-specific, since the tumour environment is known to be more acidic than blood (Greulich et al., 2011; Medeiros et al., 2011). In addition, this method of reversible loading protects the drug activity: the DOX–Fe^{2+}–SPION systems were as active or even more so than a doxorubicin solution against MCF-7 human breast cancer cells in vitro (Munnier et al., 2008).

The aim of the present study is the loading of the doxorubicin–iron (II) pre-formed complex (DOX–Fe^{2+}, Munnier et al., 2008) on the PEGylated SPION developed by our group (Hervé et al., 2008). We propose a complete study of our model: the loading process is optimized, in order to maximize the quantity of doxorubicin bound, with a simple and easily transposable method. The optimized DOX-loaded PEGylated SPION are then characterized in terms of morphology, size and zeta potential. The in vitro doxorubicin release is investigated, in order to observe how PEGylation modifies the release. Biological aspects are also explored. Confocal spectral imaging is used to follow the subcellular distribution of doxorubicin after a treatment with the nanovectors and to determine the intracellular kinetics of action of the drug. Cytotoxicity assays permit to evaluate the anticancer activity of the nanovectors and to notice the effect of vectorization.

2. Materials and methods

2.1. Nanoparticle preparation

2.1.1. Materials

Doxorubicin hydrochloride was purchased from TEVA Pharmaceuticals Ltd. (Puteaux, France). Dulbecco's phosphate buffer saline (DPBS), ferric nitrate nonahydrate ($Fe(NO_3)_3{\cdot}9H_2O$), anhydrous ferric chloride ($FeCl_3$) and iron standard solution 1 g/L (titrisol) were purchased from Fisher Bioblock Scientific (Illkirch, France). Ferrous chloride ($FeCl_2$, $4H_2O$) was obtained from Acros Organics (Noisy Le Grand, France). 3-Aminopropyltrimethoxy silane (APTES), N-(3-dimethylaminopropyl)-N′-ethylcarbodiimide hydrochloride (EDC) and methoxypoly(ethylene glycol) 5000 propionic acid N-succinimidyl ester (activated PEG, aPEG) were purchased from Sigma Aldrich (Saint-Quentin-Fallavier, France). Sodium acetate and tris-(hydroxymethyl)-aminomethane (Tris) were provided by Merck (Fontenay-sous-Bois, France), and ferrous ammonium sulphate ($(NH_4)_2Fe(SO_4)_2{\cdot}6H_2O$) by Carlo Erba (Val de Reuil, France). In all the experiments, deionized water was used.

2.1.2. PEGylated SPION

The PEGylated ferrofluids were prepared according to a method described previously (Hervé et al., 2008). Briefly, superparamagnetic iron oxide nanoparticles (SPION) were synthesized by aqueous coprecipitation of ferric and ferrous chlorides in alkaline medium. In order to stabilize the surface chemical composition, SPION were oxidized by ferric nitrate and finally peptized in nitric acid and re-suspended in a determined volume of water. SPION were then silanized by a 12 h contact with APTES, washed and peptized in water at pH 3. Finally, SPION were PEGylated by a 24 h contact with aPEG, and purified by dialysis against water. These particles will be further mentioned as "PS" for PEGylated SPION.

2.1.3. Doxorubicin (DOX) loading on PEGylated SPION

PEGylated SPION (PS) were loaded with DOX via a DOX–Fe^{2+} complex, as described elsewhere (Munnier et al., 2008). DOX–Fe^{2+} complex was pre-formed by contact between DOX and a Fe^{2+} solution (1.5 M excess of Fe^{2+} over DOX) in Tris buffer pH 7.6. PS were incubated with DOX–Fe^{2+} complex in the dark, and harvested by centrifugation at 19,000 × *g* for 1 h at 4 °C. Several parameters were modified in order to optimize drug loading, as described in Section 3.1.

These particles will be further mentioned as "DLPS" for DOX-loaded PEGylated SPION.

2.2. Nanoparticle characterization

2.2.1. Morphology and size

The morphology of nanoparticles and their diameters were examined using a Philips CM20 electronic transmission microscope (TEM), operating at 200 kV. The samples were diluted in deionized water ($[Fe] \sim 10^{-3}$ g/L), then deposited on a carbon-coated copper TEM grid, the excess of solvent was removed with filter paper, and samples were left to air-dry before TEM viewing. The size estimation was based on 30 nanoparticles on 3 different images.

The hydrodynamic diameter of the particles was determined by DLS (Dynamic Light Scattering) technique with an Autosizer 2c (Malvern Instruments, Orsay, France) after sample dilution in deionized water ($[Fe] \sim 2 \times 10^{-3}$ g/L). Each measurement was performed at 25 °C, at least in triplicate, with a He–Ne laser (4 mW) operating at 633 nm, with the scatter angle fixed at 173°. The polydispersity index PDI is a measure of the broadness of a size distribution derived from the cumulative analysis of DLS data.

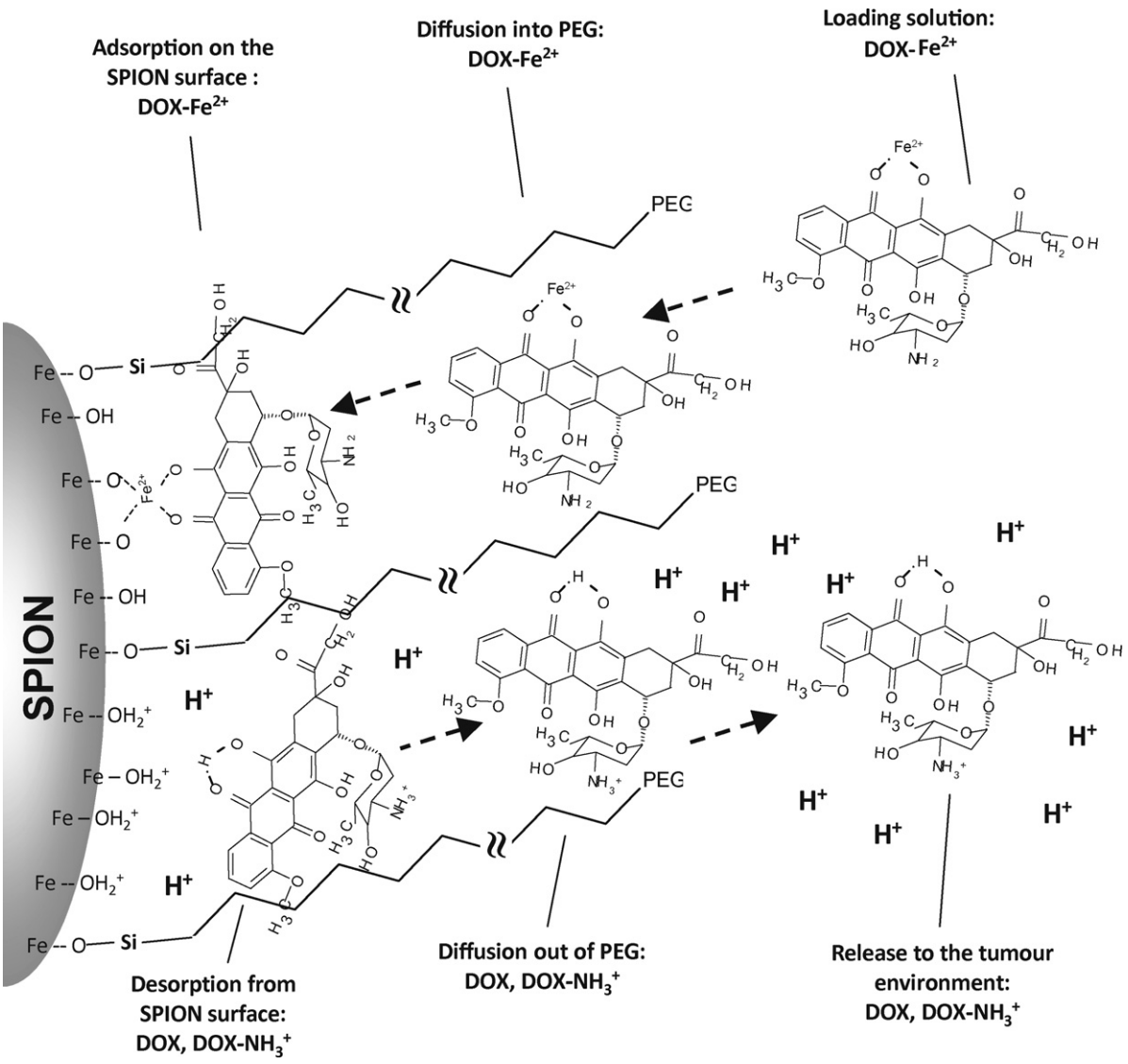

Fig. 1. Schematic diagram of loading of pre-formed DOX–Fe^{2+} complex and of release of DOX from the DLPS.

2.2.2. Zeta potential measurements

The zeta potential of the particles was determined using a Malvern NanoZ (Malvern Instruments, Orsay, France). Each measurement was performed at 25 °C, at least in triplicate, with a He–Ne laser (4 mW) operating at 633 nm, with a light scattering angle of 17°. Zeta potential was determined as a function of pH (ranging from 4.0 to 10.0) by means of a MPT-2 Titrator (Multi Purpose Titrator, Malvern Instruments, Malvern, UK) using HNO_3 and KOH 0.1 M.

2.2.3. Iron determination

The overall iron content in the ferrofluids is measured by atomic absorption spectrometry (iCE 3000 Series AA Spectrometer, ThermoFisher Scientific, France), after mineralization by a 12 h contact with HCl 6 N. A calibration curve was obtained with titrisol standard solution. Each determination was performed in triplicate. These results permit to estimate iron oxide concentration and mass in ferrofluid suspensions, considering that iron represents 71.5% w/w of SPION (Chourpa et al., 2005).

2.2.4. Drug loading determination

DLPS were suspended for 1 h in acetate buffer pH 4 in an ultrasonic bath to permit the total release of DOX, as the DOX–Fe^{2+} complex dissociates at low pH (Munnier et al., 2008). The sample was then centrifuged at 19,000 × *g* for 1 h at 15 °C. DOX concentration was determined in the supernatant by UV–visible spectrophotometry (Anthélie Advanced Spectrophotometer, Secomam, France), using its molar absorptivity determined at 500 nm. Each determination was performed at least in triplicate. Drug loading is expressed as the ratio of DOX mass over the mass of the iron oxide core of the nanovectors to permit a comparison with the non-PEGylated particles previously described (Munnier et al., 2008).

2.2.5. In vitro release kinetics of drug from DOX-loaded PEGylated SPION (DLPS)

Aliquots of DPLS suspensions, containing 10^{-4} g of iron, were made up to 2 mL with DPBS, continuously shaken and thermostated at 37 °C. At given time intervals, aliquots were centrifuged 1 h at 19,000 × *g* and 4 °C in order to separate the nanoparticles of the release medium. The drug concentration was determined in the supernatant from the intensity of the drug fluorescence at 557 nm (Hitachi F-4500 fluorescence spectrometer, excitation wavelength 500 nm), using a calibration curve.

2.3. Biological evaluation of DOX-loaded PEGylated SPION

For the biological evaluation, MCF-7 human breast carcinoma cells (American Type Culture Collection, LGC Promochem, Molsheim, France) were grown in Dulbecco's Modified Eagle Medium (DMEM) supplemented with 5% foetal bovine serum and 100 UI/mL penicillin G and 100 μg/mL streptomycin at 37 °C in a humidified 5% CO_2 atmosphere. All reagents were purchased from Fisher Bioblock Scientific (Illkirch, France).

2.3.1. Cytotoxicity evaluation of DOX-loaded PEGylated SPION

For cytotoxicity assays, cells were seeded for 48 h in standard 24-well plates (Cellstar, Greiner Bio-One, Courtaboeuf, France) at 1×10^4 cells per well. Then the culture medium was discarded and the cells were treated for 96 h with 500 μL of medium containing different doxorubicin concentrations (0.001–30 μM), either as DOX solutions or as DLPS suspensions (iron content from 1 μg/L to 333 mg/L). Cell viability was determined using a tetrazolium dye (MTT) assay (Mosmann, 1983). The cells were rinsed thrice with Hank's Buffered Salt Solution (HBSS) pH 7.4 and incubated for 4 h in 1 mL of medium containing 0.5 g/L of MTT. Then the medium was replaced by 500 μL of dimethylsulfoxide to dissolve the formazan crystals formed by viable cells. Absorbance was measured at 540 nm using a multiwell plate reader (ELX800, BioTek, Fisher Bioblock, Illkirch, France). The 50% inhibitory concentration (IC_{50}) was determined as the drug concentration that resulted in a 50% reduction in cell viability. All the experiments were performed in sextuplicate.

2.3.2. Confocal spectral imaging

Cover glasses of 1.4 cm^2 were coated with poly-D-lysine at 5 μg/mL in water for 1 h then placed in the wells of a 24-well plate. MCF-7 cells were plated (2×10^4 cells/well) and cultured for 24 h. The medium was then replaced by a suspension of DLPS in the culture medium at the concentration of 1 μM of doxorubicin. This incubation was made for 5, 30, 60, 120, 180 min at 37 °C/5% CO_2. After treatment, MCF-7 cells were washed twice in HBSS and the cover glasses were then mounted for confocal spectral imaging observation on live cells at 37 °C. Fluorescence measurements were carried out using an XploraINV confocal microspectrometer (Horiba Jobin Yvon, Villeneuve d'Ascq, France) equipped with an automated X–Y–Z scanning stage, a low dispersion grating (600 grooves/mm) and an air-cooled CCD detector. The DOX fluorescence was excited using a 532 nm line of an Ar^+ laser. The fluorescence spectra were excited and collected in confocal mode, through the 60× LWD objective. Live treated cells were placed in a closed microscopy chamber (Harvard Instruments) thermostated at 37 °C. For each cell analysis, an optical section (*x*–*y* plane) situated at half-thickness of the cell was scanned with a step of 0.7 μm that provided maps containing typically ~900 spectra (0.05 s per spectrum). Both acquisition and treatment of multispectral maps were performed with LabSpec software. Subcellular drug distribution maps were established via analysis of both the intensity and shape of DOX fluorescence spectra, as described previously (Munnier et al., 2011). Briefly, each experimental spectrum was fitted using the least-squares method to a sum of the three reference spectra of doxorubicin (see the Section 3). The fitting errors were below 5% (typically 2–4%). The cellular autofluorescence was completely neglected, because of the absence of any significant fluorescence of the untreated cells under the conditions used (laser power 5 μW on the sample, 0.05 s per spectrum). No sample photodegradation was observed. The average quantitative information (fitting scores) was extracted from each spectral map and represented as histograms.

Table 1
Physico-chemical properties of colloids PS and DPLS ($n \geq 3$).

	PEGylated SPION (PS)	DOX loaded PEGylated SPION (DLPS)
Hydrodynamic diameter (nm)	68.0 (±2.4)	62.3 (±2.5)
Polydispersity index (PDI)	0.174 (±0.018)	0.140 (±0.030)
Zeta potential (mV), pH 4–11	16 (±7.2) to −17 (±4.6)	21 (±6.3) to −21 (±3.4)
Isoelectric point (IEP)	pH 7.65 (±0.14)	pH 7.28 (±0.10)
Loading (% w/w DOX/iron oxides)	–	3.07% (±0.04)

3. Results and discussion

3.1. Optimization of DOX loading to PS

The initial SPION were prepared according to a method described previously to obtain a cationic aqueous sol (Hervé et al., 2008; Section 2.1). SPION obtained in this manner typically presented a size of 8 ± 2 nm in TEM (data not shown). The colloidal stability in acidic medium is provided by electrostatic repulsion of $FeOH_2^+$ groups on the surface of SPION and is dependent on pH value (see Fig. 2). However, for neutral particles around pH 7.4, a coating with PEG can provide stability due to steric hindrance.

In order to bind the PEG chains to SPION, the nanoparticles were treated with 3-aminopropyltrimethoxysilane (APTES). This reactant provides (i) methoxy silane groups that react with the hydroxyl groups at the surface of SPION and (ii) amino groups necessary to create an amide bond with the activated ester group of aPEG (Hervé et al., 2008). These PEGylated SPION (PS) present an excellent colloidal stability due to steric repulsion, their surface being nearly neutral over a wide range of pH as demonstrated by zeta potential measurements (Fig. 2 and Table 1).

The PS are loaded with a pre-formed DOX–Fe^{2+} complex (Fig. 1), prepared as described elsewhere (Munnier et al., 2008): doxorubicin is incubated with Fe^{2+} ions to form a chelate by replacing the hydrogen of the C11 phenolic group of DOX under strictly controlled concentration and pH conditions (pH 7.6, 1.5 iron/DOX molar ratio).

The DOX–Fe^{2+} complex solution is then incubated with PS in an aqueous buffer pH 7.6 at room temperature, since increasing temperature up to 50 °C during incubation shows no incidence on DOX loading (data not shown). In contrast, loading depends on the DOX/PS ratio (w/w ratios of DOX/PS iron varied from 0.05 to 1) and the time of incubation (30 min to 24 h). The most representative results are presented in Fig. 3.

Previously described assays on non-PEGylated, citrate stabilized SPION (Munnier et al., 2008) showed no significant loading of free DOX, because of a lack of affinity of the drug to the surface of SPION. In contrast, using DOX–Fe^{2+} chelates, the drug loading on the citrated SPION attained 14.6 ± 0.5% DOX/iron oxide w/w (Munnier et al., 2008). In the present study, free DOX loading on PS is significant (up to 1.82 ± 0.19% DOX/iron oxide w/w). It indicates that an appreciable amount of drug is diffused and captured in the PEG layer. Under similar conditions, the loading with DOX–Fe^{2+} complex is higher: up to 3% DOX/iron oxide w/w (Fig. 3). Since no additional interaction between DOX–Fe^{2+} chelate and PEG can be expected, this increase in DOX loading should indicate that the chelate adsorption on the iron oxide surface still takes place underneath the PEG layer (Fig. 1). Therefore, the drug is loaded on the PS by two mechanisms: capture in the PEG layer (Dilnawaz et al., 2010; Lübbe et al., 1996a; Yallapu et al., 2010) and iron-mediated adsorption on the SPION surface (Munnier et al., 2008).

Modulating DOX–Fe^{2+} complex/PS iron ratio has an influence on the DOX loading (Fig. 3A). Indeed, the loading is ~1% for a DOX–Fe^{2+} complex/PS iron ratio of 0.05, but increases to ~3% for a ratio of 0.1.

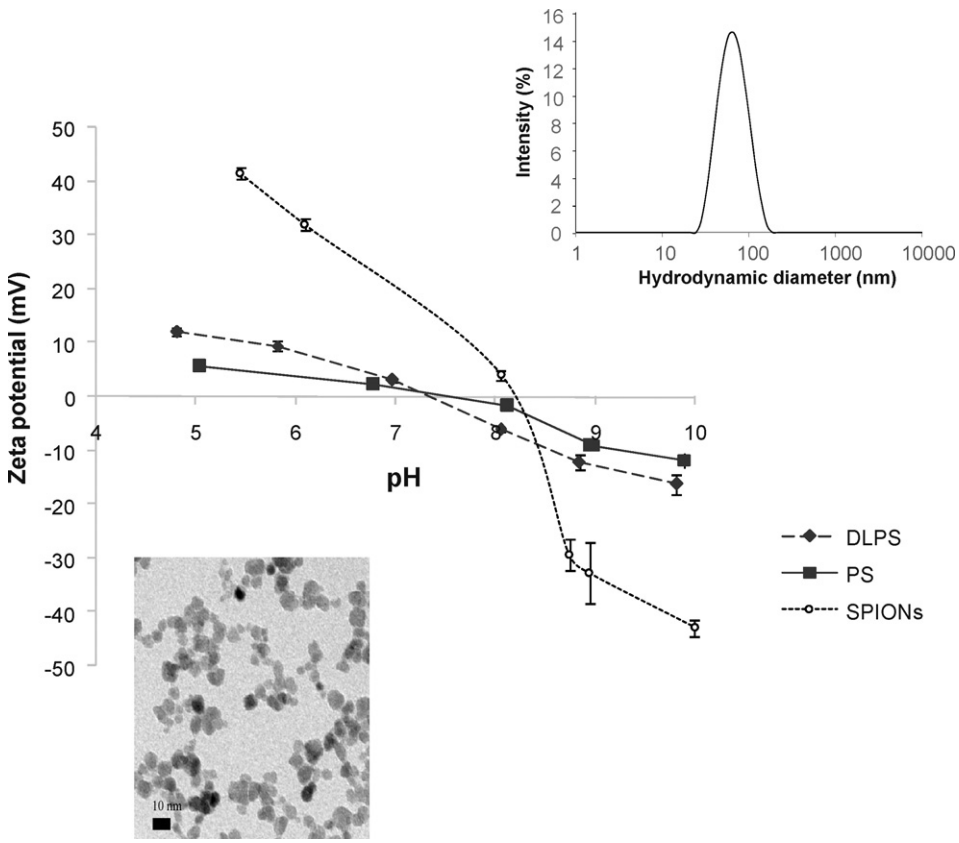

Fig. 2. Zeta potential versus pH for a batch (average of five determinations) of SPION and PEGylated SPION before (PS) and after DOX loading (DLPS). Insert: TEM image and hydrodynamic size distribution of DLPS ($n = 3$).

On the contrary, increasing the ratio to 0.5 and 1 does not seem to ameliorate the loading. The loading efficiency exhibits saturation: 27%, 7% and 3% of incubated drug was loaded respectively with ratios of 0.1, 0.5 and 1 DOX/PS iron (w/w).

The decreased DOX loading in DLPS (3%) compared to citrated SPION (14%, Munnier et al., 2008) is expected, since a part of the hydroxyl groups on the surface of SPION are occupied by silanes and/or silanes-PEG and the steric hindrance of PEG chains on the surface of SPION limits the access of the DOX–Fe^{2+} complex to the SPION surface.

In order to study the diffusion time necessary to cross the polymeric layer, we increased the incubation time from 15 min (data not shown) to 24 h. The drug loading increased between 15 and 30 min, stabilized for 2 h and decreased for 24 h (Fig. 3B). This decrease in drug loading may be due to a tendency of the complex in solution to dissociate or to precipitate over time, thus changing the equilibrium between free and PS-bound complex (Fiallo et al., 1999; Razzano et al., 1990). The results suggest that 30 min are enough to permit the DOX–Fe^{2+} complex to migrate through the PEG layer and that longer contact is useless to enhance loading, probably because of saturation of the PEG layers with the drug. The results described below correspond to DLPS prepared under the optimal conditions, i.e. 30 min incubation with DOX/PS iron ratio of 0.1 at room temperature. This method is sufficiently simple to be easily transposable for future therapeutic applications.

3.2. Physico-chemical characterization of DLPS

Transmission electron microscopy (TEM) permits to observe the morphology of the iron oxide nucleus and estimate its real

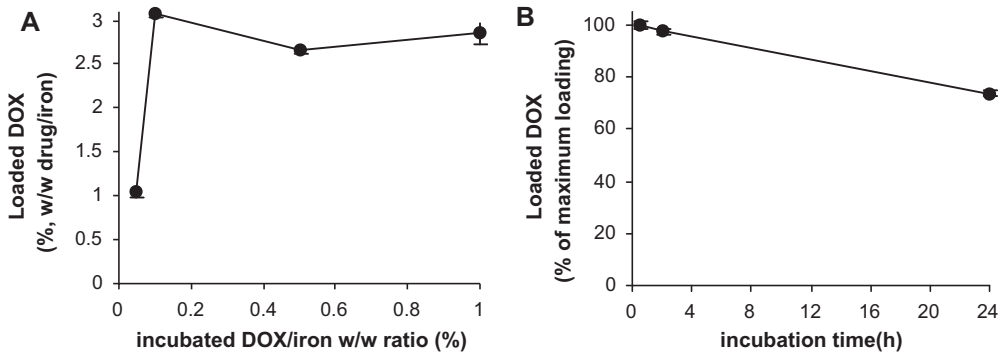

Fig. 3. DOX loading results under different conditions: (A) influence of incubated DOX/iron ratio for 30 min of incubation ($n = 3$); (B) influence of incubation time ($n = 3$) for DOX/iron ratio 0.5.

diameter. The DLPS appear to have a uniform roughly spherical shape (see insert in Fig. 2), with an average size of 10 nm ± 2 nm. These data are similar to those for SPION and PS obtained in our laboratory (Hervé et al., 2008; Munnier et al., 2008; Shkilnyy et al., 2010), and similar to those for other iron nanoparticles obtained by coprecipitation in the literature (Aqil et al., 2008; Rastogi et al., 2011; Yallapu et al., 2010). The TEM size of non-PEGylated and PEGylated particles is very similar because the polymer layer and the drug cannot be visualised on TEM images: these compounds have not sufficient electron density and their layers fold because of drying during sample preparation (Mahmoudi et al., 2010). The chemical composition of the organic layers, namely the presence of PEG and DOX, was confirmed respectively by means of FTIR and fluorescence spectroscopy (data not shown).

On the contrary, dynamic light scattering (DLS) permits to evaluate the hydrodynamic diameter of nanoparticles, which takes into account the drug/polymer layer. As shown in Table 1, values for DLPS are ~62 nm, which is close to those previously published for various PEGylated SPION (Hervé et al., 2008; Xie et al., 2007). The DLS measurements confirm the impression given by the TEM images: the distribution of the nanoparticles is monomodal (see insert in Fig. 2) with a satisfactory PDI smaller than 0.2 (see Table 1). This result shows that no large aggregates are present in the DLPS suspension.

The DLS results are completed by zeta potential measurements in function of the pH. For PS and DLPS, the zeta potential is close to zero over the pH range from 4 to 10 (Fig. 2). These results confirm prior observations (Hervé et al., 2008) and support the sterical nature of the colloidal stability of the suspensions. This implies that DPLS suspensions are physically stable in suspension at any pH, and particularly at physiological pH. We observe a slight decrease in hydrodynamic diameter (62 versus 68 nm, Table 1) and an increase in zeta potential for DLPS compared to PS. This slight modification of zeta potential cannot be due to a significant damage of the PEG layer, as the obtained profile is very far from the one of native SPION (see Fig. 2). One hypothesis could be that DOX ionizable functions, in particular the amino group ($pK_a \sim 8.2$) and the phenolic group at position C11 ($pK_a \sim 9.5$) influence the surface charge of DLPS. Nevertheless, taking into account the relatively low drug loading, and its major presence at the surface of SPION, the increased surface charge could not be directly induced by the presence of DOX in superficial PEG layers. The most plausible hypothesis seems to be that the decreased hydrodynamic diameter and the increased zeta potential are due to a change in spatial conformation of PEG chains in the presence of DOX.

Finally, the physical and chemical characteristics of DLPS like their small size, surface neutrality and good colloidal stability at physiological pH make them compatible with a systemic administration in vivo (Harris and Chess, 2003; Duan et al., 2008; Veiseh et al., 2010).

3.3. Kinetics of DOX release from DLPS

The in vitro release of DOX from DLPS was studied in a 24-fold donor/acceptor volume ratio to mimic the significant dilution of the suspension in the organism under physiological conditions of temperature and pH (37 ± 1 °C, DPBS buffer pH 7.4), as well as acidic pH to evaluate the pH dependence of the system (37 ± 1 °C acetic acid/sodium acetate buffer pH 4).

At pH 7.4, the kinetics observed with DLPS are progressive: no burst effect appears, DOX is released continuously during 2 h then reaches a plateau equivalent to ~70% of the loaded drug (see Fig. 4). The results demonstrate that the PEG layer does not prevent the drug to be released but delays this phenomenon at physiological pH.

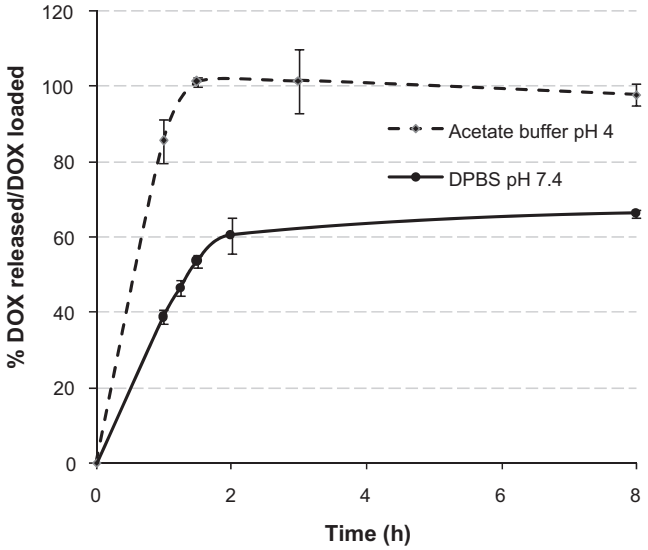

Fig. 4. In vitro release of doxorubicin from DLPS (DPBS pH 7.4, 37 °C, $n = 3$ and acetic acid/sodium acetate buffer pH 4, 37 °C, $n = 3$).

At pH 4, the release is considerably accelerated with 85% of the drug released in 1 h and practically total recovery within 2 h. A minimum duration of 1 h is imposed by the centrifugation step of the experiment, but our hypothesis is that the phenomenon is even faster, as the DOX–Fe^{2+} complex is not stable at pH 4 (Munnier et al., 2008). The time of release is then dependent on the time necessary to stabilization of the acidic pH near the SPION surface after diffusion through the PEG layer.

The kinetics at pH 7.4 seem adapted to magnetic drug targeting. In a clinical study, Lübbe et al. (2001) applied a magnetic field for 60–120 min in order to accumulate their vectors in the tumour. In our case, the moderate release during the first hour (~40% of loaded drug) should permit the nanoparticles to reach the therapeutic target without disseminating a high percentage of drug in the organism. This is important to limit the side effects generated by the free drug. In any case, this time seems reasonable compared to literature (2 weeks kinetics with glycerol monooleate coated magnetic nanoparticles loaded with paclitaxel and/or rapamycin for Dilnawaz et al., 2010; 200 h kinetics with wormlike polymer vesicles loaded with SPION and DOX for Yang et al., 2010). Once on the target, the more acidic pH of tumour tissue (Medeiros et al., 2011; Yan et al., 2007) should stimulate the release of the chelated DOX, but also of the entrapped DOX, which will then carry a positive charge on the sugar moiety (see Fig. 1). Naturally, we are conscious that the observed kinetics are only in vitro models and cannot be directly extrapolated to intracellular or in vivo kinetics. Under the experimental conditions, the appearance of a plateau indicates that a part of the loaded DOX is only slowly released from the DLPS. This kind of results is described in the literature for coated SPION. At pH 7.4, 33% of adsorbed DOX are released within 24 h from PEO-coated SPION (Maeng et al., 2010) and 31% in 48 h from composite polymer coated SPION (Rastogi et al., 2011). Our hypothesis is that the release of DOX is controlled by the drug diffusion through the polymer. In this case, the donor/acceptor volume ratio is decisive in the value of the plateau, and we can imagine that it would be displaced if the acceptor volume were larger. This is not the only explanation, since the ionic strength of the release medium may play a role in the rate of ion exchange at the surface of the SPION, as described in the literature (Li et al., 2008). Further studies could shed a light on how the DOX release from DLPS is modified in vivo. We will present some results of the intracellular release kinetics of the drug in the next section.

3.4. In vitro biological evaluation

3.4.1. Intracellular distribution and interaction of DOX delivered with DLPS

Intracellular doxorubicin release and subcellular doxorubicin redistribution are followed in living cells by confocal spectral imaging (CSI). In opposition to classical confocal fluorescence microscopy, the CSI collected not only the intensity of doxorubicin fluorescence at a given wavelength, but rather the total emission spectrum from each point scanned. This approach permits to distinguish very subtle modifications of doxorubicin intrinsic fluorescence (Fig. 5).

Three significantly different fluorescence spectra of intracellular DOX were detected in different cellular compartments (see reference spectra in Fig. 5A): a red-shifted spectrum in the nucleus and two more or less blue-shifted ones in cytoplasmic regions. Each intracellular spectrum of DOX was fitted as a weighted sum of these reference spectra. The fitting coefficients were used to generate specific maps (Fig. 5B) that can be merged and superimposed on a video image of the cell (Fig. 5D). In addition, the fitting coefficients can be statistically treated and presented in histograms (Fig. 5C).

As described before (Munnier et al., 2011), the nuclear spectrum (hereafter denoted nuc) is assigned to DOX intercalated into nuclear DNA. This corresponds only to DOX diffused through the cell membrane or intracellularly released from DLPS, since the nanoparticles cannot enter the nucleus. The two cytoplasmic spectra, denoted cyt1 and cyt2, correspond respectively to a lower and higher polarity of the molecular environment. These cytoplasmic spectra are very similar to those observed previously by Shkilnyy et al. (2010) for the cytoplasmic location of SPION–DOX–PEG where DOX was covalently bound to the SPION surface, i.e. deeply buried within the PEG layer. In the work reported by Shkilnyy et al., cells involved were MCF-7 cells as in our experiment, and the particles were similar, with a ~73 nm hydrodynamic size and were coated with PEG-5000. DOX remained fluorescent since it was bound through the amine group, outside of the fluorophore. In the present study, DOX bound to SPION by intermediate of Fe^{2+} is not fluorescent (Munnier et al., 2008). In contrast, iron-free DOX molecules entrapped/diffused inside the PEG layer are fluorescent and their fluorescence spectra are characteristic of their molecular environment within the PEG. As we determined previously, the PEG environment changes once the nanoparticles are inside cells (Shkilnyy et al., 2010). According to the blue-shifted spectral pattern of both cytoplasmic spectra, the PEG of intracellular particles creates a much more apolar environment for DOX, than when the particles are in aqueous buffer. Furthermore, this environment is even more apolar (more hydrophobic) than in the case when cells are incubated with DOX solution (Munnier et al., 2011). In general, such a blue shift of the emission spectrum is accompanied by an increase in fluorescent emission intensity. This kind of altering of the local environment around the fluorophore to a lower dielectric constant medium upon PEG–membrane interaction is known in the literature (Arnold et al., 1985). According to Ohki and Arnold (1990) PEG increases the hydrophobicity of contacting lipidic membranes by destabilizing their surface and by withdrawing free water from them. On the other hand, the decrease in dielectric constant of the PEG-related environment can be related to condensation of the PEG layers inside intracellular vesicles. This argument and the spectral similarity are both in agreement with internalization observed previously for DOX covalently bound to SPION covered with PEG (Shkilnyy et al., 2010).

From the logical consideration of the apolar environment and of the release kinetics, the major cytoplasmic fluorescence fraction (spectrum cyt1) should correspond to DOX molecules still entrapped in PEG (most apolar environment). The minor cytoplasmic fraction (spectrum cyt2) might be assigned to the drug molecules leaving the PEG layers and thus exposed to an increase of the polarity. As to a possible DOX fraction released from the particles outside the cells, under the conditions used, it is negligible in view of the recorded spectra (data not shown).

Thus, we are not able to exclude a small contribution of DOX of extracellular origin notably for nuclear fluorescence. Indeed, fluorescence of the doxorubicin administered as aqueous solution typically results in a strong nuclear staining (>90% of total intracellular drug) and a minor distribution in the cytoplasm (Munnier et al., 2011), which matches its main mechanism of action, inhibition of the nuclear enzyme DNA topoisomerase II (Hande, 2006). As it was determined before (Munnier et al., 2011) citrated SPION also deliver most of doxorubicin to the nucleus (more that 90% of fluorescence after 1 h incubation). However, when we used DLPS, the nuclear DOX fluorescence represents only 2.7% after 5 min and 22.8% after 3 h of incubation. In the latter case, the main fraction of the intracellular DOX is that of the spectrum cyt1 (Fig. 5). Thus, we deduce that the main cellular doxorubicin fluorescence did not come from doxorubicin released outside the cells, but from the drug carried by internalized nanoparticles.

The localisation of cyt1 fluorescence (Fig. 5) is concomitant with the internalization of PEGylated SPION by endocytose and accumulation inside intracellular vesicles like lysosomes as polymer nanoparticles (Harush-Frenkel et al., 2008). The kinetics of the intracellular drug distribution indicate slow migration of DOX from these cytoplasmic vesicles to the nucleus (cyt1 fluorescence is reduced from 97.5% after 5 min to 77.1% after 3 h, whereas nuc fluorescence increases from 2.7% to 22.8%). Interestingly, the cyt2 fluorescence increased temporarily during the first 30 min of incubation (2.2%) and then became negligible.

These data on subcellular DOX interaction and distribution confirm the interesting potential of PEGylated SPION as controlled delivery carriers for doxorubicin. The effect of this progressive release of doxorubicin on cellular viability is described in the next section.

3.4.2. Cytotoxicity

The aim of this biological evaluation was to determine if DOX loaded on DLPS still presents an antineoplastic activity. The CSI results described above showed that the entrance of DOX at its site of action, the nucleus, is delayed when it is vectorized by DLPS. According to these results, we chose to perform a cytotoxicity assay over 96 h in order to study the activity of the whole drug introduced in the medium. This duration corresponds to two cycles of division of MCF-7 cells, which guaranties the validity of the results. We compared the cytotoxicity on MCF-7 cancer cells of doxorubicin solution with DLPS with the same amount of loaded drug (Fig. 6). We demonstrated previously that neither drug-free SPION (Munnier et al., 2008) nor PEGylated SPION (Shkilnyy et al., 2010) adjusted for the same iron concentration produce any significant cytotoxicity on MCF-7 cells. For all concentrations tested in this study, both doxorubicin and DPLS have similar activity. The IC_{50} values are comparable for the two treatments and were determined to be 0.6 and 0.9 μM with doxorubicin and DLPS, respectively. These results show that our original loading process is reversible within 96 h and does not damage the DOX pharmacophore. The major mechanism of action of free doxorubicin is an intercalation in the DNA and an inhibition of the topoisomerase II (Hande, 2006). Several minor mechanisms of action are described in the literature as DOX-induced production of ROS (Minotti et al., 2004). As it is not very probable that the whole quantity of DLPS put into the well is internalized by the cell even in 96 h, the nanovectors could present a higher anticancer activity than the same amount of the free drug. We utter the hypothesis that in this case, several mechanisms of action are involved, as DOX has a different

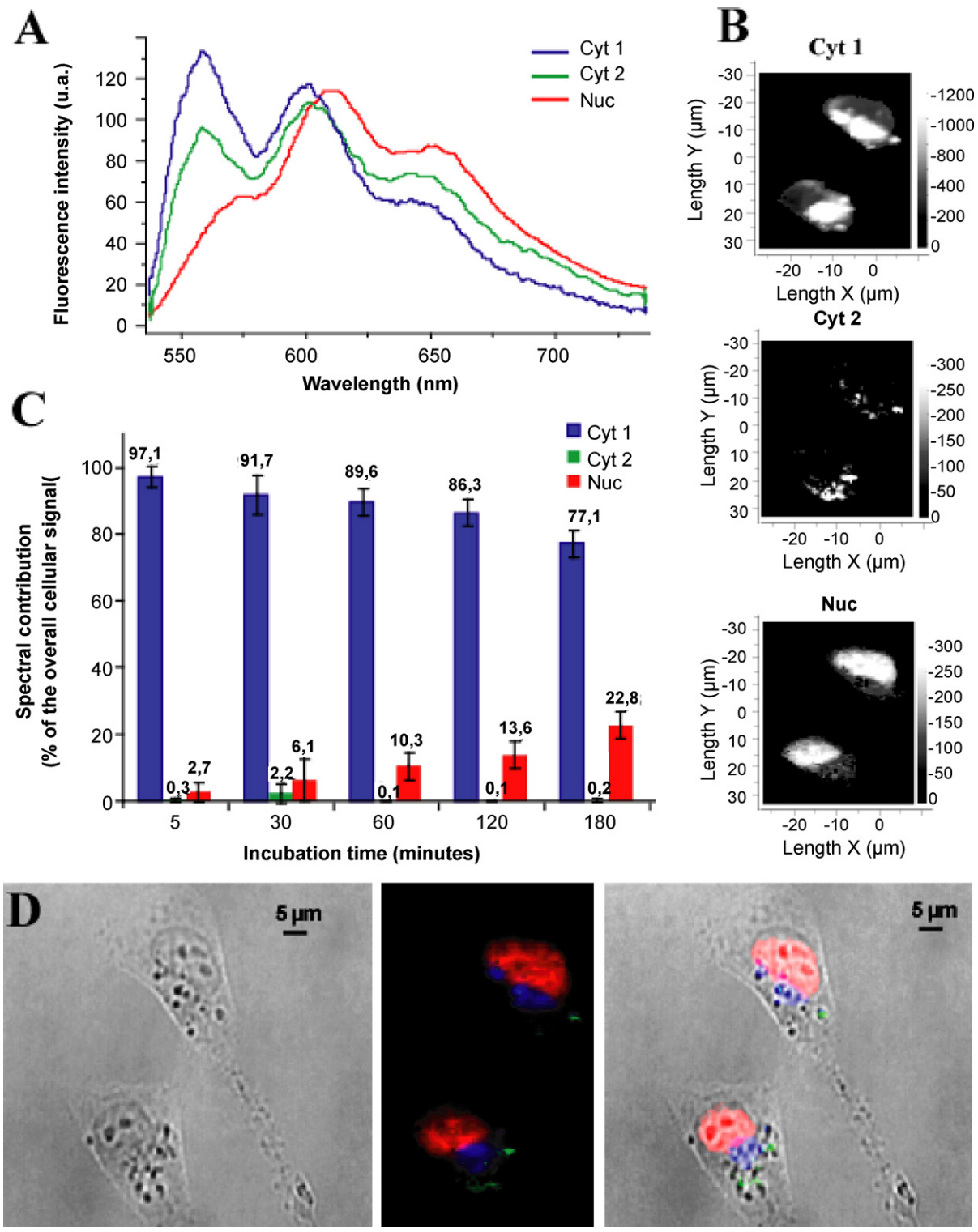

Fig. 5. Confocal spectral fluorescence imaging results on the subcellular DOX distribution in live MCF-7 cancer cells. (A) Reference spectra used to fit the intracellular DOX fluorescence: nuclear form (Nuc, red line) and two cytoplasmic forms (Cyt 1, blue line and Cyt 2, green line). (B) Typical subcellular distribution maps of the three reference spectra. (C) Statistically validated contribution to the cellular fluorescence of the three forms of fluorescence of DOX ($n \geq 6$). (D) Superposition of the maps using an extended intensity scale for colocalisation and encoded with pseudo colors. (For interpretation of the references to color in this figure legend, the reader is referred to the web version of the article.)

intracellular distribution from free DOX and DOX-loaded non PEGylated SPION (Munnier et al., 2011). The more plausible hypothesis is a joint action of DOX released in the culture medium within this long incubation time, which diffuses through the plasmic membrane, and of DOX released intracellularly. This hypothesis does not exclude the participation of supplementary mechanisms of action. Further studies can be useful to explore the mechanisms of action of these nanovectors, and to determine if they present a higher antineoplastic activity than the drug administered to cells as a solution.

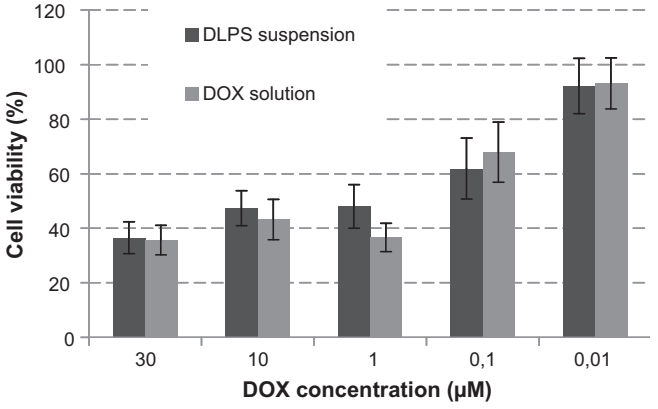

Fig. 6. Cytoxicity of DLPS versus DOX at equal drug concentration as measured on MCF-7 cancer cells (96 h, MTT assay).

4. Conclusion

The original approach of binding and pH-sensitive release of DOX to the SPION surface using a pre-formed DOX–Fe^{2+} complex is adapted to PEGylated SPION. This approach allows the preparation of DOX-loaded SPION carrying modest amounts of drug (~3% DOX/iron oxide, w/w). Nevertheless, the model is interesting in several respects. The drug is loaded on the particles following a simple and rapid protocol. The drug release kinetics is pH-dependent, and seems to be favourable for magnetic drug targeting. Moreover, drug cytotoxicity is preserved, and we suppose that several secondary mechanisms of action are involved. This study sheds a light on how PEGylation of the particles, often realized for the purpose of stealth, has an important influence on drug loading, drug release and nanoparticle distribution into the cell. Further studies will explore the cytotoxic potential of these DLPS in vivo.

Acknowledgments

This study was supported in part by grants from the Ligue Nationale contre le Cancer (Conseil Scientifique Inter-Régional Grand-Ouest (CSIRGO), Délégation Indre-et-Loire, France) and from the Region Centre, France (NANOMAG Project).

References

Aqil, A., Vasseur, S., Duguet, E., Passirani, C., Benoît, J.P., Roch, A., Müller, R., Jérôme, R., Jérôme, C., 2008. PEO coated magnetic nanoparticles for biomedical application. Eur. Polym. J. 44, 3191–3199.

Arnold, K., Herrmann, A., Pratsch, L., Gawrisch, K., 1985. The dielectric properties of aqueous solutions of poly(ethylene glycol) and their influence on membrane structure. BBA Biomembranes 815, 515–518.

Chourpa, I., Douziech-Eyrolles, L., Ngaboni-Okassa, L., Fouquenet, J.-F., Cohen-Jonathan, S., Soucé, M., Marchais, H., Dubois, P., 2005. Molecular composition of iron oxide nanoparticles, precursors for magnetic drug targeting, as characterized by confocal Raman microspectroscopy. Analyst 130, 1395–1403.

Dilnawaz, F., Singh, A., Mohanty, C., Sahoo, S.K., 2010. Dual drug loaded superparamagnetic iron oxide nanoparticles for targeted cancer therapy. Biomaterials 31, 3694–3706.

Douziech-Eyrolles, L., Marchais, H., Hervé, K., Munnier, E., Soucé, M., Linassier, C., Dubois, P., Chourpa, I., 2007. Nanovectors for anticancer agents based on superparamagnetic iron oxide nanoparticles. Int. J. Nanomed. 2, 541–550.

Duan, H.W., Kuang, M., Wang, X.X., Wang, Y.A., Mao, H., Nie, S.M., 2008. Reexamining the affects of particle size and surface chemistry on the magnetic properties of iron oxide nanocrystals: new insights into spin disorder and proton relaxivity. J. Phys. Chem. C 112, 8127–8131.

Fan, C., Gao, W., Chen, Z., Fan, H., Li, M., Deng, F., Chen, Z., 2010. Tumor selectivity of stealth multi-functionalized superparamagnetic iron nanoparticles. Int. J. Pharm., doi:10.1016/j.ijpharm.2010.10.038.

Fiallo, M.M.L., Garnier-Suillerot, A., Matzanke, B., Kozlowski, H., 1999. How Fe^{3+} binds anthracycline antitumour compounds. The myth and the reality of a chemical sphinx. J. Inorg. Biochem. 75, 105–115.

Greulich, C., Diendorf, J., Simon, T., Eggeler, G., Epple, M., Köller, M., 2011. Uptake and intracellular distribution of silver nanoparticles in human mesenchymal stem cells. Acta Biomater. 7, 347–354.

Hande, K.R., 2006. Topoisomerase II inhibitors. Update Cancer Ther. 1, 3–15.

Harris, J.M., Chess, R.B., 2003. Effect of pegylation on pharmaceuticals. Nat. Rev. Drug Discov. 2, 214–221.

Harush-Frenkel, O., Rozentur, E., Benita, S., Altschuler, Y., 2008. Surface charge of nanoparticles determines their endocytic and transcytotic pathway in polarized MDCK cells. Biomacromolecules 9, 435–443.

Hervé, K., Douziech-Eyrolles, L., Munnier, E., Cohen-Jonathan, S., Soucé, M., Marchais, H., Limelette, P., Warmont, F., Saboungi, M.L., Dubois, P., Chourpa, I., 2008. The development of stable aqueous suspensions of PEGylated SPION for biomedical applications. Nanotechnology 19, 465608, 7 pp.

Lankelma, J., Dekker, H., Luque, R.F., Luykx, S., Hoekman, K., van der Valk, P., van Diest, P.J., Pinedo, H.M., 1999. Doxorubicin gradients in human breast cancer. Clin. Cancer Res. 5, 1703–1707.

Leonard, R.C.F., Williams, S., Tulpule, A., Levine, A.M., Oliveros, S., 2009. Improving the therapeutic index of anthracycline chemotherapy: focus on liposomal doxorubicin (Myocet™). J. Breast 18, 218–224.

Li, Y., Wong, H.L., Shuhendler, A.J., Rauth, A.M., Wu, X.Y., 2008. Molecular interactions, internal structure and drug release kinetics of rationally developed polymer–lipid hybrid nanoparticles. J. Control. Release 128, 60–70.

Lübbe, A.S., Alexiou, C., Bergemann, C., 2001. Clinical applications of magnetic drug targeting. J. Surg. Res. 95, 200–206.

Lübbe, A.S., Bergemann, C., Huhnt, W., Fricke, T., Riess, H., Brock, J.W., Huhn, D., 1996a. Preclinical experiences with magnetic drug targeting: tolerance and efficacy. Cancer Res. 56, 4694–4701.

Lübbe, A.S., Bergemann, C., Riess, H., Schriever, F., Reichardt, P., Possinger, K., Matthias, M., Dörken, B., Herrmann, F., Gürtler, R., Hohenberger, P., Haas, N., Sohr, R., Sander, B., Lemke, A.J., Ohlendorf, D., Huhnt, W., Huhn, D., 1996b. Clinical experiences with magnetic drug targeting: a phase i study with 4′-epidoxorubicin in 14 patients with advanced solid tumors. Cancer Res. 56, 4686–4693.

Maeng, J.H., Lee, D.H., Jung, K.H., Bae, Y.H., Park, I.S., Jeong, S., Jeon, Y.S., Shim, C.K., Kim, W., Kim, J., Lee, J., Lee, Y.M., Kim, J.H., Kim, W.H., Hong, S.S., 2010. Multifunctional doxorubicin loaded superparamagnetic iron oxide nanoparticles for chemotherapy and magnetic resonance imaging in liver cancer. Biomaterials 31, 4995–5066.

Mahmoudi, M., Sant, S., Wang, B., Laurent, S., Sen, T., 2010. Superparamagnetic iron oxide nanoparticles (SPION): development, surface modification and applications in chemotherapy. Adv. Drug Deliv. Rev., 006, doi:10.1016/j.addr.2010.05.

Mahmoudi, M., Shokrgozar, M.A., Simchi, A., Imani, M., Milani, A.S., Stroeve, P., Vali, H., Hafeli, U.O., Bonakdar, S., 2009. Multiphysics flow modelling and in vitro toxicity of iron oxide nanoparticles coated with poly(vinyl alcohol). J. Phys. Chem. C 113, 2322–2331.

Medeiros, S.F., Santos, A.M., Fessi, H., Elaissari, A., 2011. Stimuli-responsive magnetic particles for biomedical applications. Int. J. Pharm. 403, 139–161.

Minotti, G., Menna, P., Salvatorelli, E., Cairo, G., Gianni, L., Anthracyclines:, 2004. molecular advances and pharmacologic developments in antitumor activity and cardiotoxicity. Pharmacol. Rev. 56, 185–229.

Mosmann, T., 1983. Rapid colorimetric assay for cellular growth and survival: application to proliferation and cytotoxicity assays. J. Immunol. Methods 65, 55–63.

Munnier, E., Cohen-Jonathan, S., Hervé, K., Linassier, C., Soucé, M., Dubois, P., Chourpa, I., 2011. Doxorubicin delivered to MCF-7 cancer cells by superparamagnetic iron oxide nanoparticles: effects on subcellular distribution and cytotoxicity. J. Nanopart. Res. 13, 959–971.

Munnier, E., Cohen-Jonathan, S., Linassier, C., Douziech-Eyrolles, L., Marchais, H., Soucé, M., Hervé, K., Dubois, P., Chourpa, I., 2008. Novel method of doxorubicin–SPION reversible association for magnetic drug targeting. Int. J. Pharm. 363, 170–176.

Ohki, S., Arnold, K., 1990. Surface dielectric constant, surface hydrophobicity and membrane fusion. Membr Biol. 114, 195–203.

Pütz, G., Schmah, O., Eckes, J., Hug, M.J., Winkler, K., 2009. Controlled application and scheduled removal of nanoparticle based chemotherapeutics (CARL) will reduce dose limiting adverse events in anticancer chemotherapy. Med. Hypotheses 72, 393–397.

Rastogi, R., Gulati, N., Kotnala, R.V., Sharma, U., Jayasundar, R., Koul, V., 2011. Evaluation of folate conjugated PEGylated thermosensitive magnetic nanocomposites for tumor imaging and therapy. Colloids Surf. B: Biointerfaces 82, 160–167.

Razzano, G., Rizzo, V., Vigevani, A., 1990. Determination of phenolic ionization constants of anthracyclines with modified substitution pattern of anthraquinone chromophore. Farmaco 45, 215–222.

Roch, A., Gossuin, Y., Muller, R.N., Gillis, P., 2005. Superparamagnetic colloid suspensions: water magnetic relaxation and clustering. J. Magn. Magn. Mater. 293, 532–539.

Sabaté, R., Barnadas-Rodríguez, R., Callejas-Fernández, J., Hidalgo-Álvarez, R., Estelrich, J., 2008. Preparation and characterization of extruded magnetoliposomes. Int. J. Pharm. 347, 156–162.

Shkilnyy, A., Munnier, E., Hervé, K., Soucé, M., Benoit, R., Cohen-Jonathan, S., Limelette, P., Saboungi, M.L., Dubois, P., Chourpa, I., 2010. Synthesis and evaluation of novel biocompatible super-paramagnetic iron oxide nanoparticles as magnetic anticancer drug carrier and fluorescence active label. J. Phys. Chem. C 114, 5850–5858.

Veiseh, O., Gunn, J.W., Zhang, M., 2010. Design and fabrication of magnetic nanoparticles for targeted drug delivery and imaging. Adv. Drug Deliv. Rev. 62, 284–304.
Wang, M., Thanou, M., 2010. Targeting nanoparticles to cancer. Pharmacol. Res. 62, 90–99.
Wassel, R.A., Grady, B., Kopke, R.D., Dormer, K.J., 2007. Dispersion of super paramagnetic iron oxide nanoparticles in poly(D,L-lactide-co-glycolide) microparticles. J. Colloids Surf. 292, 125–130.
Weissleder, R., Stark, D.D., Engelstad, B.L., Bacon, B.R., Compton, C.C., White, D.L., Jacobs, P., Lewis, J., 1989. Superparamagnetic iron oxide: pharmacokinetics and toxicity. Am. J. Roentgenol. 152, 167–173.
Xie, J., Xu, C., Kohler, N., Hou, Y., Sun, S., 2007. Controlled PEGylation of monodisperse Fe_3O_4 nanoparticles for reduced non-specific uptake by macrophage cells. Adv. Mater. 19, 3163–3166.
Yallapu, M.M., Othman, S.F., Curtis, E.T., Gupta, B.K., Jaggi, M., Chauhan, S.C., 2010. Multifunctional magnetic nanoparticles for magnetic resonance imaging and cancer therapy. Biomaterials, doi:10.1016/j.biomaterials.2010.11.028.
Yan, G.P., Robinson, L., Hogg, P., 2007. Magnetic resonance imaging contrast agents: overview and perspectives. J. Radiol. 13, e5–e19.
Yang, X., Grailer, J.J., Rowland, I.J., Javadi, A., Hurley, S.A., Steeber, D.A., Gong, S., 2010. Multifunctional SPIO/DOX-loaded wormlike polymer vesicles for cancer therapy and MR imaging. Biomaterials 31, 9065–9073.
Ying, E., Hwang, H.M., 2010. In vitro evaluation of the cytotoxicity of iron oxide nanoparticles with different coatings and different sizes in A3 human T lymphocytes. J. Sci. Total Env. 408, 4475–4481.
Ying, X.Y., Du, Y.Z., Hong, L.H., Yuan, H., Hu, F.Q., 2011. Magnetic lipid nanoparticles loading doxorubicin for intracellular delivery: preparation and characteristics. J. Magn. Magn. Mater. 323, 1088–1093.
Zhu, S., Hong, M., Tang, G., Qian, L., Lin, J., Jiang, Y., Pei, Y., 2010. Partly PEGylated polyamidoamine dendrimer for tumor-selective targeting of doxorubicin: the effects of PEGylation degree and drug conjugation style. Biomaterials 31, 1360–1371.

Chapitre 2 : Etude en SERS du complexe DOX-fer et de sa libération à partir des nanovecteurs

Publication 4 : SERS spectroscopic approach to study the doxorubicin complexes with Fe^{2+} ions and the drug release from SPION-based nanocarriers
Soumise dans Analyst, 2013

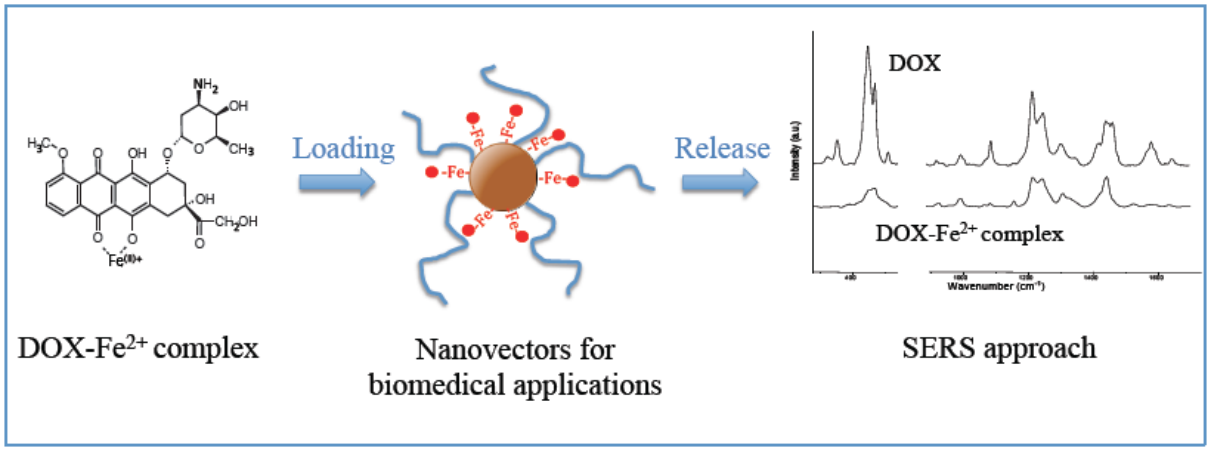

L'utilisation du complexe DOX-Fe^{2+} comme stratégie de chargement de la DOX sur les nanovecteurs soulève de nombreuses interrogations. La plus importante est la forme sous laquelle la DOX est libérée. En effet, la molécule complexée au fer pourrait présenter une cytotoxicité différente de celle de la DOX en solution, ou tout du moins des mécanismes de cytotoxicité différents, et potentiellement induire des effets indésirables nouveaux, ou connus comme la cardiotoxicité liée au complexe DOX-Fe^{3+}. De plus, la présence du fer libre dans les échantillons n'est pas souhaitable.

La DOX et le complexe DOX-Fe^{2+} ont été étudiés par spectrophotométrie UV-visible, leur spectre respectif montre en effet des modifications caractéristiques permettant de les discriminer [125]. Malheureusement, la sensibilité de cette technique est inadaptée pour des solutions diluées. Or les cinétiques de libération *in vitro* de molécules à partir de nanovecteurs se font essentiellement dans des volumes accepteurs importants. Les techniques basées sur la fluorescence ne sont pas non plus adaptées, car si la DOX fluoresce bien, la complexation avec le fer éteint sa fluorescence. Notre choix s'est donc porté sur une technique de spectrométrie possédant une sensibilité et une spécificité suffisantes pour discriminer la DOX et le complexe DOX-Fe^{2+} à des concentrations sub-micromolaires, la diffusion Raman exaltée de surface (DRES, ou SERS pour surface enhanced Raman scattering).

La spectrométrie Raman repose sur les propriétés vibrationnelles des molécules. Lorsqu'un échantillon est soumis à un rayonnement monochromatique, alors que la majorité du rayonnement est diffusé sans changement de fréquence (diffusion Rayleigh ou élastique), une minorité de photons est diffusée avec un changement de longueur d'onde, suite à un transfert d'énergie entre la molécule et le photon : il s'agit de la diffusion inélastique ou Raman [131]. Cet échange d'énergie provoque les vibrations des liaisons de la molécule. Lors d'une diffusion Raman Stokes, la plus probable et donc celle utilisée par défaut en spectroscopie Raman, le photon diffusé présente une longueur d'onde supérieure à celle du photon incident. La diffusion Raman anti-Stokes donne des photons bien plus rares, encore moins nombreux qu'en Stokes, elle est donc peu utilisée. Les décalages des bandes de diffusion inélastiques par rapport à la bande de diffusion Rayleigh correspondent donc aux énergies de vibration de la molécule. Comme ces phénomènes de diffusion inélastiques sont de faible probabilité, la spectrométrie Raman conventionnelle est une méthode peu sensible. Par contre, la technique du SERS (surface enhanced Raman scattering) ou DRES (diffusion Raman exaltée de surface) permet d'améliorer cette sensibilité d'un facteur 10^6 en moyenne. L'intensité du signal Raman peut en effet être augmentée pour des molécules se trouvant près d'une surface d'un métal

noble (argent ou or, le plus souvent) [132,133]. Cette exaltation en présence de colloïdes serait due à l'augmentation locale du champ électrique au voisinage de la surface métallique, et/ou à l'augmentation de la polarisabilité de la molécule suite à sa liaison chimique avec la surface métallique.

La mise en contact d'une molécule comme la DOX avec un colloïde d'argent a permis, dans l'étude qui suit, d'obtenir le spectre SERS de cette molécule. Comme les phénomènes d'exaltation sont plus importants pour les vibrations moléculaires perpendiculaires à la surface métallique, l'orientation de la DOX par rapport à cette surface a pu être élucidée, en fonction notamment des conditions de concentration, de pH, et donc de l'état de protonation de la DOX.

Le complexe DOX-Fe^{2+}, également caractérisé en SERS, présente une affinité accrue pour les nanoparticules d'argent. Son spectre est non seulement très intense, mais il est aussi facilement distinguable de celui de la DOX en solution. Cela a permis d'étudier la DOX libérée à partir des SPIONs PEGylés, directement dans le milieu de relargage, et de constater que la DOX est très majoritairement relarguée à pH physiologique sous forme non complexée. Ainsi, l'ion fer reste attaché aux SPIONs.

Cette étude qualitative souligne l'intérêt de l'utilisation du complexe DOX-Fe^{2+} comme stratégie d'attachement à des nanovecteurs, tout en révélant le potentiel du SERS dans les applications bioanalytiques.

Cite this: DOI: 10.1039/c0xx00000x

www.rsc.org/xxxxxx

ARTICLE TYPE

SERS spectroscopic approach to study the doxorubicin complexes with Fe^{2+} ions and the drug release from SPION-based nanocarriers

Juliette Gautier,[a] Emilie Munnier,[a] Laurence Douziech-Eyrolles,[a] Archibald Paillard,[a,b] Pierre Dubois,[a] and Igor Chourpa*[a]

Received (in XXX, XXX) Xth XXXXXXXXX 200X, Accepted Xth XXXXXXXXX 200X
DOI: 10.1039/b000000x

The aim of this work is to present a surface-enhanced Raman scattering (SERS) spectroscopic approach to study complexes of a frequently used antineoplastic agent, doxorubicin (DOX), with ferrous ions, at sub-micromolar concentrations in aqueous solution. The SERS bands of DOX were assigned according to the synthetic analysis of literature. Prior to the complexation study, the spectral changes related to the drug orientation on the silver surface and to its protonation state were highlighted. The SERS spectra of DOX-Fe^{2+} complexes showed several features distinguishing them from the free drug, protonated or not on the phenolic part of its chromophore. This property is particularly interesting from the analytical point of view, since it allows studying the drug-iron interactions upon the drug loading on and release from magnetic drug carriers based on the superparamagnetic iron oxide nanoparticles (SPIONs), stabilized with citrate ions or coated with polyethylene glycol (PEG) polymer. Our SERS data indicate that the drug loaded on magnetic nanocarriers as DOX-iron chelate was mainly released in free DOX form. These results demonstrate the analytical interest of the SERS approach to study DOX-iron interactions in relation with delivery issues and its action mechanisms.

Introduction

The antineoplastic agent of the anthracycline family, doxorubicin (DOX) (Figure 1), is used to treat a large number of cancers [1]. This molecule was so extensively studied [2–8], because of its therapeutic interest as well as the variety of conceivable analytical techniques. It is well-known that the anthracycline chromophore of DOX, rich in π→ π* and n→ π* transitions, sensitive to the ring interactions with various molecules, is suitable for spectroscopic studies, namely using UV-visible absorption, circular dichroism (CD) [5] and fluorescence [8,9]. DOX is also well known to have a high affinity for ferric iron Fe (III), forming DOX-Fe^{3+} complexes. These complexes were particularly explored since their formation in the organism was believed to induce the cardiotoxicity of the molecule [10–12,6,13,8,7,14]. Contrary to the ferric iron complexes, only a few authors studied the DOX complex with ferrous iron [15,16,9], DOX-Fe^{2+}.

Recently, we developed a novel method of reversible association of doxorubicin to superparamagnetic iron oxide nanoparticles (SPIONs), using a pre-formed DOX-Fe^{2+} chelate [16] (Figure 1). The chelated iron bound to OH groups on the SPION surface and thus played the role of an intermediary between the DOX molecule and nanoparticles, ensuring the DOX loading to SPIONs, bare or coated with PEG polymer [16]. Since the DOX-Fe^{2+} complex dissociates at pH < 6, the drug release is pH–dependent and is expected to be accelerated in tumor environment known to be more acidic than blood [17,18]. So the use of the DOX-Fe^{2+} complex permitted to control both DOX loading and release. The choice of Fe (II) ion for this purpose was also motivated by the fact that Fe (III) oxidizes DOX to cardiotoxic products [19].

Characterization of this type of complexes in aqueous environment presents several technical difficulties. UV-visible spectrophotometry allows studying both free and iron-bound DOX, but this method is not very sensitive. To study DOX-iron complexes in presence of SPIONs, the additional difficulty with UV-visible technique is that light scattering from nanoparticles disturbs the absorption spectra. A more sensitive and selective detection of intrinsically fluorescent DOX is possible by spectrofluorimetry; however, the DOX-Fe^{2+} complex does not fluoresce. So there is a need for an analytical technique offering a good sensitivity and structural specificity to study DOX iron interactions.

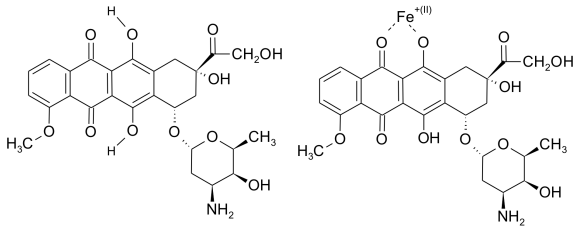

- **Fig.1** Structure of the DOX molecule and of the most probable DOX Fe^{2+} complex.

The above requirements can be satisfied using surface-enhanced Raman scattering (SERS) spectroscopy based on aqueous colloids of silver nanoparticles. Nanosized noble metal (most often Ag, Au) surfaces are able to enhance the Raman scattering of adsorbed chromophores. Raman scattering is dependent on the induced dipole moment that is proportional to the electric field component of the incident light and to the polarisability of the molecule. Therefore, two enhancement mechanisms are assumed to cooperate in SERS effect: (i) "electromagnetic" - EM field around the plasmonic NP is enhanced due to interaction between the excitation light and plasmons (coherent oscillations of the metal surface conducting electrons); (ii) "chemical" – the molecular polarisability of chromophore changed due to the chemical interaction with metal surface [20]. The cooperation depends on the molecular structure, the surface characteristics, the molecule-metal bonding and the microenvironment.

Most of the analytical and bioanalytical applications of SERS spectroscopy involve aqueous suspensions of Ag and Au NPs, typically prepared by low-cost soft chemistry methods, where the NP size and shape can be controlled by reaction conditions to obtain the desired optical properties [21]. Colloidal stability of those suspensions is insured either by electrostatic repulsion of nanoparticles carrying counter-ions like citrates [22], or by sterical hindering of nanoparticles coated with polymers like PEG [23]. Before use, electrostatically stabilized colloids are typically aggregated by increasing ionic strength, in order to favor interparticle junctions (named 'hot spots') particularly favorable for enhancement of Raman scattering. SERS permits to obtain detection limits as low as 10^{-10} M for DOX, without any perturbation of its structure [24] and SERS spectra of DOX are well described in literature since the 1980s [25,24,26,27].

In the present article, we report a SERS study of DOX and its interactions upon chelating Fe^{2+} ions. The study was managed in aqueous medium, DOX being loaded on SPIONs, stabilized with citrates or coated with PEG, to build an injectable drug carrier. Furthermore, the SERS approach was used to analyze the DOX molecular state after its release from the magnetic nanocarriers. To the best of our knowledge, these aspects have never been described in published reports.

1. Results and discussion

DOX aromatic chromophore contains two phenolic groups in positions C11 and C6 (pK_a 9.5 and 11.5, respectively, Figure 1). The deprotonation of the phenols logically leads to a bathochromic effect in the UV-visible absorption spectrum of DOX, *i.e.* to the rise of an additional absorption band at *ca.* 600 nm and the decrease of the main maxima at 480 and 500 nm. In contrast, the protonation state of the third ionisable function of DOX, the amine group (pK_a 8.2) situated on the sugar moiety, does not influence the chromophore's electronic structure. These considerations will be useful to recall for the discussion of the SERS data below.

Prior to DOX-iron complex study, we established SERS spectral features for free DOX at different experimental conditions, in order to analyze how the SERS band positions and relative intensities depend on the molecular environment and orientation of DOX adsorbed on the silver surface.

1.1. Characteristic SERS bands of DOX and their assignment

Considering the very low intensity of the CH stretching region situated arround 3000 cm^{-1} (data not shown) in the SERS spectra of DOX, our analysis will focus on the bands between 300 and 1700 cm^{-1}. The typical vibrational frequencies of major SERS bands of DOX found in this study are presented in Figure 2 and Table I. These data corresponded well to those from literature, namely from the historical study by Smulevich and Feiss [25] who assigned the SERS bands of DOX on the basis of detailed analysis of the excitation profiles in solid, the concentration effect in solution, and the fluorescence in non-polar solvents. More recent data on the band shifts upon drug deuteration in resonance Raman (RR) [25], SERS [24] and resonance SERS (SERRS) [26] allowed to introduce some additional precisions in the assignment of the DOX SERS bands, as we attempted to resume in the present study.

The majority of structure-specific SERS bands of DOX were comprised in the region between 300 and 1800 cm^{-1}. The very weak band at 1638 cm^{-1} was assigned to the stretching mode of hydrogen-bonded carbonyl group [24]. This assignment was in agreement with the fact that the band underwent a downward shift upon deuteration (isotopic shift) [31,26]. Different stretching vibration modes of aromatic rings of DOX [24], slightly sensitive

Table I Vibrational frequencies (cm^{-1}) of major bands in SERS spectra of DOX. Legend: *vw - very weak; w - weak; m - medium; s - strong; vs - very strong, sh – shoulder. Most of the assignments were made accordingly to Smulevich and Feis, 1986 [25], and were completed if specified.

Free DOX, position, cm^{-1}	Temptative assignments
1638 vw*	ν(C=O)[a,b]
1586 sh	Ring stretch + ν(C=O)[c]
1576 w	Ring stretch
1564 w	Ring stretch
1456 m	Ring stretch + δ(CC-O)[b]
1434 m	Ring stretch+ δ(CC-O)[b]
1413 w	Ring stretch
1343 w	Ring stretch
1296 w	Ring stretch + ν(C-O)
1244 s	Ring stretch symmetry B_1 + δ(O-H)
~1224 sh	Ring stretch
1210 s	Ring stretch symmetry A_1 + δ(O-H)
1152 vw	δ(C-H)
1082 w	Skeletal deformation
990 w	Ring breath
917 vw	Skeletal deformation
795 vw	Skeletal deformation
679 vw	Skeletal deformation
504 vw	Skeletal deformation
465 vs	δ(C=O)
~450 sh	Skeletal deformation
443 vs	δ(C-O)

(a) Beljebbar *et al.* [24]; (b) Yan *et al.* [26]; (c) Nonaka *et al.* [31].

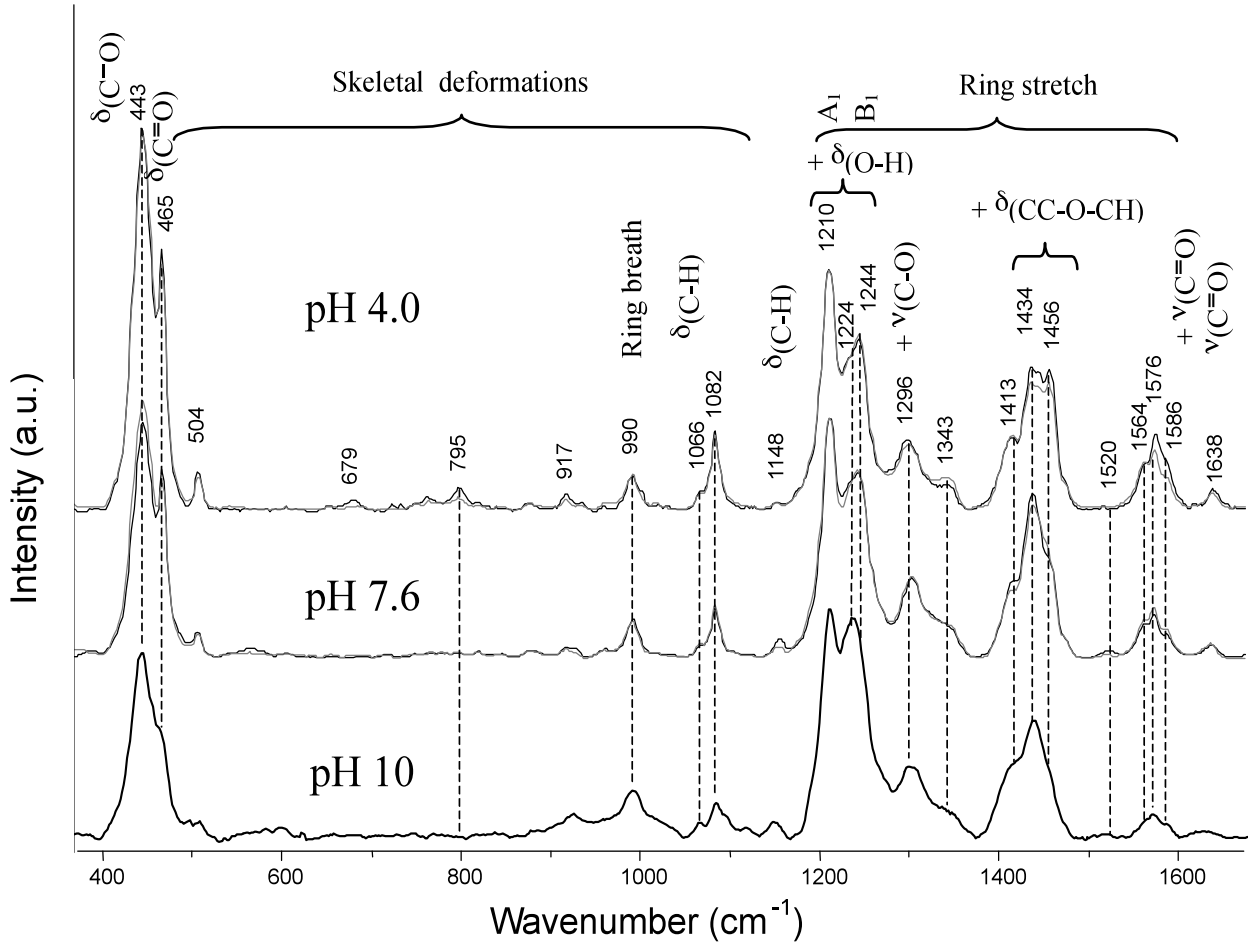

Fig. 2 Effect of pH increase (black curves, 8 μM DOX) and of the dilution (grey curves, 0.8 μM) on the SERS spectra of DOX. The spectra were normalized on the intensity of the band at 990 cm^{-1} (ring breath). The assignments were suggested according to the literature and were summarized in the Table I. Experimental conditions: laser power ~0.95 mW (632.8 nm); 36 scans of 1 s.

to deuteration, formed three groups of bands at 1586-1576-1564 cm^{-1}, then at 1456-1434-1413 cm^{-1} and finally at 1345-1296 cm^{-1}. Some of them were supposed to be additionally contributed from carbonyl and carboxyl movements: the band at 1586 cm^{-1} was presumably coupled with C=O stretching [31], those at 1434-1456 cm^{-1} were coupled with CCOCH bending [31] and that at 1296 cm^{-1} was coupled with C-O stretching [24]. The two strong bands at 1244 and 1210 cm^{-1} were from ring stretching, in relation to long molecular axis, but different in symmetry (B_1 and A_1 respectively), both strongly contributed from in-plane bending motions from C-O [24].

In contrast, the shoulder observed at *ca.* 1235 cm^{-1} was related to ring stretching only. The weak bands at 1152 and 990 cm^{-1} were due to a δ(C-H) and ring breath modes, respectively. The weak to very weak bands at 1082 and between 950 and 500 cm^{-1} were those of skeletal deformations [24]. The very strong doublet observed at 465 and 443 cm^{-1} was assigned to deformational modes (in plane bending) δ(C=O) and δ(C-O), respectively. Between them, one could reveal a shoulder at *ca.* 450 cm^{-1} corresponding to a skeletal deformation.

1.2. Effect of the DOX/silver adsorption geometry on the SERS spectra

Interpretation of the SERS spectra requires to understand the mechanism of binding of adsorbed molecules to metal surfaces [25]. In fact, both the adsorption geometry and the surface forces may induce spectral changes in SERS compared to Raman spectra. The changes can be related to a selective short-range enhancement of certain vibrations situated closer to the surface and oriented perpendicularly to it ("surface selection rule" proposed by Moskovits [32]). Moreover, the surface forces can induce some structural alterations.

Therefore, we examined the possible changes in chromophore orientation due to the drug concentration decrease/increase

Cite this: DOI: 10.1039/c0xx00000x

www.rsc.org/xxxxxx

ARTICLE TYPE

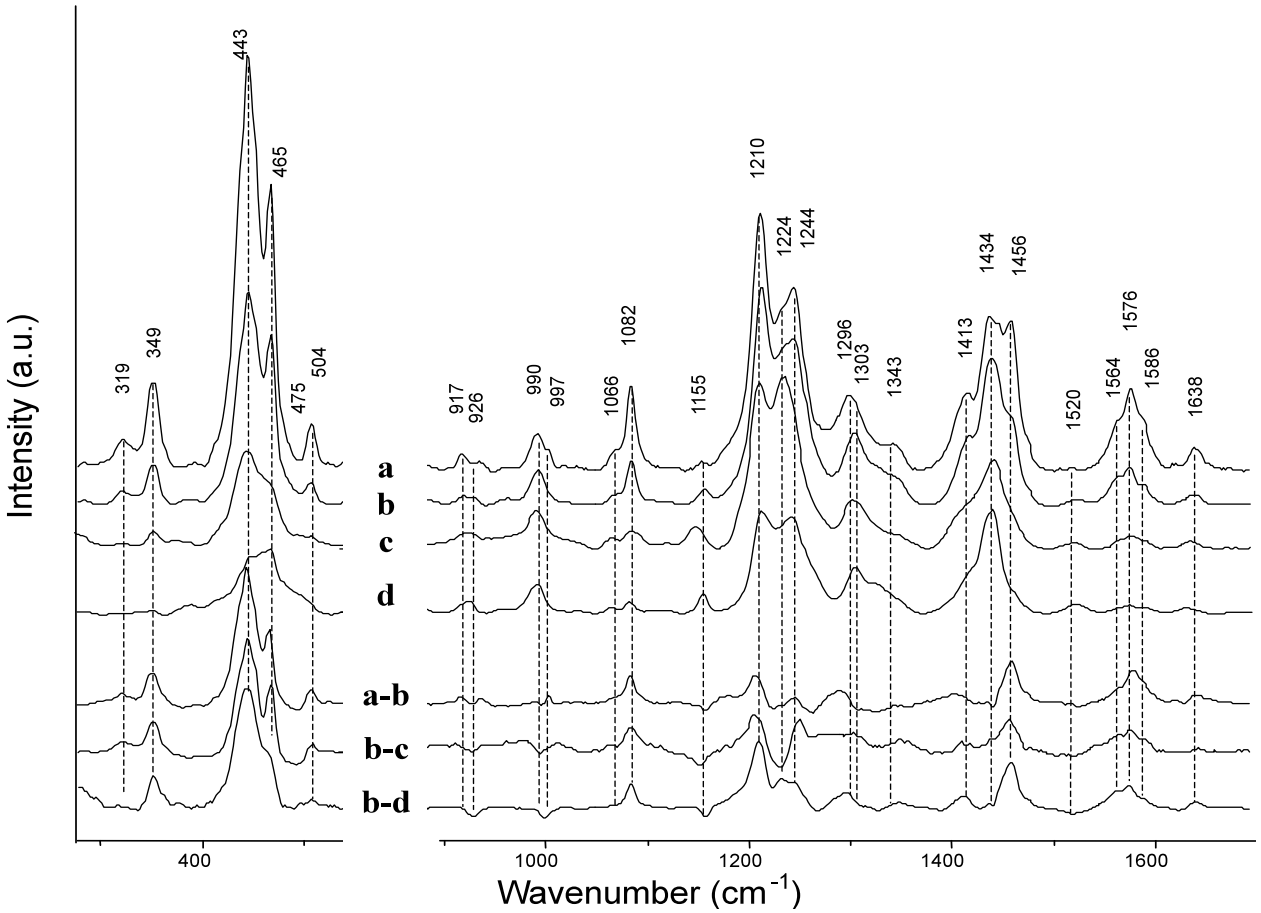

Fig. 3 Characteristic SERS spectra of doxorubicin: (a) free drug at pH 4.0; (b) free drug at pH 7.6; (c) free drug at pH 10; (d) drug-Fe (II) complex at pH 7.6, drug/iron molar ratio 1/3. The difference spectra in the bottom revealed certain similarity in terms of changes upon the amine group deprotonation (a-b), the phenol in C11 deprotonation (b-c) and in the drug-iron interaction (b-d). Experimental conditions: DOX concentration 0.8 μM for all the spectra except spectrum c (8 μM); laser power ~0.95 mW (632.8 nm); 36 scans of 1 s.

(Figure 2, black or grey curves for 8 and 0.8 μM, respectively). The commonly admitted hypothesis is that, because of additional steric hindrance at higher concentration, DOX molecules adsorbed on silver colloids recover a more perpendicular chromophore-to-surface orientation. We chose two concentration values, 0.8 μM (grey spectra) and 8 μM (black spectra), both being below 10 μM in order to avoid the stacking self-association known to take place for the anthracycline molecules at high concentrations in aqueous media [11,12].

The orientation-related effect was compared for two different pH values, 4.0 (protonated, positively charged DOX carrying NH_3^+ on its sugar moiety) and 7.6 (DOX partially deprotonated at amino group with pKa 8.2). At pH 10, the dominating form was anionic DOX, deprotonated at the phenol function in C_{11} position of the chromophore (pKa 9.5). Therefore, the pH increase from 4.0 to 7.6 should reveal the side chain effect on the chromophore orientation, while the comparison of the pH 7.6 versus 10 corresponds to the protonation state of the chromophore phenol in C11 of DOX. This should also influence the drug-surface orientation, however its main role was expected to change the electronic distribution within the chromophore, as seen in the UV-visible spectra (data not shown).

As seen in Figure 2, the SERS bands of DOX were only slightly affected by a 10-fold drug concentration increase: for both pH 4.0 and 7.6, some minor changes in relative intensities were observed, the spectra being quite superimposable. These minor changes were in agreement with the initial hypothesis about more perpendicular than flat chromophore orientation on the silver surface, for both the concentrations and pH studied here. Nevertheless, the concentration increase exhibited a slightly different effect at two pH: at pH 4.0, the main effect was the intensity increase for the bands situated above 1230 cm^{-1} (ring stretchings coupled with C=O stretching and CC-O bendings), while at pH 7.6, we observed the intensity decrease for the bands below 500 cm^{-1} (the C-O and C=O in-plane bendings). These differences indicated that the positive charge on the side chain of DOX influenced the chromophore orientation relatively to the silver surface. The latter argument was much stronger when

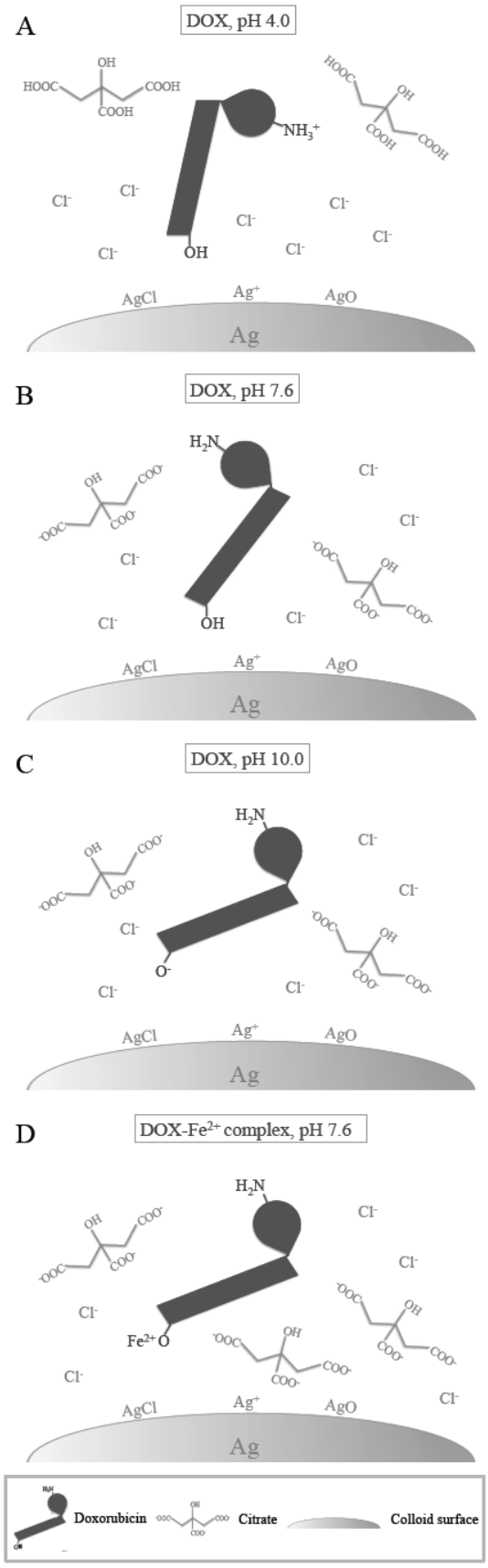

Fig. 4 Scheme illustrating the supposed geometry of DOX adsorption on the Ag NP surface at different pH and when chelated with Fe^{2+}.

comparing similar concentrations at two pH, 4.0 (Figure 3a) and 7.6 (Figure 3b): one could observe several significant orientation-related effects for the SERS bands at 1413, 1456, 443 and 465 cm^{-1}, that could be visually revealed with help of the difference spectrum (Figure 3 a-b).

The pH effect was analyzed in Figure 3. The difference spectra in the bottom of Figure 3 shed a light on similarities and differences in spectral changes observed both upon the pH increase from pH 4 to 7.6 (chromophore orientation effect, difference spectrum a-b) and from pH 7.6 to 10 (chromophore orientation plus C11 phenol deprotonation, difference spectrum b-c). Moreover, one could also remark in Figure 3 that there was also a certain similarity in the effect of pH and of ferrous iron chelation by DOX described in the next section (difference spectrum b-d quite similar to other difference spectra a-b and b-c).

A significant increase of the overall SERS intensity could be observed on going from pH 7.6 to pH 4.0. This intensity increase at pH 4 should be conditioned both by the drug/NP adsorption efficiency (probably favored (i) by electrostatic attraction of the cationic drug to the anionic solvation layers around Ag NPs and (ii) by the easier replacement of non-charged citrates by DOX) and adsorption geometry (Figure 4A). Indeed, the increase of the relative intensity (positive signals on the difference spectrum a-b in Figure 3) of several bands related to aromatic rings vibrations coupled to those of C=O and hydroxyl groups showed that, when the side chain was positively charged, the chromophore's orientation became significantly more perpendicular and the C=O and C-OH groups became closer to the surface (Figure 4A). In agreement with that reported by Fabriciova et al. (2004) [33] for anthraquinones, we could also comment on few upward and downward shifts of certain SERS bands (1303 to 1296 cm^{-1} and 1623 to 1638 cm^{-1}) for DOX on going from neutral to acidic conditions. Nevertheless, these very few and weak frequency shifts confirmed that the chromophore protonation state did not change between the pH 4.0 and 7.6. On the contrary, on going from pH 7.6 to pH 10, the phenol C11 of the chromophore was deprotonated, generating some more pronounced effect in the SERS spectra of DOX (revealed in spectrum b-c in Figure 3).

The pH increase from pH 7.6 to 10 resulted in a significant decrease of the overall SERS intensity, which was indicative of the flattening of the adsorption geometry and/or of the loss of the adsorption efficiency. Indeed, the appearance of negative charges on the chromophore may undergo some repulsion from the anions in the solvation layers around Ag NPs (Figure 4B and 4C).

To summarize the orientational aspects discussed in this section, we concluded that: (i) doxorubicin adsorbed on the silver surface was more inclined to a perpendicular orientation rather than to a flat one, even at sub-micromolar concentrations; (ii) positively charged amine groups of doxorubicin at acidic environment made the chromophore's orientation relatively to the silver surface even more perpendicular, thus making more intense the in-plane vibrational modes of aromatic rings and ring-coupled groups; (iii) on the contrary, the phenol deprotonation in basic environment flattened the orientation of the chromophore; (iv) finally, no structural alteration upon adsorption could be commented.

1.3. DOX-Fe^{2+} complexes

The ability of DOX to bind Fe^{3+} and Fe^{2+} ions in aqueous solution at neutral and basic pH conditions is well known and is

Cite this: DOI: 10.1039/c0xx00000x

www.rsc.org/xxxxxx

ARTICLE TYPE

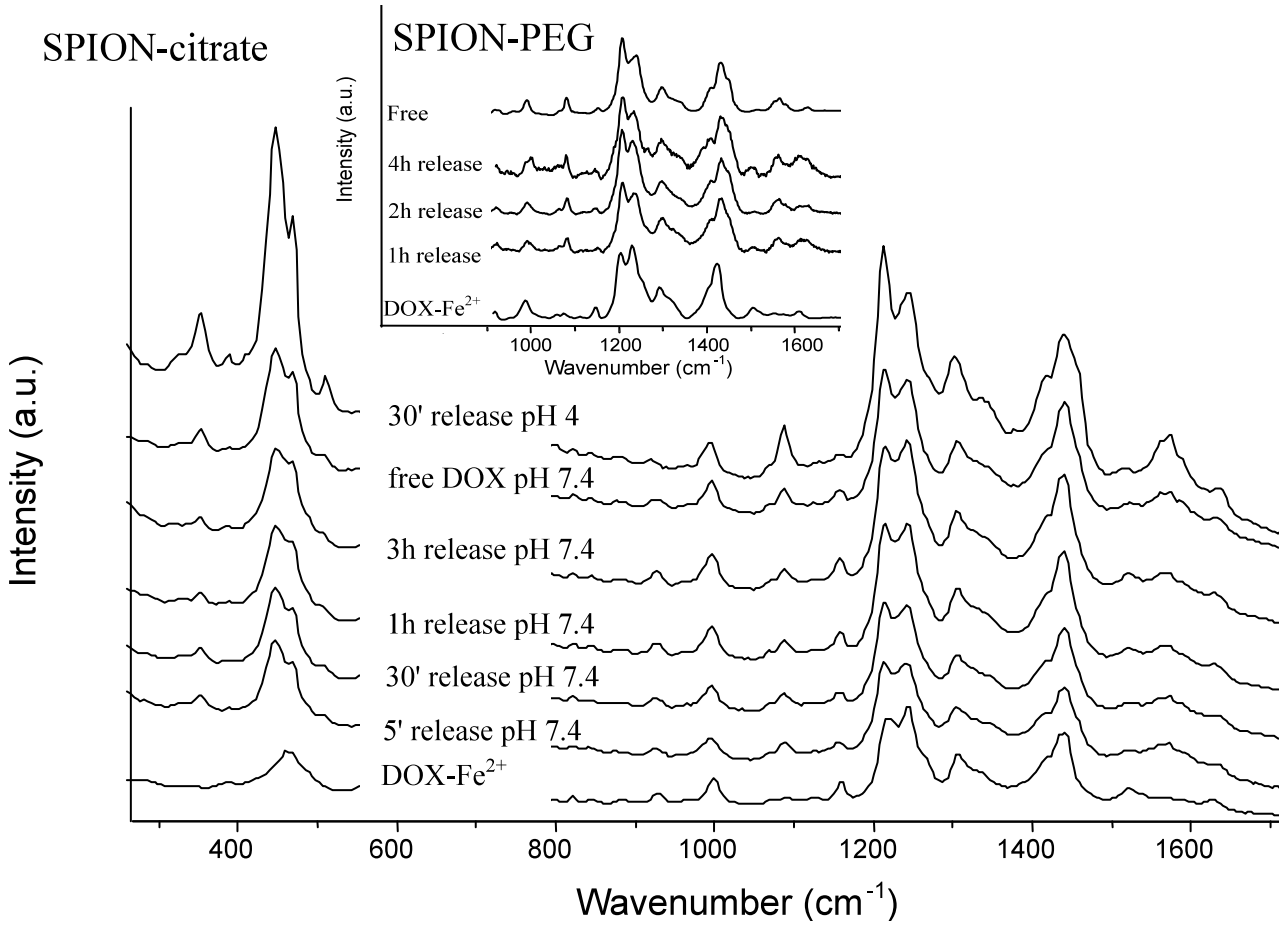

Fig.5 SERS spectra obtained during release of DOX at pH 7.4 from citrated SPIONs (from the bottom up: DOX-Fe^{2+} complex, release in 5 min, 30 min, 1h, and 3h at pH 7.4, free DOX at pH 7.4, and DOX released in 30 minutes at pH 4.0). Insert: release from PEGylated SPIONs (from the bottom up: DOX-Fe^{2+} complex, release in 1h, 2h, 4h and free DOX).

described elsewhere [16,6,11]. The binding is thought to imply the chelate formation involving one carbonyl group and its hydroxyl neighbor, where the hydrogen is replaced by iron ion (Figure 1). The reprotonation of DOX upon pH decrease dissociates these complexes. In the DOX molecule, there are two sites that can be involved in the iron chelation: the higher affinity site (C=O in position C12 and C-OH in C11) and the lower affinity site (C=O in C5 and C-OH in C6). Nevertheless, at aggregate-free drug concentration and with low iron excess, the chelation involves mainly the upper affinity site (positions C11 and C12) [11], thus resulting in a complex stoechiometry of 1:1 for DOX:iron, independently on the ferrous or ferric nature. Since the chelate concerns the electronic structure of the chromophore, there is a characteristic bathochromic effect in the UV-visible spectrum of the drug observed as an increase of the absorption band at *ca.* 600 nm which also increases upon the phenol deprotonation at higher pH, but to a much lower extend than in case of iron ions chelation.

As we reported recently, the iron ion of DOX-Fe^{2+} chelate was able to coordinate the Fe-OH groups present on the surface of SPIONs in neutral aqueous medium. This favored the drug adsorption and therefore the drug loading on SPIONs-based magnetic nanocarriers [15,16]. The most interesting was that this loading mechanism resulted in a pH-dependent release, accelerated when pH was below 6. To load DOX on the magnetic nanocarriers, the optimal operating conditions were pH 7.6 and 1.5 molar excess of Fe^{2+} (in order to favor the stoechiometry 1 Fe^{2+}:1 DOX, Figure 1) [16].

The SERS spectrum of DOX-Fe^{2+} complex (Figure 3d) formed at pH 7.6 for 0.8 µM drug concentration and 3-fold molar excess of iron showed significant changes compared to that of free DOX taken at the same pH (Figure 3b) and concentration (difference spectrum b-d). A decrease of the bands at 1576 cm^{-1} together with its shoulders changed, relatively to the band at 1520 cm^{-1} (increased), as the bands at 1456 and 1413 cm^{-1} relatively to the band at 1434 cm^{-1} (nearly constant). The same observation was

made for the band at 1287 cm^{-1} relatively to that at 1322 cm^{-1} (increased), for the bands at 1210 and 1224 cm^{-1} relatively to the band at 1244 cm^{-1} (nearly constant), for the band at 1082 cm^{-1} and all the bands below 500 cm^{-1} relatively to the band at 990 cm^{-1} (nearly constant).

Interestingly, a comparison of the difference spectra b-c and b-d (Figure 3) highlighted that most of the modifications noticed in the SERS spectra of DOX upon the pH increase were similar to those observed when DOX chelated Fe^{2+} at pH 7.6. Here again, the similarity should indicate some additional flattening of the drug adsorption on the silver surface (Figure 4D). The main features that allowed to distinguish the SERS spectra of DOX-iron complex from those of free DOX deprotonated on the phenol C11 were: (i) the shift of the strong band from 1224 to 1244 cm^{-1}; (ii) the significantly lower intensity of the band at 1576 together with its shoulders at 1586 and 1564 cm^{-1} compared to their neighbors situated at 1638 and 1520 cm^{-1}; (iii) the higher intensity ratio for the bands at 1434/1413, 1244/1224, 1210/1224 cm^{-1} and 465/443 cm^{-1}. These SERS bands seemed to be more sensitive to the electronic density redistribution over a chromophore when chelated with iron. Interestingly, in spite of the flattened adsorption on silver, the DOX-iron complexes gave quite intense SERS spectra, 2 to 3-fold more intense than those of the free drug at the same concentration. This could be explained by the increased adsorption efficiency for the complexes carrying positive charge due to coordination of one ferrous iron (Figure 4D).

Apart from these mechanistic considerations, the remarkable experimental fact was that the DOX-Fe^{2+} complex had the characteristic SERS pattern, which allowed to selectively detect and distinguish it from the free DOX spectrum. Thereafter, we will use this pattern for analytical purposes.

1.4. Study of DOX-Fe^{2+} complex released from magnetic nanovectors based on SPIONs

In this section, we will analyze the DOX released from SPIONs, citrate-stabilized and coated with PEG.

The citrate-stabilized SPIONs were efficiently loaded with DOX by their incubation with pre-formed DOX-Fe^{2+} complexes at pH 7.6. The loading attained 14 % drug/iron oxides w/w and the loaded SPIONs were more cytotoxic to MCF-7 cancer cells than the free DOX solution at the same sub-micromolar concentration [16]. One of the hypothesis was that the nanocarriers released the drug-ion complexes, which may be more cytotoxic that the DOX alone. The question about the origin of the increased cytotoxicity remained very interesting to elucidate. The release of the drug at pH 7.4 was measured by means of UV-visible spectrometry and HPLC. However, both of these approaches had significant limitations related to the low sensitivity of the former and to the dissociating complexes with the latter. Therefore, we attempted to use SERS to check if there were some DOX-iron complexes in the release medium.

After the drug released from the DLCS (Figure 5), the SERS spectrum showed certain modifications compared to the free DOX spectrum. However, the overall spectral shape and in particular the high intensity ratio for the bands at 1576/1520 and 443/465 cm^{-1} was indicative that the dominant fraction in the release media was the free DOX and not the DOX-Fe^{2+} complex. Indeed, the DOX-Fe^{2+} complex should exhibit a lower intensity of the bands between 1576 and 1520 cm^{-1}, with a higher intensity ratio for the bands at 465/443 cm^{-1}, 1244/1224 and 1210/1224 cm^{-1}. In fact, the presence of some minor fraction of DOX-Fe^{2+} complexes could not be excluded, in particular at early release stages. We supposed this minor fraction may remain in bulk solution after NP incubation. This could explain the minor differences observed between the SERS spectrum at 5 min and free DOX at the same pH, the main being the slight change in intensity ratio for the bands at 1210/1244/1224 cm^{-1}. In spite of the fact that the DOX-iron complex showed a superior affinity for the silver colloids and presented an increased SERS detection sensitivity compared to the free DOX, we did not detect any further increase of the presumed complex signal, even over release times of 3-4 hours (Figure 5).

Thus, neither DOX-iron nor iron release from the citrated SPIONs could be commented. This was also the case with SPIONs coated with PEG and loaded with DOX-iron complexes: the drug was mainly released under its free form (Figure 5 insert), as shown by the minor change in intensity ratio for the bands at 1210/1244/1224 cm^{-1}, and the quantity of free DOX increased with time. The absence of iron traces in the release medium was in agreement with the work of Pang et al. [34], who established that iron oxides did not release ionic iron at physiological pH. So the ferric ion playing the role of intermediate in the DOX-SPION binding stood on the nanoparticles.

The spectrum of DOX released in 30 minutes at pH 4.0 was typical of DOX in acidic medium, which was also concomitant with the hypothesis that the release of DOX under acidic conditions was under free form, and was expected to be total.

2. Materials and methods

2.1. Samples

Chemicals Doxorubicin hydrochloride was purchased from TEVA Pharmaceuticals Ltd. (Puteaux, France). PBS, ferric nitrate nonahydrate ($Fe(NO_3)_3.9H_2O$), anhydrous ferric chloride ($FeCl_3$), silver nitrate, trisodium citrate and citric acid were purchased from Fisher Bioblock Scientific (Illkirch, France). Ferrous chloride ($FeCl_2$, $4H_2O$) was obtained from Acros Organics (Noisy Le Grand, France). 3-aminopropyltrimethoxy silane (APTES) and methoxypoly(ethylene glycol) 5000 propionic acid N-succinimidyl ester (activated PEG, aPEG) were purchased from Sigma Aldrich (Saint-Quentin-Fallavier, France). Sodium acetate and tris-(hydroxymethyl)-aminomethane (Tris) were provided by Merck (Fontenay-sous-Bois, France), and ferrous ammonium sulphate ($(NH_4)_2Fe(SO_4)_2.6H_2O$) by Carlo Erba (Val de Reuil, France).

All other reagents were of analytical grade. In all the experiments, water was previously deionized. Dialysis tubing (cellulose, molecular weight cut off 8000 Da) was furnished by Interchim (Montluçon, France).

DOX-Fe^{2+} complexes In Tris buffer pH 7.4, some increasing quantities of Fe^{2+} ions (ferrous ammonium sulphate) were added to DOX solution, in order to obtain molar ratios Fe^{2+}/DOX from 0.1 to 3. These conditions permitted to form complexes with different stoechiometries. The complex with stoechiometry 1:1 was loaded on nanovectors.

SPIONs and SPION-DOX The ferrofluids, the citrated SPIONs

and the PEGylated SPIONs were prepared according to methods described previously [28,16]. Briefly, superparamagnetic iron oxide nanoparticles (SPIONs) were synthesized by aqueous coprecipitation of ferric and ferrous chlorides in alkaline medium. In order to stabilize the surface chemical composition, SPIONs were oxidized by ferric nitrate and finally peptized in nitric acid and re-suspended in a determined volume of water. These SPIONs exhibit a size of 10 nm in TEM, as described elsewhere [28].

In order to increase the stability of ferrofluids at physiological pH, the SPIONs were incubated with 1.5 g/L citric acid under agitation for 2h, as described elsewhere [16]. Then the pH was readjusted to 7.0, and the citrated SPION were purified from excess citrate by dialysis against water. These particles, characterized by a hydrodynamic diameter of 20 nm, as described elsewhere [16] will be further mentioned as "CS" for citrated SPIONs.

The PEGylated ferrofluids were prepared according to a method described previously [28]. SPIONs were silanized by a 12h contact with APTES, washed and peptized in water at pH 3. Then SPIONs were PEGylated by a 24h contact with a-PEG, and purified by dialysis against water. These particles, characterized by a hydrodynamic diameter around 70-80 nm, as described elsewhere [15,28], will be further mentioned as "PS" for PEGylated SPIONs.

Citrated (CS) and PEGylated SPIONs (PS) were loaded by contact with pre-formed DOX-Fe^{2+} complex, as described elsewhere [16,15]. These particles will be further mentioned as "DLCS" for DOX-loaded citrated SPIONs and "DLPS" for DOX-loaded PEGylated SPIONs. The DLCS were loaded with 10 % of DOX (w/w iron oxides), and the DLPS with 3.0% of DOX (w/w iron oxides), as described elsewhere [15,16].

Ag NPs Silver colloids were prepared using a well-known Lee and Meisel method [29] consisting in reducing silver nitrate in presence of an excess of trisodium citrate and heat. Just before use, the silver colloids were aggregated by adding $NaClO_4$ and activated either by adding NaCl or by simple dilution in Cl^--containing PBS buffer pH 7.4, as described elsewhere [30].

2.2 SERS Study

DOX and DOX-Fe^{2+} complex Small aliquots of samples were added to activated colloids. For each sample series, ratio of colloids, buffer and sample were optimized in order to obtain maximum signal detection.

Drug loading/release on/from SPIONs

The kinetics of DOX-Fe^{2+} loading in PEGylated SPIONs was studied by regular measurements of SERS spectra from small aliquots mixed with activated colloids and incubated for 5 minutes, to favor the binding of DOX on colloids.

The release of DOX from citrated and PEGylated nanovectors was studied in a fixed volume of Tris buffer pH 7.4, continuously shaken and thermostated at 37°C. At given time intervals, aliquots were centrifuged in order to separate the nanoparticles of the release medium, and then added to activated silver colloids.

Instrumental SERS measurements were carried out using a LabRAM confocal microspectrometer (Horiba Jobin-Yvon, France) equipped with an Olympus BX-40 microscope, a 300 mm focal length spectrograph (dispersion grating of 1800 grooves per mm) and an air-cooled CCD detector. The samples (30 µL drop) were loaded into a small quartz cell for measurements. Sample irradiation and collection of SERS spectra were performed through a 10× microscope objective (numerical aperture 0.50; LMPlan Fl, Olympus, Japan), in a non-confocal mode (confocal hole opened to 800 µm). The DOX SERS spectra were excited with a 632.8 nm line of a He-Ne laser and the laser power on the samples did not exceed 1 mW. No sample photodegradation was observed under the conditions used. Each spectrum was recorded as an average of 36 scans (0.1–2 s per scan). The spectra presented in the figures are averages of at least three independent measurements. Both experiment control and following data treatment were performed using the LABSPEC software package.

Conclusions

SERS spectroscopy using Ag nanoparticles was successfully applied to study DOX and its complex with Fe^{2+}. Free DOX was characterized at different concentrations and pH. By this way, we assigned the typical modifications of DOX spectra to the drug protonation state and its orientation on the silver surface. Then, the SERS spectra of DOX-Fe^{2+} complexes and the main features discriminating them from the free DOX spectra were finely described. Finally, the SERS technique was demonstrated to be able to characterize the drug released from magnetic nanocarriers, namely to confirm its release in a free form. These results highlighted the potent of the SERS approach to study DOX-iron interactions in relation with drug delivery and its biological activity.

Acknowledgments

This study was supported in part by grants from the Ligue Nationale contre le Cancer (Délégation Indre-et-Loire, France) and from the Region Centre, France (NANOMAG Project). The authors acknowledge Delphine Perron for the technical assistance in the SERS measurements and Dr. Martin Soucé for the fruitful discussions.

Notes and references

[a] *Université François-Rabelais, EA 6295 « Nanomédicaments et Nanosondes», Tours, F-37200 France. Fax: (33)-247367270; Tel: (33)-247367162; E-mail: igor.chourpa@univ-tours.fr*

[b] *Wake Forest Institute for Regenerative Medicine, Winston-Salem, North Carolina, 27157 United States.*

1. J. Lankelma, H. Dekker, F. R. Luque, S. Luykx, K. Hoekman, P. van der Valk, P. J. van Diest, and H. M. Pinedo, *Clin. Cancer Res. Off. J. Am. Assoc. Cancer Res.*, 1999, **5**, 1703–1707.
2. X. Li, D. J. Hirsh, D. Cabral-Lilly, A. Zirkel, S. M. Gruner, A. S. Janoff, and W. R. Perkins, *Biochim. Biophys. Acta Bba - Biomembr.*, 1998, **1415**, 23–40.
3. A. W. El-Kareh and T. W. Secomb, *Neoplasia New York N*, 2005, **7**, 705–713.
4. C. Eliasson, A. Lorén, K. V. Murty, M. Josefson, M. Käll, J. Abrahamsson, and K. Abrahamsson, *Spectrochim. Acta. A. Mol. Biomol. Spectrosc.*, 2001, **57**, 1907–1915.
5. L. Gallois, M. Fiallo, and A. Garnier-Suillerot, *Biochim. Biophys. Acta*, 1998, **1370**, 31–40.
6. N. R. Bachur, R. D. Friedman, and R. G. Hollenbeck, *Cancer Chemother. Pharmacol.*, 1984, **12**, 5–9.
7. D. Gelvan, E. Berg, P. Saltman, and A. Samuni, *Biochem. Pharmacol.*, 1990, **39**, 1289–1295.

8. M. Fiallo, A. Laigle, A. Garnier-Suillerot, C. Amirand, J. P. Ballini, L. Chinsky, M. Duquesne, B. Jolles, F. Sureau, and P. Y. Turpin, *Biochim. Biophys. Acta*, 1993, **1177**, 236–244.
9. M. Feng, Y. Yang, P. He, and Y. Fang, *Spectrochim. Acta. A. Mol. Biomol. Spectrosc.*, 2000, **56**, 581–587.
10. Y. Octavia, C. G. Tocchetti, K. L. Gabrielson, S. Janssens, H. J. Crijns, and A. L. Moens, *J. Mol. Cell. Cardiol.*, 2012, **52**, 1213–1225.
11. M. M. Fiallo, A. Garnier-Suillerot, B. Matzanke, and H. Kozlowski, *J. Inorg. Biochem.*, 1999, **75**, 105–115.
12. R. Kiraly and R. B. Martin, *Inorganica Chim. Acta*, 1982, **67**, 13–18.
13. F. Capolongo, M. Giomini, A. M. Giuliani, B. F. Matzanke, U. Russo, A. Silvestri, A. X. Trautwein, and R. Barbieri, *J. Inorg. Biochem.*, 1997, **65**, 115–122.
14. A. Samuni, P. L. Chong, Y. Barenholz, and T. E. Thompson, *Cancer Res.*, 1986, **46**, 594–599.
15. J. Gautier, E. Munnier, A. Paillard, K. Hervé, L. Douziech-Eyrolles, M. Soucé, P. Dubois, and I. Chourpa, *Int. J. Pharm.*, 2012, **423**, 16–25.
16. E. Munnier, S. Cohen-Jonathan, C. Linassier, L. Douziech-Eyrolles, H. Marchais, M. Soucé, K. Hervé, P. Dubois, and I. Chourpa, *Int. J. Pharm.*, 2008, **363**, 170–176.
17. C. Greulich, J. Diendorf, T. Simon, G. Eggeler, M. Epple, and M. Köller, *Acta Biomater.*, 2011, **7**, 347–354.
18. S. F. Medeiros, A. M. Santos, H. Fessi, and A. Elaissari, *Int. J. Pharm.*, 2011, **403**, 139–161.
19. M. Tokarska-Schlattner, M. Zaugg, C. Zuppinger, T. Wallimann, and U. Schlattner, *J. Mol. Cell. Cardiol.*, 2006, **41**, 389–405.
20. K. A. Willets and R. P. Van Duyne, *Annu. Rev. Phys. Chem.*, 2007, **58**, 267–297.
21. X.-M. Lin, Y. Cui, Y.-H. Xu, B. Ren, and Z.-Q. Tian, *Anal. Bioanal. Chem.*, 2009, **394**, 1729–1745.
22. M. V. Cañamares, J. V. Garcia-Ramos, S. Sanchez-Cortes, M. Castillejo, and M. Oujja, *J. Colloid Interface Sci.*, 2008, **326**, 103–109.
23. A. Shkilnyy, M. Soucé, P. Dubois, F. Warmont, M.-L. Saboungi, and I. Chourpa, *The Analyst*, 2009, **134**, 1868.
24. A. Beljebbar, G. . Sockalingum, J. . Angiboust, and M. Manfait, *Spectrochim. Acta. A. Mol. Biomol. Spectrosc.*, 1995, **51**, 2083–2090.
25. G. Smulevich and A. Feis, *J. Phys. Chem.*, 1986, **90**, 6388–6392.
26. Q. Yan, W. Priebe, J. B. Chaires, and R. S. Czernuszewicz, *Biospectroscopy*, 1997, **3**, 307–316.
27. I. R. Nabiev, H. Morjani, and M. Manfait, *Eur. Biophys. J. Ebj*, 1991, **19**, 311–316.
28. K. Hervé, L. Douziech-Eyrolles, E. Munnier, S. Cohen-Jonathan, M. Soucé, H. Marchais, P. Limelette, F. Warmont, M. L. Saboungi, P. Dubois, and I. Chourpa, *Nanotechnology*, 2008, **19**, 465608.
29. P. C. Lee and D. Meisel, *J. Phys. Chem.*, 1982, **86**, 3391–3395.
30. I. Chourpa, F. H. Lei, P. Dubois, M. Manfait, and G. D. Sockalingum, *Chem. Soc. Rev.*, 2008, **37**, 993–1000.
31. Y. Nonaka, M. Tsuboi, and K. Nakamoto, *J. Raman Spectrosc.*, 1990, **21**, 133–141.
32. M. Moskovits, *J. Chem. Phys.*, 1982, **77**, 4408.
33. G. Fabriciova, J. . García-Ramos, P. Miskovsky, and S. Sanchez-Cortes, *Vib. Spectrosc.*, 2004, **34**, 273–281.
34. S. C. Pang, S. F. Chin, and M. A. Anderson, *J. Colloid Interface Sci.*, 2007, **311**, 94–101.

Chapitre 3 : Etude *in vivo* des nanovecteurs magnétiques pour la délivrance de la DOX sur un modèle animal de cancer du sein

Publication 5 : Efficacy and hemotoxicity of stealth magnetic nanovectors of doxorubicin on breast cancer xenografts

Soumise dans Nanoscale, 2013

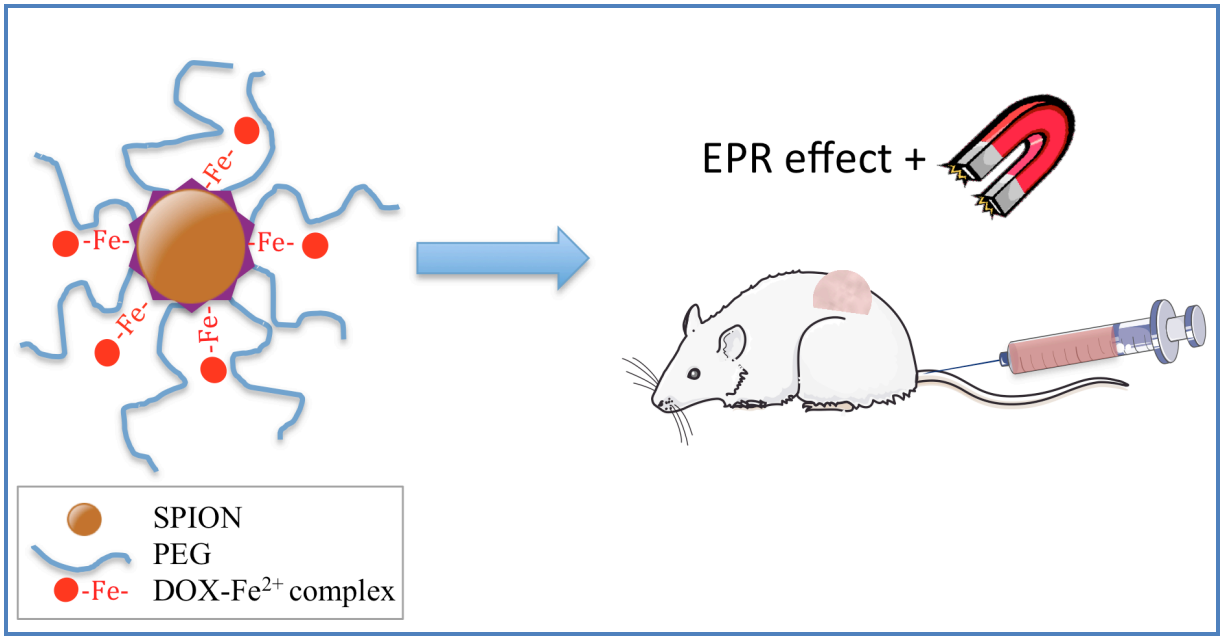

Pour l'évaluation *in vivo* des nanovecteurs magnétiques de DOX, les DLPS (DOX-loaded PEGylated SPIONs), un modèle animal a été développé. Des cellules MDA-MB 435 (carcinome du sein humain) ont été injectées en sous-cutané dans le flanc droit de souris femelles NMRI nude. L'immunodéficience de ces souris (déficit en lymphocytes T) permet d'induire une croissance tumorale à partir de lignées cellulaires cancéreuses humaines.

Avant toute évaluation *in vivo*, les nanovecteurs ont été incubés avec les cellules MDA-MB 435. Si l'internalisation des nanovecteurs a été vérifiée précédemment sur cellules MCF-7, dans cet article nous nous intéressons aux voies d'endocytose. La microscopie électronique en transmission (MET) a permis de révéler que les SPIONs PEGylés entrent dans les cellules à la fois par la voie des clathrines et la voie des cavéoles. Cette constatation est de première importance, dans la mesure où le devenir intracellulaire des nanovecteurs dépend de ces voies. Les SPIONs PEGylés internalisés par la voie des cavéoles sont retrouvés dans des cavéosomes (pH 7,4) alors que ceux pénétrant par endocytose clathrine-dépendante sont retrouvés dans les endosomes, puis les lysosomes (pH 5). La libération pH-dépendante de la DOX à partir des DLPS se retrouverait donc modulée par le fait que les nanovecteurs empruntent les deux voies.

L'essai de viabilité cellulaire réalisé sur les cellules MDA-MB 435 a mis en évidence que la cytotoxicité des DLPS dépend du nombre de nanovecteurs internalisés par les cellules. A une concentration de 1 µM, les DLPS sont internalisés et dirigés efficacement vers les compartiments intracellulaires, entraînant une cytotoxicité comparable à celle de la DOX en solution. Ce phénomène est saturable, ce qui explique qu'à 10 µM, la baisse de la viabilité cellulaire n'est pas supérieure à celle observée à 1 µM.

Un protocole thérapeutique a été initié sur des souris NMRI nude, après injection sous-cutanée dans le flanc droit de cellules MDA-MB 435. Le groupe des souris témoin a reçu du sérum physiologique en injection intraveineuse. Les autres animaux ont reçu au total 6 mg/kg de DOX ou équivalent (3 injections de 2 mg/kg de DOX, à 1 semaine d'intervalle) : un groupe a reçu la DOX en solution, un autre les DLPS, un dernier les DLPS avec application d'un aimant au niveau de la tumeur pendant l'heure suivant l'injection. Malgré la variabilité du modèle animal, il apparaît que le traitement avec DLPS limite significativement la croissance tumorale, par rapport au témoin. Par contre, l'application d'un aimant ne semble pas apporter de bénéfice. Les modalités du ciblage magnétique sont à étudier avec plus de développements méthodologiques.

Enfin, les effets secondaires des traitements ont été appréciés sur des échantillons sanguins des animaux. Le traitement avec les DLPS limite les effets secondaires ordinairement liés à l'administration de la DOX. Ce premier essai *in vivo* pose les bases de futures évaluations des DLPS et d'autres nanovecteurs.

Nanoscale

Dynamic Article Links ►

Cite this: DOI: 10.1039/c0xx00000x

www.rsc.org/xxxxxx

ARTICLE TYPE

Efficacy and hemotoxicity of stealth magnetic nanovectors of doxorubicin on breast cancer xenografts

Juliette Gautier,*[a] Emilie Allard-Vannier, *[a] Julien Gaillard,[b] Jorge Domenech,[c] and Igor Chourpa[a]

Received (in XXX, XXX) Xth XXXXXXXXX 20XX, Accepted Xth XXXXXXXXX 20XX

DOI: 10.1039/b000000x

In the field of oncology, research is now turned to theragnostic nanosystems, ensuring drug delivery, tumor targeting, and imaging for diagnosis/monitoring. In this context, we designed PEGylated SPIONs for the delivery of doxorubicin (DOX), an antineoplastic agent. These DOX-loaded PEGylated SPIONs or DLPS already exhibited a pH-dependent release of DOX *in vitro*, and should be relevant for DOX delivery *in vivo*, as well as for magnetic drug targeting (MDT) and magnetic resonance imaging (MRI). The aim of this study was to evaluate the potential applications of DLPS *in vivo,* as drug carrier systems for tumor reduction on breast xenograft bearing mice. Prior to the animal model, the main internalization pathways of the nanovectors were identified as caveolae- and clathrin-mediated endocytosis on breast MDA-MB435 cells. The time- and quantity-dependence of the NP uptake by the cells modified the *in vitro* cytotoxicity of DLPS in MTT assays. The *in vitro* antiproliferative effect of DLPS not only depended on DOX concentration but also on the NP internalization efficacy that explained the slight differences observed between DLPS and DOX in solution. On bearing xenograft tumors NMRI nude mice, DLPS exhibited a limitation of tumor growth equivalent to that of free DOX, in normal conditions of tumor growth. The application of an external magnetic field on tumors, *i.e.* MDT, did not improve the efficacy of the DLPS treatment. Nevertheless, the vectorization of DOX via DLPS seemed to limit the hematologic side effects usually related for DOX (anemia, thrombocytopenia and leukopenia).

Introduction

In the field of nanomedicine applied to oncology, some nano-objects are already available on the market, for imaging and diagnosis (Feridex®/Endorem®, Resovist®/Cliavist®) or for anticancer drug delivery (Doxil®, Abraxane®). The research efforts are now turned to the design of multifunctional nano-objects, associating imaging functions, specific targeting of the tumor microenvironment, and anticancer drug controlled release. Such "theragnostic" nanosystems are now extensively studied [1–9]. In this context, we designed polymer-coated nanovectors for the delivery of doxorubicin, an anticancer molecule of the anthracycline family. These potential theragnostic nanosystems were hybrid nanocarriers, that is metallic inorganic cores based on superparamagnetic iron oxide nanoparticles (SPIONs) [10–13] functionalized with organic compounds [1,14]. SPIONs often present interesting nanosizes below 100 nm allowing their intravenous administration and their uptake by the target cells. The high atomic number of iron provides good contrast for visualizing SPIONs after the realization of sections in tissue or in culture cells by transmission electron microscopy (TEM). Furthermore, the magnetic properties of magnetite (Fe_3O_4) or maghemite (γ-Fe_2O_3) cores confer them properties of negative T2 contrast agents in magnetic resonance imaging (MRI) [15,13,16]. Lastly, SPIONs are commonly involved in magnetic drug targeting of tumors (MDT), that is the application of an external magnetic field in order to retain nanovectors in the vicinity of tumors [17–19]. So SPIONs can assume the functions of drug cargos, *in vitro/in vivo* imaging agents and tumor targeting systems [20,5,13].

SPION surface was functionalized with biocompatible polyethylene glycol (PEG 5000), covalently bound to the iron core via an aminopropylsilane (APTES) (figure 1) [21]. These PEGylated SPIONs, also called PS, presented an hydrodynamic diameter of 70 nm, a neutral surface charge at physiological pH, and a narrow size distribution [22]. They also exhibited a reduced uptake by monocytes and macrophages, a poor *in vitro* complement activation and a prolonged blood circulation time (blood half-life $t_{1/2} = 76 \pm 6$ min) [23]. This shown stealthiness made them suitable for novel drug carrier systems in an *in vivo* cancer model.

Doxorubicin (DOX) was loaded on PS using a pre-formed DOX-Fe^{2+} complex (figure 1) [24]. The chelated iron bound DOX to the PS surface. The complex dissociated in acidic conditions, ensuring an accelerated release [22]. As the tumor environment is known to be more acidic (6.8-6.9) than healthy tissues (7.4), such a strategy is especially attractive for achieving tumor drug delivery. Moreover, most of the nanocarriers can easily penetrate into cells by endocytosis and end up into endosomes/lysosomes, where the decreasing pH values (6.5 to 4.5) can accelerate the release of the entrapped drug. These nanocarriers were called "DLPS" for DOX-loaded PEGylated SPIONs. DLPS demonstrated their *in vitro* ability to penetrate into cancer cells, to

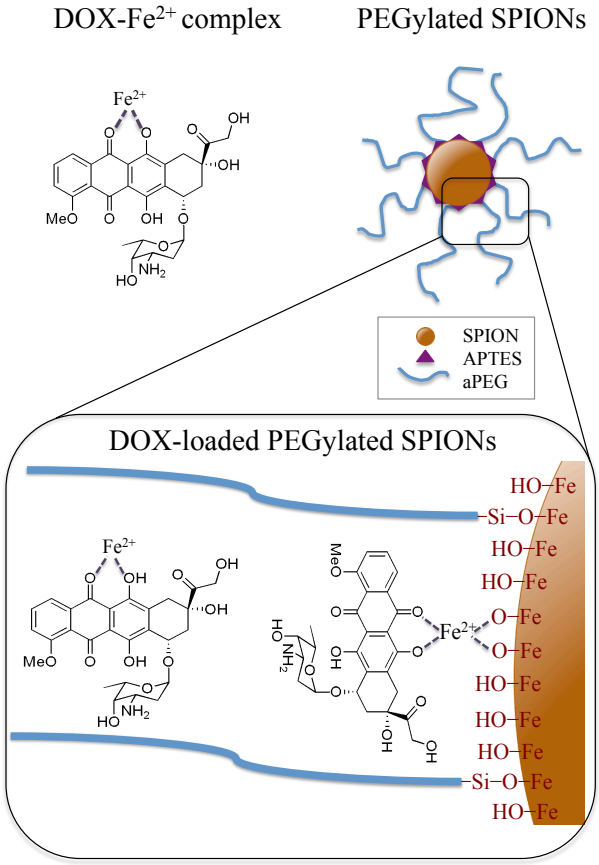

Figure 1. Schematic representation of the nanocarrier structure

release DOX in a sustained and pH-sensitive manner, and demonstrated an *in vitro* cytotoxicity on breast cancer cells MCF-7 [22]. The presence of DOX close to the NP core did not alter the SPION surface as the *in vitro* and *in vivo* stealthiness was not affected compared to PS [23].

These previous *in vitro* studies were concrete foundations to plan *in vivo* studies with DLPS. The purpose of the present study is now to evaluate the potentiality of DLPS to induce tumor reductions in an animal model. Before using MDA-MB435 cells (human breast carcinoma cells) to induce tumors on mice, we identified the main endocytosis pathways for DLPS into these cells, using transmission electron microscopy (TEM). As the endocytosis mechanisms involved in nanocarriers uptake can be expected to affect their intracellular localization and trafficking, this is of first importance to understand and study these pathways. Indeed, in the present study, this could influence the DOX release from DLPS, and then their antiproliferative efficacy, as determined by an MTT assay on MDA-MB435 cells. After subcutaneous injection of these cells and the development of solid tumors, nude mice were involved in a therapeutical protocol (6 mg/kg of DOX or equivalent, 2 mg/kg once a week, three times). The DLPS were injected intravenously and compared to a treatment with saline or DOX in solution by monitoring the tumor growth. An external magnet was also tested to evaluate the feasibility of magnetic drug targeting on mice receiving DLPS. Finally, the side effects and the hemotoxicity were explored on mice treated with vectorized DOX or DOX in solution. To our knowledge, this paper is one of the very few studies dealing with tumor reduction using SPIONs to vectorize doxorubicin anticancer agent. [25,26].

1. Results and discussion

1.1. Internalization pathways of nanovectors

To visualize the uptake of nanocarriers, MDA-MB435 cells were incubated with PS at 200 mg/L for 1 to 48 h, then washed to eliminate the untaken nanocarriers, fixed and examined in transmission electron microscopy (TEM). DLPS were not used as it was supposed to generate modifications in the metabolism or cell death, even for short incubation times. After 1h, some nanocarriers were found in the close proximity of cell membranes, in the form of clusters of few nano-objects (figure 2A and B) or small aggregates (2C) near filopodia. Observations of single objects near the cell membrane were reported with phospholipid-coated SPIONs on murine macrophages and hepatocytes [27], and clusters were observed with PEG-coated SPIONs on human fibroblasts [28]. The presence of clusters on images can have further explanations. First, the formation of small aggregates of iron oxide cores during PEG grafting should not be excluded. Nevertheless, this aggregation was minor as demonstrated both by superparamagnetic behavior and by polydispersity index values below 0.2 characteristic of monodisperse colloids [21]. Moreover, aggregation phenomena of PS and DLPS were never observed in culture media. It could also be due to the high PS concentration used for incubation (200 mg/L). In any case, clusters exhibited a limited size, under 100 nm, which should not have hampered their uptake by the cells.

On the same images, flask-shaped invaginations in plasma membrane appeared (2A and B), and some clusters were already internalized in intracellular structures (2C). After 2h, invaginations in plasma membrane around PS clusters were also observed (2D and E). Internalized nanocarriers were found in rosette-shaped structures, near the membrane (2F) or deeper in the cell. For longer times of incubation, PS were found in intracellular compartments, in more or less dense populations (for example after 24h (figures 2G and H) and 48h (figure 2I)).

The presence of invaginations in the plasma membrane and the uptake of external fluid suggested that PS were internalized by endocytosis. This result was expected, since endocytosis is the prevalent way for the uptake of nano-objects below 100 nm in size into non-phagocytic mammalian cells (cesium oxide nanoparticles [29], TiO_2 nanoparticles [30], lipid-based nanoparticles [31], coated SPIONs [32]). The typical morphology of invaginations indicated a caveolae and clathrin-mediated phenomenon [33]. Indeed, figures 2A-D show membrane invagination with electron-dense layer and a size of about 50-100 nm characteristic of clathrin-coated pits [34].

Moreover, the vesicles merging (figure 2C, 2F) with a famous rosette aspect were typical of caveolae [35,36,34]. The invaginations without electron-dense layer and the size in the lower end of the 50-100 nm range strengthened the hypothesis of caveolae structures (figure 2E). Caveolae vesicles are known to continuously dock and fuse with early endosomes, then dissociate, in a “kiss-and-run” interaction [37]. The observation of both caveolae and clathrin structures was coherent with other studies found in the literature [31,38–40], as these two pathways were

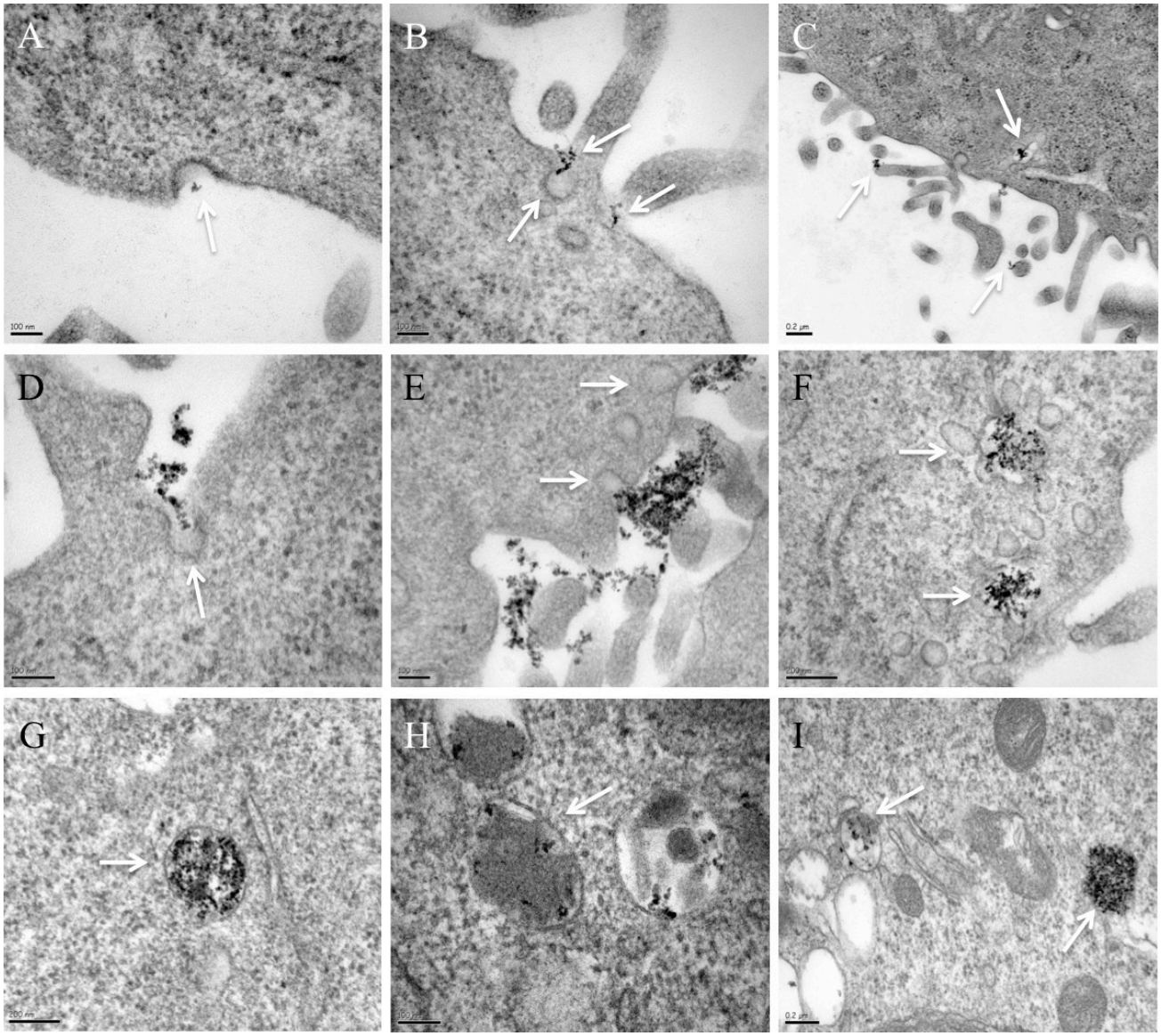

Figure 2. TEM images after incubation of PS on MDA-MB435 cells. (A-C) 1h incubation; (D-F) 2h; (G-H) 24h; (I) 48h.

often involved in internalization of nano-objects, clathrin pathway being recognized as more specific than caveolae pathway [34]. In our case, caveolae pathway could be the major mechanism of internalization for PS, without excluding the participation of clathrin-mediated endocytosis.

These mechanisms rule the fate of PS into cells, because caveolae and clathrin-mediated endocytosis involve different intracellular traffickings [41]. Indeed, dramatic differences in subcellular distribution and trafficking were observed for nanocargos like quantum dots in prostate cancer cells with different phenotypes [42]. Caveolae are known to merge in caveosomes, whereas clathrin vesicles merge with endosomes, then with lysosomes, even if the possibility of travel between caveosomes and endosomes was not excluded [34]. After 24h, PS were grouped together in late endosomes (figure 2G), but also in lysosomes (figure 2H), as suggested by the less defined aspect of contents. These two types of intracellular compartments coexisted after 48h (figure 2I). As the stability of the DOX-Fe^{2+} complex depends on pH, the DOX release from DLPS in caveosomes (pH 7.4) could be more progressive than from those stained in lysosomes (pH 5.0). So the delayed cytotoxicity of DLPS compared to free DOX observed in our previous study on MCF-7 cells [22] could also be explained by a dual endocytosis mechanism, modulating DOX release in function of the pH of intracellular compartments. These observations must be taken into account in the evaluation of cytotoxicity generated by DLPS.

1.2. *In vitro* evaluation of antiproliferative effect on MDA-MB435 cells

The aim of this biological evaluation was to determine an *in vitro* antineoplastic activity of DLPS on MDA-MB435 cells, a breast human carcinoma cell line chosen to induce a xenograft solid tumor on nude mice model. Breast cancer cells were incubated during 4h with free DOX, PS, or DLPS, in a DOX concentration range from 0.01 to 10 µM. PS were used at the same iron concentrations as DLPS (0.2 to 200 mg/L of iron). After 4h, the

preparations were replaced by fresh medium, and a MTT viability assay was realized after 72h, *i.e.* after two replication cycles of the cells.

First, the presence of PS on cells had no effect on cell viability, even for high iron concentrations equivalent to 200 mg/L (figure 3). Free DOX induced a decrease of the MDA-MB435 cell viability, with an IC_{50} around 0.08 µM. DLPS had a delayed effect on cells, with a 10-fold higher IC_{50}, around 0.8 µM. Interestingly, cell viability did not decrease on going from 0.1 to 1 µM of free DOX and from 1 to 10 µM of DLPS. On the other hand, both free and vectorized DOX presented similar cell viability at a concentration of 1 µM.

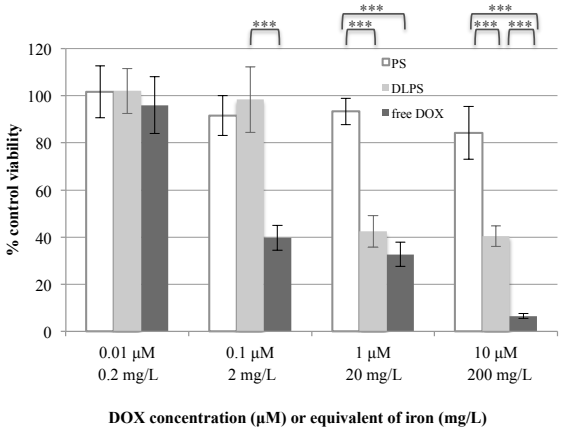

Figure 3. Viability of MDA-MB435 cells after 4h of incubation with PS, DLPS or DOX in solution, and a delay of 72h.

We previously demonstrated that PEGylated SPIONs did not provide any detectable cytotoxicity on another carcinoma cell line MCF-7 [22]. On this cell line, we also demonstrated that DLPS had a cytotoxic activity in the same range compared to DOX in solution, with a IC_{50} of 0.9 and 0.6 µM, respectively, after an incubation of 96h on cells [22]. Since the activity of free and vectorized DOX was different in the present study on MDA-MB435 cells ($P < 0{,}001$), further remarks must be made.

A first remark concerns the chosen protocol. In the literature, the *in vitro* time of contact between nanocarriers and cells is often quite long, equivalent to 24h or more [22,43–45]. This can be justified by the fact that free DOX is rapidly internalized into cells, whereas the nanocarriers uptake and the sustained release of vectorized DOX disadvantage DOX-loaded nanovectors for short-term cytotoxicity. Nevertheless, for further reasons, in the present study, we intentionally chose 4h of contact, followed by 72h of incubation in a fresh medium. First, this 4h time of contact was coherent with previously established DOX release kinetics from DLPS *in vitro* [22]. Secondly, the fresh medium permitted to eliminate non-internalized DLPS or DOX as it should probably take place in the body. Indeed, in the organism, free drugs as well as nanocarriers are conveyed by the blood flow, so probably have a limited time of contact with the target site. This is convenient with the blood half-life of DLPS estimated at 76±6 min [23]. We are obviously conscious that *in vitro* cell viability assays are only models, but the chosen protocol could supply clues for *in vivo* behavior of DLPS.

A second remark is that in the literature, similar nanosystems based on SPIONs often present a 4 to 10-fold decreased efficacy compared to free DOX. Park *et al.* evaluated the cytotoxicity of DOX-loaded Pluronic®-coated SPIONs on human lung cancer cells, incubated with DOX concentrations from 0 to 160 µM for 48h [43]. They observed a 10-fold lower IC_{50} for DOX in solution compared to their DOX-loaded nanocarriers. The authors attributed these results to the slow and incomplete release kinetics of DOX out of the nanocarriers. He *et al.* observed a 4-fold decreased cytotoxicity of DOX-loaded copolymer-coated SPIONs compared to DOX in solution after 24h of incubation on HeLa cells [46]. The authors indicated that the coating could slow down the release of the drug out of the nanocarriers. In our case, previous *in vitro* studies demonstrated a progressive release of DOX from DLPS, where 60% of the loaded drug was released in 2h at pH 7.4. The release was also pH-dependent, considerably accelerated at pH 4 (85% of loaded DOX was released in 1h) [22]. In addition, the relatively low cytotoxicity of DLPS can be related to a lack of specificity of PEG-coating with respect to cellular membranes. Indeed, similar DOX nanovectors based on polymer-coated SPIONs and carrying on their surface biological ligands like folic acid [25] or cRGD [47] showed a cytotoxicity equivalent to that of free DOX.

A third remark concerns the difference in the interactions of a DOX molecule and a nanocarrier with the cell membrane. Free DOX molecules diffuse passively through the cell membrane, whereas the uptake of nanocarriers by the cell, as an active phenomenon could take some time. This hypothesis of uptake kinetics was already evoked in our previous study of DLPS on MCF-7 cells, where the DLPS cytotoxicity compared to that of DOX was similar to lower after 96h or 4h of contact, respectively [22]. These data also confirmed that free DOX was internalized more rapidly by cells than nanovectors.

The active uptake of nanocarriers into MDA-MB435 cells is also dependent on the quantity of nanoparticles in the medium. For a DOX concentration equivalent to 0.1 µM, nanocarrier formulations could be diluted in the medium, and then the number of nano-objects per cell would be low. Nanocarriers could be internalized as single objects, limiting the quantity of vectorized DOX reaching the lysosomes. So the quantity of DOX delivered to cells would be insufficient to lead to a cytotoxic effect. For 1 µM, the concentration of DLPS would be adequate compared to the number of incubated cells, nanoparticles being internalized as clusters, reaching the lysosomes with efficacy, and leading to a similar cytotoxicity compared to DOX in solution. On the contrary, a higher concentration of 10 µM could induce a saturation effect of the uptake. The clusters being numerous, as shown in figure 2E, they could not be internalized simultaneously, limiting the quantity of DOX delivered to cells. This could explain that a DLPS concentration of 10 µM did not improve the cytotoxicity compared to the 1µM concentration. These remarks concerning the time- and quantity-dependence of the NP uptake by the MDA-MB435 cells imply to explore more precisely the *in vivo* behavior of such nanocarriers, in order to appreciate the real impact of such observations. Namely the enhanced retention and permeation (EPR) effect could favor the delivery of DLPS preferentially to tumor cells. The magnetic drug targeting strategy could also influence the toxicity on tumors.

1.3. *In vivo* evaluation: inhibition of tumor growth on NMRI nude mice bearing MDA-MB435 tumor xenografts

To evaluate the anticancer effect of DLPS in an animal model, NMRI nude mice bearing MDA-MB435 tumors were injected intravenously with DLPS for a total amount of DOX of 6 mg/kg (2 mg/kg once a week, three times). This group of interest was compared to a group of mice injected with saline solution (control group), and with DOX in solution. Lastly, we tested the impact of the application of an external magnetic field (1.2 T) for 1h on the tumor, after the injection of DLPS in another group of mice. The 4 groups (saline solution, DOX, DLPS and DLPS + magnet) were monitored during 5 weeks after the end of the treatment (tumor volume, weight of the animals and side effects). The tumor volumes at the end of the period of monitoring (in percentage of initial tumor volume) are presented in figure 4A.

Data were summarized with box-and-whisker diagrams. We chose this statistic presentation to analyze the results, as great differences in the tumor volumes appeared in each group: the means and confidence intervals were not significant, namely because of outliers. This permitted to compare populations without making any assumptions concerning the statistical distribution of results in the group of mice. This graphical representation first highlighted the dispersion of data (figure 4A). The maximal and minimal values as well as the size of the boxes indicated that the results for mice treated with saline solution or DOX were more dispersed than those for mice having received DLPS. The results were also dispersed for the group having received DLPS with the application of an external magnetic field. The dispersion of values could be due partially explained by the presence of outliers in the group of mice treated with DOX in solution and with DLPS with the application of an external magnetic field. As the median within the boxes was not equidistant, this indicated that the data were skewed: data distribution was quite asymmetric, especially for the group DLPS + magnet.

The tumor growth kinetics after the injection of cancerous cells could explain the dispersion of values. The final volume of tumor for each mouse was presented in figure 4B. We decided to define 3 groups in function of tumor growth before the beginning of the treatment. Tumors developing in 6 weeks were considered as "normal". Tumors reaching the required size for treatment in 7-8 weeks were considered as "moderate". To finish, tumors developing in more than 9 weeks were named "slow".

The size of tumors for mice having received saline confirmed the difference in tumor development. When tumors grew normally, mice developed large tumors with saline treatment (until 3500 mm^3). The final size of tumors with saline was more limited when their growth was moderate (968 and 257 mm^3), whereas the tumor grown lately kept a limited size (308 mm^3). In comparison, the sizes of tumors for groups treated with DOX or DLPS (with or without the application of a magnet) were lower than control when their growth was normal or moderate. But delayed tumors which received DLPS + magnet or DOX treatments reached important sizes (3402 and 2299 mm^3, respectively). These values corresponded to the outliers observed in the figure 4A, generating an asymmetric distribution of data.

These observations can be related to the physiology of tumors. The tumors that developed in 6 weeks grew regularly, with the development of neovascularization. DOX, under free as well as vectorized form, could access tumors, and limited their growth, as shown by the limited sizes in all groups, excepted control, in figure 4A. For tumors developed moderately in 7-8 weeks, their growth was probably hampered by a reaction of the immune system of the mice, tumors developing less easily. Neoangiogenesis could be limited, and the tumors were less irrigated. In that case, the lack of irrigation could limit the access of DOX and DLPS to the tumor environment: the sizes of tumors

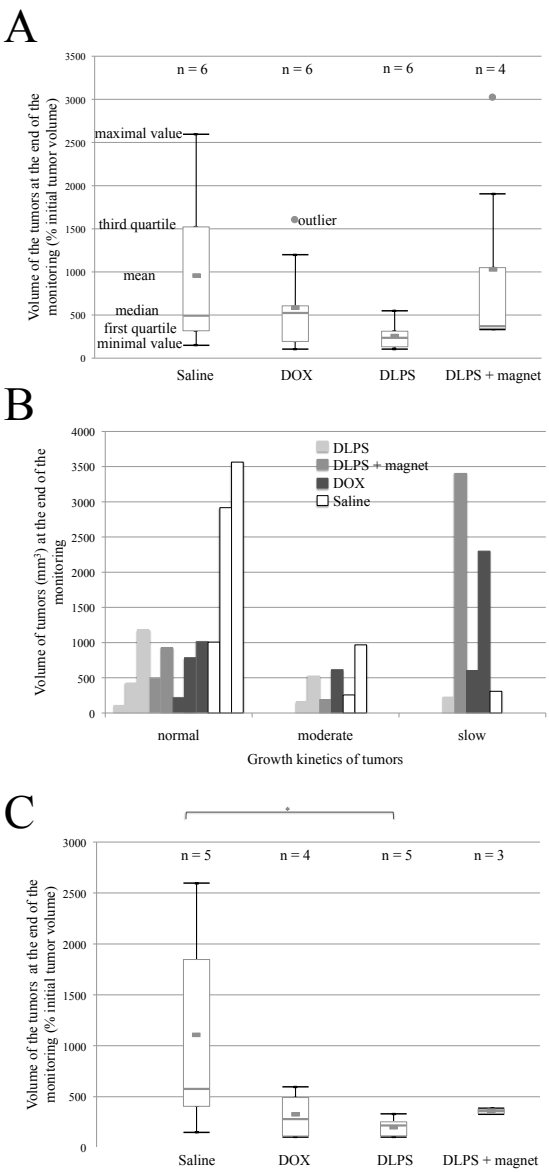

Figure 4. (A) Box-and-whisker diagram of the volume of the tumors at the end of the period of observation (saline, solution of DOX, DLPS without and with application of an external magnetic field). (B) Volumes of tumors at the end of the period of observation in function of the growth kinetics of tumors (normal, moderate or slow) for each group treated. (C) Box-and-whisker diagram of the tumor volume at the end of the period of observation (saline, solution of DOX, DLPS without and with application of an external magnetic field) without data concerning late tumors.

are in the same range, independently of the treatment, as shown in figure 4B. This hypothesis reinforced the idea of an accumulation of DLPS in tumors by an enhanced permeability retention (EPR) effect. For very late tumors (9 weeks and later), two cases were observed: tumors developed slowly during all the time of the experiments, but some of them grew exponentially after a latent time.

This could be due to the selection of resistant cancer cells by the immune system of mice. In that case, tumor volumes must be considered cautiously, as it appeared irrespective of the treatment administered (some tumors grew faster with treatments than with saline solution). The variability of this animal model must be taken into consideration for next *in vivo* experiments.

The figure 4C shows the volumes of tumors grown normally or moderately at the end the period of monitoring (in percentage of initial tumor volume). In that case, outliers were excluded; distributions of data in treated groups were symmetric. DLPS and DLPS + magnet treatments limited the tumor growth of mice compared to non-treated animals, as showed by the narrow dispersion of values and the lower mean and median. Nevertheless, the treatments made with vectorized DOX were not more efficacious than the treatments with DOX in solution. Secondly, no significant difference was observed on results obtained with DLPS with or without the application of an external magnetic field for 1h after the injection. It could be made the hypothesis that the magnetic field was not adapted. Even if applying for 1h a magnet on tumors seems to be a good compromise between the blood half-life of PEGylated SPIONs (~76 min) [23] and the comfort of mice, recent studies reported longer application times, between 18 to 24h [18,19]. Furthermore, numerous studies recognized that even with powerful magnets, the question remained to focus the magnetic field on the target [48–51]. Ruenraroengsak *et al*. suggested recently that the wait for the arrival of more powerful and focused magnets has been the delaying factor for the development of magnetic drug targeting nanosystems [48].

It could be also hypothesized that a static field will not be adequate for targeting, since it could lead to a local aggregation of DLPS [52]. In that case, the size of clusters could limit their extravasation, and then limit the efficacy of the delivery. The use of an alternating magnetic field could be a clue, limiting the formation of clusters. Another source of work would be the addition of another targeting strategy in the design of DLPS. Maeng *et al.* recently published one of the few studies reporting an *in vivo* anticancer effect of DOX-loaded polymer-coated SPIONs targeted with folic acid (FA) [25]. The FA targeting significantly facilitated the specific delivery of DOX to targeted cells, and induced a significant inhibition on liver tumor growth.

To resume, these preliminary results seemed to show further tendencies. First, in normal conditions of tumor growth, DLPS showed a limitation of tumor growth equivalent to DOX in solution. They may be captured in tumors by EPR effect. Secondly, this study gave clues for new experiments, namely the improvement of tumor model, as well as a longer time of application for the external alternative magnetic field, in order to demonstrate the tendencies seen in this paper. We also recently reported the design of SPIONs coated with PEG-FA [53], so studies with FA targeted DLPS should also be conducted soon.

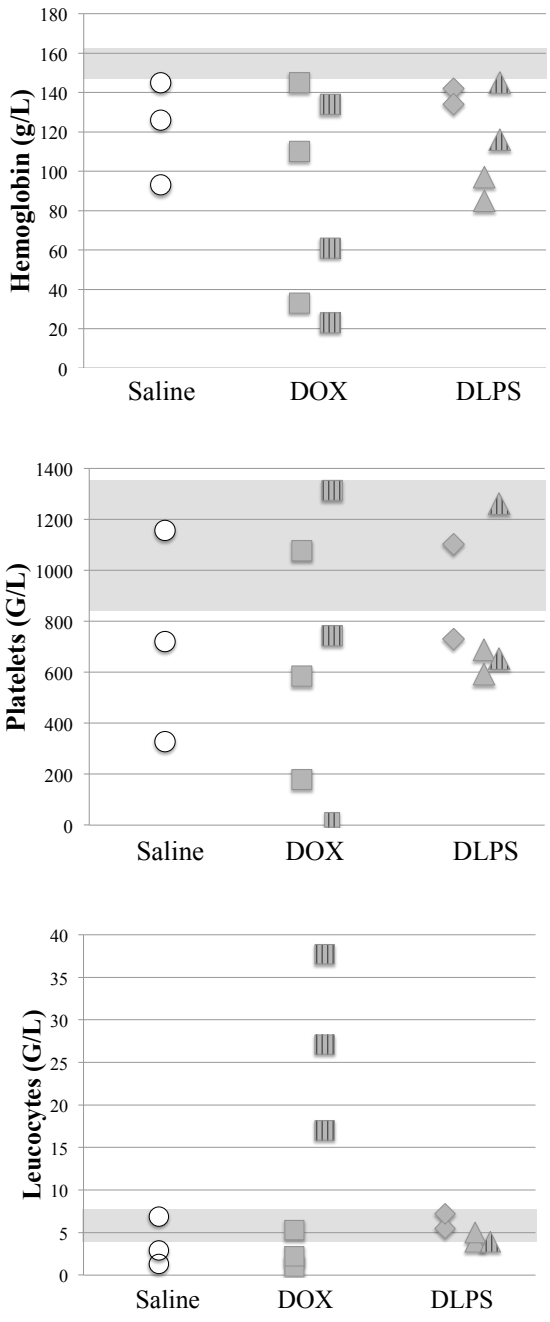

Figure 5. Hematologic data of mice involved in the therapeutical protocol, before sacrifice: hemoglobin (g/L) (normal values in the grey area, 153 ± 8 g/L), number of platelets (G/L) (normal values 1118 ± 254 G/L) and number of leucocytes (G/L) (normal values 6 ± 1.3 G/L). Results for mice treated with saline were circles, DOX were squares, DLPS were diamonds, DLPS + magnet were triangles; the markers were striped for the biggest tumors.

1.4. *In vivo* evaluation of side effects and hemotoxicity

During the therapeutical protocol, no clinical sign of toxicity was observed. Mice gained weight regularly, and had a normal activity. No sign of lameness (splaying and dragging of the hind limbs) was observed for mice treated with DOX or DLPS, this clinical sign being reported in some studies concerning DOX [54,55]. After the mice sacrifice, mains organs were weighted. A

significant increase in spleen weights was noticed, correlating with the size of tumors. The spleens of mice having developed tumors of a limited size (less than 600 mm^3) represented 0.68 ± 0.28% of the body weight, whereas the spleens of mice having developed bigger tumors represented a significantly different percentage (1.32 ± 0.51%, P = 0,002). The observation of an increase in spleen weight was found in the literature after exposition of mice to stressful conditions, namely anticancer drugs [56,57]. Desai *et al.* related this event to a reaction to a drug-induced hematologic toxicity [58]. In our case, the increased spleen weights were also observed in the control group, treated with saline, and could be just a sign of inflammation, due to the tumor growth.

At the end of the therapeutical protocol, blood samples were taken immediately before the sacrifice of mice and analyzed. The individual results of blood samples tests are presented in figure 5. Mice were grouped in three categories: saline for control mice (circles), DOX for mice having received DOX in solution (squares), and DLPS for mice having received the nanovectors, with (diamonds) or without the application of a magnet (triangles). The latter two groups were presented together because they received the same type of treatments *i.e.* DLPS. Furthermore, as the application of an external magnetic field had no influence on the efficacy of DLPS, it could have neither influence on hematologic parameters. The blood tests were representative of the health of animals when they were sacrificed, and appeared independent of the growth kinetics of tumors. Nevertheless, the final size of tumors seemed to influence hematological parameters. That is why the symbols were striped when the data corresponded to mice that developed sizeable tumors, to highlight this tumor size parameter.

The first graph in figure 5 shows the hemoglobin concentration for each mouse. The grey area corresponds to the normal values for healthy NMRI nude mice (153 ± 8 g/L). The control mice showed decreased hemoglobin values, compared to healthy mice. This decrease was also observed for the groups treated with DOX in solution or DLPS. For all animals, this hemoglobin decrease was associated with a microcytosis: the mean corpuscular volume (MCV) of 52.5 ± 6.3 fL was significantly different of values for healthy mice (60 ± 1 fL, $P < 0.001$). The mean corpuscular hemoglobin concentration (MCHC) was also significantly modified (33.2 ± 4.3 g/dL instead of 26 ± 1 g/dL, $P < 0.001$). The origin of this microcytic anemia is not probably explained by an iron deficiency or a bone marrow infiltration by tumor cells. This abnormality should rather be a sign of an inflammatory state induced by the tumor bearing.

Nevertheless, if individual values were comparable between control and DLPS group, the mice having received DOX showed more pronounced anemias, independently of the final size of tumors (striped symbols). This suggests that DOX treatment could induce a supplementary toxicity on red blood cells when DOX was in solution, compared to DLPS.

The second graph in figure 5 represents platelet count for each mouse. Some control mice presented a decreased platelet count compared to the values of healthy nude mice (1118 ± 254 G/L). Although bone marrow infiltration by tumor cells could contribute to thrombocytopenia, as previously found, the most marked cases appeared in the group treated with DOX in solution, independently of the final size of tumors. So the treatment with DOX in solution could induce *per se* thrombocytic toxicity.

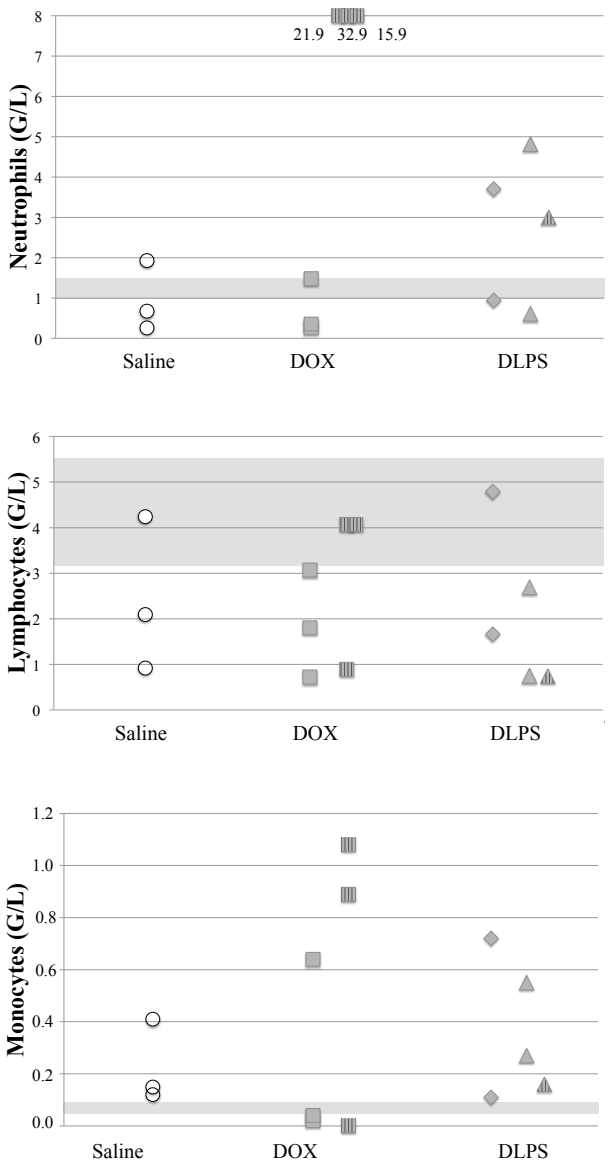

Figure 6. Detail of leukocyte cells for mice involved in the therapeutical protocol, before sacrifice: number of neutrophils, lymphocytes and monocytes (G/L). The symbols were striped for the biggest tumors.

Lastly, the third graph in figure 5 represents the white cell count for each mouse. Data related to neutrophils, lymphocytes, and monocytes are detailed in figure 6. Control mice exhibited a normal or decreased quantity of leucocytes compared to the values of healthy nude mice (6 ± 1.3 G/L). So leukopenia could also be attributed to tumor bone marrow infiltration, as for anemia and for thrombocytopenia. The raise of monocytes (figure 6) for most of mice was a supplementary clue in favor of an inflammation due to the development of tumors. Normal or decreased values of leucocytes were observed in all groups, but unlike previous data concerning hemoglobin and platelets, leucocyte count seemed to depend on the final size of tumors.

Indeed, the mice treated with DOX in solution and having developed important tumors exhibited a marked leukocytosis. This could be attributed to an inflammatory effect, due to tumor growth. This hypothesis could be reinforced by the fact that the main white cells involved in this increase were the neutrophils and the monocytes, whereas the lymphocytes amounts were normal or decreased (figure 6).

In other cases, it could be considered that the normal values or the leukopenia observed were in accordance with the observations made with the control mice, and conclude that neither DOX nor DLPS could influence the white cell count. Moreover, the results were closed to normal values for the DLPS group.

Nevertheless, it must be noticed that for control, leukopenia was due both to neutropenia and lymphocytopenia, the tumor generating a toxicity effect for the both white cell lineages. The same observation was made for the group of mice injected with DOX in solution. On the contrary, in the DLPS group, leucocyte counts appeared quite normal, but in one case from two, the lymphocytopenia was offset by a neutrophilia (figure 6). So the fact that the DLPS treatment did not influence the leukocytes could be only apparent. Nevertheless, while neutropenia represents the critical factor to evaluate the toxicity of chemotherapy, inducing a vital risk, the DLPS treatment appeared to limit such a toxicity.

Globally, the respective hematologic effects of tumor development and treatments were difficult to distinguish. It seemed that the DLPS treatment involved fewer modifications of blood cell counts than DOX in solution. Therefore, vectorization through a modification of DOX biodistribution could limit the bone marrow failure, described in the literature for doxorubicin anticancer drug [58,54,59–61].

2. Experimental

2.1. Synthesis and characterization of SPION-based nanoparticles

2.1.1. Materials

Doxorubicin hydrochloride was purchased from TEVA Pharmaceuticals Ltd. (Puteaux, France). Ferric nitrate nonahydrate ($Fe(NO_3)_3.9H_2O$), anhydrous ferric chloride ($FeCl_3$), ferrous chloride ($FeCl_2$, $4H_2O$) were purchased from Fisher Bioblock Scientific (Illkirch, France). 3-aminopropyltrimethoxy silane (APTES) and methoxypoly(ethylene glycol) 5000 propionic acid N-succinimidyl ester (activated PEG, aPEG) were purchased from Sigma Aldrich (Saint-Quentin-Fallavier, France). Sodium acetate, tris-(hydroxymethyl)-aminomethane (Tris), mannitol and iron standard solution 1g/L (CertiPUR®) were provided by Merck (Fontenay-sous-Bois, France), and ferrous ammonium sulphate ($(NH_4)_2Fe(SO_4)_2.6H_2O$) by Carlo Erba (Val de Reuil, France). Dialysis membranes (Spectra/Por 6, cut off 25,000) were purchased from Biovalley, Marne-la-Vallée, France). All solutions were prepared with deionized water, and all reagents were of analytical grade.

2.1.2. Preparation of PEGylated SPIONs (PS)

PEGylated SPIONs were synthesized according to a previously published protocol [21]. Briefly, ferrofluids prepared by coprecipitation were first silanized by bonding of APTES molecules on the surface hydroxyl groups of the SPIONs. Then, PEGylated ferrofluids were prepared by mixing silanized ferrofluids with aPEG (molecular weight 5000) in water under stirring for 24h. The PS were then purified by dialysis against water.

2.1.3. Preparation of doxorubicin-loaded PEGylated SPIONs (DLPS)

PS were loaded with doxorubicin (DOX) via a DOX-Fe^{2+} complex, as described elsewhere [22]. Mixing a solution of DOX hydrochloride and a Fe^{2+} solution (1.5 molar excess of Fe^{2+} over DOX) in TRIS buffer pH 7.6 permitted to pre-form the DOX-Fe^{2+} complex. The complex was incubated with PS in the dark, and nano-objects were harvested by centrifugation at 19,000*g* for 1h at 4°C. For determining drug loading, as the DOX-Fe^{2+} complex dissociates at low pH [24,22], the DLPS were sonicated for 1h in an acetate buffer pH 4 to allow total DOX release. The sample was then centrifuged at 19,000g for 1h at 15°C. DOX concentration was determined in the supernatant by UV-visible spectrophotometry (Anthélie Advanced Spectrophotometer, Secomam, France), using its molar absorptivity determined at 500 nm. Each determination was performed at least in triplicate. Drug loading is expressed as the mass ratio of DOX over the mass of the iron oxide core of the nanovectors.

2.1.4. Determination of hydrodynamic diameter and zeta potential

The mean hydrodynamic diameter (D_H) of NPs (PS and DLPS) was determined by DLS (Dynamic Light Scattering) with an Autosizer 2c (Malvern Instruments, Orsay, France). The ferrofluids were also characterized with respect to the zeta potential ζ of NPs by using a Malvern NanoZ (Malvern Instruments, Malvern, UK). For the measurements, ferrofluids were diluted in deionized water (1:100 V:V, ≈ 2.10^{-3} g/L)). Each measurement was done in triplicate, was performed at 25°C, with a He-Ne laser (4 mW, 633 nm, scatter angle 173° for DLS, light scattering angle 17° for ζ).

2.1.5. Determination of iron content by AAS

Total iron content was quantified by flame atomic absorption spectrometry (AAS) (air/C_2H_2 flame mode with deuterium background correction, slit width: 0.2 nm, wavelength: 248.3 nm, sensitivity 0.12 ppm, A: 1%) (iCE 3000 Series AA Spectrometer, ThermoFisher Scientific, France). One mL of NPs suspension was mineralized by a 12h contact with 5mL of hydrochloric acid 6N, and the resultant solution was diluted with hydrochloric acid 0.1M before measurement. A calibration curve was obtained with dilutions of an iron standard solution. Each determination was done in triplicate.

2.2. *In vitro* methods using cells

MDA-MB 435 is an estrogen receptor-negative cell line isolated from the pleural effusion of a patient with breast carcinomas [3]. The cells were routinely cultured in Dulbecco's Modified Eagle Medium (DMEM) supplemented with foetal bovine serum FBS (5%), and antibiotics 100X (1%) in a humidifier-incubator (5% CO_2/37°C). All reagents were purchased from Fisher Bioblock Scientific (Illkirch, France).

2.2.1. Cell viability study

The MDA-MB435 cells were first plated at 4.10^4 cells/mL on 24-

well plates for 48h and then treated with increasing concentrations of various preparations. DOX in solution and DLPS were diluted in culture medium to obtain the higher concentration tested on cells (10µM). PS were tested as controls, and used at the same iron concentration than DLPS. The cells were incubated at 37°C/5% CO_2 for 4h, then the preparations were removed and replaced by fresh medium. Thereafter, cell viability was determined using tetrazolium dye (MTT) assay [62], after 72h. Briefly, 40 µL of MTT solution at 5 mg/mL in PBS 1X were added to each well, and the plates were incubated at 37 °C for 4h. The medium was removed and 500 µL of DMSO was added to each well and mixed thoroughly to completely dissolve the dark blue crystals. The optical density values were measured at 580 nm using a multiwell-scanning spectrophotometer (Multiskan Ascent, Labsystems SA, Cergy-Pontoise, France). The 50% inhibitory concentration (IC_{50}) was determined as the DOX (or equivalent) concentration inducing a 50% reduction of cell viability. Six independent repetition experiments were conducted, each with at least 6 repeated samples.

2.2.2. TEM imaging

The MDA-MB435 cells were first routinely cultured 24h in flasks. Then the medium was replaced by dilutions of P-SPIONs (200 mg/L iron) in DMEM and cells were incubated for 1, 2, 4, 8, 24 or 48h. Media were removed, cells were washed 3 times, harvested, concentrated and fixed in Trump's solution. Cells were post-fixed with 2% osmium tetroxide, dehydrated with series of increasing ethanol solutions and embedded in Epon® resin. Ultrathin sections (90 nm) were stained with 2% aqueous uranyl acetate and 1% lead citrate. Images were acquired using a JEOL 1011 transmission electron microscope (TEM) operating at an acceleration voltage of 100 kV. It has to be underlined that the images obtained were not necessary representative for the whole cell population, because the ultrathin cuts observed were chosen at random.

2.3. *In vivo* evaluations

Female athymic nude mice (six weeks-old; NMRI-nu (nu/nu NUDE: France) were purchased from Janvier Laboratory (Le Genest St Isle, France). They were housed in a pathogen-free isolation facility with rodent chow and water ad libitum. The animals were manipulated under isoflurane/oxygen anaesthesia, and treated in accordance with institutional guidelines for animals of French Ministry of Agriculture.

2.3.1. Tumor animal model

MDA-MB 435 cells (8 x 10^6 in 0.150 mL PBS sterile) were injected subcutaneously on the right flank of NMRI nude mice. Tumor growth curves were obtained using vernier calliper twice a week and the estimate tumor weight formula,

$$\text{Tumor weight TW } (cm^3 \text{ or g}) = l^2.L/2$$

where l and L are the short and the long axis of the tumor, respectively. Tumor-bearing mice were used in the studies when tumor volume was approximately 150 mm^3.

2.3.2. Therapeutical protocol

24 tumor-bearing mice were divided in 4 groups (6 mice per group): control (injected with saline solution), DOX (injected with DOX in solution), DLPS (injected with DOX-loaded nanocarriers) and DLPS + magnet (injected with DOX-loaded nanocarriers and with application of an external magnetic field for 1h). When possible, as soon as 4 mice developed tumors with equivalent growth kinetics and reaching the limit volume, mice were paired: one received serum, one DOX in solution, one DLPS, the last DLPS with the application of an external magnetic field for 1h. Each preparation was injected intravenously at a dose of 2mg/kg of DOX or equivalent, under anaesthesia, three times at 7-days intervals. Animals were monitored (weight, tumor growth and apparent side effects) for 8 weeks after the first injection (3 weeks of treatment, 5 weeks of observation).

Animals were sacrificed at the end of the monitoring or when the tumor reached 8% of the body weight. Before sacrifice, blood samples were taken in tubes containing EDTA, for haematological analysis with a LH 785 Beckman Counter. The tumor, heart, lungs, spleen, kidneys and liver were removed, weighted and frozen in isopentane for further investigations.

For technical reasons, the number of results in each group of mice could have varied.

2.4. Statistical analysis

In vivo data of the therapeutical protocol were presented as box-and-whisker diagrams. Boxes were built with the first and third quartile, so contained 50% of the data, as well as the mean and the median. Minimal and maximal values were also represented with whiskers. Outliers are values distant from the rest of the data (upper than 1.5 times the interquartile range). The statistical significance for the *in vivo* results was determined between groups for each experiment by a Student *t*-test ($P < 0.05$ was considered to be significant).

Conclusions

This paper shed a light on the need to understand the cellular mechanisms involved in the cellular uptake of DOX nanocarriers. The internalization of DLPS both by caveolae- and clathrin-mediated endocytosis, as well as the time- and quantity-dependence of this phenomenon, modified the *in vitro* cytotoxicity of these nanocargos on MDA-MB435 cells. If DLPS, in certain conditions of time and concentration, showed a decreased *in vitro* antiproliferative effect compared to DOX in solution, this was not the case for *in vivo* studies. On mice bearing breast xenograft tumors, DLPS exhibited a limitation of tumor growth equivalent to that of free DOX, in normal conditions of tumor development. This *in vivo* evaluation also highlighted the variability in the animal model, and the need to improve the magnetic targeting protocol. To finish, if tumor growth involved modifications in mice blood tests (pancytopenia), non vectorized DOX seemed to accentuate this phenomenon, contrary to DLPS. This paper is one of the few tumor reduction studies dealing with SPION-based nanosystems for DOX delivery.

Acknowledgments

The authors would like to thank the U1069 INSERM unit for the gift of MDA-MB435 cells. This study was supported in part by grants from the Ligue Nationale contre le Cancer (Conseil Scientifique Inter-Régional Grand-Ouest (CSIRGO), Délégation

Indre-et-Loire, France and from the Region Centre, France (NANOMAG Project).

Notes and references

[a] *Université François-Rabelais, EA 6295 "Nanomédicaments et Nanosondes", 37200 Tours, France. Fax: (33)-24736 7200; Tel: (33)-24736 7198; E-mail: Emilie.allard@univ-tours.fr*
[b] *Université François-Rabelais, Plateau Technologique Analyse des systèmes Biologiques, 37032 Tours, France.*
[c] *CNRS UMR 7292, Equipe 2 LNOx, UFR de Médecine, 37200 Tours, France.*

1. S. Chandra, K. C. Barick, and D. Bahadur, *Adv. Drug Deliv. Rev.*, 2011, **63**, 1267–1281.
2. A. J. Cole, V. C. Yang, and A. E. David, *Trends Biotechnol.*, 2011, **29**, 323–332.
3. E. Cukierman and D. R. Khan, *Biochem. Pharmacol.*, 2010, **80**, 762–770.
4. A. S. de Dios and M. E. Díaz-García, *Anal. Chim. Acta*, 2010, **666**, 1–22.
5. H.-C. Huang, S. Barua, G. Sharma, S. K. Dey, and K. Rege, *J. Controlled Release*, 2011, **155**, 344–357.
6. S. Parveen, R. Misra, and S. K. Sahoo, *Nanomedicine Nanotechnol. Biol. Med.*, 2012, **8**, 147–166.
7. R. E. Serda, B. Godin, E. Blanco, C. Chiappini, and M. Ferrari, *Biochim. Biophys. Acta Bba - Gen. Subj.*, 2011, **1810**, 317–329.
8. N. T. K. Thanh and L. A. W. Green, *Nano Today*, 2010, **5**, 213–230.
9. J. Xie, S. Lee, and X. Chen, *Adv. Drug Deliv. Rev.*, 2010, **62**, 1064–1079.
10. T. Islam and L. Josephson, *Cancer Biomarkers Sect. Dis. Markers*, 2009, **5**, 99–107.
11. T. Schlorf, M. Meincke, E. Kossel, C.-C. Glüer, O. Jansen, and R. Mentlein, *Int. J. Mol. Sci.*, 2010, **12**, 12–23.
12. P. Rai, S. Mallidi, X. Zheng, R. Rahmanzadeh, Y. Mir, S. Elrington, A. Khurshid, and T. Hasan, *Adv. Drug Deliv. Rev.*, 2010, **62**, 1094–1124.
13. J. E. Rosen, L. Chan, D.-B. Shieh, and F. X. Gu, *Nanomedicine Nanotechnol. Biol. Med.*, 2012, **8**, 275–290.
14. S. Prakash, M. Malhotra, W. Shao, C. Tomaro-Duchesneau, and S. Abbasi, *Adv. Drug Deliv. Rev.*, 2011, **63**, 1340–1351.
15. T. Neuberger, B. Schöpf, H. Hofmann, M. Hofmann, and B. von Rechenberg, *J. Magn. Magn. Mater.*, 2005, **293**, 483–496.
16. Y.-X. J. Wang, *Quant. Imaging Med. Surg.*, 2011, **1**, 35–40.
17. S. Dandamudi, V. Patil, W. Fowle, B.-A. Khaw, and R. B. Campbell, *Cancer Sci.*, 2009, **100**, 1537–1543.
18. J.-P. Fortin-Ripoche, M. S. Martina, F. Gazeau, C. Ménager, C. Wilhelm, J.-C. Bacri, S. Lesieur, and O. Clément, *Radiology*, 2006, **239**, 415–424.
19. M.-Y. Hua, H.-W. Yang, H.-L. Liu, R.-Y. Tsai, S.-T. Pang, K.-L. Chuang, Y.-S. Chang, T.-L. Hwang, Y.-H. Chang, H.-C. Chuang, and C.-K. Chuang, *Biomaterials*, 2011, **32**, 8999–9010.
20. J. Gautier, E. Allard-Vannier, E. Munnier, M. Soucé, and I. Chourpa, *J. Controlled Release*.
21. K. Hervé, L. Douziech-Eyrolles, E. Munnier, S. Cohen-Jonathan, M. Soucé, H. Marchais, P. Limelette, F. Warmont, M. L. Saboungi, P. Dubois, and I. Chourpa, *Nanotechnology*, 2008, **19**, 465608.
22. J. Gautier, E. Munnier, A. Paillard, K. Hervé, L. Douziech-Eyrolles, M. Soucé, P. Dubois, and I. Chourpa, *Int. J. Pharm.*, 2012, **423**, 16–25.
23. E. Allard-Vannier, S. Cohen-Jonathan, J. Gautier, K. Hervé-Aubert, E. Munnier, M. Soucé, P. Legras, C. Passirani, and I. Chourpa, *Eur. J. Pharm. Biopharm.*, 2012, **81**, 498–505.
24. E. Munnier, S. Cohen-Jonathan, C. Linassier, L. Douziech-Eyrolles, H. Marchais, M. Soucé, K. Hervé, P. Dubois, and I. Chourpa, *Int. J. Pharm.*, 2008, **363**, 170–176.
25. J. H. Maeng, D.-H. Lee, K. H. Jung, Y.-H. Bae, I.-S. Park, S. Jeong, Y.-S. Jeon, C.-K. Shim, W. Kim, J. Kim, J. Lee, Y.-M. Lee, J.-H. Kim, W.-H. Kim, and S.-S. Hong, *Biomaterials*, 2010, **31**, 4995–5006.
26. Q. Quan, J. Xie, H. Gao, M. Yang, F. Zhang, G. Liu, X. Lin, A. Wang, H. S. Eden, S. Lee, G. Zhang, and X. Chen, *Mol. Pharm.*, 2011, **8**, 1669–1676.
27. T. Skajaa, D. P. Cormode, P. A. Jarzyna, A. Delshad, C. Blachford, A. Barazza, E. A. Fisher, R. E. Gordon, Z. A. Fayad, and W. J. M. Mulder, *Biomaterials*, 2011, **32**, 206–213.
28. A. K. Gupta and M. Gupta, *Biomaterials*, 2005, **26**, 3995–4021.
29. S. Singh, A. Kumar, A. Karakoti, S. Seal, and W. T. Self, *Mol. Biosyst.*, 2010, **6**, 1813–1820.
30. K. T. Thurn, H. Arora, T. Paunesku, A. Wu, E. M. B. Brown, C. Doty, J. Kremer, and G. Woloschak, *Nanomedicine Nanotechnol. Biol. Med.*, 2011, **7**, 123–130.
31. N. Zeng, X. Gao, Q. Hu, Q. Song, H. Xia, Z. Liu, G. Gu, M. Jiang, Z. Pang, H. Chen, J. Chen, and L. Fang, *Int. J. Nanomedicine*, 2012, **7**, 3703–3718.
32. L. Zhu, D. Wang, X. Wei, X. Zhu, J. Li, C. Tu, Y. Su, J. Wu, B. Zhu, and D. Yan, *J. Controlled Release*, 2013.
33. C. G. Hansen and B. J. Nichols, *J. Cell Sci.*, 2009, **122**, 1713–1721.
34. L. Pelkmans and A. Helenius, *Traffic Cph. Den.*, 2002, **3**, 311–320.
35. I. R. Nabi, *J. Cell Biol.*, 2003, **161**, 673–677.
36. J. E. Ziello, Y. Huang, and I. S. Jovin, *Mol. Med. Camb. Mass*, 2010, **16**, 222–229.
37. Z. Wang, C. Tiruppathi, J. Cho, R. D. Minshall, and A. B. Malik, *Iubmb Life*, 2011, **63**, 659–667.
38. C. Morelli, P. Maris, D. Sisci, E. Perrotta, E. Brunelli, I. Perrotta, M. L. Panno, A. Tagarelli, C. Versace, M. F. Casula, F. Testa, S. Andò, J. B. Nagy, and L. Pasqua, *Nanoscale*, 2011, **3**, 3198–3207.
39. H. Li, Y. Xiao, J. Niu, X. Chen, and Q. Ping, *J. Nanosci. Nanotechnol.*, 2011, **11**, 8547–8555.
40. S. Sunoqrot, Y. Liu, D.-H. Kim, and S. Hong, *Mol. Pharm.*, 2012.
41. M. Bastiani and R. G. Parton, *J. Cell Sci.*, 2010, **123**, 3831–3836.
42. S. Barua and K. Rege, *Small Weinh. Bergstr. Ger.*, 2009, **5**, 370–376.
43. S. Park, H. S. Kim, W. J. Kim, and H. S. Yoo, *Int. J. Pharm.*, 2012, **424**, 107–114.
44. S. K. Sahu, S. Maiti, A. Pramanik, S. K. Ghosh, and P. Pramanik, *Carbohydr. Polym.*, 2012, **87**, 2593–2604.
45. X.-Y. Ying, Y.-Z. Du, L.-H. Hong, H. Yuan, and F.-Q. Hu, *J. Magn. Magn. Mater.*, 2011, **323**, 1088–1093.
46. X. He, X. Wu, X. Cai, S. Lin, M. Xie, X. Zhu, and D. Yan, *Langmuir Acs J. Surfaces Colloids*, 2012, **28**, 11929–11938.
47. X. Yang, H. Hong, J. J. Grailer, I. J. Rowland, A. Javadi, S. A. Hurley, Y. Xiao, Y. Yang, Y. Zhang, R. J. Nickles, W. Cai, D. A. Steeber, and S. Gong, *Biomaterials*, 2011, **32**, 4151–4160.
48. P. Ruenraroengsak, J. M. Cook, and A. T. Florence, *J. Controlled Release*, 2010, **141**, 265–276.
49. A. S. Lübbe, C. Bergemann, J. Brock, and D. G. McClure, *J. Magn. Magn. Mater.*, 1999, **194**, 149–155.
50. S. F. Medeiros, A. M. Santos, H. Fessi, and A. Elaissari, *Int. J. Pharm.*, 2011, **403**, 139–161.
51. Q. A. Pankhurst, N. K. T. Thanh, S. K. Jones, and J. Dobson, *J. Phys. Appl. Phys.*, 2009, **42**, 224001.
52. J.-E. Bae, M.-I. Huh, B.-K. Ryu, J.-Y. Do, S.-U. Jin, M.-J. Moon, J.-C. Jung, Y. Chang, E. Kim, S.-G. Chi, G.-H. Lee, and K.-S. Chae, *Biomaterials*, 2011, **32**, 9401–9414.
53. K. Kaaki, K. Hervé-Aubert, M. Chiper, A. Shkilnyy, M. Soucé, R. Benoit, A. Paillard, P. Dubois, M.-L. Saboungi, and I. Chourpa, *Langmuir Acs J. Surfaces Colloids*, 2012, **28**, 1496–1505.
54. R. Duncan, J. K. Coatsworth, and S. Burtles, *Hum. Exp. Toxicol.*, 1998, **17**, 93–104.
55. G. Molyneux, M. Andrews, W. Sones, M. York, A. Barnett, E. Quirk, W. Yeung, and J. Turton, *Cell Biol. Toxicol.*, 2010, **27**, 13–40.
56. A. M. Yeager, J. Levin, and F. C. Levin, *Exp. Hematol.*, 1983, **11**, 944–952.
57. K. S. Zuckerman, R. Sullivan, and P. J. Quesenberry, *Blood*, 1978, **51**, 957–969.
58. V. G. Desai, E. H. Herman, C. L. Moland, W. S. Branham, S. M. Lewis, K. J. Davis, N. I. George, T. Lee, S. Kerr, and J. C. Fuscoe, *Toxicol. Appl. Pharmacol.*, 2013, **266**, 109–121.
59. R. C. F. Leonard, S. Williams, A. Tulpule, A. M. Levine, and S. Oliveros, *The Breast*, 2009, **18**, 218–224.

60. J. Lankelma, H. Dekker, F. R. Luque, S. Luykx, K. Hoekman, P. van der Valk, P. J. van Diest, and H. M. Pinedo, *Clin. Cancer Res. Off. J. Am. Assoc. Cancer Res.*, 1999, **5**, 1703–1707.
61. T. Lei, S. Srinivasan, Y. Tang, R. Manchanda, A. Nagesetti, A. Fernandez-Fernandez, and A. J. McGoron, *Nanomedicine Nanotechnol. Biol. Med.*, 2011, **7**, 324–332.
62. T. Mosmann, *J. Immunol. Methods*, 1983, **65**, 55–63.

Troisième partie
Discussion générale

Les différentes étapes de développement et de caractérisation, aussi bien *in vitro* qu'*in vivo*, des nanovecteurs magnétiques pour la délivrance de la doxorubicine exposés dans cette thèse ont permis de soulever de très nombreuses questions. Il s'agit non seulement d'évaluer un modèle, mais aussi de comprendre son comportement et ses interactions, en solution, avec une cellule ou un organisme. Cela nécessite de poser un regard sur les résultats obtenus, mais aussi sur les techniques employées, de façon à donner des interprétations justes, tout en gardant à l'esprit leurs limites.

Toutes les publications faisant état de nanovecteurs théragnostiques ont le même point de départ : la construction d'un nano-objet correspondant au plus près à un nanovecteur idéal. La formulation de celui-ci, comme tout médicament, doit être adaptée à la voie d'administration. Plus qu'un simple véhicule, le nano-objet protège le principe actif de la dégradation et de l'élimination précoce par l'organisme. Il permet également une délivrance ciblée et prolongée de la molécule active, permettant une efficacité accrue du traitement, tout en limitant les effets indésirables liés à la molécule active, et le vecteur n'est pas toxique. Les fonctions d'imagerie permettent de visualiser la tumeur et de suivre la distribution du traitement. Toutes ces qualités attendues sont abordées dans cette partie.

Dans cette discussion, pour des raisons de clarté, les dénominations utilisées dans les articles précédents sont reprises. Les nanovecteurs magnétiques ou SPIONs PEGylés sont nommés PS (pour PEGylated SPIONs), et les nanovecteurs magnétiques chargés de DOX sont nommés DLPS (pour DOX-loaded PEGylated SPIONs).

1. Formulation des nanovecteurs magnétiques de la DOX

La formulation des nanovecteurs magnétiques de la DOX est basée sur des matériaux biocompatibles, comme les oxydes de fer. La voie systémique impose d'autres contraintes, liées à la reconnaissance précoce des SPIONs par le système immunitaire et leur élimination rapide. Le greffage de chaînes de PEG est une méthode classique pour fonctionnaliser les nanoparticules inorganiques, et leur conférer un état de surface compatible avec une circulation prolongée dans l'organisme.

La caractérisation poussée de l'architecture des SPIONs PEGylés est un point essentiel pour la connaissance approfondie des interactions des nanovecteurs et leur administration *in vivo*. De plus, la formulation qui a permis de conférer aux DLPS toutes les propriétés explorées

dans cette thèse peut être modifiée, en vue de remédier à certaines problématiques rencontrées.

1.1. Configuration du cœur inorganique

Les SPIONs initiaux présentent une taille de 8 ±1,9 nm en MET, et un diamètre hydrodynamique de 56,3 ± 9,5 nm [123]. La PEGylation augmente le diamètre hydrodynamique de 20 nm environ. La différence observée entre taille et diamètre hydrodynamique des SPIONs initiaux est expliquée par la couche de solvatation autour des SPIONs, due aux charges présentes à la surface. Néanmoins, l'hypothèse d'une agrégation partielle et mineure sous forme d'assemblages de quelques SPIONs ne peut pas être exclue. Les PS se présenteraient alors sous forme des SPIONs PEGylés individuellement et d'agrégats de quelques SPIONs PEGylés, comme l'illustre la figure 4.

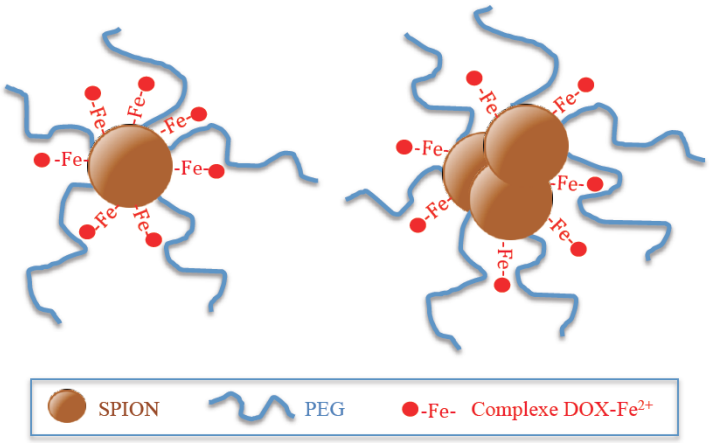

Figure 4 : configurations possibles des DLPS.

Cette hypothèse a été évoquée dans les publications concernant les PS et les DLPS [124,134]. Cette distinction peut avoir des conséquences notamment en termes d'élimination et de persistance des nanovecteurs dans l'organisme. En effet, des agrégats de SPIONs présentent une surface de contact inférieure à celle des SPIONs individualisés, ce qui pourrait ralentir leur dégradation par l'environnement acide des compartiments intracellulaires. Une telle hypothèse a été récemment mise à profit par Jenkins *et al.* [135]. Des agrégats de nanoparticules d'or avec des oxydes de fer ont été formulés pour que la biodégradation rapide du fer favorise la division des nanovecteurs en unités d'or plus petites, éliminées plus rapidement de l'organisme. Dans le cas des DLPS, la formation d'agrégats pourrait être un des paramètres sur lequel travailler pour limiter leur persistance dans l'organisme.

1.2. Opsonisation, phagocytose et PEGylation

In vivo, les nanovecteurs administrés par voie intraveineuse subissent des phénomènes d'opsonisation, c'est-à-dire leur couverture par des protéines appelées opsonines. Ces protéines sont présentes dans le flux sanguin, les plus communes étant les protéines C3, C4, C5 du système du complément, et les immunoglobulines. Elles facilitent la reconnaissance et l'élimination des nano-objets par les cellules phagocytaires du système réticulo-endothélial (SRE) [65,109]. Ce faisant, le temps de circulation des nano-objets dans l'organisme est réduit, limitant leurs interactions possibles avec les tissus et/ou les cellules cibles : ils s'accumulent préférentiellement dans les principaux organes d'élimination (foie et rate). Il s'agit donc du principal obstacle à la délivrance ciblée de molécules actives dans les organes autres que les organes d'élimination [41].

Ces phénomènes d'opsonisation dépendent étroitement de la formulation des nanovecteurs. Typiquement, les NPs hydrophobes sont opsonisées plus rapidement que les NPs hydrophiles, les protéines sériques s'adsorbant plus facilement sur ce type de surfaces. Le port de charges est également un facteur favorisant l'opsonisation [61,136,137]. Une méthode largement utilisée pour limiter le phénomène est donc le greffage de molécules à la surface des nanovecteurs pour bloquer les interactions hydrophobes et électrostatiques qui favorisent l'attachement des opsonines. Il s'agit généralement de longues chaînes hydrophiles, par exemple des polysaccharides [138], des dérivés de polyacrylamide [139], de l'alcool polyvinylique [140]. Le polymère le plus largement utilisé et le plus efficace est le polyéthylène glycol ou PEG, seul ou sous forme de copolymères, car il est à la fois très hydrophile et neutre, et sa grande flexibilité permet de « camoufler » efficacement les NPs hydrophobes ou chargées [15,16,32,33]. La présence de PEG assure en même temps une stabilité colloïdale des NPs, par encombrement stérique, empêchant l'agrégation. Le PEG est également biocompatible, et approuvé par la FDA pour des applications biomédicales. Les nanovecteurs PEGylés sont reconnus comme ayant une certaine « furtivité » dans l'organisme, c'est-à-dire une capacité à échapper à la reconnaissance par le système immunitaire [18,36,141]. C'est pour toutes ces raisons que les nanovecteurs magnétiques pour la délivrance de la DOX ont été fonctionnalisés avec du PEG [123].

Le greffage des PEG sur les nanovecteurs magnétiques est difficile à confirmer directement. La présence du PEG dans les suspensions de nanoparticules après purification par dialyse a été confirmée par la présence de bandes caractéristiques en spectroscopie infrarouge à

transformée de Fourier (FT-IR). Selon notre estimation, basée sur le dosage du fer total par spectrométrie d'absorption atomique (SAA) et les pesées de matière sèche après lyophilisation, le fer représente 0,046 g par g de matière sèche, soit 0,09 mmol de PEG pour 0,41 mmol de fer [123]. Apprécier l'épaisseur du revêtement est problématique par les techniques courantes comme la MET, car le polymère se contracte lors de la déshydratation de l'échantillon ; de plus, la couche de PEG est transparente aux électrons, et de ce fait invisible en microscopie électronique. Les conséquences de la PEGylation des nanovecteurs peuvent cependant être visualisées : les PS et les DLPS présentent un potentiel zêta proche de zéro sur une large gamme de pH, et leur diamètre hydrodynamique, augmenté par la PEGylation (de 60 à 80 nm environ), ne présente pas de variation en fonction du pH. Les changements de force ionique n'affectent pas non plus leur stabilité. Ainsi, bien qu'indirectes, les mesures de diamètre hydrodynamique et de potentiel zêta sont une meilleure confirmation de la PEGylation.

1.3. Configuration des PEG à la surface des SPIONs

Si la PEGylation est reconnue comme une méthode de choix pour assurer une certaine furtivité des nanovecteurs, il faut souligner que la densité du greffage ainsi que la longueur et la conformation des chaînes de PEG peuvent fortement moduler les interactions des nanovecteurs avec l'organisme.

De nombreuses études soulignent l'importance de la longueur des chaînes de PEG : le poids moléculaire (PM) minimum requis est de 2000, pour pouvoir assurer des propriétés de furtivité [36,41]. En dessous de ce PM, la flexibilité des chaînes est insuffisante pour pouvoir « camoufler » efficacement les nanoparticules, et pour empêcher l'opsonisation. Au-dessus de ce PM, l'allongement de la chaîne jusqu'à un PM de 5000 entraîne une réduction drastique de l'adsorption des protéines plasmatiques [18]. Par contre, allonger encore la chaîne n'apporte aucun bénéfice supplémentaire. Le PEG 5000 apparaît donc comme un compromis optimal pour la formulation des PS [123,124,134,142]. Un autre paramètre à prendre en compte est la densité du greffage : le revêtement doit en effet couvrir correctement les nanoparticules pour prévenir l'opsonisation. Lorsque la densité de greffage est faible, les chaînes de PEG peuvent se conformer librement, et ont tendance à prendre une conformation dite en « champignon » (figure 5) : l'épaisseur du revêtement est faible, et il peut même présenter des lacunes favorisant l'opsonisation [143]. Lorsque le greffage est plus dense, la conformation des

chaînes est contrainte, et les molécules de PEG prennent une conformation semi-linéaire ou en « brosse » (figure 5).

La configuration idéale se situe entre ces deux exemples, les chaînes de PEG possédant assez de liberté pour se mouvoir et assurer une répulsion stérique, mais en densité suffisante pour couvrir efficacement toute la surface. La littérature propose une épaisseur de PEG minimale représentant 5% du diamètre total d'une nanoparticule [144,145], ou, pour des formules liposomales, une fraction molaire de 4 à 8% de PEG par rapport aux lipides mis en œuvre [36]. Gref *et al*. proposent de calculer la densité de greffage du PEG sur des nanoparticules polymériques [18]. Cela soulève donc la question de la quantification du PEG à la surface des nanoparticules.

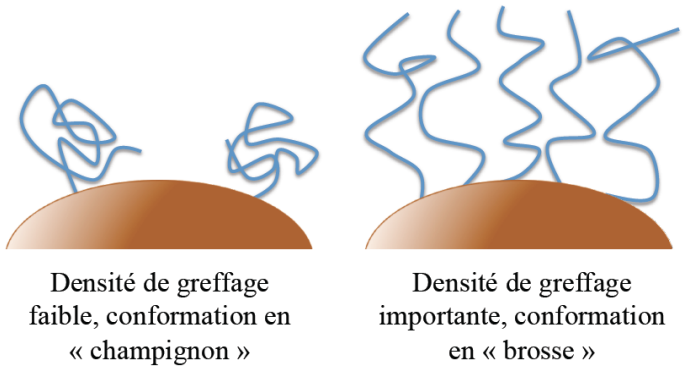

Figure 5 : Représentation de la conformation des chaînes de PEG à la surface de nanoparticules, en fonction de la densité de leur greffage.

Pour les PS et les DLPS, comme pour d'autres nanosystèmes, si les quantités de matériaux mises en œuvre sont connues (ici 0,12 mmol de PEG pour 0,41 mmol de fer), les quantités de polymère greffées sont plus délicates à quantifier, l'excès de PEG étant éliminé par dialyse [123]. Les PEG ne possédant aucun groupement spécifique susceptible d'être dosé, une technique classique consiste à greffer un fluorophore sur les PEG. D'abord, cette stratégie n'est valable que si le nombre de molécules de fluorophore greffées par chaîne de PEG est constant. De plus, l'ajout du fluorophore avant greffage sur les nanoparticules risque de modifier le comportement des chaînes de PEG lors de cette étape, de par l'encombrement stérique généré, par exemple. Le greffage ne serait alors pas comparable avec et sans le fluorophore. L'ajout du fluorophore après PEGylation des nanovecteurs pose le problème de l'accessibilité du site d'attache et de la diffusion probable des molécules fluorescentes dans le revêtement. Enfin, l'intensité de fluorescence peut varier énormément en fonction du

microenvironnement dans lequel le fluorophore se trouve (en solution aqueuse, attaché aux PEG à la surface externe de la couche polymérique recouvrant les nanovecteurs, ou dans le revêtement de PEG à proximité de la nanoparticule).

Pour les PS, la quantité de PEG greffés a été estimée sur matière sèche. La lyophilisation ou le passage à la balance à humidité d'un volume précis de suspension de PS a permis de déterminer que la quantité de PEG est de 0,09 mmol de PEG pour 0,41 mmol de fer. Cette estimation concorde avec les quantités mises en œuvre lors de la PEGylation (0,12 mmol de PEG pour 0,41 mmol de fer), l'excès de PEG étant éliminé par dialyse. Par contre, la densité du greffage ne peut pas être déterminée par cette méthode. Néanmoins, la surface des SPIONs présentés dans cette thèse semble intégralement couverte, ne présentant pas ou peu de lacunes dans le revêtement, au vu de la réduction drastique de l'opsonisation et de la capture diminuée par les cellules du système immunitaire, et du temps de demi-vie allongé dans l'organisme, résultats présentés dans la deuxième partie de cette discussion. De plus, la diminution de l'adsorption du complexe DOX-Fe^{2+} de 14% m/m (masse d'oxydes de fer) sur des SPIONs citratés à 3% m/m sur des SPIONs PEGylés suggère un encombrement stérique important des chaînes de PEG, et donc une conformation plutôt contrainte.

Ces observations amènent à envisager plusieurs hypothèses de travail quant à la formulation des PS et des DLPS :

- La densité de greffage des PEG génère un encombrement stérique, et détermine donc la place laissée pour l'adsorption du complexe DOX-Fe^{2+}. Une densité moindre de PEG pourrait permettre un compromis favorisant un chargement accru de molécule anticancéreuse, tout en préservant la stabilité colloïdale et la furtivité. Cela permettrait de diminuer :

⇒ La quantité de nanovecteurs administrés *in vivo* nécessaire pour atteindre la dose thérapeutique ;

⇒ La quantité de nanovecteurs accumulée au niveau des organes d'élimination, favorisant peut-être leur dégradation dans les cellules phagocytaires ;

⇒ Les coûts de fabrication de la nanoformulation, les PEG activés étant, comme de nombreux polymères, des matériaux onéreux, ainsi que le coût du traitement pour le patient.

- La question se pose aussi quant à la stratégie d'attachement covalent des PEG aux nanosystèmes. Ce revêtement semblant protéger les SPIONs de la dégradation par l'organisme, des liaisons réversibles seraient plus adaptées pour favoriser une

élimination plus rapide des nanosystèmes. Par exemple, une liaison hydrolysable pourrait favoriser la défonctionnalisation des nanovecteurs dans les compartiments intracellulaires. Cette stratégie permettrait :

⇒ D'exposer plus précocement les vecteurs hybrides à la désintégration des compartiments intracellulaires, et ainsi de favoriser une biodégradation plus rapide du cœur inorganique;

⇒ D'accélérer la libération de la DOX, ce qui pourrait augmenter la cytotoxicité de la nanoformulation vis-à-vis des cellules cibles.

2. Furtivité des nanovecteurs magnétiques et devenir dans l'organisme

La PEGylation des nanovecteurs doit leur conférer une certaine furtivité vis-à-vis du système immunitaire, et permettre une circulation prolongée dans l'organisme. Ces deux aspects sont cruciaux pour envisager la délivrance de la DOX *in vivo* : les nanovecteurs doivent circuler suffisamment longtemps pour qu'ils soient accumulés préférentiellement dans la tumeur. En effet, le ciblage de la tumeur, physique (par application d'un champ magnétique externe) ou biologique (par effet EPR ou par reconnaissance moléculaire type ligand-récepteur) nécessite également une circulation prolongée des nanovecteurs. Enfin, la connaissance de la biodistribution des nanovecteurs dans l'organisme est essentielle pour juger de leur efficacité, élimination et éventuelle toxicité.

2.1. Évaluation *in vitro* de la furtivité des nanovecteurs magnétiques

L'impact de cette PEGylation sur les interactions des PS et des DLPS avec le système immunitaire a été évalué récemment [124]. Les phénomènes d'opsonisation ont été mesurés *in vitro* par un test d'activation du complément, le test CH50. Le principe de ce test est illustré par la figure 6.

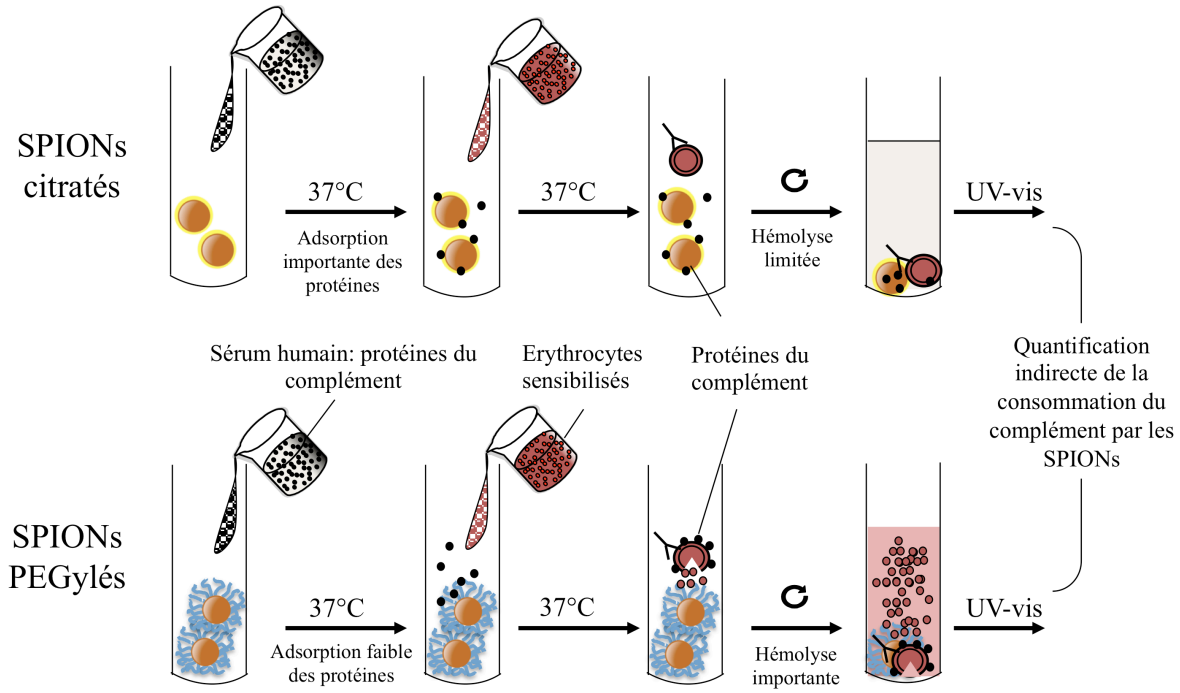

Figure 6 : schéma de principe du test CH50 (activation du complément).

Il s'agit d'un test évaluant la capacité hémolytique résiduelle du système du complément dans du sérum humain. Après contact avec les nanovecteurs, les protéines du complément non consommées sont mises en présence d'une quantité donnée d'érythrocytes ovins sensibilisés avec des anticorps érythrocytaires rabiques anti-ovins. La quantité de sérum humain nécessaire pour lyser 50% des érythrocytes ovins est appelée CH50. La consommation du complément a été mesurée avec des SPIONs citratés et PEGylés (PS), de façon à visualiser l'intérêt de la PEGylation. Cette consommation a aussi été mesurée pour des SPIONs PEGylés et chargés de DOX (DLPS) : même si la présence de la molécule sur les nanovecteurs ne provoque pas de variation du potentiel zêta [134], de par sa localisation à la surface des SPIONs, enfouie dans la couche de PEG, le nanovecteur doit être évalué sous sa forme finale. Les résultats sont présentés dans la figure 7, en fonction de la surface des NPs ou de la concentration en fer.

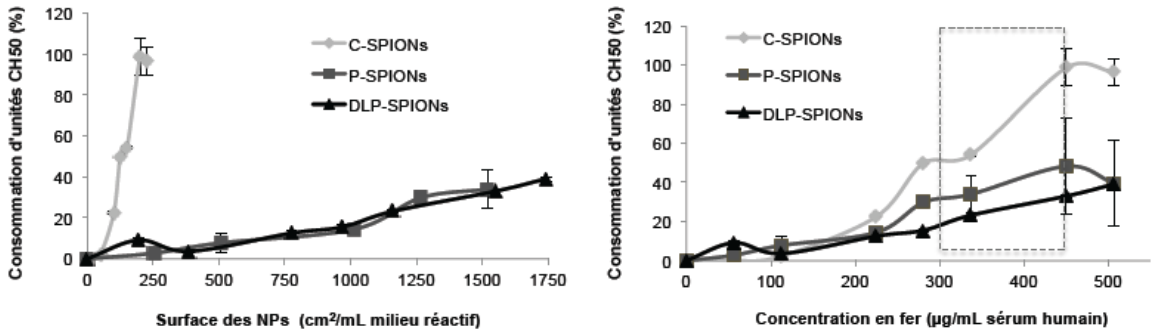

Figure 7 : activation du complément par les SPIONs citratés (C-SPIONs), PEGylés (P-SPIONs) ou PEGylés et chargés de DOX (DLP-SPIONs), en fonction de leur surface ou de la concentration en fer.

Sans surprise, les SPIONs citratés, chargés négativement, consomment les protéines du complément de façon importante, même pour des surfaces de contact limitées (250 cm^2/mL de milieu réactionnel). La consommation entraînée par la présence de SPIONs PEGylés avec ou sans DOX reste limitée, pas plus de 40% pour des surfaces de contact importantes (1750 cm^2/mL de milieu réactionnel). Cette quantité correspond aux valeurs trouvées dans la littérature : Aqil et al. ont décrit une activation inférieure à 25% pour des surfaces de 1000 cm^2/mL pour des nanosystèmes équivalents [146]. L'équivalence des résultats en présence ou en absence de DOX chargée sur les nanovecteurs PEGylés confirme que la molécule n'altère en rien les propriétés de surface du nanosystème. Comme les SPIONs citratés et PEGylés ne présentent pas les mêmes surfaces par NP, les résultats exprimés en fonction de la

concentration en fer permettent de comparer les deux systèmes pour un même nombre de NPs. Là aussi, les SPIONs citratés activent le complément de façon plus importante que les SPIONs PEGylés, avec ou sans DOX. En tenant compte du volume sanguin ou sérique d'une souris (2 à 2,4 mL de sang, 0,8-1,2 mL de sérum) et de la quantité de fer injectée lors du protocole thérapeutique *in vivo* (200 µL à 1,8 g/L de fer, soit 360 µg de fer par souris), la zone d'intérêt *in vivo* de la concentration en fer est située entre 300 et 450 µg/mL de sérum. Or c'est dans cette zone que la différence d'activation du complément est la plus favorable aux nanovecteurs PEGylés, comparés aux SPIONs citratés.

Pour compléter ces résultats de faible activation du complément, les mêmes nanosystèmes ont été incubés 1 à 4h sur des cellules THP-1, puis un dosage de fer a été réalisé par spectrométrie d'absorption atomique. Les cellules THP-1 sont des monocytes issus d'une lignée leucémique humaine. Elles peuvent se différencier et présenter un phénotype de macrophages lorsqu'elles sont cultivées en présence de PMA (acétate myristate de phorbol). L'intérêt est que leur capacité phagocytaire est augmentée par rapport à des monocytes. Les résultats sont présentés dans la figure 8. Les concentrations utilisées (500 mg/L de fer dans le milieu de culture), bien qu'importantes, n'ont pas généré de baisse de la viabilité cellulaire, de même que la présence de la DOX. En effet, les temps d'incubation courts et le traitement immédiat des cellules après incubation n'ont pas permis un délai suffisant pour que les cellules réalisent un cycle cellulaire, et donc que la DOX puisse interférer dans la réplication.

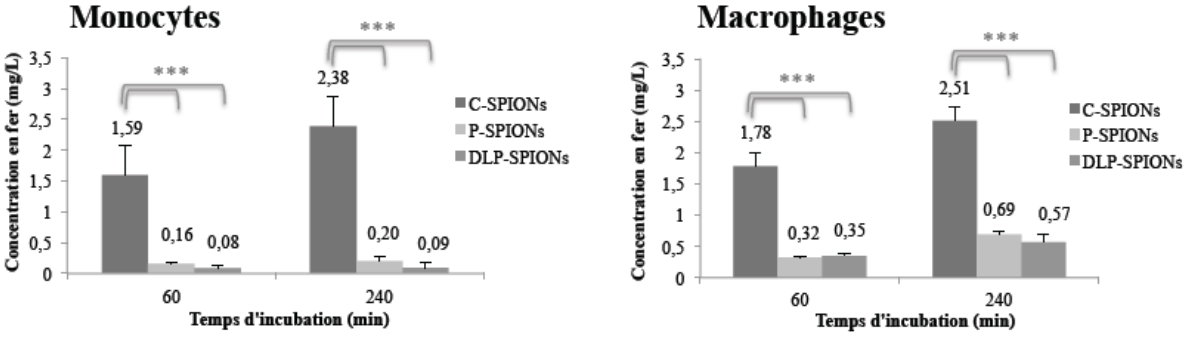

Figure 8 : Concentration en fer dans des cellules THP-1 traitées avec des SPIONs citratés (C-SPIONs, PEGylés (P-SPIONs) ou PEGylés et chargés de DOX (DLP-SPIONs), après 60 et 240 min d'incubation.

La capture par les cellules mimant des monocytes et des macrophages est largement diminuée pour les SPIONs PEGylés avec ou sans DOX par rapport aux SPIONS citratés, et ce pour les

2 temps d'incubation ($p < 0,01$), et pour les deux phénotypes de cellules. La capture est globalement plus importante pour les cellules mimant des macrophages, du fait de leurs capacités phagocytaires plus importantes que les monocytes. Aucune différence significative n'a été mise en évidence entre SPIONs PEGylés avec ou sans DOX. Là encore, la présence de la molécule sur les nanovecteurs ne semble pas altérer leur comportement *in vitro*.

Ainsi, au vu de ces essais *in vitro* (test CH50 et capture par des cellules mimant des monocytes et des macrophages), la PEGylation des nanovecteurs permet une faible opsonisation et une activation limitée du complément, ainsi qu'une diminution drastique de leur capture par les cellules de type monocyte et macrophage. Ces constatations renforcent l'hypothèse que ces nanovecteurs seraient furtifs dans l'organisme.

Pour conclure cette partie, plusieurs remarques peuvent être faites :

- Les propriétés générales recherchées avec la mise en œuvre de PEG 5000 ont été obtenues, que ce soit la stabilité colloïdale et la furtivité *in vitro*. Ces points sont capitaux pour envisager une administration *in vivo*.
- La PEGylation est une stratégie maintenant bien connue et étudiée, depuis les années 90. Si elle a démontré son intérêt dans l'allongement de la demi-vie sanguine des nanovecteurs administrés par voie intraveineuse, une circulation systémique prolongée n'est pas sans conséquences. Le Doxil® a certes permis de réduire la toxicité cardiaque de la DOX, mais sa demi-vie sanguine d'environ 80h chez l'adulte provoque l'apparition d'autres effets indésirables, comme le syndrome main-pieds, ce qui limite la dose maximale tolérée [36]. Dans la littérature, il est aussi rapporté que l'injection répétée de systèmes PEGylés peut provoquer la fabrication par l'organisme d'anticorps (IgM) anti-PEG, ce qui diminue la demi-vie des nanovecteurs lors des injections suivantes [147,148].

2.2. Devenir dans l'organisme : biodistribution

Les PS et les DLPS présentent un potentiel zêta proche de zéro, notamment à pH physiologique, du fait de la PEGylation, ainsi qu'une taille limitée (diamètre hydrodynamique inférieur à 80 nm). Comme l'ont démontré les essais de furtivité *in vitro*, ces propriétés sont favorables à une circulation prolongée dans l'organisme, du fait de la faible activation du complément et une capture diminuée par les cellules phagocytaires [124]. La taille des nanovecteurs entre 10 et 100 nm devrait favoriser une élimination plutôt hépatique, la taille des éléments pouvant être éliminés par voie rénale n'excédant 5 à 10 nm. Ces hypothèses ont

été vérifiées chez des souris Swiss saines ayant reçu une injection de 200 µL de SPIONs citratés (C-SPIONs), de PS ou de DLPS (concentration en fer 1,8 g/L). Des échantillons sanguins ont été prélevés à intervalles réguliers, pour estimer la demi-vie sanguine des nanovecteurs. Des souris ont également été sacrifiées à des temps donnés, et les organes d'élimination prélevés (foie, reins et rate), pour quantifier la biodistribution des nanovecteurs dans ces organes.

Le suivi des nanoformulations dans les échantillons sanguins et les organes a été réalisé par dosage du fer en spectrométrie d'absorption atomique (SAA). Cette démarche est peu courante dans la littérature. En effet, de nombreuses études se basent sur un changement de l'intensité du signal en IRM, ou sur un marquage spécifique des nanovecteurs, comme un isotope [149,150] ou un fluorophore [26,117], voire sur le suivi de la molécule active (comme la fluorescence de la DOX [6]). Toutes ces méthodes sont moins sensibles (à l'exemple de l'IRM) et/ou moins spécifiques (les fluorophores peuvent se désolidariser des nanovecteurs) comparées à la SAA. Cette méthode possède en effet une sensibilité de l'ordre du ppm ou du ppb pour le fer, et le fer dosé ne peut provenir que du cœur métallique des nanovecteurs (après soustraction du fer physiologique), conférant ainsi à cette méthode une grande spécificité.

La figure 9A présente la concentration sanguine de fer en fonction du temps, après injection de C-SPIONs et PS. La concentration physiologique de fer a été déterminée et soustraite. La figure 9B présente la concentration en fer totale (nanovecteurs et fer physiologique) en fonction du temps dans différents organes d'élimination, après injection de PS. Pour des raisons éthiques, les injections de DLPS n'ont été réalisées que pour des temps courts, jusqu'à 30 min ; les résultats (non exposés ici) sont comparables à ceux obtenus pour les PS.

Les SPIONs citratés disparaissent très rapidement du flux sanguin : la concentration en fer chute de 90% en 15 min, puis de 80% en 30 min (figure 9A). Leur demi-vie plasmatique a été estimée à 15 ± 9 min. Leur capture précoce par le SRE peut être imputée au port de charges négatives. Au contraire, la concentration en fer reste élevée dans les 30 premières minutes pour les PS (et les DLPS). Plus de 50% des PS circulent encore après 60 min, leur demi-vie sanguine a été estimée à 76 ± 6 min. Cet allongement du temps de circulation des PS dans l'organisme est certes attendu, il conforte les essais de furtivité *in vitro*, mais la demi-vie plasmatique de 76 min permet aussi de quantifier le délai laissé aux nanovecteurs pour une capture tumorale par effet EPR. Ce délai a également servi de base de réflexion pour la mise

au point du protocole thérapeutique chez la souris tumorisée, notamment pour l'évaluation du ciblage magnétique de la tumeur. Une application de l'aimant pendant 1h après injection des DLPS concorde également avec les essais cliniques réalisés par Lübbe *et al.* (60 à 120 min d'application [52,151,152]), et ne semble pas excessive au regard du confort des animaux.

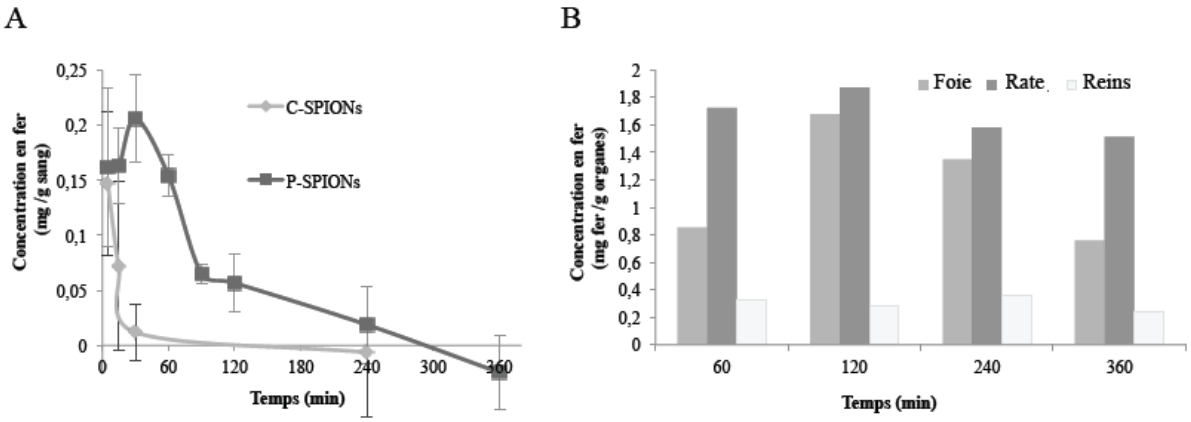

Figure 9 : (A) Pharmacocinétique des SPIONs citratés et PEGylés, suivie par la concentration de fer (dosé par SAA) dans le sang pendant 360 min (n = 4 souris). (B) Variation de la concentration en fer (en mg/g d'organes, dosé par SAA) dans les principaux organes d'élimination à 60, 120, 240 et 360 min après injection de SPIONs PEGylés (mesure sur les organes réunis de 5 souris).

Si les PS disparaissent très progressivement du flux sanguin, la concentration en fer dans le foie augmente progressivement entre 60 et 120 min, pour décroître doucement à 240 et 360 min (figure 9B). La même observation peut être faite pour la rate. En revanche, la concentration en fer reste constante dans les reins. Les principales voies d'élimination des PS et donc des DLPS sont donc hépatique et splénique, avec une accumulation progressive, concordant avec la demi-vie plasmatique.

Pour compléter cet essai de biodistribution *in vivo*, un essai préliminaire a été mené sur une souris NMRI nude tumorisée. L'animal a été sacrifié 1h après injection de PS (200 µL à 1,8 g/L de fer), les organes et la tumeur ont été prélevés. Des coupes ont été réalisées pour la microscopie électronique en transmission (MET). Cette technique a déjà été employée *in vitro* pour suivre les PS incubés sur des cellules MDA-MB 435. Cet essai préliminaire avait pour but de déterminer si la technique était pertinente dans le cadre d'essais *in vivo*. Les images obtenues sont présentées en figure 10.

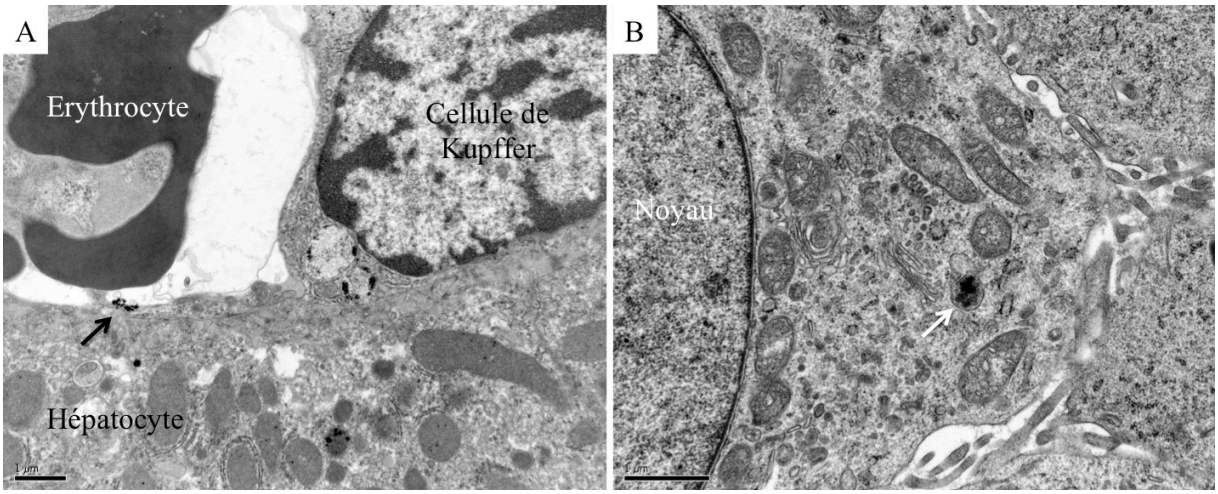

Figure 10 : Coupes d'organes en MET, 1h après injection de 200 µL de PS à 1,8 g/L chez une souris NMRI nude tumorisée. (A) foie ; (B) tumeur.

La figure 10A est une coupe du foie de la souris. La présence de nanovecteurs a été détectée au niveau des capillaires sinusoïdes (flèche noire), à proximité de cellules de Kupffer, qui ont des propriétés de phagocytose. En 1h, des PS sont donc drainés par le système sanguin jusqu'au foie, ce qui est cohérent avec leur demi-vie plasmatique. Par contre, aucune coupe n'a montré la présence de PS au sein des cellules hépatocytes ou des cellules de Kupffer. Le temps choisi est sans doute trop court pour que les PS puissent être amenés jusqu'au foie et internalisés en nombre suffisant pour pouvoir être vus facilement sur les images. Au niveau de la tumeur, quelques structures plus denses aux électrons apparaissent, sans qu'elles puissent être formellement identifiées comme des PS, notamment en raison de leur aspect moins défini (figure 10B). Si le TEM a permis de visualiser quelques DLPS au niveau du foie, cette technique ne permet pas de mettre en évidence une accumulation précoce de PS au niveau de la tumeur.

Ces essais *in vivo* concernant la biodistribution permettent de souligner quelques points importants :

- Pour les PS, un temps de demi-vie plasmatique allongé et une élimination principalement hépatique et splénique étaient prévisibles, au vu de leurs propriétés physico-chimiques et des essais *in vitro* de furtivité. Néanmoins, une élimination rénale ne peut pas être exclue : après dégradation des nanosystèmes, il est possible que le fer soit réabsorbé au niveau des tubules proximaux des reins, et ainsi incorporé au métabolisme du fer physiologique [153]. La non-observation de ce phénomène

voudrait indiquer que cette élimination est négligeable dans les conditions expérimentales utilisées ici.

- La pharmacocinétique des PS et des DLPS, et leur temps de demi-vie plasmatique de 76 min montrent que leur capture est un phénomène progressif. Ainsi, si les essais *in vitro* ont montré une opsonisation et une capture par les cellules phagocytaires largement diminués, ces phénomènes ne sont pas totalement supprimés, ils sont ralentis *in vivo*.

3. Imagerie et ciblage des tumeurs à l'aide des nanovecteurs magnétiques de la DOX

3.1. Nanovecteurs et IRM

Afin d'évaluer l'efficacité des nanovecteurs en tant qu'agents de contraste en IRM, des injections ont été réalisées sur des souris Swiss saines; l'intensité du signal a été mesurée pendant plus de 2h. Pour des raisons éthiques évidentes, ce sont des SPIONs PEGylés sans DOX qui ont été injectés. Les résultats ont été comparés à ceux obtenus avec des injections de Cliavist®, un agent de contraste commercial pour l'IRM, à base de SPIONS habillés de carboxydextran. La dose administrée de fer était équivalente dans les deux cas (11,67 µM/kg). Des images IRM en coupes morphologiques axiales ont été réalisées pour les principaux organes d'élimination (foie, reins et rate). La figure 11A montre les images obtenues pour le foie en fonction du temps, après injection de SPIONS PEGylés. Sur les images avant injection, la tache noire dans le quart supérieur gauche correspond à l'estomac vide, le foie occupant le reste de la cavité abdominale à ce niveau de coupe. Après injection, un assombrissement du foie est visible à l'œil nu (figure 11A) et une décroissance de l'intensité du signal est observée (figure 11B et C).

L'intensité du signal a décru drastiquement dans le foie quelques minutes seulement après l'injection de Cliavist® (à 12 min, figure 11B). Ce résultat était attendu, car cet agent de contraste commercial est utilisé pour la détection et la caractérisation des petites lésions du foie. Ces NPs sont en effet immédiatement capturées et accumulées par phagocytose dans les cellules du système réticulo-endothélial du foie, de par la nature de leur revêtement [95]. La baisse de l'intensité du signal dans le foie a atteint 50% après 20 min (figure 11C). En revanche, aucune baisse de l'intensité du signal n'a été notée dans les reins et la rate, le foie étant le principal organe d'élimination pour cette formulation (figure 11B).

Pour les SPIONs PEGylés, l'intensité du signal dans le foie a décru de façon plus progressive (assombrissement sur la figure 11A, et figure 11B). La rate a également montré une décroissance de l'intensité du signal, suivant la même cinétique que dans le foie, et atteignant un plateau à 80 min (figure 11B). La baisse de l'intensité du signal dans le foie due aux SPIONs PEGylés atteint 50% après 70 min (figure 11C). La PEGylation des SPIONs a, de fait, modifié leur biodistribution.

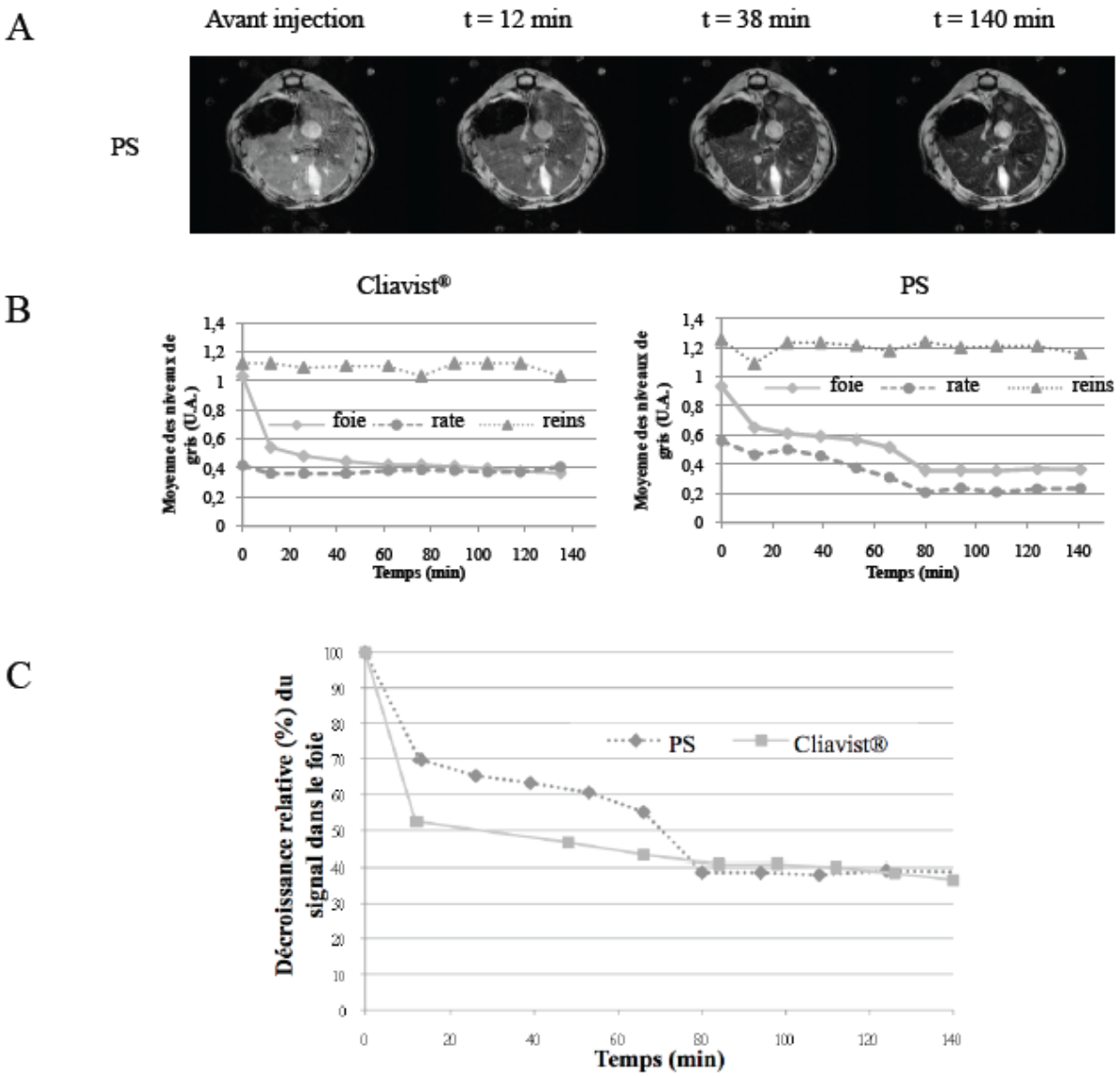

Figure 11: (A) Coupes morphologiques axiales en IRM du foie de souris après injection de Cliavist® ou de SPIONs PEGylés (11,67 µM/kg de fer) en fonction du temps. (B) Décroissance de l'intensité du signal en fonction du temps après injection de Cliavist® ou de SPIONS PEGylés, pour le foie, les reins et la rate de souris. (C) Décroissance relative de l'intensité du signal dans le foie de souris, en fonction du temps, pour le Cliavist® et les SPIONS PEGylés. Données de S. Même et J. C. Beloeil du CBM d'Orléans.

Leur demi-vie sanguine $t_{1/2}$, estimée à 76 ± 6 min [124], concorde avec une décroissance maximale du signal dans le foie et la rate à 80 min, de même que l'élimination principalement dirigée vers ces organes [124]. Ces observations concordent aussi avec les données concernant le Clariscan®, un autre agent de contraste à base de SPIONs PEGylés, développé pour l'angiographie. Cet agent de contraste possède une demi-vie sanguine de plus de 2h chez l'homme, ainsi qu'une biodistribution principalement dirigée vers le foie et la rate [95]. Les

SPIONs PEGylés, et par là même les SPIONs PEGylés chargés de DOX sont donc de bons candidats comme agents de contraste en IRM.

Si les nanovecteurs offrent un contraste équivalent au Cliavist®, formulation commerciale, leur capacité à servir d'agents de contraste en IRM n'est pas remise en cause. Cependant, le Cliavist® est utilisé pour l'imagerie du foie, objectif tout à fait différent de l'application théragnostique recherchée pour les nanovecteurs de la DOX. Ces résultats, ainsi que la biodistribution, doivent donc être accompagnés de plusieurs remarques :

- La cinétique de distribution des SPIONS PEGylés dans les organes, avec une arrivée retardée dans le foie et la rate, est un élément favorable à leur application théragnostique. La demi-vie sanguine des nanovecteurs leur offre la possibilité de s'accumuler au niveau de la tumeur par différents mécanismes, notamment par effet EPR. Ce délai est aussi favorable à un ciblage magnétique, avec application d'un champ magnétique externe au niveau de la tumeur, de façon à y retenir les nanovecteurs.
- L'étude préliminaire effectuée sur souris saines, hors ciblage tumoral, permet de modéliser la biodistribution des nanovecteurs excédentaires, non retenus dans les tumeurs, chez des souris tumorisées. Cependant, la rétention des nanovecteurs au niveau des tumeurs doit être prise en compte pour la biodistribution globale.
- En plus de la toxicité, la biodistribution des nanovecteurs est importante pour l'imagerie. En effet, l'imagerie à l'aide d'un nanovecteur théragnostique a pour but le diagnostic et/ou le suivi du traitement. Les nanovecteurs doivent donc montrer une certaine spécificité pour la tumeur, de façon à la détecter en imagerie.
- Pour finir, même si leur biodistribution semble favorable, il n'en reste pas moins que les SPIONs PEGylés sont finalement capturés par le système réticulo-endothélial, et sont accumulés au niveau du foie. La question est donc de savoir quelle proportion de nanovecteurs peut s'accumuler au niveau de la tumeur lorsqu'elle n'est pas située dans le foie, et donc quelle est la dose thérapeutique du principe actif anticancéreux spécifiquement délivrée au niveau de la tumeur.

3.2. Nanovecteurs et ciblage des tumeurs

Si des essais de quantification de la distribution de nanovecteurs dans les tumeurs sont trouvés dans la littérature, les méthodes varient. Yang *et al.* ont rapporté l'évaluation *in vivo* chez la souris tumorisée de SPIONs PEGylés chargés de DOX, et ciblant spécifiquement l'intégrine

$\alpha_v\beta_3$, grâce au peptide cRGD [149]. Les résultats sont présentés en pourcentage de la dose injectée par g de tissu : par effet EPR, environ 2,5% de la dose injectée est retenue au niveau de la tumeur, contre environ 5% avec le ciblage actif du peptide. La majorité de la dose d'oxydes de fer injectée est retrouvée précocement dans le foie. Hua *et al.* ont rapporté des résultats en ppm, pour l'évaluation *in vivo* de SPIONs revêtus de dérivé de polyaniline chargés de DOX, utilisant un ciblage magnétique [83] : 18h après injection d'une dose de 5mg/kg de la formulation, 630 ppm ont été retrouvés au niveau de la tumeur. Dandamudi *et al.* ont quant à eux évalué l'accumulation au niveau des vaisseaux tumoraux de magnétoliposomes chargés de vinblastine, marqués d'un fluorophore, avec application d'un champ magnétique externe [154] : le pourcentage de fluorescence observé dans les vaisseaux tumoraux était de 16% en présence de l'aimant, au lieu de 5% sans. D'autres études sont basées sur la décroissance du signal observée en IRM dans les tumeurs [155,156].

Ces quelques exemples montrent que ces quantifications sont surtout indirectes, et sont rarement comparées à la dose totale administrée, encore moins à celle retrouvée au niveau des organes d'élimination. La raison en est que si l'effet EPR existe, il n'est certes pas suffisant pour accumuler des quantités appréciables de nanovecteurs au niveau tumoral, et que les différentes techniques de ciblage employées, même efficaces, ne permettent pas en l'état actuel des recherches de détourner la grande majorité des nanovecteurs des organes d'élimination.

Ainsi, les stratégies de ciblage des tumeurs restent d'une importance prioritaire pour le développement de nanovecteurs. D'abord, *in vitro*, elles permettent de compenser la cytotoxicité moindre des nanovecteurs, due à des cinétiques d'internalisation plus lentes que la molécule active sous forme libre [81,155,157,158]. Deuxièmement, elles sont constamment améliorées, et couplées à l'augmentation des temps de demi-vie des nanovecteurs dans l'organisme, elles permettent de détourner une partie des nanovecteurs des cellules saines, limitant ainsi les effets secondaires liés à l'administration de la molécule active seule.

3.3. Une nanoformulation théragnostique ?

Le protocole thérapeutique *in vivo* initié dans le cadre de cette thèse (deuxième partie, chapitre 3) n'a pas permis de valider expérimentalement le ciblage magnétique au moyen d'un petit aimant stationnaire en terre rare. Pour des raisons d'effectifs, les tests statistiques ne possédaient pas la puissance nécessaire à la mise en évidence d'une différence significative

entre les groupes traités à la DOX en solution, avec les DLPS et les DLPS avec application d'un champ magnétique externe. De plus, les modalités d'application de l'aimant doivent être repensées, notamment parce que le champ magnétique n'a pas été optimisé, et que la plupart des études de ciblage magnétique sont conduites sur des durées largement supérieures à 1h [154,156,159]. Par contre, notre étude a montré que les effets des traitements étaient étroitement dépendants de la croissance tumorale et de sa vascularisation, l'effet EPR est donc un élément-clé de l'activité des DLPS. C'est probablement un facteur important pour expliquer la réduction de la toxicité de la DOX observée avec l'administration des DLPS.

Pour être qualifiée de théragnostique, une nanoformulation doit pouvoir justifier de fonctions d'imagerie et de délivrance d'un médicament. Face à ces considérations, les évaluations du potentiel théragnostique des nanovecteurs magnétiques décrites par la suite seront axées sur ces aspects, ainsi que sur la possibilité d'un ciblage magnétique :

- Un protocole en IRM a été initié, sur souris NMRI nude tumorisées avec injection sous-cutanée de cellules MDA-MB 435. L'objectif est de visualiser et quantifier la décroissance de l'intensité du signal au niveau des tumeurs après injection des SPIONS PEGylés. La fonction d'imagerie des nanovecteurs, c'est-à-dire la possibilité de visualiser la tumeur et/ou de suivre le traitement va donc être évaluée. De plus, le sacrifice des souris et le prélèvement des tumeurs à des temps déterminés vont permettre de doser le fer par SAA, et donc de quantifier de façon objective la proportion de nanovecteurs retenue au niveau de l'environnement tumoral, par effet EPR.
- La stratégie de ciblage magnétique peut être évaluée par le même biais, grâce aux données d'IRM. L'application pendant des temps croissants d'un aimant à proximité de la tumeur après injection de PS, associée au suivi de la décroissance du signal devrait permettre de faire des choix rationnels quant au protocole à adopter pour un ciblage magnétique optimal. Le premier point sera de vérifier si ce ciblage magnétique permet une rétention accrue des PS au niveau de la tumeur, et si oui, pour quel temps d'application de l'aimant. Un autre point à explorer sera la possibilité de faire varier les modalités d'application du champ magnétique (focalisation, champ constant ou alternatif), après avoir mieux caractérisé le dispositif.

- L'amélioration du protocole thérapeutique est indispensable avant d'engager d'autres essais.

⇒ Cela passe par l'amélioration du modèle animal choisi, en raison de la variabilité observée dans les cinétiques de croissance tumorale, et de la difficulté des interprétations qui en découlent (deuxième partie, chapitre 3). Une nouvelle lignée murine et de nouvelles lignées cellulaires de cancer du sein vont être expérimentées pour mettre au point un modèle d'animal tumorisé présentant moins de variabilité inter-individuelle.

⇒ Ensuite, les effectifs doivent être suffisamment importants pour pouvoir mettre en évidence une différence significative entre les croissances tumorales des différents groupes traités, même si quelques animaux doivent être écartés du protocole.

⇒ Enfin, les modalités d'administration doivent être revues (dose administrée et fréquence), pour que l'efficacité de la DOX en solution puisse être mise en évidence, et ainsi permettre une comparaison avec le traitement avec les DLPS.

4. Persistance dans l'organisme des nanovecteurs magnétiques et toxicité:

Les études classiques de cytotoxicité des nanovecteurs pour la délivrance d'agents anticancéreux *in vitro* se font généralement sur le court terme. En effet, la plupart des essais de viabilité cellulaire (MTT ou équivalent) sont réalisés sur 24, 48 ou 72h, de façon à vérifier qu'aucune mortalité cellulaire ne peut être imputée aux nanovecteurs non chargés de molécule active [119,160]. Il est rare que les cultures cellulaires soient prolongées au delà. De même, les essais *in vivo*, portant la plupart du temps sur la capacité des nanovecteurs à servir en imagerie, font l'objet d'un suivi court sur quelques heures [157,161], certains allant jusqu'à 48h [149]. Cependant, la question des conséquences à plus long terme d'une exposition à des nanovecteurs est de plus en plus abordée dans la littérature. Des études *in vitro* récentes explorent les effets d'une exposition de certaines lignées cellulaires à des SPIONs revêtus de dextran sur plusieurs jours [162,163]. Si aucune mortalité cellulaire n'est détectée précocement (24 à 48h), la production de cytokines pro-inflammatoires et de radicaux libres oxygénés a été mise en évidence, pouvant induire une apoptose sur des périodes plus longues (jusqu'à 7 jours). De même, de plus en plus d'études *in vivo*, centrées sur les effets de nanovecteurs sans molécule active, revêtus de dextran ou de dérivés de glucose, sont poussées sur des périodes longues, pouvant aller jusqu'à 3 semaines [163] ou même 3 mois [164].

Ces études *in vivo* explorent la rémanence des nanosystèmes dans l'organisme, notamment au niveau des principaux organes d'élimination. Il est généralement admis qu'en tant que matériau non toxique, les SPIONs sont bien tolérés et offrent une certaine sécurité quant à leur usage clinique, surtout sous forme fonctionnalisée. Le métabolisme régulant le fer dans l'organisme est considéré comme apte à prendre en charge l'élimination des nanoparticules d'oxydes de fer. Néanmoins, le cycle de biotransformation de ces nanovecteurs est encore loin d'être complètement élucidé. Ainsi, Levy et *al.*, après injection de SPIONs de 8 nm, revêtus de dérivés de glucose, dont les doses administrées chez la souris allaient de 50 à 1000 µmol de fer/kg (de 84 µg à 1,68 mg de fer pour une souris de 30g), suivent la quantité de fer dans les organes d'élimination (foie, rate et rein), ainsi que leur magnétisation, afin de juger de l'état de dégradation des SPIONs [164]. Sans surprise, les nanoparticules sont retrouvées majoritairement dans le foie et la rate, très précocement, et y sont encore détectées après 90 jours. Il semble que leur dégradation soit lente, et les auteurs supposent qu'une partie des produits de dégradation, sous forme de ferritine, est redirigée vers la rate à partir du foie.

D’autres études confirment une rémanence magnétique des SPIONs persistant sur plusieurs semaines au niveau du foie [93,165,166].

Dans le cadre de cette thèse, les organes des souris ayant pris part au protocole thérapeutique ont été prélevés et congelés pour de plus amples investigations. Des coupes du foie et de la tumeur de l’une d’elles ont été observées en MET. Ici, les quantités injectées de DLPS sont trois fois supérieures à celles des PS utilisées pour l’étude présentée précédemment à la figure 10, et les DLPS ont eu le temps de s’accumuler dans les principaux organes d’élimination (foie et rate) ainsi que dans la tumeur; les DLPS devraient donc être visualisées par cette technique. Les images MET du foie de souris traitées sont présentées à la figure 12.

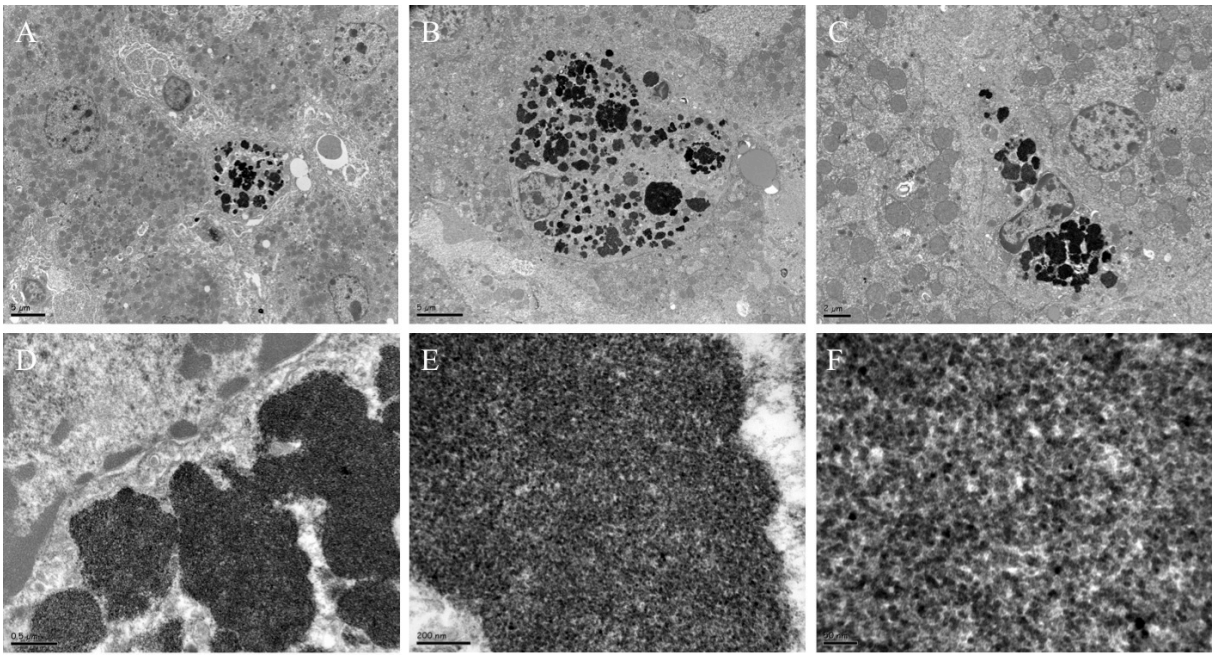

Figure 12 : Images MET de coupes de foie de souris NMRI nude tumorisées, 5 semaines après arrêt du protocole thérapeutique (3 injections de DLPS de 360 µg de fer, soit 1,08 mg de fer en tout). (A-C) Cellules de Kupffer ; (D-F) différents grossissements de l’image C.

Sans surprise, des amas de nanoparticules sont facilement visibles au niveau du foie. Comme le montrent les clichés A à C, les hépatocytes sont exempts de SPIONs, qui sont exclusivement concentrés dans les cellules de Kupffer. Cette constatation a également été faite par Lunov *et al.* [163,166], qui soulignent que ces macrophages ne représentent que 2% des cellules du foie. Il est à noter que la morphologie des tissus du foie est normale. Par contre, les clichés réalisés sur la tumeur n’ont pas permis de mettre en évidence la présence de DLPS au sein des cellules. La quantité de nanovecteurs accumulée par effet EPR dans une

tumeur est généralement de quelques pourcents par rapport à la dose totale injectée, cette quantité rend difficile une visualisation en MET des DLPS dans les cellules tumorales.

En ce qui concerne le foie, le deuxième point à souligner est que les grossissements D à F font apparaître des SPIONs qui ont le même aspect que ceux retrouvés dans les cellules MDA-MB435 après une courte incubation (voir la figure 2, chapitre 3). Leur aspect bien défini semble indiquer une dégradation limitée. Ceci pourrait avoir deux causes : d'abord la quantité injectée est relativement importante, de plus le sacrifice des souris a été fait 5 semaines après la fin du traitement. Les macrophages pourraient avoir besoin de plus de temps pour dégrader les nanoparticules, et gérer un apport si conséquent. Les DLPS sont donc des systèmes possédant un temps de persistance important dans le foie. Cette constatation peut être mise en relation avec la coloration du foie et de la rate observée lors du prélèvement des organes (figure 13) : ces deux organes semblent plus foncés que ceux des témoins ayant reçu du sérum physiologique. Il est donc probable que des quantités importantes de DLPS seraient également observées au niveau de la rate, au vu de la baisse de l'intensité du signal observée en IRM au niveau de cet organe, et au vu de l'étude de biodistribution (chapitres 2 et 3 de cette discussion).

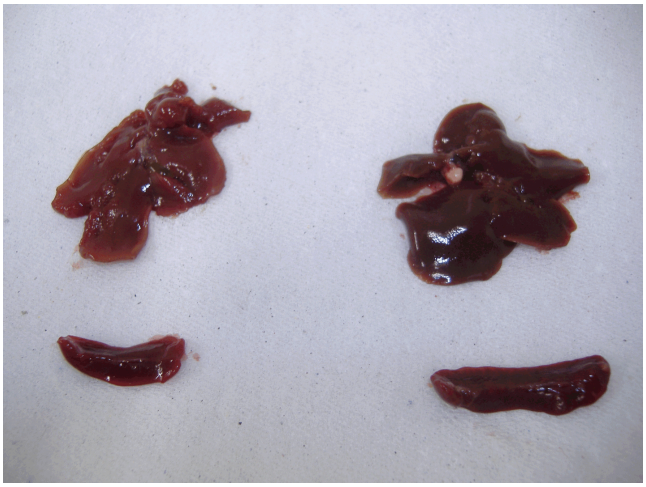

Figure 13 : foies et rates prélevés après sacrifice de souris ayant reçu du sérum physiologique (à gauche) et des DLPS (à droite).

La dégradation lente de DLPS pourrait être reliée à sa formulation, notamment à son revêtement de PEG. Plusieurs études s'intéressent au temps de dégradation de SPIONs en fonction de leur revêtement [163,164,167]. Lunov *et al.* relèvent la diminution de 50% du diamètre hydrodynamique de SPIONs revêtus de carboxydextran après 3 jours d'internalisation dans des macrophages, ainsi qu'une baisse de la fluorescence due à un

fluorophore relié covalemment à l'enveloppe, ce qui est un indice de la dégradation du revêtement [163]. Levy *et al.* ont exposé différentes formulations à un environnement lysosomal artificiel : des SPIONs revêtus de citrates, de dérivés de glucose, ou de dextran montrent une dégradation pH-dépendante, pouvant aller de 10 à 53 jours en fonction du revêtement [164]. La couche de PEG pourrait donc protéger les SPIONs de la dégradation au sein des cellules de Kupffer.

Cette évaluation *in vivo* concernant la persistance des DLPS dans l'organisme permet de souligner quelques points importants :

- Cette persistance ne semble pas affecter le foie de façon visible, puisque les tissus semblent sains morphologiquement, y compris à l'échelle microscopique. Cependant, une évaluation des fonctions hépatiques (dosage des phosphatases alcalines, bilirubine, ASAT et ALAT) peut être envisagée pour confirmer le bon fonctionnement de cet organe [135].
- La persistance au niveau de la rate doit être évaluée, ainsi qu'au niveau des reins. En effet, il n'est pas exclu que le fer issu de la dégradation des nanovecteurs soit redirigé vers ces organes [135,163,164].

Conclusion

Les applications de la « nanomédecine » en sont encore à leurs balbutiements. Si un certain nombre de formulations sont déjà disponibles sur le marché pour l'imagerie ou la délivrance d'agents anticancéreux, ou approuvées dans le cadre d'essais cliniques (247 applications ou produits, selon Etheridge *et al.* [168]), une large proportion de nanoformulations est encore au stade de la recherche ou du développement. Parmi elles, les systèmes à base de SPIONs sont en bonne place, majoritairement en tant qu'agents de contraste en IRM, ou dans des thérapies combinées comme MagForce NanoTherm®, des SPIONs utilisés en thérapie thermique, ayant démontré une synergie avec la chimiothérapie et la radiothérapie, permettant de diminuer les doses de ces traitements anticancéreux. Néanmoins, les plateformes théragnostiques permettant à la fois (i) un ciblage spécifique de l'environnement ou des cellules tumorales, (ii) des fonctions d'imagerie pour le diagnostic et/ou le suivi du traitement (iii) la délivrance d'une molécule anticancéreuse, se font attendre.

De plus, depuis la mise sur le marché des premières nanoformulations, les autorités de santé ont durci les critères et les exigences pour obtenir une autorisation de mise sur le marché, par principe de précaution. Un exemple typique est l'absence de générique du Doxil®, alors que les brevets sont tombés dans le domaine public depuis 2010. Barenholz, l'un des pères de cette nanoformulation, a récemment exposé les difficultés liées aux caractérisations physico-chimiques complémentaires exigées par la FDA [21].

Ces constatations soulignent la nécessité d'une caractérisation poussée des nanosystèmes, et d'une connaissance approfondie des interactions de ces nano-objets à l'échelle de la cellule et de l'organisme. Les travaux présentés dans cette thèse concernant les DLPS sont une base de travail pour le développement futur de cette nanoformulation. La fonctionnalisation de leur surface avec de l'acide folique a déjà été réalisée dans notre laboratoire, et les DLPS folatés ont démontré une internalisation accrue par les cellules cancéreuses [169]. Les évaluations *in vivo* des DLPS folatés sont programmées dans un futur très proche. De plus, le ciblage plus spécifique des tumeurs grâce à la fonctionnalisation des DLPS avec des fragments ScFv d'anticorps est développé dans le cadre d'un nouveau projet en collaboration avec l'équipe du professeur Dimier-Poisson. La stratégie d'attachement de la doxorubicine par l'intermédiaire d'un complexe avec le fer peut être transposée à d'autres molécules connues pour former des chélates avec le fer, comme la curcumine [170]. Enfin, le couplage de la chimiothérapie vectorisée avec la thérapie hyperthermique peut être envisagée. Le potentiel des DLPS n'a pas fini d'être exploré.

Bibliographie

[1] V.P. Torchilin, Drug targeting, Eur J Pharm Sci. 11 Suppl 2 (2000) S81–91.

[2] J. Klostergaard, C.E. Seeney, Magnetic nanovectors for drug delivery, Maturitas. 73 (2012) 33–44.

[3] Z. Gao, L. Zhang, Y. Sun, Nanotechnology applied to overcome tumor drug resistance, Journal of Controlled Release. 162 (2012) 45–55.

[4] C.-M.J. Hu, L. Zhang, Nanoparticle-based combination therapy toward overcoming drug resistance in cancer, Biochemical Pharmacology. 83 (2012) 1104–1111.

[5] A. Shapira, Y.D. Livney, H.J. Broxterman, Y.G. Assaraf, Nanomedicine for targeted cancer therapy: Towards the overcoming of drug resistance, Drug Resist Update. 14 (2011) 150–163.

[6] L.M. Kaminskas, V.M. McLeod, B.D. Kelly, G. Sberna, B.J. Boyd, M. Williamson, et al., A comparison of changes to doxorubicin pharmacokinetics, antitumor activity, and toxicity mediated by PEGylated dendrimer and PEGylated liposome drug delivery systems, Nanomedicine: Nanotechnology, Biology and Medicine. 8 (2012) 103–111.

[7] G.D. Bothun, A. Lelis, Y. Chen, K. Scully, L.E. Anderson, M.A. Stoner, Multicomponent folate-targeted magnetoliposomes: design, characterization, and cellular uptake, Nanomedicine: NBM. 7 (2011) 797–805.

[8] A. Etzerodt, M.B. Maniecki, J.H. Graversen, H.J. Møller, V.P. Torchilin, S.K. Moestrup, Efficient intracellular drug-targeting of macrophages using stealth liposomes directed to the hemoglobin scavenger receptor CD163, Journal of Controlled Release. 160 (2012) 72–80.

[9] J. Qi, P. Yao, F. He, C. Yu, C. Huang, Nanoparticles with dextran/chitosan shell and BSA/chitosan core—Doxorubicin loading and delivery, International Journal of Pharmaceutics. 393 (2010) 177–185.

[10] X.-Y. Ying, D. Cui, L. Yu, Y.-Z. Du, Solid lipid nanoparticles modified with chitosan oligosaccharides for the controlled release of doxorubicin, Carbohyd Polym. 84 (2011) 1357–1364.

[11] S. Bae, K. Ma, T.H. Kim, E.S. Lee, K.T. Oh, E.-S. Park, et al., Doxorubicin-loaded human serum albumin nanoparticles surface-modified with TNF-related apoptosis-inducing ligand and transferrin for targeting multiple tumor types, Biomaterials. 33 (2012) 1536–1546.

[12] A.O. Elzoghby, W.M. Samy, N.A. Elgindy, Albumin-based nanoparticles as potential controlled release drug delivery systems, Journal of Controlled Release. 157 (2012) 168–182.

[13] G. Fanali, A. di Masi, V. Trezza, M. Marino, M. Fasano, P. Ascenzi, Human serum albumin: From bench to bedside, Mol Aspects Med. 33 (2012) 209–290.

[14] S.K. Agrawal, N. Sanabria-DeLong, J.M. Coburn, G.N. Tew, S.R. Bhatia, Novel drug release profiles from micellar solutions of PLA–PEO–PLA triblock copolymers, J Control Release. 112 (2006) 64–71.

[15] A. Brownlie, I.. Uchegbu, A.. Schätzlein, PEI-based vesicle-polymer hybrid gene delivery system with improved biocompatibility, Int J Pharm. 274 (2004) 41–52.

[16] F. Danhier, E. Ansorena, J. Azeitao, R. Coco, A. Le Breton, V. Préat, PLGA-based nanoparticles: An overview of biomedical applications, Journal of Controlled Release. (n.d.).

[17] T.K. Dash, V.B. Konkimalla, Poly-ϵ-caprolactone based formulations for drug delivery and tissue engineering: A review, Journal of Controlled Release. 158 (2012) 15–33.

[18] R. Gref, M. Lück, P. Quellec, M. Marchand, E. Dellacherie, S. Harnisch, et al., "Stealth" corona-core nanoparticles surface modified by polyethylene glycol (PEG): influences of the corona (PEG chain length and surface density) and of the core composition on phagocytic uptake and plasma protein adsorption, Colloid Surface B. 18 (2000) 301–313.
[19] Z.W. Huang, V. Laurent, G. Chetouani, J.Y. Ljubimova, E. Holler, T. Benvegnu, et al., New functional degradable and bio-compatible nanoparticles based on poly(malic acid) derivatives for site-specific anti-cancer drug delivery, International Journal of Pharmaceutics. 423 (2012) 84–92.
[20] C. Zhang, N. Awasthi, M.A. Schwarz, S. Hinz, R.E. Schwarz, Superior antitumor activity of nanoparticle albumin-bound Paclitaxel in experimental gastric cancer, PLoS ONE. 8 (2013) e58037.
[21] Y. (Chezy) Barenholz, Doxil® — The first FDA-approved nano-drug: Lessons learned, J Control Release. 160 (2012) 117–134.
[22] T. Safra, F. Muggia, S. Jeffers, D.D. Tsao-Wei, S. Groshen, O. Lyass, et al., Pegylated liposomal doxorubicin (doxil): reduced clinical cardiotoxicity in patients reaching or exceeding cumulative doses of 500 mg/m2, Ann. Oncol. 11 (2000) 1029–1033.
[23] C. Sanson, O. Diou, J. Thévenot, E. Ibarboure, A. Soum, A. Brûlet, et al., Doxorubicin Loaded Magnetic Polymersomes: Theranostic Nanocarriers for MR Imaging and Magneto-Chemotherapy, ACS Nano. 5 (2011) 1122–1140.
[24] C. Sanson, C. Schatz, J.-F. Le Meins, A. Soum, J. Thévenot, E. Garanger, et al., A simple method to achieve high doxorubicin loading in biodegradable polymersomes, J Control Release. 147 (2010) 428–435.
[25] H. Oliveira, E. Pérez-Andrés, J. Thevenot, O. Sandre, E. Berra, S. Lecommandoux, Magnetic field triggered drug release from polymersomes for cancer therapeutics, Journal of Controlled Release. (n.d.).
[26] D. Kim, Z.G. Gao, E.S. Lee, Y.H. Bae, In vivo evaluation of doxorubicin-loaded polymeric micelles targeting folate receptors and early endosomal pH in drug-resistant ovarian cancer, Mol. Pharm. 6 (2009) 1353–1362.
[27] D. Kim, E.S. Lee, K.T. Oh, Z.G. Gao, Y.H. Bae, Doxorubicin-loaded polymeric micelle overcomes multidrug resistance of cancer by double-targeting folate receptor and early endosomal pH, Small. 4 (2008) 2043–2050.
[28] J.O. Kim, A.V. Kabanov, T.K. Bronich, Polymer micelles with cross-linked polyanion core for delivery of a cationic drug doxorubicin, J Control Release. 138 (2009) 197–204.
[29] Y.-Z. Zhao, C.-Z. Sun, C.-T. Lu, D.-D. Dai, H.-F. Lv, Y. Wu, et al., Characterization and anti-tumor activity of chemical conjugation of doxorubicin in polymeric micelles (DOX-P) in vitro, Cancer Letters. 311 (2011) 187–194.
[30] K.W. Kang, M.-K. Chun, O. Kim, R.K. Subedi, S.-G. Ahn, J.-H. Yoon, et al., Doxorubicin-loaded solid lipid nanoparticles to overcome multidrug resistance in cancer therapy, Nanomedicine: NBM. 6 (2010) 210–213.
[31] Y.-C. Kuo, C.-T. Liang, Catanionic solid lipid nanoparticles carrying doxorubicin for inhibiting the growth of U87MG cells, Colloid Surface B. 85 (2011) 131–137.
[32] H.-J. Cho, I.-S. Yoon, H.Y. Yoon, H. Koo, Y.-J. Jin, S.-H. Ko, et al., Polyethylene glycol-conjugated hyaluronic acid-ceramide self-assembled nanoparticles for targeted delivery of doxorubicin, Biomaterials. 33 (2012) 1190–1200.
[33] S. Dietrich, S. Schulze, M. Hietschold, H. Lang, Au nanoparticles stabilised by PEGylated low generation PAMAM dendrimers: Design, characterisation and properties, J Colloid Interf Sci. 359 (2011) 454–460.

[34] S. Dietrich, S. Chandra, C. Georgi, S. Thomas, D. Makarov, S. Schulze, et al., Design, characterization and magnetic properties of Fe3O4-nanoparticle arrays coated with PEGylated-dendrimers, Mater Chem Phys. 132 (2012) 292–299.
[35] L.M. Kaminskas, B.D. Kelly, V.M. McLeod, G. Sberna, D.J. Owen, B.J. Boyd, et al., Characterisation and tumour targeting of PEGylated polylysine dendrimers bearing doxorubicin via a pH labile linker, Journal of Controlled Release. 152 (2011) 241–248.
[36] S.-D. Li, L. Huang, Stealth nanoparticles: High density but sheddable PEG is a key for tumor targeting, Journal of Controlled Release. 145 (2010) 178–181.
[37] E. Fleige, M.A. Quadir, R. Haag, Stimuli-responsive polymeric nanocarriers for the controlled transport of active compounds: Concepts and applications, Advanced Drug Delivery Reviews. (n.d.).
[38] S.A. Krovi, D. Smith, S.T. Nguyen, "Clickable" polymer nanoparticles: a modular scaffold for surface functionalization, Chem. Commun. (Camb.). 46 (2010) 5277–5279.
[39] W.B. Liechty, N.A. Peppas, Expert opinion: Responsive polymer nanoparticles in cancer therapy, European Journal of Pharmaceutics and Biopharmaceutics. 80 (2012) 241–246.
[40] E. Markovsky, H. Baabur-Cohen, A. Eldar-Boock, L. Omer, G. Tiram, S. Ferber, et al., Administration, distribution, metabolism and elimination of polymer therapeutics, Journal of Controlled Release. (n.d.).
[41] D.E. Owens III, N.A. Peppas, Opsonization, biodistribution, and pharmacokinetics of polymeric nanoparticles, International Journal of Pharmaceutics. 307 (2006) 93–102.
[42] S. Prakash, M. Malhotra, W. Shao, C. Tomaro-Duchesneau, S. Abbasi, Polymeric nanohybrids and functionalized carbon nanotubes as drug delivery carriers for cancer therapy, Advanced Drug Delivery Reviews. 63 (2011) 1340–1351.
[43] S. Vrignaud, J.-P. Benoit, P. Saulnier, Strategies for the nanoencapsulation of hydrophilic molecules in polymer-based nanoparticles, Biomaterials. 32 (2011) 8593–8604.
[44] A.M. Chen, M. Zhang, D. Wei, D. Stueber, O. Taratula, T. Minko, et al., Co-delivery of doxorubicin and Bcl-2 siRNA by mesoporous silica nanoparticles enhances the efficacy of chemotherapy in multidrug-resistant cancer cells, Small. 5 (2009) 2673–2677.
[45] W. Di, X. Ren, H. Zhao, N. Shirahata, Y. Sakka, W. Qin, Single-phased luminescent mesoporous nanoparticles for simultaneous cell imaging and anticancer drug delivery, Biomaterials. 32 (2011) 7226–7233.
[46] H. Tang, J. Guo, Y. Sun, B. Chang, Q. Ren, W. Yang, Facile synthesis of pH sensitive polymer-coated mesoporous silica nanoparticles and their application in drug delivery, International Journal of Pharmaceutics. 421 (2011) 388–396.
[47] Y. Zhu, Y. Fang, L. Borchardt, S. Kaskel, PEGylated hollow mesoporous silica nanoparticles as potential drug delivery vehicles, Microporous and Mesoporous Materials. 141 (2011) 199–206.
[48] J.-M. Li, Y.-Y. Wang, M.-X. Zhao, C.-P. Tan, Y.-Q. Li, X.-Y. Le, et al., Multifunctional QD-based co-delivery of siRNA and doxorubicin to HeLa cells for reversal of multidrug resistance and real-time tracking, Biomaterials. 33 (2012) 2780–2790.
[49] E. Muro, T. Pons, N. Lequeux, A. Fragola, N. Sanson, Z. Lenkei, et al., Small and stable sulfobetaine zwitterionic quantum dots for functional live-cell imaging, J. Am. Chem. Soc. 132 (2010) 4556–4557.
[50] Y. Chen, H. Chen, S. Zhang, F. Chen, S. Sun, Q. He, et al., Structure-property relationships in manganese oxide - mesoporous silica nanoparticles used for T1-weighted MRI and simultaneous anti-cancer drug delivery, Biomaterials. 33 (2012) 2388–2398.

[51] A.K. Gupta, M. Gupta, Synthesis and surface engineering of iron oxide nanoparticles for biomedical applications, Biomaterials. 26 (2005) 3995–4021.
[52] A.S. Lübbe, C. Alexiou, C. Bergemann, Clinical Applications of Magnetic Drug Targeting, J Surg Res. 95 (2001) 200–206.
[53] T. Neuberger, B. Schöpf, H. Hofmann, M. Hofmann, B. von Rechenberg, Superparamagnetic nanoparticles for biomedical applications: Possibilities and limitations of a new drug delivery system, J Magn Magn Mater. 293 (2005) 483–496.
[54] O. Veiseh, J.W. Gunn, M. Zhang, Design and fabrication of magnetic nanoparticles for targeted drug delivery and imaging, Adv. Drug Deliv. Rev. 62 (2010) 284–304.
[55] F.K. Alanazi, A.A. Radwan, I.A. Alsarra, Biopharmaceutical applications of nanogold, Saudi Pharmaceutical Journal. 18 (2010) 179–193.
[56] A.M. Alkilany, L.B. Thompson, S.P. Boulos, P.N. Sisco, C.J. Murphy, Gold nanorods: Their potential for photothermal therapeutics and drug delivery, tempered by the complexity of their biological interactions, Advanced Drug Delivery Reviews. 64 (2012) 190–199.
[57] B. Book Newell, Y. Wang, J. Irudayaraj, Multifunctional gold nanorod theragnostics probed by multi-photon imaging, Eur J Med Chem. 48 (2012) 330–337.
[58] B. Duncan, C. Kim, V.M. Rotello, Gold nanoparticle platforms as drug and biomacromolecule delivery systems, J Control Release. 148 (2010) 122–127.
[59] P. Ghosh, G. Han, M. De, C.K. Kim, V.M. Rotello, Gold nanoparticles in delivery applications, Advanced Drug Delivery Reviews. 60 (2008) 1307–1315.
[60] J.E. Ziello, Y. Huang, I.S. Jovin, Cellular endocytosis and gene delivery, Mol. Med. 16 (2010) 222–229.
[61] O. Harush-Frenkel, Y. Altschuler, S. Benita, Nanoparticle-cell interactions: drug delivery implications, Crit Rev Ther Drug Carrier Syst. 25 (2008) 485–544.
[62] H. Hillaireau, P. Couvreur, Nanocarriers' entry into the cell: relevance to drug delivery, Cell. Mol. Life Sci. 66 (2009) 2873–2896.
[63] K. Kawano, E. Onose, Y. Hattori, Y. Maitani, Higher liposomal membrane fluidity enhances the in vitro antitumor activity of folate-targeted liposomal mitoxantrone, Mol. Pharm. 6 (2009) 98–104.
[64] Y. Octavia, C.G. Tocchetti, K.L. Gabrielson, S. Janssens, H.J. Crijns, A.L. Moens, Doxorubicin-induced cardiomyopathy: From molecular mechanisms to therapeutic strategies, J Mol Cell Cardiol. 52 (2012) 1213–1225.
[65] F. Danhier, O. Feron, V. Préat, To exploit the tumor microenvironment: Passive and active tumor targeting of nanocarriers for anti-cancer drug delivery, Journal of Controlled Release. 148 (2010) 135–146.
[66] S. Dufort, L. Sancey, J.-L. Coll, Physico-chemical parameters that govern nanoparticles fate also dictate rules for their molecular evolution, Adv. Drug Deliv. Rev. 64 (2012) 179–189.
[67] H. Maeda, J. Wu, T. Sawa, Y. Matsumura, K. Hori, Tumor vascular permeability and the EPR effect in macromolecular therapeutics: a review, J Control Release. 65 (2000) 271–284.
[68] I. Altintas, R.J. Kok, R.M. Schiffelers, Targeting epidermal growth factor receptor in tumors: From conventional monoclonal antibodies via heavy chain-only antibodies to nanobodies, Eur J Pharm Sci. 45 (2012) 399–407.
[69] I.K. Kwon, S.C. Lee, B. Han, K. Park, Analysis on the current status of targeted drug delivery to tumors, Journal of Controlled Release. (n.d.).
[70] P. Ruenraroengsak, J.M. Cook, A.T. Florence, Nanosystem drug targeting: Facing up to complex realities, J Control Release. 141 (2010) 265–276.

[71] Y. Lu, P.S. Low, Folate-mediated delivery of macromolecular anticancer therapeutic agents, Adv. Drug Deliv. Rev. (2012).
[72] K.J. Widder, A.E. Senyel, G.D. Scarpelli, Magnetic microspheres: a model system of site specific drug delivery in vivo, Proc. Soc. Exp. Biol. Med. 158 (1978) 141–146.
[73] R. Ganguly, A.P. Gaind, S. Sen, I.K. Puri, Analyzing ferrofluid transport for magnetic drug targeting, J Magn Magn Mater. 289 (2005) 331–334.
[74] T. Islam, L. Josephson, Current state and future applications of active targeting in malignancies using superparamagnetic iron oxide nanoparticles, Cancer Biomark. 5 (2009) 99–107.
[75] J.E. Rosen, L. Chan, D.-B. Shieh, F.X. Gu, Iron oxide nanoparticles for targeted cancer imaging and diagnostics, Nanomedicine: Nanotechnology, Biology and Medicine. 8 (2012) 275–290.
[76] M.S. Shim, Y.J. Kwon, Stimuli-responsive polymers and nanomaterials for gene delivery and imaging applications, Advanced Drug Delivery Reviews. 64 (2012) 1046–1059.
[77] R. Lehner, X. Wang, M. Wolf, P. Hunziker, Designing switchable nanosystems for medical application, Journal of Controlled Release. 161 (2012) 307–316.
[78] A.L. Kiss, Caveolae and the regulation of endocytosis, Adv. Exp. Med. Biol. 729 (2012) 14–28.
[79] C. Fang, F.M. Kievit, O. Veiseh, Z.R. Stephen, T. Wang, D. Lee, et al., Fabrication of magnetic nanoparticles with controllable drug loading and release through a simple assembly approach, J Control Release. 162 (2012) 233–241.
[80] F.M. Kievit, F.Y. Wang, C. Fang, H. Mok, K. Wang, J.R. Silber, et al., Doxorubicin loaded iron oxide nanoparticles overcome multidrug resistance in cancer in vitro, J Control Release. 152 (2011) 76–83.
[81] M. Prabaharan, J.J. Grailer, S. Pilla, D.A. Steeber, S. Gong, Amphiphilic multi-arm-block copolymer conjugated with doxorubicin via pH-sensitive hydrazone bond for tumor-targeted drug delivery, Biomaterials. 30 (2009) 5757–5766.
[82] M. Prabaharan, J.J. Grailer, S. Pilla, D.A. Steeber, S. Gong, Gold nanoparticles with a monolayer of doxorubicin-conjugated amphiphilic block copolymer for tumor-targeted drug delivery, Biomaterials. 30 (2009) 6065–6075.
[83] M.-Y. Hua, H.-W. Yang, H.-L. Liu, R.-Y. Tsai, S.-T. Pang, K.-L. Chuang, et al., Superhigh-magnetization nanocarrier as a doxorubicin delivery platform for magnetic targeting therapy, Biomaterials. 32 (2011) 8999–9010.
[84] J. You, C. Xiong, M. Zhong, M. Melancon, S. Gupta, A.M. Nick, et al., Effective photothermal chemotherapy using doxorubicin-loaded gold nanospheres that target EphB4 receptors in tumors, Cancer Res. (2012).
[85] J. You, G. Zhang, C. Li, Exceptionally High Payload of Doxorubicin in Hollow Gold Nanospheres for Near-Infrared Light-Triggered Drug Release, ACS Nano. 4 (2012) 1033–1041.
[86] J. You, R. Zhang, G. Zhang, M. Zhong, Y. Liu, C.S. Van Pelt, et al., Photothermal-chemotherapy with doxorubicin-loaded hollow gold nanospheres: A platform for near-infrared light-trigged drug release, J Control Release. 158 (2012) 319–328.
[87] S.M. Janib, A.S. Moses, J.A. MacKay, Imaging and drug delivery using theranostic nanoparticles, Advanced Drug Delivery Reviews. 62 (2010) 1052–1063.
[88] M.P. Melancon, R.J. Stafford, C. Li, Challenges to effective cancer nanotheranostics, Journal of Controlled Release. (2012).
[89] S. Mura, P. Couvreur, Nanotheranostics for personalized medicine, Adv. Drug Deliv. Rev. (2012).

[90] A. Astolfo, E. Schültke, R.H. Menk, R.D. Kirch, B.H.J. Juurlink, C. Hall, et al., In vivo visualization of gold-loaded cells in mice using x-ray computed tomography, Nanomedicine: NBM. (2012).
[91] X. Huang, M.A. El-Sayed, Gold nanoparticles: Optical properties and implementations in cancer diagnosis and photothermal therapy, J Adv Res. 1 (2010) 13–28.
[92] D. Kim, S. Jon, Gold nanoparticles in image-guided cancer therapy, Inorg Chim Acta. (2012).
[93] P.-W. Lee, S.-H. Hsu, J.-J. Wang, J.-S. Tsai, K.-J. Lin, S.-P. Wey, et al., The characteristics, biodistribution, magnetic resonance imaging and biodegradability of superparamagnetic core-shell nanoparticles, Biomaterials. 31 (2010) 1316–1324.
[94] S.F. Medeiros, A.M. Santos, H. Fessi, A. Elaissari, Stimuli-responsive magnetic particles for biomedical applications, Int J Pharm. 403 (2011) 139–161.
[95] Y.-X.J. Wang, Superparamagnetic iron oxide based MRI contrast agents: Current status of clinical application, Quant Imaging Med Surg. 1 (2011) 35–40.
[96] J. Xie, K. Chen, J. Huang, S. Lee, J. Wang, J. Gao, et al., PET/NIRF/MRI triple functional iron oxide nanoparticles, Biomaterials. 31 (2010) 3016–3022.
[97] M. Adeli, M. Kalantari, M. Parsamanesh, E. Sadeghi, M. Mahmoudi, Synthesis of new hybrid nanomaterials: promising systems for cancer therapy, Nanomedicine: Nanotechnology, Biology and Medicine. 7 (2011) 806–817.
[98] K. Susumu, E. Oh, J.B. Delehanty, J.B. Blanco-Canosa, B.J. Johnson, V. Jain, et al., Multifunctional compact zwitterionic ligands for preparing robust biocompatible semiconductor quantum dots and gold nanoparticles, J. Am. Chem. Soc. 133 (2011) 9480–9496.
[99] P. Pericleous, M. Gazouli, A. Lyberopoulou, S. Rizos, N. Nikiteas, E.P. Efstathopoulos, Quantum dots hold promise for early cancer imaging and detection, Int. J. Cancer. 131 (2012) 519–528.
[100] C.E. Probst, P. Zrazhevskiy, V. Bagalkot, X. Gao, Quantum dots as a platform for nanoparticle drug delivery vehicle design, Adv. Drug Deliv. Rev. (2012).
[101] M. Ryvolova, J. Chomoucka, J. Drbohlavova, P. Kopel, P. Babula, D. Hynek, et al., Modern micro and nanoparticle-based imaging techniques, Sensors (Basel). 12 (2012) 14792–14820.
[102] N.G. Khlebtsov, L.A. Dykman, Optical properties and biomedical applications of plasmonic nanoparticles, Journal of Quantitative Spectroscopy and Radiative Transfer. 111 (2010) 1–35.
[103] P. Mohan, N. Rapoport, Doxorubicin as a molecular nanotheranostic agent: effect of doxorubicin encapsulation in micelles or nanoemulsions on the ultrasound-mediated intracellular delivery and nuclear trafficking, Mol. Pharm. 7 (2010) 1959–1973.
[104] R. Kizek, V. Adam, J. Hrabeta, T. Eckschlager, S. Smutny, J.V. Burda, et al., Anthracyclines and ellipticines as DNA-damaging anticancer drugs: Recent advances, Pharmacol Therapeut. 133 (2012) 26–39.
[105] X. Li, D.J. Hirsh, D. Cabral-Lilly, A. Zirkel, S.M. Gruner, A.S. Janoff, et al., Doxorubicin physical state in solution and inside liposomes loaded via a pH gradient, BBA-Biomembranes. 1415 (1998) 23–40.
[106] G. Molyneux, M. Andrews, W. Sones, M. York, A. Barnett, E. Quirk, et al., Haemotoxicity of busulphan, doxorubicin, cisplatin and cyclophosphamide in the female BALB/c mouse using a brief regimen of drug administration, Cell Biol Toxicol. 27 (2010) 13–40.
[107] M. Heijn, S. Roberge, R.K. Jain, Cellular membrane permeability of anthracyclines does not correlate with their delivery in a tissue-isolated tumor, Cancer Res. 59 (1999) 4458–4463.

[108] M. Sui, W. Liu, Y. Shen, Nuclear drug delivery for cancer chemotherapy, J Control Release. 155 (2011) 227–236.
[109] R.E. Serda, B. Godin, E. Blanco, C. Chiappini, M. Ferrari, Multi-stage delivery nanoparticle systems for therapeutic applications, BBA-Gen Subjects. 1810 (2011) 317–329.
[110] E. Cukierman, D.R. Khan, The benefits and challenges associated with the use of drug delivery systems in cancer therapy, Biochem Pharmacol. 80 (2010) 762–770.
[111] DOXIL_PI_Booklet.pdf, (n.d.).
[112] M.R. Mirza, B. Lund, J.C. Lindegaard, N. Keldsen, A. Mellemgaard, R. dePont Christensen, et al., A phase II study of combination chemotherapy in early relapsed epithelial ovarian cancer using gemcitabine and pegylated liposomal doxorubicin, Gynecologic Oncology. 119 (2010) 26–31.
[113] P. Power, G. Stuart, A. Oza, D. Provencher, J.R. Bentley, W.H. Miller Jr, et al., Efficacy of pegylated liposomal doxorubicin (PLD) plus carboplatin in ovarian cancer patients who recur within six to twelve months: A phase II study, Gynecologic Oncology. 114 (2009) 410–414.
[114] F. Joly, E. Sevin, A. Lortholary, F. Priou, J.F. Paitel, M. Fabbro, et al., Association of pegylated liposomal doxorubicin and ifosfamide in early recurrent ovarian cancer patients: A Multicenter Phase II Trial, Gynecologic Oncology. 116 (2010) 312–316.
[115] J. Jiang, S. Yang, J. Wang, L. Yang, Z. Xu, T. Yang, et al., Sequential treatment of drug-resistant tumors with RGD-modified liposomes containing siRNA or doxorubicin, European Journal of Pharmaceutics and Biopharmaceutics. 76 (2010) 170–178.
[116] R.E. Eliaz, S. Nir, C. Marty, F.C. Szoka Jr, Determination and modeling of kinetics of cancer cell killing by doxorubicin and doxorubicin encapsulated in targeted liposomes, Cancer Res. 64 (2004) 711–718.
[117] A. Lowery, H. Onishko, D.E. Hallahan, Z. Han, Tumor-targeted delivery of liposome-encapsulated doxorubicin by use of a peptide that selectively binds to irradiated tumors, Journal of Controlled Release. 150 (2011) 117–124.
[118] S. Wagner, F. Rothweiler, M.G. Anhorn, D. Sauer, I. Riemann, E.C. Weiss, et al., Enhanced drug targeting by attachment of an anti αv integrin antibody to doxorubicin loaded human serum albumin nanoparticles, Biomaterials. 31 (2010) 2388–2398.
[119] M. Mahmoudi, A. Simchi, A.S. Milani, P. Stroeve, Cell toxicity of superparamagnetic iron oxide nanoparticles, Journal of Colloid and Interface Science. 336 (2009) 510–518.
[120] L. Douziech-Eyrolles, H. Marchais, K. Hervé, E. Munnier, M. Soucé, C. Linassier, et al., Nanovectors for anticancer agents based on superparamagnetic iron oxide nanoparticles, Int J Nanomedicine. 2 (2007) 541–550.
[121] R.A. Frimpong, J.Z. Hilt, Magnetic nanoparticles in biomedicine: synthesis, functionalization and applications, Nanomedicine (Lond). 5 (2010) 1401–1414.
[122] S.K. Sahu, S. Maiti, A. Pramanik, S.K. Ghosh, P. Pramanik, Controlling the thickness of polymeric shell on magnetic nanoparticles loaded with doxorubicin for targeted delivery and MRI contrast agent, Carbohyd Polym. 87 (2012) 2593–2604.
[123] K. Hervé, L. Douziech-Eyrolles, E. Munnier, S. Cohen-Jonathan, M. Soucé, H. Marchais, et al., The development of stable aqueous suspensions of PEGylated SPIONs for biomedical applications, Nanotechnology. 19 (2008) 465608.
[124] E. Allard-Vannier, S. Cohen-Jonathan, J. Gautier, K. Hervé-Aubert, E. Munnier, M. Soucé, et al., Pegylated magnetic nanocarriers for doxorubicin delivery: A quantitative determination of stealthiness in vitro and in vivo, Eur J Pharm Biopharm. 81 (2012) 498–505.

[125] E. Munnier, S. Cohen-Jonathan, C. Linassier, L. Douziech-Eyrolles, H. Marchais, M. Soucé, et al., Novel method of doxorubicin–SPION reversible association for magnetic drug targeting, Int J Pharm. 363 (2008) 170–176.
[126] C. Greulich, J. Diendorf, T. Simon, G. Eggeler, M. Epple, M. Köller, Uptake and intracellular distribution of silver nanoparticles in human mesenchymal stem cells, Acta Biomaterialia. 7 (2011) 347–354.
[127] M. Fiallo, A. Laigle, A. Garnier-Suillerot, C. Amirand, J.P. Ballini, L. Chinsky, et al., Interactions of iron-anthracycline complexes with living cells: a microspectrofluorometric study, Biochim. Biophys. Acta. 1177 (1993) 236–244.
[128] M.M. Fiallo, A. Garnier-Suillerot, B. Matzanke, H. Kozlowski, How Fe3+ binds anthracycline antitumour compounds. The myth and the reality of a chemical sphinx, J. Inorg. Biochem. 75 (1999) 105–115.
[129] E.L. Kostoryz, D.M. Yourtee, Oxidative mutagenesis of doxorubicin-Fe(III) complex, Mutat. Res. 490 (2001) 131–139.
[130] S. Singh, A. Kumar, A. Karakoti, S. Seal, W.T. Self, Unveiling the mechanism of uptake and sub-cellular distribution of cerium oxide nanoparticles, Mol Biosyst. 6 (2010) 1813–1820.
[131] X.-M. Lin, Y. Cui, Y.-H. Xu, B. Ren, Z.-Q. Tian, Surface-enhanced Raman spectroscopy: substrate-related issues, Anal Bioanal Chem. 394 (2009) 1729–1745.
[132] I. Chourpa, F.H. Lei, P. Dubois, M. Manfait, G.D. Sockalingum, Intracellular applications of analytical SERS spectroscopy and multispectral imaging, Chem Soc Rev. 37 (2008) 993–1000.
[133] K.A. Willets, R.P. Van Duyne, Localized surface plasmon resonance spectroscopy and sensing, Annu Rev Phys Chem. 58 (2007) 267–297.
[134] J. Gautier, E. Munnier, A. Paillard, K. Hervé, L. Douziech-Eyrolles, M. Soucé, et al., A pharmaceutical study of doxorubicin-loaded PEGylated nanoparticles for magnetic drug targeting, Int J Pharm. 423 (2012) 16–25.
[135] J.T. Jenkins, D.L. Halaney, K.V. Sokolov, L.L. Ma, H.J. Shipley, S. Mahajan, et al., Excretion and toxicity of gold–iron nanoparticles, Nanomedicine: Nanotechnology, Biology and Medicine. 9 (2013) 356–365.
[136] M. Beija, R. Salvayre, N. Lauth-de Viguerie, J.-D. Marty, Colloidal systems for drug delivery: from design to therapy, Trends in Biotechnology. 30 (2012) 485–496.
[137] J. Nam, N. Won, J. Bang, H. Jin, J. Park, S. Jung, et al., Surface engineering of inorganic nanoparticles for imaging and therapy, Advanced Drug Delivery Reviews. (n.d.).
[138] A.M.G.C. Dias, A. Hussain, A.S. Marcos, A.C.A. Roque, A biotechnological perspective on the application of iron oxide magnetic colloids modified with polysaccharides, Biotechnol. Adv. 29 (2011) 142–155.
[139] M. Rahimi, A. Wadajkar, K. Subramanian, M. Yousef, W. Cui, J.-T. Hsieh, et al., In vitro evaluation of novel polymer-coated magnetic nanoparticles for controlled drug delivery, Nanomedicine: Nanotechnology, Biology and Medicine. 6 (2010) 672–680.
[140] M. Mahmoudi, A. Simchi, M. Imani, P. Stroeve, A. Sohrabi, Templated growth of superparamagnetic iron oxide nanoparticles by temperature programming in the presence of poly(vinyl alcohol), Thin Solid Films. 518 (2010) 4281–4289.
[141] A. Gabizon, H. Shmeeda, T. Grenader, Pharmacological basis of pegylated liposomal doxorubicin: Impact on cancer therapy, Eur J Pharm Sci. 45 (2012) 388–398.
[142] E. Munnier, S. Cohen-Jonathan, K. Hervé, C. Linassier, M. Soucé, P. Dubois, et al., Doxorubicin delivered to MCF-7 cancer cells by superparamagnetic iron oxide nanoparticles: effects on subcellular distribution and cytotoxicity, J Nanopart Res. 13 (2011) 959–971.

[143] M. Wang, M. Thanou, Targeting nanoparticles to cancer, Pharmacol Res. 62 (2010) 90–99.
[144] S. Stolnik, L. Illum, S.S. Davis, Long circulating microparticulate drug carriers, Advanced Drug Delivery Reviews. 16 (1995) 195–214.
[145] G. Storm, S.O. Belliot, T. Daemen, D.D. Lasic, Surface modification of nanoparticles to oppose uptake by the mononuclear phagocyte system, Advanced Drug Delivery Reviews. 17 (1995) 31–48.
[146] A. Aqil, S. Vasseur, E. Duguet, C. Passirani, J.P. Benoît, A. Roch, et al., PEO coated magnetic nanoparticles for biomedical application, European Polymer Journal. 44 (2008) 3191–3199.
[147] K. Shiraishi, M. Hamano, H. Ma, K. Kawano, Y. Maitani, T. Aoshi, et al., Hydrophobic blocks of PEG-conjugates play a significant role in the accelerated blood clearance (ABC) phenomenon, Journal of Controlled Release. 165 (2013) 183–190.
[148] T. Tagami, Y. Uehara, N. Moriyoshi, T. Ishida, H. Kiwada, Anti-PEG IgM production by siRNA encapsulated in a PEGylated lipid nanocarrier is dependent on the sequence of the siRNA, Journal of Controlled Release. 151 (2011) 149–154.
[149] X. Yang, H. Hong, J.J. Grailer, I.J. Rowland, A. Javadi, S.A. Hurley, et al., cRGD-functionalized, DOX-conjugated, and 64Cu-labeled superparamagnetic iron oxide nanoparticles for targeted anticancer drug delivery and PET/MR imaging, Biomaterials. 32 (2011) 4151–4160.
[150] C. Alexiou, A. Schmidt, R. Klein, P. Hulin, C. Bergemann, W. Arnold, Magnetic drug targeting: biodistribution and dependency on magnetic field strength, Journal of Magnetism and Magnetic Materials. 252 (2002) 363–366.
[151] A.S. Lübbe, C. Bergemann, H. Riess, F. Schriever, P. Reichardt, K. Possinger, et al., Clinical experiences with magnetic drug targeting: a phase I study with 4'-epidoxorubicin in 14 patients with advanced solid tumors, Cancer Res. 56 (1996) 4686–4693.
[152] A.S. Lübbe, C. Bergemann, J. Brock, D.G. McClure, Physiological aspects in magnetic drug-targeting, J Magn Magn Mater. 194 (1999) 149–155.
[153] D. Hellstern, K. Schulze, B. Schöpf, A. Petri-Fink, B. Steitz, S. Kamau, et al., Systemic distribution and elimination of plain and with Cy3.5 functionalized poly(vinyl alcohol) coated superparamagnetic maghemite nanoparticles after intraarticular injection in sheep in vivo, J Nanosci Nanotechnol. 6 (2006) 3261–3268.
[154] S. Dandamudi, V. Patil, W. Fowle, B.-A. Khaw, R.B. Campbell, External magnet improves antitumor effect of vinblastine and the suppression of metastasis, Cancer Sci. 100 (2009) 1537–1543.
[155] L. Deng, X. Ke, Z. He, D. Yang, H. Gong, Y. Zhang, et al., A MSLN-targeted multifunctional nanoimmunoliposome for MRI and targeting therapy in pancreatic cancer, Int J Nanomedicine. 7 (2012) 5053–5065.
[156] J.-P. Fortin-Ripoche, M.S. Martina, F. Gazeau, C. Ménager, C. Wilhelm, J.-C. Bacri, et al., Magnetic targeting of magnetoliposomes to solid tumors with MR imaging monitoring in mice: feasibility, Radiology. 239 (2006) 415–424.
[157] J.H. Maeng, D.-H. Lee, K.H. Jung, Y.-H. Bae, I.-S. Park, S. Jeong, et al., Multifunctional doxorubicin loaded superparamagnetic iron oxide nanoparticles for chemotherapy and magnetic resonance imaging in liver cancer, Biomaterials. 31 (2010) 4995–5006.
[158] C. Liao, Q. Sun, B. Liang, J. Shen, X. Shuai, Targeting EGFR-overexpressing tumor cells using Cetuximab-immunomicelles loaded with doxorubicin and superparamagnetic iron oxide, Eur J Radiol. 80 (2011) 699–705.

[159] A.J. Wagstaff, S.D. Brown, M.R. Holden, G.E. Craig, J.A. Plumb, R.E. Brown, et al., Cisplatin drug delivery using gold-coated iron oxide nanoparticles for enhanced tumour targeting with external magnetic fields, Inorganica Chimica Acta. (n.d.).
[160] L. Zhu, D. Wang, X. Wei, X. Zhu, J. Li, C. Tu, et al., Multifunctional pH-sensitive superparamagnetic iron-oxide nanocomposites for targeted drug delivery and MR imaging, J Control Release. (2013).
[161] G. Lamanna, M. Kueny-Stotz, H. Mamlouk-Chaouachi, C. Ghobril, B. Basly, A. Bertin, et al., Dendronized iron oxide nanoparticles for multimodal imaging, Biomaterials. 32 (2011) 8562–8573.
[162] M. Geppert, M.C. Hohnholt, S. Nürnberger, R. Dringen, Ferritin up-regulation and transient ROS production in cultured brain astrocytes after loading with iron oxide nanoparticles, Acta Biomaterialia. 8 (2012) 3832–3839.
[163] O. Lunov, T. Syrovets, C. Röcker, K. Tron, G. Ulrich Nienhaus, V. Rasche, et al., Lysosomal degradation of the carboxydextran shell of coated superparamagnetic iron oxide nanoparticles and the fate of professional phagocytes, Biomaterials. 31 (2010) 9015–9022.
[164] M. Levy, N. Luciani, D. Alloyeau, D. Elgrabli, V. Deveaux, C. Pechoux, et al., Long term in vivo biotransformation of iron oxide nanoparticles, Biomaterials. 32 (2011) 3988–3999.
[165] Y. Liu, K. Yang, L. Cheng, J. Zhu, X. Ma, H. Xu, et al., PEGylated FePt@Fe2O3 core-shell magnetic nanoparticles: Potential theranostic applications and in vivo toxicity studies, Nanomedicine: Nanotechnology, Biology and Medicine. (2013).
[166] O. Lunov, T. Syrovets, B. Büchele, X. Jiang, C. Röcker, K. Tron, et al., The effect of carboxydextran-coated superparamagnetic iron oxide nanoparticles on c-Jun N-terminal kinase-mediated apoptosis in human macrophages, Biomaterials. 31 (2010) 5063–5071.
[167] J.L. Winer, C.Y. Liu, M.L.J. Apuzzo, The Use of Nanoparticles as Contrast Media in Neuroimaging: A Statement on Toxicity, World Neurosurgery. 78 (2012) 709–711.
[168] M.L. Etheridge, S.A. Campbell, A.G. Erdman, C.L. Haynes, S.M. Wolf, J. McCullough, The big picture on nanomedicine: the state of investigational and approved nanomedicine products, Nanomedicine: Nanotechnology, Biology and Medicine. 9 (2013) 1–14.
[169] K. Kaaki, K. Hervé-Aubert, M. Chiper, A. Shkilnyy, M. Soucé, R. Benoit, et al., Magnetic nanocarriers of doxorubicin coated with poly(ethylene glycol) and folic acid: relation between coating structure, surface properties, colloidal stability, and cancer cell targeting, Langmuir. 28 (2012) 1496–1505.
[170] M.I. Khalil, A.M. Al-Zahem, M.H. Al-Qunaibit, Synthesis, Characterization, Mössbauer Parameters, and Antitumor Activity of Fe(III) Curcumin Complex, Bioinorg Chem Appl. 2013 (2013) 982423.

Annexes

Annexe 1 PEGylated magnetic nanocarriers for doxorubicin : a quantitative determination of stealthiness *in vitro* and *in vivo*

Publication 6, publiée dans European Journal of Pharmaceutics and Biopharmaceutics, 2012

European Journal of Pharmaceutics and Biopharmaceutics 81 (2012) 498–505

Contents lists available at SciVerse ScienceDirect

European Journal of Pharmaceutics and Biopharmaceutics

journal homepage: www.elsevier.com/locate/ejpb

Research paper

Pegylated magnetic nanocarriers for doxorubicin delivery: A quantitative determination of stealthiness *in vitro* and *in vivo*

E. Allard-Vannier [a,*], S. Cohen-Jonathan [a], J. Gautier [a], K. Hervé-Aubert [a], E. Munnier [a], M. Soucé [a], P. Legras [b], C. Passirani [c], I. Chourpa [a]

[a] *EA 6295 Nanomédicaments et Nanosondes, Université François-Rabelais de Tours, Tours, France*
[b] *Animalerie Hospitalo-universitaire, UFR médecine, Angers, France*
[c] *Inserm UMR_S 1066, Université d'Angers, Angers, France*

ARTICLE INFO

Article history:
Received 24 October 2011
Accepted in revised form 2 April 2012
Available online 10 April 2012

Keywords:
Superparamagnetic iron oxide nanoparticles (SPIONs)
Doxorubicin
Polyethylene glycol
Macrophage uptake
Blood half-life
Atomic absorption spectrometry

ABSTRACT

The aim of this work was to elucidate the impact of polyethylene glycol (PEG) polymeric coating on the *in vitro* and *in vivo* stealthiness of magnetic nanocarriers loaded or not with the anticancer drug doxorubicin. The comparison was made between aqueous suspensions of superparamagnetic iron oxide nanoparticles (SPIONs) stabilized by either citrate ions (C-SPIONs) or PEG_{5000} (P-SPIONs), the latter being loaded or not with doxorubicin via the formation of a DOX-Fe^{2+} complex (DLP-SPIONs).

After determination of their relevant physico-chemical properties (size and surface charge), nanoparticle (NP) stealthiness was studied *in vitro* (ability to activate the complement system and uptake by monocytes and macrophage-like cells) and *in vivo* in mice (blood half-life; $t_{1/2}$, and biodistribution in main clearance organs). These aspects were quantitatively assessed by atomic absorption spectrometry (AAS). Complement activation dramatically decreased for sterically stabilized P-SPIONs and DLP-SPIONs in comparison with C-SPIONs stabilized by charge repulsion. Monocyte and macrophage uptake was also largely reduced for pegylated formulations loaded or not with doxorubicin. The $t_{1/2}$ in blood for P-SPIONs was estimated to be 76 ± 6 min, with an elimination mainly directed to liver and spleen. Thanks to their small size (<80 nm) and a neutral hydrophilic polymer-extended surface, P-SPIONs exhibit prolonged blood circulation and thus potentially an increased level in tumor delivery suitable for magnetic drug targeting applications.

1. Introduction

Magnetic drug targeting (MDT) is a treatment concept consisting in the intravenous delivery of cytostatic drugs associated to magnetic nanoparticles (NPs) that can be retained in a tumor by an external magnetic field [1,2]. The main advantage of this and other targeting techniques is to increase the local drug dose in tumors [3]. Consequently, the dose effect is enhanced while the side effects often observed in chemotherapy treatment are decreased [4]. The success of MDT generally depends on tumor location, on magnetic properties [5], but also on the NP composition and structure [6]. Superparamagnetic iron oxide nanoparticles (SPIONs) are nanocrystals of sizes below 10 nm [7] that are investigated as a promising platform for MDT and magnetic resonance imaging (MRI) [8,9]. Superparamagnetic behavior means that the NPs are highly magnetized in a magnetic field but lose their magnetization when the field is switched off. This behavior is important for injectable formulations, because it reduces the risk of thrombosis from magnetically aggregated NPs. Moreover, to avoid non-magnetic aggregation, the SPIONs need to be coated with organic materials like polymers as described below and the coating will determine the physical parameters of final NPs like apparent hydrodynamic diameter (D_H) and surface charge (ζ-potential) [10].

These physical parameters will also dictate the interaction of the NPs in live organisms. Indeed, when NPs enter the bloodstream, they immediately encounter a complex environment of plasma proteins and immune cells. According to their nature, NPs in the blood can be more or less rapidly captured by the mononuclear phagocyte system (MPS) and directed to the clearance organs like liver and spleen. Nanoparticle uptake by cells of the MPS is known to be facilitated by the electrostatic adsorption of opsonins (plasma proteins) on the particle surface [11]. Among the opsonins, the C3 protein of the complement system plays a major role in the foreign NP recognition by the immune system [12]. The complement activation test (hemolytic CH50 test) in Normal Human Serum (NHS) has been reported as a relevant *in vitro* evaluation of the NP opsonization [13]. On the other hand, the NP stealthiness

* Corresponding author. EA 6295 Nanomédicaments et Nanosondes, Laboratoire de pharmacie galénique, Faculté de pharmacie, 31 avenue Monge, 37200 Tours, France. Tel.: +33 247 367200; fax: +33 247 367198.
E-mail address: emilie.allard@univ-tours.fr (E. Allard-Vannier).

0939-6411/$ - see front matter © 2012 Elsevier B.V. All rights reserved.
http://dx.doi.org/10.1016/j.ejpb.2012.04.002

can be assessed *in vitro* via their uptake by phagocytic cells, like monocytes and macrophages [11,14].

For a nanocarrier to be "stealth," that is, almost undetectable by the immune system, the opsonin adsorption on the NP surface needs to be as low as possible [14]. This is expected for NPs with charge-free surface, that is, with a ζ-potential close to zero [15]. Stealth NPs can circulate in the blood for a longer time and, in addition to magnetic retention, can be accumulated in tumors by so-called "enhanced permeability retention," the EPR effect [16]. For this, the NP D_H needs to be below a critical size which is defined in the literature as between 10 and 100 nm, depending on tumors and studies [17,18]. Polyethylene glycol (PEG) is known to be an attractive material to reduce opsonization because it is uncharged, hydrophilic, and non-immunogenic [19,20]. The presence of PEG chains on the NP surface has been shown to increase both their colloidal stability in aqueous suspension [21] and the blood half-life *in vivo* [22]. The stealthiness of PEG-coated NPs depends on their D_H and on parameters such as polymer molecular weight, its density, and its conformation on the particle surface [23,24]. As such, understanding nanoparticle hematocompatibility is an important step during the initial biological evaluation of each newly designed injectable nanomaterial.

The present study is devoted to PEG-coated SPIONs (P-SPIONs) developed as a platform for magnetic carrier of doxorubicin (DOX) anticancer drug. DOX is a suitable model for targeted delivery since it is known for its low therapeutic index and for important side effects like cardiotoxicity and hematotoxicity [25]. The effect of the polymeric coating on the *in vitro* hematocompatibility was assessed by comparison of PEG-coated and non-coated, citrated SPIONs (C-SPIONs). Negative charges of citrate ions adsorbed on C-SPION surface protect them from aggregation in aqueous media at pH 7.4. In addition, DOX was adsorbed on the iron oxide surface of P-SPIONs in a reversible, pH dependent manner [26,27] to obtain DOX-loaded pegylated SPIONs (DLP-SPIONs). The P-SPIONs and DLP-SPIONs were compared *in vitro* to investigate the possible effect of the drug loading on the NP stealthiness. Our *in vitro* study includes the complement consumption test and the quantification of the NP uptake by two immune blood cell lines (human monocytes and macrophage-like cells). After intravenous administration of P-SPIONs on Swiss mice, we examined their blood clearance and biodistribution in main organs such as liver, spleen, and kidney. The originality of this approach is that the iron oxide-based NPs were monitored *in vitro* and *in vivo* by the quantitative determination of iron by atomic absorption spectrophotometry (AAS). Compared to other techniques, AAS offers the main advantage to be label-free [28] and therefore more objective. Furthermore, AAS is known to be both user-friendly and sensitive enough to quantify the iron content in cells [29] and in wet-ashed organs [30].

2. Materials and methods

2.1. Synthesis and characterization of SPION-based nanoparticles

2.1.1. Materials

Doxorubicin hydrochloride was purchased from TEVA Pharmaceuticals Ltd. (Puteaux, France). Ferric nitrate nonahydrate ($Fe(NO_3)_3{\cdot}9H_2O$), anhydrous ferric chloride ($FeCl_3$), ferrous chloride ($FeCl_2$, $4H_2O$), and citric acid were purchased from Fisher Bioblock Scientific (Illkirch, France). 3-Aminopropyltrimethoxy silane (APS), N-(3-dimethylaminopropyl)-N′-ethylcarbodiimide hydrochloride (EDC), and methoxypoly(ethylene glycol) 5000 propionic acid N-succinimidyl ester (activated PEG, aPEG) were purchased from Sigma Aldrich (Saint-Quentin-Fallavier, France). Sodium acetate, tris-(hydroxymethyl)-aminomethane (Tris), mannitol, and iron standard solution 1 g/L (CertiPUR®) were provided by Merck (Fontenay-sous-Bois, France), and ferrous ammonium sulfate ($(NH_4)_2Fe(SO_4)_2{\cdot}6H_2O$) by Carlo Erba (Val de Reuil, France). All solutions were prepared with deionized water.

2.1.2. Preparation of citrated SPIONs (C-SPIONs)

SPIONs were synthesized as aqueous ferrofluids by a coprecipitation of ferric and ferrous chlorides in alkaline medium followed by a surface oxidation by ferric nitrate, as described elsewhere [31]. To increase the stability of the ferrofluid suspension at neutral pH, the SPION surface was treated with citrate ions [27]. The particles were then purified from excess citrate by 48 h dialysis (Float-a-Lyzer dialysis membrane, MWCO 8000, Interchim, France) against a 150-fold acceptor volume of distilled water.

2.1.3. Preparation of pegylated SPIONs (P-SPIONs)

Pegylated SPIONs were synthesized according to a previously published protocol [21]. Briefly, ferrofluids were first silanized by bonding of trialkoxyaminosilane molecules on the surface hydroxyl groups of the SPIONs. Then, pegylated ferrofluids were prepared by mixing silanized ferrofluids with methoxypoly(ethylene glycol) 5000 propionic acid *N*-succinimidyl ester (aPEG) in water under stirring for 24 h. The dispersion was then purified by dialysis against water.

2.1.4. Preparation of doxorubicin-loaded pegylated SPIONs (DLP-SPIONs)

Pegylated SPIONs were loaded with doxorubicin (DOX) via a DOX-Fe^{2+} complex, as described elsewhere [26]. The DOX-Fe^{2+} complex was pre-formed by mixing a solution of DOX hydrochloride and a Fe^{2+} solution (1.5 M excess of Fe^{2+} over DOX) in TRIS buffer pH 7.6. Pegylated SPIONs were incubated with the DOX-Fe^{2+} complex in the dark, and harvested by centrifugation at 19,000*g* for 1 h at 4 °C. For determining drug loading, DLP-SPIONs were sonicated for 1 h in an acetate buffer pH 4 to allow total DOX release, as the DOX-Fe^{2+} complex dissociates at low pH [26]. The sample was then centrifuged at 19,000*g* for 1 h at 15 °C. DOX concentration was determined in the supernatant by UV–visible spectrophotometry (Anthélie Advanced Spectrophotometer, Secomam, France), using its molar absorptivity determined at 500 nm. Each determination was performed at least in triplicate. A SPION suspension of 1 g/L of iron corresponds to a DOX concentration of $3.6 \pm 0.3 \times 10^5$ mol/L.

2.1.5. Determination of hydrodynamic diameter and zeta potential

The mean hydrodynamic diameter (D_H) of NPs was determined by DLS (Dynamic Light Scattering) with an Autosizer 2c (Malvern Instruments, Orsay, France). The ferrofluids were also characterized with respect to the zeta potential of NPs by using a Malvern NanoZ (Malvern Instruments, Malvern, UK). For the measurements, ferrofluids were diluted in deionized water (1:100 V:V). Each measurement was done in triplicate.

2.1.6. Determination of iron content by AAS

Total iron content was quantified by flame atomic absorption spectrometry (AAS) (air/C_2H_2 flame mode with deuterium background correction, slit width: 0.2 nm, wavelength: 248.3 nm, sensitivity 0.12 ppm, A: 1%) (iCE 3000 Series AA Spectrometer, ThermoFisher Scientific, France). One milliliter of SPION suspension was digested by 5 mL of hydrochloric acid 6 N. The digestion was maintained up to one night and the resultant solution was diluted with hydrochloric acid 0.1 M before measurement. A calibration curve was obtained with a standard solution (CertiPUR®, Merck Darmstadt Germany). Each determination was performed in triplicate.

2.1.7. pH and osmolarity measurements

KOH 0.1 M was added to adjust the pH of the SPION suspension to a physiological value. Mannitol was dissolved in the formulations in order to obtain iso-osmotic media. pH measurements and osmolarity of SPION suspensions were performed on a Cyberscan 500 pHmeter (Fisher Bioblock, Illkirch, France) and an automatic micro osmometer Roebling type 13DR (Berlin, Germany), respectively. Osmotic measurements were expressed in mOsm/kg.

2.2. In vitro stealthiness evaluation

2.2.1. Complement activation (CH50 test)

Complement consumption was assessed in normal human serum (NHS) (provided by the Etablissement Francais du Sang, CHU, Angers, France) by measuring the residual hemolytic capacity of the complement system after contact with NPs. The final dilution of NHS in the mixture was 1:4 (V/V) in 1 mL of reactive media. The technique consisted in determining the amount of serum able to lyze 50% of a fixed number of sensitized sheep erythrocytes with rabbit antisheep erythrocyte antibodies (CH50), according to the procedure described elsewhere [13]. Complement activation was first expressed as a function of the surface area in order to compare NPs with different D_H. Nanoparticle surface areas were estimated using the equation: $S = 3\ m/r\rho$, where S is the surface area [cm^2], m *is* the weight [μg] in 1 mL of suspension, r *is* the average radius [cm] determined by DLS, and ρ *is* the volumetric mass [$\mu g/cm^3$] of the nanoparticles estimated at 10^6 $\mu g/cm^3$. Complement activation was also expressed as a function of iron concentration to estimate the impact of the polymer coating for a similar quantity of SPIONs. The *in vivo* iron concentration of interest is in the range of 300–450 μg/mL of NHS, taking into account the blood-serum volume per mouse (2–2.4 mL blood or 0.8–1.2 mL serum) and the ferrofluid quantity that will be injected per mouse (200 μL at 1.8 μg/μL or 360 μg of iron per mouse).

2.2.2. THP-1 cell culture and differentiation

THP-1 cells (human monocytic leukemia cells) were grown in a humidifier-incubator (5% CO_2/37 °C) in suspension in a RPMI 1640 medium supplemented with FCS (10%), HEPES 1 M 10 mM, sodium pyruvate 100× 1 mM, antibiotics 100× 1×, and β-mercaptoethanol (0.05 mM) (Fisher Bioblock Scientific, Illkirch, France). For the differentiation in macrophage phenotype, cells were cultured in the same medium supplemented with 100 n phorbol 12-myristate 13-acetate (PMA, Sigma Saint-Quentin Fallavier, France) for 48 h [32]. The medium was then removed and the cells were subsequently incubated in a fresh medium (without PMA) for an additional 24 h prior to uptake studies.

2.2.3. Qualitative study of SPION uptake by cells

Four-chamber glass slides (Lab-teks™, Nunc, Fisher Bioblock Scientific, Illkirch, France) were seeded with 5×10^4 cells per chamber. After 24 h, the medium was discarded and replaced by fresh medium with PMA. 48 h later, cells were treated by C-SPIONs or P-SPIONs freshly prepared in culture medium (iron content of 500 μg/mL). The slides were placed at 37 °C for 60 min. Then, the suspension was discarded and the cells were washed 6 times with PBS to eliminate excess SPIONs. Cells were fixed with paraformaldhedyde (PFA) 4%. The slides were immerged in a freshly prepared 5% ferrocyanide/5% HCl solution. After 20 min incubation, the slides were washed 5 times with PBS. Cells were then observed with an optical microscope (objective ×40) with an integrated camera.

2.2.4. Quantitative study of SPION uptake by cells

Quantitative uptake of SPIONs was evaluated on monocytes (THP-1 cells) and on macrophage-like cells (PMA-stimulated THP-1 cells). THP-1 were seeded in 6-well clusters, at 1.5×10^6 cells per well (0.16×10^6 cells/cm^2). After 24 h, the cell suspension was transferred to an Eppendorf tube and centrifuged at 1000*g* for 5 min. The supernatant was discarded and replaced by 2 mL of C-SPION, P-SPION, or DLP-SPION suspension in culture medium (iron content of 200 μg/mL). Clusters were then placed in a 37 °C, 5% CO_2 incubator during 60 and 240 min. After this delay, cells were centrifuged for 5 min at 1000*g* and washed with HBSS (with Ca^{2+}–Mg^{2+}) for three times. The cell pellets of each well were then digested by 1 mL of HCl 37% during 24 h. After this delay, a 1:4 dilution in HCl 0.1 M was made and the iron content of the cell lysate was analyzed by AAS. For the macrophage-like cell uptake, THP-1 were seeded in 6-well clusters, at 1.5×10^6 cells per well (0.16×10^6 cells/cm^2) with a PMA media (C = 100 nM). After 48 h, the medium was discarded and replaced by 2 mL of fresh media without PMA. 24 h later, the medium was replaced by SPION suspension in culture medium (iron content of 200 μg/mL). Flasks were placed in a 37 °C, 5% CO_2 incubator during 60 and 240 min. After this delay, cells were washed with HBSS (with Ca^{2+}–Mg^{2+}) for 5 times. The cells were then digested by HCl 37% during 24 h. After a 1:4 dilution in HCl 0.1 M, the iron content of the cell lysate was analyzed by AAS.

2.3. In vivo stealthiness evaluation

2.3.1. Animals

Swiss female mice weighing 30–35 g were obtained from Janvier Laboratories (Le Genest St Ile, France). All experiments were performed on 6–8-week-old female Swiss mice. The animals were manipulated under isoflurane/oxygen anesthesia. Animal care was provided in strict accordance with French Ministry of Agriculture regulations.

2.3.2. Blood half-life of C-, P-, and DLP-SPIONs

A 200 μL of C-SPIONs, P-SPIONs, or DLP-SPIONs was injected in the tail vein of Swiss mice ([Fe] = 1.8 g/L = 10–12 mg/kg body wt). After 5, 15, and 30 min, a blood sample (0.3–0.4 mL) was collected by retro-orbital or sub-mandibulary puncture. For P-SPIONs and C-SPIONs, blood punctions were continued from 60 to 360 min. Samples were prepared by wet ashing with a mixture of HNO_3–H_2O_2 (2:1, V:V) for 12 h in a sand bath with electric hot plate and evaporation to dryness. Finally, 3 mL of 37% HCl solution was added to each sample and the iron content was determined by AAS after a 1:10 dilution in HCl 0.1 M.

2.3.3. Biodistribution of P-SPIONs in clearance organs

After blood sampling, Swiss mice injected with P-SPIONs were euthanized at the end of 60, 120, 240, and 360 min. The clearance organs (liver, spleen, and kidney) were excised and washed quickly with cold water to remove surface blood. Organs were digested in a beaker with a mixture of HNO_3–H_2O_2 (2:1, V:V) for 12 h in a sand bath with electric hot plate, and then evaporated to dryness. Then, samples were placed in a muffle furnace at 450 °C during 12H. Finally, the dry residues were dissolved in a 37% HCl solution (10 mL: liver and 3 mL: spleen-kidney) and kept for 24 h. Iron solutions were filtered using a PES syringe filter and diluted in HCl 0.1 M (1:10, V:V). Iron content was then determined by AAS.

2.4. Statistical analysis

The Student's t-test was used for the statistical analysis of the experimental data. Values of $p < 0.05$ were considered to indicate statistical significance.

3. Results

3.1. Surface and colloidal properties of SPION-based nanoparticles

The physico-chemical properties of the three types of NPs evaluated in this study (C-SPIONs, P-SPIONs, and DLP-SPIONs) are summarized in Table 1. As previously described, C-SPIONs were obtained by mixing original SPIONs with citrate ions, thus conferring an electrostatic repulsion to the particles allowing their stability in suspension [27]. C-SPIONs have a final hydrodynamic diameter of about 50 nm and a negative zeta potential of −26 ± 3 mV at pH 7.4 (Table 1). Pegylation of SPIONs was made by the formation of an amide bond between the amino group of the silanized ferrofluids and the activated ester group of methoxy-poly(ethylene glycol) 5000 propionic acid N-succinimidyl ester [21]. For P-SPIONs, hydrodynamic diameters were slightly increased and were about 75 nm. When doxorubicin was associated to the SPION surface via the DOX-Fe(II) complex (DLP-SPIONs), no change in hydrodynamic diameter was noted. Indeed, the mean diameter was about 76.5 ± 3.1 nm in the presence of DOX at the SPION surface. At pH = 7.4, zeta potential values of the two pegylated formulations (P-SPIONs and DLP-SPIONs) were not significantly different and close to zero. All batches of SPIONs were monodisperse as indicated by a polydispersity index below 0.2. For stealthiness studies, the colloid suspensions were adjusted to be iso-osmotic via addition of mannitol, and the osmolarity values measured varied between 304 and 312 ± 0.6 mOsm/kg.

3.2. In vitro stealthiness

3.2.1. Complement consumption

NPs intended for systemic administration were tested for their tendency to activate the complement system. Complement consumption was evaluated as the lytic capacity of the serum toward 50% of antibody-sensitized sheep erythrocytes (CH50 units) after exposure to C-SPIONs, P-SPIONs, and DLP-SPIONs (Fig. 1). C-SPIONs, which are negatively charged, were strong activators with 100% of CH50 unit consumption for a surface area as small as 250 cm^2/mL (Fig. 1A). For the same surface area of 250 cm^2/mL, the consumption of CH50 by P-SPIONs led to only 3% of consumption. For both P- and DLP-SPIONs, the maximum activation levels remained below 40% of CH50 even with a surface area of ca. 1750 cm^2/mL. The CH50 profiles obtained for P- and DLP-SPIONs were very similar, both when they were expressed as a function of NP surface (Fig. 1A) or as a function of iron concentration per mL of NHS (Fig. 1B). However, the difference between pegylated and citrated SPIONs is significant over a concentration range between 300 and 450 μg/mL of iron, which roughly corresponds to *in vivo* doses.

3.2.2. NP uptake by monocytes and macrophage-like cells

Stealthiness of C-SPIONs, P-SPIONs, and DLP-SPIONs was also evaluated by measuring their uptake in monocytes and macrophage-like cells (derived from THP-1 cell lines) as representative of the MPS. Fig. 2 shows their intracellular iron content (in mg/L) determined by atomic absorption spectrometry (AAS) after the incubation of the three formulations. For the monocytic cells, on going from 60 to 240 min of incubation, the amount of intracellular iron increased from 1.59 ± 0.27 to 2.38 ± 0.20 mg/L in the cells incubated with C-SPIONs while it remained very low in the cells treated by pegylated formulations: 0.16 ± 0.02 to 0.20 ± 0.06 mg/L for P-SPIONs and from 0.08 ± 0.05 to 0.09 ± 0.05 mg/L for DLP-SPIONs. It is obvious that C-SPIONs are much more readily internalized by monocytes than pegylated SPIONs loaded or not with doxorubicin ($p < 0.01$). Moreover, there is no significant difference in iron contents for the cells treated with P- and DLP-SPIONs for the two time tested ($p > 0.05$). For the macrophage-like cells, between 60 and 240 min, the cell iron content increased from 1.78 ± 0.22 to 2.51 ± 0.21 mg/L for C-SPIONs, from 0.32 ± 0.02 to 0.69 ± 0.04 mg/L for P-SPIONs, and from 0.35 ± 0.05 to 0.57 ± 0.14 mg/L for DLP-SPIONs. The iron content found in macrophages after 60 (or 240) min of incubation was more than 5 (or 3–4) fold higher for C-SPIONs versus P-SPIONs or DLP-SPIONs ($p < 0.01$). For all formulations tested, the intracellular iron content was higher in macrophages compared to monocytes. Cytotoxicity at 60 and 240 min was not observed on monocytes and macrophages incubated with doxorubicin-loaded pegylated SPIONs (data not shown). To confirm qualitatively that the iron measured by AAS is associated with cells, the rapid uptake of non-pegylated SPIONs by macrophage-like cells was easily visualized by a Prussian blue staining (Fig. 3).

Table 1
Physico-chemical properties of SPION formulations.

	C-SPIONs	P-SPIONs	DLP-SPIONs
Size (nm) (*Z* average mean)	48.7 ± 6.3	74.7 ± 5.0	76.5 ± 3.1
Polydispersity index	0.196 (±0.022)	0.180 (±0.016)	0.187 (±0.022)
Zeta potential at pH 7.4 (mV)	−26 ± 3	+3 ± 2	−2 ± 4
Osmolarity (mOsm/kg)	312 ± 0.6	304 ± 0.6	308 ± 0.3

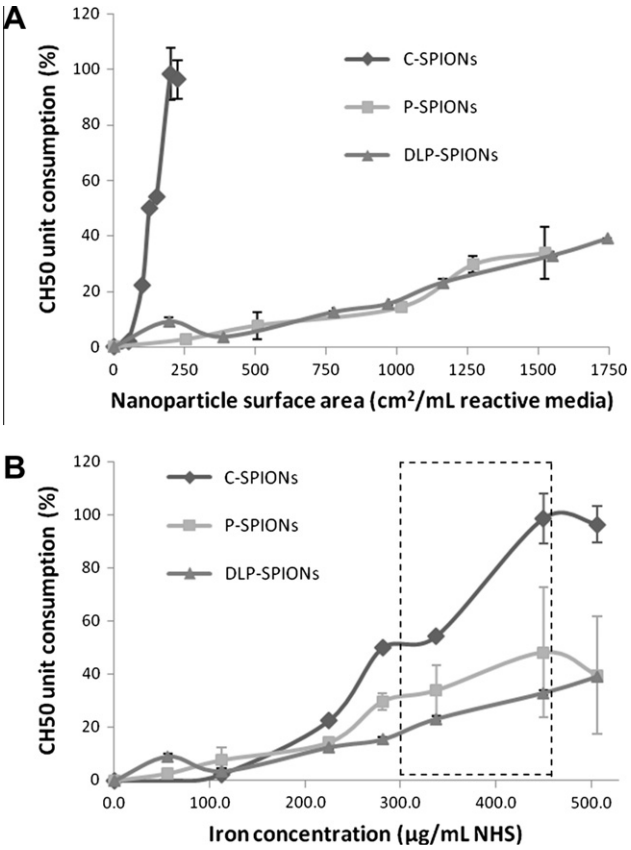

Fig. 1. Complement consumption by citrated SPIONs (C-SPIONs), pegylated SPIONs (P-SPIONs), and doxorubicin-loaded pegylated SPIONs (DLP-SPIONs) according to their nanoparticle surface area (A) in cm^2/mL of reactive media or their iron concentration (B) expressed in μg of iron/mL of normal human serum (NHS).

3.3. In vivo behavior

3.3.1. Blood concentration kinetics

To assess NP blood distribution kinetics in mice, C-, P-, and DLP-SPIONs were injected in the tail vein at iron concentrations of 10–12 mg/kg of animal. This concentration is known to be compatible

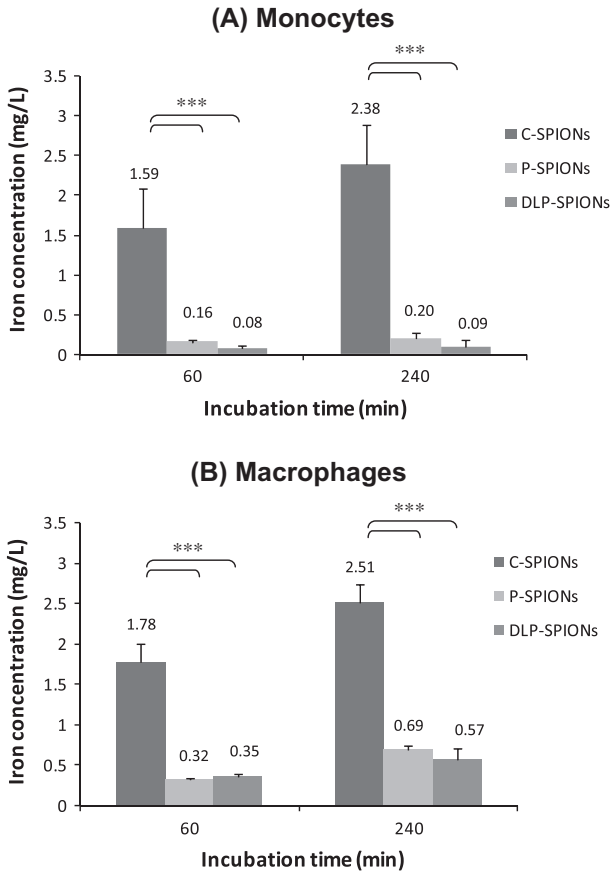

Fig. 2. Iron content of THP-1 cells treated with citrated SPIONs (C-SPIONs), pegylated SPIONs (P-SPIONs), or doxorubicin-loaded pegylated SPIONs (DLP-SPIONs) after 60 and 240 min. A. represents the nanoparticle uptake by the monocyte THP-1 cells and B. represents the nanoparticle uptake by the macrophages (differentiated THP-1) ($p < 0.01^{***}$ Student t-test).

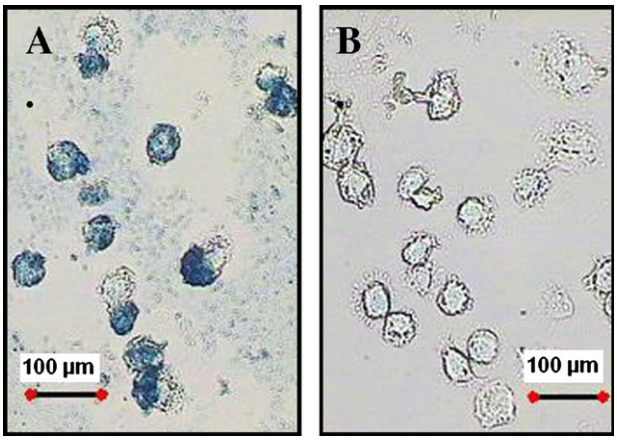

Fig. 3. Microscopic observations of iron in macrophage-like cells after treatment for 60 min with citrated SPIONs (A) and pegylated SPIONs (B). Iron was stained by Prussian blue technique on PMA-treated THP-1 cells and observed with an optical microscope (objective ×40).

with an attraction by a magnetic field [33]. First, no toxic or allergic reaction occurred during and after nanoparticle injection, and reflex status was normal, even for the group injected with DOX. Thereafter, blood samples were collected at 5, 15, and 30 min after injection. The iron concentration in blood at 5 min was considered to be the hundred percent for all injected formulations. Results

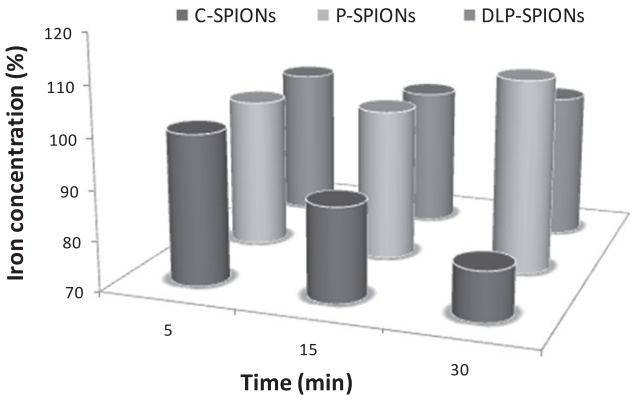

Fig. 4. Elimination kinetics of iron in blood for mice injected with C-SPIONs, P-SPIONs, and DLP-SPIONs. Iron concentration was determined by AAS. Data are expressed as a percentage of initial iron concentration (iron concentration at 5 min = 100%) and are the mean of four injected mice.

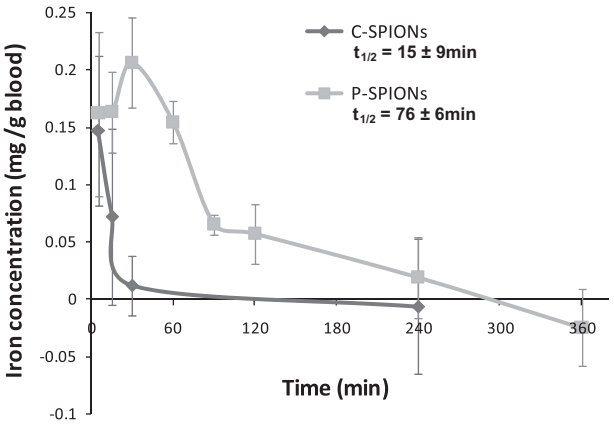

Fig. 5. Pharmacokinetics of citrated and pegylated SPIONS monitored by iron concentration in blood during 360 min. Iron concentration was determined by AAS and was corrected for physiological iron concentration in mice. Data are the mean of four mice ± standard deviation.

were first expressed in total iron concentration, that is, included physiologic iron concentration (Fig. 4). For the group of mice injected with pegylated formulations loaded or not with DOX, the iron concentration in blood remained more or less constant up to 30 min (Fig. 4). On the contrary, for the group treated with C-SPIONs, the iron concentration in the bloodstream dropped to below 88.8% in 15 min and to 79.9% in 30 min. Thus, the C-SPIONs were rapidly removed from the blood. To go further, and with the aim of determining the clearance half-life ($t_{1/2}$) of C- and P-SPIONs in Swiss mice blood, we continued monitoring until 360 min. The contribution of iron was then calculated as the total iron concentration minus physiologic iron concentration of each group of mice (Fig. 5). Results showed that elimination kinetics of C-SPIONs was very quick because the average concentration of iron related to nanoparticles was closed to zero after 30 min. The $t_{1/2}$ for C-SPIONs was very short and estimated to be around 15 ± 9 min. On the contrary, Fig. 5 shows that more than 50% of the P-SPIONs were still circulating in the blood after 60 min to finally totally disappear after 360 min. The $t_{1/2}$ for P-SPIONs was estimated to be 76 ± 6 min. For ethical reasons, we did not perform the long-term kinetics study with DLP-SPIONs.

3.3.2. Biodistribution of P-SPIONs in main clearance organs

Iron concentrations given correspond to the sum of physiological iron and that from NPs (mg of iron per gram of organ tissue).

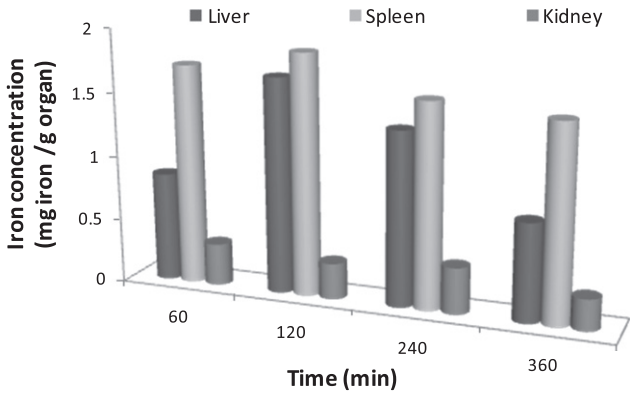

Fig. 6. Variation of iron concentration (in mg iron/g organ tissue) determined by AAS in different organs of elimination, 60, 120, 240, and 360 min after injection of pegylated SPIONs. Data are the concentrations measured for pooled organs of five mice.

Fig. 6 shows the kinetics of iron concentration in the main clearance organs. For the mice injected with P-SPIONs, we clearly observed a significant variation of iron concentration in the liver: it increased from 0.85 to 1.68 mg/g between 60 and 120 min and then decreased steadily. After 360 min, it had returned to approximately its "initial" value after 60 min. The kinetics of iron content in spleen was quite different: it exhibited a slight increase between 60 (1.72 mg/g) and 120 min (1.87 mg/g) and a slight decrease from 120 to 360 min (1.5 mg/g). On the contrary, iron concentration observed in kidneys was quite constant between 60 and 360 min, teetering around 0.3 mg/g (from 0.33, 0.28, 0.36, and 0.24 mg/g).

4. Discussion

The aim of this work was to elucidate the impact of PEG coating (MW = 5000 g/mol) on the *in vitro* and *in vivo* stealthiness of superparamagnetic nanocarriers loaded or not with doxorubicin anticancer drug.

The main physical parameters influencing the stealthiness of NPs are D_H and ζ-potential. For all the NPs studied here, the experimental D_H values were below 80 nm: ~48 nm for C-SPIONs and ~75–76 nm for P- and DLP-SPIONs (Table 1). These D_H values should not be directly compared with the diameters of the iron oxide cores (6–10 nm) observed by electron microscopy (TEM, data not shown). The hydrodynamic diameters of hybrid NPs in aqueous suspension include a solvation layer [34]. In addition, the presence of small aggregates of iron oxide cores could also contribute to the difference between D_H values and TEM diameters [21]. Both partial aggregation and solvation may contribute to the D_H of pegylated NPs [26]. It should be underlined that the aggregation of iron oxide cores was minor for all the NPs described here, as demonstrated both by superparamagnetic behavior [21] and by polydispersity index values below 0.2 characteristic of monodisperse colloids (Table 1). Constant and reproducible D_H values obtained for all the batches confirmed the excellent colloidal stability of our NPs at physiological pH 7.4. At this pH, C-SPIONs displayed a significant negative zeta potential of ca. −26 mV. Therefore, C-SPIONs were stabilized by an electrostatic repulsion of citrate ions. In contrast, the stability of pegylated NPs was of sterical nature, since P- and DLP-SPIONs were neutral and stable in a wide range of pH 3–11 [21,35]. Neutral surface charge and D_H well below 100 nm observed for P-SPIONs and DLP-SPIONs are in accordance with their stealthiness and accumulation in tumors by the EPR effect [11,36].

Knowing these physico-chemical properties, complement consumption by NPs was evaluated. Basically, the amount of serum needed to hemolyze 50% of a fixed number of sensitized sheep erythrocytes was determined after NHS exposure to increasing concentrations of NPs. As expected [14], negatively charged C-SPIONs adsorbed larger amounts of serum proteins and were thus stronger activators of the complement system than their neutral counterparts (Fig. 1A). At all concentrations studied, P- and DLP-SPIONs did not trigger any major response of the complement system, the activation being lower than 40% even for high surface contact (>1500 cm^2/mL). These results confirm that for NP opsonization, the role of the hydrophilic coating is much more important than the role of the particle size. For the same type of nanoobjects, Aqil et al. described a complement activation below 25% for surface areas of 1000 cm^2/mL [37]. Our results are in good agreement with their observations as P- and DLP-SPIONs activated the complement system to less than 20% for the same range of NP surface areas. The presence of DOX did not alter the SPION surface thanks to its localization close to the NP core, far from the surface or buried inside the polymer layer [26,27].

Alternatively, we expressed the CH50 unit consumption (%) for the three nanocarriers as a function of iron concentration expressed in iron mass (μg) per volume of NHS (mL) (Fig. 1B). In this manner, complement activation is explained in terms of the number of NPs, showing the effect of the shielding by the PEG layer. At low iron concentrations (C < 200 μg iron/mL NHS), there is no effect of PEG coating at the SPION surface since the number of NPs is too low compared to the amount of complement proteins. From 250 up to 500 μg/mL, results show that P-SPIONs and DLP-SPIONs are significantly weaker activators than C-SPIONs, which is explained by their near-zero zeta potential. Considering the quantity of iron injected per mouse, we can make an *in vitro/in vivo* correlation, showing that the region of interest may be located between 300 and 450 μg/mL of NHS. In this zone, the pegylation effect is clearly notable and the difference between pegylated and non-pegylated formulations is highly significant (Fig. 1B).

Nanoparticle uptake by the immune cells may occur both in the bloodstream by monocytes, platelets, leukocytes, and dendritic cells and in tissues by resident phagocytes (e.g., Kupffer cells in liver, macrophages and B cells in spleen). Phagocytes are known to favor the uptake of negatively charged compounds as they preferentially endocyte liposomes containing negatively charged lipids or liposomes modified by poly-anions [38]. Blood monocytes are the first trap to fear because they can migrate into pathological sites, thus carrying their load to tissue macrophages. In this context, we first measured the uptake of C-, P-, and DLP-SPIONs by THP-1 cells, which is a human monocytic leukemia cell line. With monocytic THP-1 cells, we clearly see that, whatever the incubation time, C-SPIONs were much more readily taken up compared to P- and DLP-SPIONs (Fig. 2A). This cell line was also converted into mature cells with macrophage functions [32]. The uptake of C-SPIONs by macrophage-like THP-1 cells is higher than that by monocytes and increases with time (Fig. 2B). Phagocytosis capacity is known to be more efficient for macrophagic cells compared to monocytes [32,39]. As expected, the ability of phagocytes to catch coated or uncoated SPIONs is clearly significant (p < 0.01), and largely reduced for pegylated formulations. In the conditions of this study, the presence of doxorubicin within the polymeric layer of P-SPIONs did not change the physical properties and consequently did not increase the uptake by monocytes or macrophage-like cells (p > 0.05).

For *in vivo* monitoring of NPs, we used atomic absorption spectrophotometry (AAS) for the determination of iron content in blood. To the best of our knowledge, there are very few studies that used AAS for the monitoring of magnetic NPs *in vivo* via a determination of iron content in biological samples (blood and organs). Indeed, most of the studies evaluated iron content by measuring the change in the MRI signal intensity [40] or by phenanthroline colorimetric methods [41] which are not as sensitive and specific as

AAS. Atomic absorption spectrometry provides fast and accurate analysis of samples with a sensibility in the range of ppm–ppb. For short times of 15 and 30 min, the total iron concentration in blood was unchanged which means that no clearance was noted for P-SPIONs and DLP-SPIONs confirming the conclusions made *in vitro* (Fig. 4). On the contrary, C-SPIONs were quickly taken up by phagocytes and suffered from clearance by the reticuloendothelial system (RES), mainly due to their negative potential value [10]. The blood half-life *in vivo* ($t_{1/2}$) was estimated to be 15 ± 9 min for C-SPIONs and 76 ± 6 min for P-SPIONs (Fig. 5). The half-life of pegylated formulation is considerably longer than those observed with different kinds of magnetic nanostructures. Jain et al. described a very rapid blood clearance of 6.4 min for commercial Feridex IV (SPION coated by dextrans) and a blood clearance of 31.2 min for SPIONs coated by oleic acid and covered by an amphiphilic coating of Pluronic F-127 (PEO-PPO-PEO) [40]. SPIO-alginate described by Ma et al. was rapidly eliminated from serum with a half-life of 16.2 min (0.27 h) [41]. The latter results could mainly be explained by larger particle sizes (D_H = 150–250 nm) and high negative zeta potentials. For MDT applications, a magnetic drug delivery system has to remain in the bloodstream for time durations compatible with the application of a magnetic field. According to clinical experiences of Lübbe et al., a realistic duration of the treatment assisted with magnetic field should be comprised between 60 and 120 min [4]. From this point of view, our drug delivery system appears interesting for MDT applications.

As regards their clearance, P-SPIONs seem to be eliminated by a hepatic and splenic process. Considering the physiological status of iron on Swiss mice [42], iron concentration in liver increased from 0 to 120 min and decreased slowly after that time (Fig. 6). We particularly observed a clear increase of iron concentration in liver between 60 and 120 min. This observation was linked with the result of a blood half-life corresponding to 50% elimination of iron at the end of 76 ± 6 min. This proves that elimination from blood is far from instantaneous which is in accordance with stealth properties. The increase of iron concentration in the spleen was smaller, and no net variation was observed in kidneys. With their hydrodynamic diameter of 75 nm, P-SPIONs are too large to be rapidly removed through renal clearance because the cutoff size for renal excretion is approximatively 5.5 nm according to recent research using quantum dots [43]. Moreover, they are too small to be quickly sequestered by phagocytic cells of the liver and spleen [44]. This result can inform us on the hypothetic main elimination route of P-SPIONs after their intravenous administration. However, it cannot be excluded that the iron component of SPION can be filtrated and reabsorbed within the proximal tubules of the kidney to finally be incorporated into the physiological iron metabolism, than degradated in the RES [45].

To sum up, if a nanoparticle formulation is well understood (i.e., if its physico-chemical properties, hematocompatibility, *in vivo* interaction, etc., are well known), it is easier to predict potential interferences and thus avoid them. These preliminary but essential results give us information about the possibility to use P-SPIONs and DLP-SPIONs for magnetic drug targeting. In our future studies, we plan to evaluate how a magnetic field applied to a tumor can help to concentrate P-SPIONs within it, and can reduce NPs accumulation in liver.

5. Conclusion

In this study, we demonstrate that SPIONs coating with PEG_{5000} improves their stealthiness. Indeed, P-SPIONs exhibited adequate physico-chemical properties allowing them to remain stable in suspension and stealth *in vitro* and *in vivo*. The blood half-life of P-SPIONs of ca. 76 min enables us to be optimistic about the use of those NPs for magnetic drug targeting. The presence of the anticancer drug within the polymeric coating of P-SPIONs did not alter their stealthiness *in vitro*. The elimination kinetics of DLP-SPIONs in blood mice *in vivo* seems to be unchanged compared to P-SPIONs until 30 min but needs to be completed on tumor-bearing mice.

Acknowledgments

This study was supported in part by grants from the Ligue Nationale contre le Cancer (Conseil Scientifique Inter-Régionnal Grand-Ouest (CSIRGO), Délégation Indre-et-Loire, France, and from the Region Centre, France (NANOMAG Project). The authors would like to thank Nolwenn Lautram (INSERM UMR_S 1066) and Yaël Victor (EA 6295) for their technical assistance.

References

[1] C. Alexiou, W. Arnold, R.J. Klein, F.G. Parak, P. Hulin, C. Bergemann, W. Erhardt, S. Wagenpfeil, A.S. Lubbe, Locoregional cancer treatment with magnetic drug targeting, Cancer Res. 60 (2000) 6641–6648.
[2] J. Dobson, Cancer therapy: a twist on tumour targeting, Nat. Mater. 9 (2010) 95–96.
[3] A.S. Lubbe, C. Bergemann, W. Huhnt, T. Fricke, H. Riess, J.W. Brock, D. Huhn, Preclinical experiences with magnetic drug targeting: tolerance and efficacy, Cancer Res. 56 (1996) 4694–4701.
[4] A.S. Lubbe, C. Bergemann, H. Riess, F. Schriever, P. Reichardt, K. Possinger, M. Matthias, B. Dorken, F. Herrmann, R. Gurtler, P. Hohenberger, N. Haas, R. Sohr, B. Sander, A.J. Lemke, D. Ohlendorf, W. Huhnt, D. Huhn, Clinical experiences with magnetic drug targeting: a phase I study with 4′-epidoxorubicin in 14 patients with advanced solid tumors, Cancer Res. 56 (1996) 4686–4693.
[5] C. Alexiou, R.J. Schmid, R. Jurgons, M. Kremer, G. Wanner, C. Bergemann, E. Huenges, T. Nawroth, W. Arnold, F.G. Parak, Targeting cancer cells: magnetic nanoparticles as drug carriers, Eur. Biophys. J. 35 (2006) 446–450.
[6] F.M. Kievit, M. Zhang, Surface engineering of iron oxide nanoparticles for targeted cancer therapy, Acc. Chem. Res. (2011).
[7] E. Duguet, S. Vasseur, S. Mornet, G. Goglio, A. Demourgues, J. Portier, F. Grasset, P. Veverka, E. Pollert, Towards a versatile platform based on magnetic nanoparticles for in vivo applications, Bull. Mater. Sci. 29 (2006) 581–586.
[8] C. Sun, J.S. Lee, M. Zhang, Magnetic nanoparticles in MR imaging and drug delivery, Adv. Drug Deliv. Rev. 60 (2008) 1252–1265.
[9] J. Xie, J. Huang, X. Li, S. Sun, X. Chen, Iron oxide nanoparticle platform for biomedical applications, Curr. Med. Chem. 16 (2009) 1278–1294.
[10] C. Chouly, D. Pouliquen, I. Lucet, J.J. Jeune, P. Jallet, Development of superparamagnetic nanoparticles for MRI: effect of particle size, charge and surface nature on biodistribution, J. Microencapsul. 13 (1996) 245–255.
[11] A. Vonarbourg, C. Passirani, P. Saulnier, J.P. Benoit, Parameters influencing the stealthiness of colloidal drug delivery systems, Biomaterials 27 (2006) 4356–4373.
[12] E. Allemann, P. Gravel, J.C. Leroux, L. Balant, R. Gurny, Kinetics of blood component adsorption on poly(D, L-lactic acid) nanoparticles: evidence of complement C3 component involvement, J. Biomed. Mater. Res. 37 (1997) 229–234.
[13] A. Vonarbourg, C. Passirani, P. Saulnier, P. Simard, J.C. Leroux, J.P. Benoit, Evaluation of pegylated lipid nanocapsules versus complement system activation and macrophage uptake, J. Biomed. Mater. Res. A 78 (2006) 620–628.
[14] M.A. Dobrovolskaia, P. Aggarwal, J.B. Hall, S.E. McNeil, Preclinical studies to understand nanoparticle interaction with the immune system and its potential effects on nanoparticle biodistribution, Mol. Pharm. 5 (2008) 487–495.
[15] S. Laurent, S. Boutry, I. Mahieu, L. Vander Elst, R.N. Muller, Iron oxide based MR contrast agents: from chemistry to cell labeling, Curr. Med. Chem. 16 (2009) 4712–4727.
[16] H. Maeda, J. Wu, T. Sawa, Y. Matsumura, K. Hori, Tumor vascular permeability and the EPR effect in macromolecular therapeutics: a review, J. Control. Release 65 (2000) 271–284.
[17] P.P. Adiseshaiah, J.B. Hall, S.E. McNeil, Nanomaterial standards for efficacy and toxicity assessment, Wiley Interdiscip. Rev. Nanomed. Nanobiotechnol. 2 (2009) 99–112.
[18] P. Couvreur, C. Vauthier, Nanotechnology: intelligent design to treat complex disease, Pharm. Res. 23 (2006) 1417–1450.
[19] X. Shan, Y. Yuan, C. Liu, X. Tao, Y. Sheng, F. Xu, Influence of PEG chain on the complement activation suppression and longevity in vivo prolongation of the PCL biomedical nanoparticles, Biomed. Microdev. 11 (2009) 1187–1194.
[20] A.S. Karakoti, S. Das, S. Thevuthasan, S. Seal, PEGylated inorganic nanoparticles, Angew. Chem. Int. Ed. Engl. 50 (2011) 1980–1994.
[21] K. Herve, L. Douziech-Eyrolles, E. Munnier, S. Cohen-Jonathan, M. Souce, H. Marchais, P. Limelette, F. Warmont, M. Saboungi, P. Dubois, I. Chourpa, The development of stable aqueous suspensions of PEGylated SPIONs for biomedical applications, Nanotechnology 19 (2008) 465608. 465607pp.
[22] D.P. Lankveld, R.G. Rayavarapu, P. Krystek, A.G. Oomen, H.W. Verharen, T.G. van Leeuwen, W.H. De Jong, S. Manohar, Blood clearance and tissue

distribution of PEGylated and non-PEGylated gold nanorods after intravenous administration in rats, Nanomedicine (Lond) 6 (2011) 339–349.
[23] R. Gref, M. Luck, P. Quellec, M. Marchand, E. Dellacherie, S. Harnisch, T. Blunk, R.H. Muller, 'Stealth' corona-core nanoparticles surface modified by polyethylene glycol (PEG): influences of the corona (PEG chain length and surface density) and of the core composition on phagocytic uptake and plasma protein adsorption, Colloids Surf. B: Biointerfaces 18 (2000) 301–313.
[24] M.T. Peracchia, C. Vauthier, C. Passirani, P. Couvreur, D. Labarre, Complement consumption by poly(ethylene glycol) in different conformations chemically coupled to poly(isobutyl 2-cyanoacrylate) nanoparticles, Life Sci. 61 (1997) 749–761.
[25] R.C. Leonard, S. Williams, A. Tulpule, A.M. Levine, S. Oliveros, Improving the therapeutic index of anthracycline chemotherapy: focus on liposomal doxorubicin (Myocet), Breast 18 (2009) 218–224.
[26] J. Gautier, E. Munnier, A. Paillard, K. Herve, L. Douziech-Eyrolles, M. Souce, P. Dubois, I. Chourpa, A pharmaceutical study of doxorubicin-loaded PEGylated nanoparticles for magnetic drug targeting, Int. J. Pharm. 423 (2012) 16–25.
[27] E. Munnier, S. Cohen-Jonathan, C. Linassier, L. Douziech-Eyrolles, H. Marchais, M. Souce, K. Herve, P. Dubois, I. Chourpa, Novel method of doxorubicin-SPION reversible association for magnetic drug targeting, Int. J. Pharm. 363 (2008) 170–176.
[28] M. Hoenig, A. De Kersabiec, Sample preparation steps for analysis by atomic spectroscopy methods: present status, Spectrochim. Acta B 51 (1996) 1297–1307.
[29] I. Bohm, Magnetic resonance cell-tracking studies: spectrophotometry-based method for the quantification of cellular iron content after loading with superparamagnetic iron oxide nanoparticles, Mol. Imaging 10 (2011) 270–277.
[30] G. McAuley, M. Schrag, S. Barnes, A. Obenaus, A. Dickson, W. Kirsch, In vivo iron quantification in collagenase-induced microbleeds in rat brain, Magn. Reson. Med. (2011).
[31] I. Chourpa, L. Douziech-Eyrolles, L. Ngaboni-Okassa, J.F. Fouquenet, S. Cohen-Jonathan, M. Souce, H. Marchais, P. Dubois, Molecular composition of iron oxide nanoparticles, precursors for magnetic drug targeting, as characterized by confocal Raman microspectroscopy, Analyst 130 (2005) 1395–1403.
[32] S. Tsuchiya, Y. Kobayashi, Y. Goto, H. Okumura, S. Nakae, T. Konno, K. Tada, Induction of maturation in cultured human monocytic leukemia cells by a phorbol diester, Cancer Res. 42 (1982) 1530–1536.
[33] B. Chertok, B.A. Moffat, A.E. David, F. Yu, C. Bergemann, B.D. Ross, V.C. Yang, Iron oxide nanoparticles as a drug delivery vehicle for MRI monitored magnetic targeting of brain tumors, Biomaterials 29 (2008) 487–496.
[34] M.R. Gittings, D.A. Saville, The determination of hydrodynamic size and zeta potential from electrophoretic mobility and light scattering measurements, Colloids Surf. A: Physicochem. Eng. Aspects 141 (1998) 111–117.
[35] A. Shkilnyy, E. Munnier, K. Hervé, M. Soucé, R. Benoît, S. Cohen-Jonathan, P. Limelette, M. Saboungi, P. Dubois, I. Chourpa, Synthesis and evaluation of novel biocompatible superparamagnetic iron oxide nanoparticles as magnetic anticancer drug carrier and fluorescence active label, J. Phys. Chem. C 114 (2010) 5850–5858.
[36] C. Fang, B. Shi, Y.Y. Pei, M.H. Hong, J. Wu, H.Z. Chen, In vivo tumor targeting of tumor necrosis factor-alpha-loaded stealth nanoparticles: effect of MePEG molecular weight and particle size, Eur. J. Pharm. Sci. 27 (2006) 27–36.
[37] A. Aqil, S. Vasseur, E. Duguet, C. Passirani, J.P. Benoît, A. Roch, R. Müller, R. Jérôme, C. Jérôme, PEO coated magnetic nanoparticles for biomedical application, Eur. Polym. J. 44 (2008) 3191–3199.
[38] S. Jain, V. Mishra, P. Singh, P.K. Dubey, D.K. Saraf, S.P. Vyas, RGD-anchored magnetic liposomes for monocytes/neutrophils-mediated brain targeting, Int. J. Pharm. 261 (2003) 43–55.
[39] S. Gordon, P.R. Taylor, Monocyte and macrophage heterogeneity, Nat. Rev. Immunol. 5 (2005) 953–964.
[40] T.K. Jain, J. Richey, M. Strand, D.L. Leslie-Pelecky, C.A. Flask, V. Labhasetwar, Magnetic nanoparticles with dual functional properties: drug delivery and magnetic resonance imaging, Biomaterials 29 (2008) 4012–4021.
[41] H.L. Ma, Y.F. Xu, X.R. Qi, Y. Maitani, T. Nagai, Superparamagnetic iron oxide nanoparticles stabilized by alginate: pharmacokinetics, tissue distribution, and applications in detecting liver cancers, Int. J. Pharm. 354 (2008) 217–226.
[42] D. Mishra, M. Sudarshan, A. Chakraborty, Elemental alteration, iron overloading and metallothionein induction in experimental hepatocarcinogenesis: a free radical-mediated process?, Toxicol Lett. 203 (2011) 40–47.
[43] H.S. Choi, W. Liu, P. Misra, E. Tanaka, J.P. Zimmer, B. Itty Ipe, M.G. Bawendi, J.V. Frangioni, Renal clearance of quantum dots, Nat. Biotechnol. 25 (2007) 1165–1170.
[44] L.T. Chen, L. Weiss, The role of the sinus wall in the passage of erythrocytes through the spleen, Blood 41 (1973) 529–537.
[45] D. Hellstern, K. Schulze, B. Schopf, A. Petri-Fink, B. Steitz, S. Kamau, M. Hilbe, S. Koch-Schneidemann, L. Vaughan, M. Hottiger, M. Hofmann, H. Hofmann, B. von Rechenberg, Systemic distribution and elimination of plain and with Cy3.5 functionalized poly(vinyl alcohol) coated superparamagnetic maghemite nanoparticles after intraarticular injection in sheep in vivo, J. Nanosci. Nanotechnol. 6 (2006) 3261–3268.

Annexe 2 Curriculum vitae

Pharmacien galéniste

Juliette GAUTIER
31 ans, célibataire
25 rue de l'Elysée, 37000 TOURS
06.07.90.96.93 / 02.47.61.05.13
juliette.gautier@etu.univ-tours.fr, j.gautier@groupe-imt.com

Cursus Scientifique

Depuis 2010	Doctorat en cours Sciences de la Vie et de la Santé, Université de Tours, au sein de l'EA 6295 «Nanomédicaments et Nanosondes » Laboratoires de Pharmacie Galénique et de Chimie Analytique UFR des Sciences Pharmaceutiques Philippe Maupas,Tours, France
2005-2006	6ème année de Pharmacie Master 2 Pro « Développement et industrialisation des produits de santé » (pharmacie galénique, chimie analytique, affaires règlementaires), Université de Tours, mention bien
2004-2005	5ème année de Pharmacie filière industrie, mention développement production (M1), faculté de Limoges
2001-2004	1er et 2ème cycle des études de Pharmacie, faculté de Pharmacie de Limoges 2 Maîtrises en Sciences Biologiques et Médicales (« Biochimie métabolique et régulations » et « Biotechnologies et ingénierie biomédicale »)
1999	Bac S option biologie mention bien

Expérience professionnelle

2012-2013	ATER Chimie Analytique à l'Université de Tours (37)
2011-2012	Vacataire enseignement Pharmacie Galénique à l'Université de Tours (37)
Depuis 2007	Formateur galénique au sein du groupe IMT (37)
2005-2006	Stage de M2Pro au sein de l'unité de développement galénique des laboratoires Ethypharm (Houdan, 78)
2004-2005	Concours Campus Entrepreneur, création d'une entreprise de formulation de cosmétiques, 3ème prix Stage de M1 à l'unité d'appui clinique (UAC) Laboratoires Servier (Gidy, 45) : stage ouvrier Stages hospitaliers au CHRU de Limoges (87) : toxicologie (techniques analytiques)
2001-2004	Aide en pharmacie d'officine (87)

ACTIVITES DE RECHERCHE ET DEVELOPPEMENT

Doctorat (en cours) à l'UFR Sciences Pharmaceutiques de Tours, à l'EA 6295 « Nanomédicaments et Nanosondes », responsable I. Chourpa.
Sujet de thèse "Développement, mise en forme et caractérisation de vecteurs nanoparticulaires d'agents anticancéreux à base de nanoparticules superparamagnétiques" ; directeur de thèse Pr I. Chourpa.

Coopération internationale avec l'équipe de Marek Procházka de l'Institut de Physique de la Charles University de Prague (République Tchèque), étude de porphyrines en SERS.

Stage de M2Pro au sein de laboratoires Ethypharm : étude et modification de formule d'un comprimé matriciel

Stage de M1 au sein des Laboratoires Servier : fabrication de lots de comprimés/gélules pour essais cliniques, rodage des procédés de fabrication (granulation en MGS, compression, pelliculage, masquage)

Stage hospitalier en toxicologie : mise au point d'une méthode de dosage du glyphosate (actif du Roundup®) dans les liquides biologiques (sang total, sérum, urines) en spectrométrie de masse

Compétences spécifiques :

1) ***Formulation et développement :*** élaboration de nanovecteurs magnétiques d'agents anticancéreux et de nanosondes d'argent
- Fabrication de nanoparticules d'oxydes de fer fonctionnalisées (obtention des nanoparticules par coprécipitation, PEGylation de leur surface, fixation d'un agent anticancéreux)
- Fabrication de nanoparticules d'argent fonctionnalisées (synthèse et PEGylation par chimie « one-pot »)
- Optimisation du protocole de fabrication

2) ***Physico-chimie :*** caractérisation de principes actifs et de nanoformes galéniques, et utilisation comme sondes
- Quantification des éléments par spectrométrie d'absorption atomique
- taille des nanovecteurs (granulométrie laser) et potentiel de surface (zétamétrie)
- teneur en principe actif et cinétiques de libération *in vitro* (dialyse, spectroscopies UV-visible et de fluorescence, CLHP)
- étude de complexes de principes actifs à l'aide de sondes nanoparticulaires en SERS (Surface Enhanced Raman Scattering)

3) ***Biologie :*** évaluation des nanovecteurs
- activité *in vitro*, sur cellules cancéreuses des lignées MCF-7 et MDA-MB435 (culture cellulaire, essais de cytotoxicité au MTT en microplaques; cinétiques de mortalité ; étude sub-cellulaire du devenir du principe actif par imagerie confocale multispectrale)
- activité *in vivo*, sur modèle animal, souris NMRI nude tumorisées avec des cellules MDA-MB435 (induction tumorale, suivi des animaux, administration intraveineuse, prélèvement sub-mandibulaire, prélèvement des organes)

ACTIVITES D'ENSEIGNEMENT UNIVERSITAIRE ET DE FORMATION

ATER Chimie Analytique à l'Université de Tours, travaux pratiques 2ème et 5ème année Industrie en 2012/2013, 240h (dosages volumétriques, spectrophotométrie UV-visible, HPLC, titrateurs automatiques, CPG)

Intervention à l'Université de Tours en travaux pratiques de Pharmacie Galénique de 2ème année de Pharmacie en 2011/2012, 100h (formes orales liquides, émulsions et formes semi-solides, formes liquides stériles, formes sèches industrielles).

Formateur galénique au sein du groupe IMT (formations professionnelles pour les industries pharmaceutiques et cosmétiques) depuis 2007

- Interventions pour techniciens en pharmacie et cosmétique industrielle (TPCI, niveau IV), techniciens supérieurs en pharmacie industrielle (TSPI, niveau III) et techniciens spécialisés en bioproduction industrielle (TSBI, niveau II) :
    - cours, création de supports de cours et travaux pratiques
- Interventions sur sites industriels et travaux pratiques pour la formation de salariés :
    - Dior (Orléans): formes cosmétiques et leur formulation (poudres libres/compactées, mascaras, vernis, rouges à lèvres…)
    - Theramex (Monaco) : paramètres de formulation des émulsions
    - GSK Biologicals (Saint-Amand-les-Eaux et sites de Belgique) : la vaccination (principes, formulation et procédés industriels), les cGMP
    - Sanofi (Vitry) : procédés de biotechnologie (culture cellulaire, fermentation, filtrations frontale/tangentielle, techniques séparatives, de purification…)

Compétences spécifiques :

1) ***Création de supports*** de formation, de supports de cours et de supports de travaux pratiques adaptés au public ciblé

2) maîtrise des ***procédés industriels*** et ***pilotage des équipements***
- formes sèches : granulateurs, lit d'air fluidisé, compacteur, mélangeurs, presse à comprimer rotative, géluleuse alternative, turbines de pelliculage
- formes liquides : remplisseuse ampoules/flacons, bancs de filtration, autoclave, lyophilisateur, manipulations en PSM, habillage en ZAC, bioréacteurs
- formes pâteuses : disperseur-homogénéisateur, homogénéisateur à filière

3) maîtrise des ***procédés de contrôles*** en cours et en fin de production, et des équipements associés
- contrôles Pharmacopées,
- contrôles sur ligne comme le mirage, l'étanchéité, la line clearance
- contrôles physico-chimiques

4) maîtrise des ***techniques analytiques***
- techniques séparatives : HPLC, CPG
- techniques spectroscopiques : spectrophotométrie UV-visible, imagerie confocale multi spectrale, SERS

5) ***Formulation*** des formes galéniques industrielles et cosmétiques

6) ***Connaissance du milieu industriel*** pharmaceutique, biotechnologique et cosmétique

PRODUCTIONS SCIENTIFIQUES

Publications

1 publication en cours de soumission (15 mai)

5. **Efficacy and hemotoxicity of stealth magnetic nanovectors of doxorubicin on breast cancer xenografts.** J. Gautier, E. Allard-Vannier, J. Gaillard, J. Domenech, I. Chourpa. Soumis à Nanoscale.

4. **SERS spectroscopic approach to study the doxorubicin complexes with Fe^{2+} ions and the drug release from SPION-based nanocarriers.** J. Gautier, E. Munnier, L. Douziech-Eyrolles,A. Paillard, P. Dubois, I. Chourpa. Soumis à Analyst.

3. **Recent advances in theranostic nanocarriers of doxorubicin based on iron oxide and gold nanoparticles.** J. Gautier, E. Allard-Vannier, E. Munnier, M. Soucé, I. Chourpa. J Control Release 2013, doi:10.1016/j.jconrel.2013.03.018, *in press*

2. **Pegylated magnetic nanocarriers for doxorubicin delivery: A quantitative determination of stealthiness in vitro and in vivo.** E. Allard-Vannier, S. Cohen-Jonathan, J. Gautier, K. Hervé-Aubert, E. Munnier, M. Soucé, P. Legras, C. Passirani, I. Chourpa. Eur J Pharm Biopharm 2012, **81**: 498-505, doi: 10.1016/j.ejpb.2012.04.002

1. **A pharmaceutical study of doxorubicin-loaded PEGylated nanoparticles for magnetic drug targeting.** J. Gautier, E. Munnier, A. Paillard, K. Hervé, L. Douziech-Eyrolles, M. Soucé, P. Dubois, I. Chourpa. Int J Pharm 2012, **423**: 16-25, doi:10.1016/j.ijpharm.2011.06.010

Communications

10. ***In vitro* and *in vivo* study of theranostic magnetic nanocarriers of doxorubicin.** J. Gautier, E. Allard-Vannier, S. Même, A. Carrouée, E. Munnier, K. Hervé-Aubert, J.C. Beloeil, I. Chourpa (Communication orale)
E-MRS Spring Meeting, Strasbourg, May 27-31, 2013

9. **Nanovecteurs magnétiques pour la délivrance de la doxorubicine: caractérisations et évaluations *in vitro/in vivo* d'un outil théragnostique potentiel.** J. Gautier, E. Allard-Vannier, I. Chourpa (Communication orale)
XV^{ème} colloque Louis Néel, Tours, 19-22 mars 2013

8. **PEGylated iron oxide magnetic nanocarriers for doxorubicin delivery: *in vitro* and *in vivo* study of a potential theranostic system.** J. Gautier, E. Allard-Vannier, E. Munnier, K. Hervé-Aubert, S. Même, J.C. Beloeil, I. Chourpa (Communication orale)
« Medicine in Oncology » workshop at Berder Island, September 26-29, 2012

7. **Stealthiness of injectable magnetic nanoparticles for nanotheranostic applications**, E. Allard-Vannier, Y. Victor, J. Gautier, K. Kaaki, S. Cohen-Jonathan, C. Passirani and I. Chourpa.
26èmes Journées Scientifiques du GTRV, Bruxelles, 5-7 Décembre 2011.

6. **Etude pharmaceutique de nanovecteurs magnétiques d'anticancéreux.** J. Gautier (communication orale)

Journée des Jeunes Scientifiques des Universités d'Orléans, de Tours et du CEA Le Ripault, « Chimie – Physique – Matériaux », 20 octobre 2011

5. **Magneto-optical nanoparticles for delivery and detection of anti-cancer drug**, I.Chourpa, K.Kaaki, J. Gautier, E. Allard, A. Paillard, K. Hervé, A. Shkilnyy, L. Douziech-Eyrolles, S. Cohen-Jonathan, M. Soucé, H. Marchais, P. Dubois, et M.L. Saboungi. 25èmes Journées Scientifiques du GTRV, Toulouse, 6-10 Décembre 2010.

1-4. **Pharmaceutical study of DOX-loaded PEGylated nanoparticles for magnetic drug targeting.** J. Gautier, E. Munnier, K. Hervé, A. Paillard, P. Dubois, I. Chourpa.
23ème colloque Biotechnocentre, Seillac, 21-22 octobre 2010.
25èmes Journées Scientifiques du GTRV, Toulouse, 6-10 Décembre 2010.
Forum des Ecoles Doctorales « Santé, Sciences, Technologies » de Tours et « Sciences et Technologies » d'Orléans, Tours, 23 juin 2011
Journée Nanosciences et Nanotechnologies en Région Centre, Orléans, 6 juillet 2011

Récompenses

2. **Lauréate du soutien financier colloque international de l'Axe Vectorisation et Radiothérapies du Cancéropôle Grand Ouest,** pour l'E-MRS Spring Meeting, Strasbourg, May 27-31, 2013.

1. **Prix de la meilleure communication** session Poster, Forum des Ecoles Doctorales « Santé, Sciences, Technologies » de Tours et « Sciences et Technologies » d'Orléans, Tours, 23 juin 2011.

Juliette GAUTIER

Nanoparticules d'oxydes de fer PEGylées pour la délivrance de la doxorubicine : développement et évaluation de leur potentiel théragnostique

Résumé

Des nanoparticules d'oxydes de fer superparamagnétiques (SPIONs) PEGylées ont servi de plateforme pour la formulation de nanovecteurs théragnostiques pour la délivrance d'un agent anticancéreux, la doxorubicine (DOX). Le chargement de la DOX sur les nanovecteurs à l'aide d'un complexe avec l'ion fer (II) a été optimisé. Ce complexe se dissocie en milieu acide, typique des compartiments intracellulaires. La spectroscopie Raman exaltée de surface (SERS) a confirmé que les nanovecteurs libèrent la DOX sous forme non complexée. La cytotoxicité *in vitro* induite par la libération de la DOX a été évaluée sur différentes lignées cellulaires de cancer du sein, et comparée à celle de la DOX en solution. Les voies d'internalisation des nanovecteurs ont été explorées en microscopie électronique en transmission (MET), et le devenir intracellulaire de la DOX a été suivi en imagerie confocale multispectrale (ICMS). Enfin, un protocole thérapeutique *in vivo* chez la souris tumorisée a permis d'évaluer la capacité de la nanoformulation à limiter la croissance tumorale, la possibilité d'un ciblage magnétique, et la réduction des effets secondaires induits par la DOX.

Mots-clés

Nanoparticules d'oxydes de fer superparamagnétiques (SPIONs), doxorubicine (DOX), complexe DOX-Fe^{2+}, nanovecteur théragnostique, délivrance, protocole thérapeutique, furtivité, imagerie

Abstract

PEGylated superparamagnetic iron oxide nanoparticles (SPIONs) were used as a platform to build theranostic nanovectors for the delivery of an anticancer drug, doxorubicin (DOX). The DOX loading on nanocarriers via a DOX-iron (II) complex was optimized. The complex dissociates at low pH, typical of intracellular compartments. Surface enhanced Raman scattering (SERS) confirmed that the nanovectors released DOX under free form. *In vitro* cytotoxicity due to DOX loaded on nanocarriers was performed on different breast cancer cells, and compared to that of DOX in solution. Internalization pathways of nanovectors were explored with transmission electron microscopy (TEM), and intracellular fate of DOX was monitored by confocal spectral imaging (CSI). To finish, a therapeutical protocol was performed on tumorized mice, in order to evaluate the efficacy of the nanoformulation on tumor reduction, the possibility of magnetic targeting, and the decrease of side effects induced by DOX.

Keywords

Superparamagnetic iron oxide nanoparticles (SPIONs), doxorubicin (DOX), DOX-Fe^{2+} complex, theranostic nanovector, delivery, therapeutical protocol, stealthiness, imaging